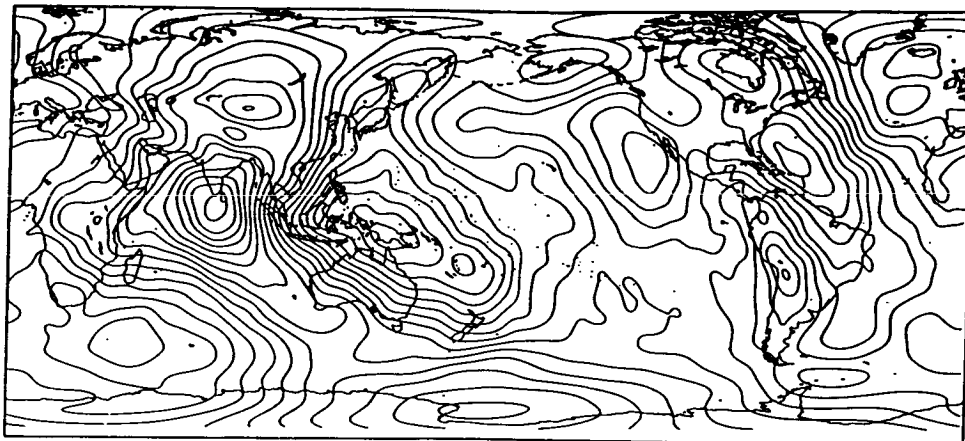# NASA Technical Memorandum 4019

An Improved Model of the Earth's Gravitational Field: *GEM-T1*

J. G. Marsh, F. J. Lerch, B. H. Putney,
D. C. Christodoulidis, T. L. Felsentreger,
B. V. Sanchez, D. E. Smith, S. M. Klosko,
T. V. Martin, E. C. Pavlis, J. W. Robbins,
R. G. Williamson, O. L. Colombo,
N. L. Chandler, K. E. Rachlin, G. B. Patel,
S. Bhati, and D. S. Chinn

NASA

NASA Technical Memorandum 4019

An Improved Model of the Earth's Gravitational Field: *GEM-T1*

J. G. Marsh, F. J. Lerch, B. H. Putney,
D. C. Christodoulidis, T. L. Felsentreger,
B. V. Sanchez, and D. E. Smith
Geodynamics Branch

S. M. Klosko, T. V. Martin, E. C. Pavlis,
J. W. Robbins, R. G. Williamson,
O. L. Colombo, N. L. Chandler, and
K. E. Rachlin
*EG&G Washington Analytical Services
Center, Inc.*

G. B. Patel, S. Bhati, and D. S. Chinn
*Science Applications and Research
Corporation*

JULY 1987

NASA

National Aeronautics and
Space Administration

Goddard Space Flight Center

1987

TABLE OF CONTENTS

TABLE OF CONTENTS (cont.)

TABLE OF CONTENTS (cont.)

SECTION 1.0

INTRODUCTION

Ground-based tracking of artificial satellites has provided an observational data set which has been used to develop spherical harmonic models of the global long wavelength gravity field of the earth. Analyses of these data by the authors and many others have provided a major advance in the field of Geodesy. Since the creation of the National Geodetic Satellite Program in the middle 1960's, a continuous effort has been underway at NASA/Goddard Space Flight Center (GSFC) and other research centers (notably the Smithsonian Astrophysical Observatory, the U.S. Department of Defense, and a cooperative effort between Germany's Deutsches Geodaetisches Forschungsinstitut and France's Groupe de Recherches de Geodesie Spatiale -- to name a few) to use satellite observations to improve our understanding of the gravity field and enhance our capabilities for modeling near-earth satellite orbital motion. Better knowledge of the geopotential has created dramatic advances in point positioning, in the study of the earth's kinematics and tectonics, in understanding the earth's rheology and interior, and in the study of global oceanic processes with spaceborne instrumentation.

The geopotential models developed by GSFC are known by their acronym, GEM, standing for Goddard Earth Models. The GEM have generally kept pace with the rapid advances made in the precision by which near-earth satellites are tracked and the orbital accuracy requirements of the missions themselves. However, new NASA missions foreseen for the 1990's require further gravity model improvement to achieve their mission objectives. Of most immediate concern is geodetic support (e.g., for orbit computations and the marine geoid) for the TOPEX oceanographic satellite which is under development for launch in 1991. The 10 to 15 cm radial orbit accuracy requirement of TOPEX, driven by the radar altimeter system, is at least a factor of three beyond the

1

capability of gravity models existing in 1985. There is an additional need for an Interim model which enhances our present knowledge of the earth's gravity field at intermediate and short wavelengths to the accuracy needed to support a low orbiting Geopotential Research Mission which is under consideration as a new flight project by NASA. Both of these objectives can be satisfied with a substantial improvement in global gravity modeling and the development of an Interim Model.

The recovery of a gravity model from satellite observations is both costly and time consuming. It requires the arduous analysis of large numbers of observations spanning diverse data types and the building of large numerical systems of equations permitting a simultaneous solution of several thousand unknowns. Consequently, the preparation of an improved model requires extensive pre-launch research.

To achieve the accuracy required for TOPEX, an experimental plan has been devised which builds towards a final geopotential solution in stages with harmonics extending to higher degree as the earth's gravity field is more completely sampled. Therein, each type of data is to be carefully scrutinized and separately evaluated to extract optimal subset gravity solutions. The final model, and one that will satisfy the TOPEX criterion, will be obtained from the combination of all of these validated data. This model will utilize a large amount of available laser, altimeter, satellite-to-satellite tracking and surface gravimetric observations.

This report describes the first of these preliminary gravity models, GEM-T1, which is exclusively based upon direct satellite tracking observations. This spherical harmonic model, complete to degree and order 36 is a direct result of the gravity field improvement effort which has been undertaken by GSFC and the University of Texas' Center for Space Research to produce an Interim Model. This "satellite-only" model was developed by GSFC and is reported herein. In regard to data selection, GEM-T1 although more complete in spherical harmonics, is

like earlier GSFC models, for example, GEM-9 (Lerch et al., 1979) and GEM-L2 (Lerch et al., 1982) which also exclusively used satellite tracking observations. Models which will include satellite-to-satellite tracking, spaceborne radar altimeter observations and surface gravity measurements are in the planning stages. These later fields will all be built upon the long wavelength information contained within GEM-T1.

The demands of future orbital missions made the recovery of a more accurate gravity model necessary and required their extension to higher degree. The availability of the CYBER 205 "super-computer" at GSFC played a major role in making this task both feasible within the time constraints imposed upon us and practical from a resource assessment. Adapting our orbit determination GEODYN Program and the SOLVE least squares solution system to the Cyber vector processor was a major step in laying the foundation for a complete and total re-iteration of our previous gravity modeling activities. The last recalculation of all least-squares normal matrices occured more than ten years ago in preparation for GEM-7 (Wagner, et al., 1977).

In the computation of the GEM-T1 model a total re-iteration of the data analysis and matrix generation activities was performed. This permitted a consistency lacking in the earlier GEM models in terms of adopted constants, data treatment, non-conservative force modeling and in the definition of a reference frame. In particular, the aliasing error has been reduced by consistently evaluating all orbital data in the normal equations for a spherical harmonic representation to degree and order 36. For many data sets, terms extending to degree 50 are available although they have not been used to solve GEM-T1. In the past, as the state of the science evolved, only the most recent data sets benefitted from improved modeling. The inconsistencies associated with an evolving science and the lag-time required for their implementation in our data analysis have been avoided by design in the creation of GEM-T1. A model with improved parentage has now been produced which is based largely upon the standard set of constants

adopted for the MERIT Campaign (Melbourne, et al 1983) with some significant improvements. Additionally, other NASA Geodynamics research activities like the Crustal Dynamics Program, have provided improved a priori tracking station coordinates and earth rotation series which have been used in the development of GEM-T1. These models, values and treatments are described in detail within this report. In subsequent models planned for the next few years, a simultaneous solution including tracking station adjustments with the gravity field will also be explored.

Although the title of this report might indicate otherwise, there is more than one gravitational model discussed within its pages. We deliberately sacrificed brevity for the sake of completeness to permit a more thorough discussion of the approach we have pursued to design, compute, calibrate, and test the GEM-T1 solution. In so doing, we have presented material pertaining to many additional fields which were in some cases developed specifically for test purposes. Generally, these models were used to illustrate specific points and show the response of the model to new weights and/or new data contributions. As an aide in keeping track of them all and to assist in an easy understanding of their differences, these models are summarized in Table 1. Therein we present a brief description of these fields, and a cross reference which highlights specific tables, figures and sections where they are used.

TABLE 1. KEY TO GSFC GRAVITATIONAL FIELDS: DESCRIPTIVE SUMMARY AND CROSS REFERENCE

FIELD NAME

DESCRIPTION

GEM-T1

is a "satellite-only" gravitational field model developed from tracking data acquired on 17 unique satellite orbits (Table 5.4). A summary of the observations utilized is presented on Table 5.3 and the weighting used is shown in Figure 8.4. The spherical harmonic coefficients for GEM-T1 are found in Table 9.1 and their uncertainties are shown in Figure 10.1. This model is the focus of this manuscript. GEM-T1 had an internal GSFC field number of PGS 3113. Note also, certain data sets were corrected to improve the overall model.

PGS-T2

is an earlier model presented at the American Geophysical Union Meeting in the spring of 1986. It did not contain data from 6 low inclination satellite (Section 5.2.8 and 10.4) and contained a serious GEOS-2 matrix back-substitution problem (Figure 8.3).

PGS-T2'   is the PGS-T2 field (above) with
                 the GEOS-2 problem corrected.

GEM-9   is a pre-Lageos "satellite-only"
                 model (Lerch et al, 1977).

GEM-L2'   is the GEM-L2 model (Lerch et al,
                 1982) solved with the C,S (2,1)
                 coefficients constrained to
                 equal zero. This was GSFC's
                 general recommended "satellite
                 only" model prior to the completion
                 of GEM-T1.

PGS-1331'   is the PGS-1331 model (Marsh
                 et al, 1985), like Gem-L2,
                 solved with C,S (2,1) constrained
                 to equal zero. PGS-1331 was a
                 model "tailored" for the Starlette
                 satellite orbital computations.

PGS-S4'   is the PGS-S4 model (Lerch et al,
                 1982b) solved with the C,S (2,1)
                 coefficients constrained to
                 equal zero. PGS-S4 was a model
                 "tailored" for SEASAT orbital
                 computations.

GEM-10B'   is the GEM-10B model (Lerch et al,
                 1981) solved with the C,S (2,1)
                 coefficients constrained to equal
                 zero. GEM-10B is a comprehensive
                 model which contained altimetry
                 and surface gravimetry.

PGS-3013   is the PGS-T2 model where the
                    data weight was increased by a
                    factor of 5 with respect to
                    the collocation matrix (Table 8.2)
                    and was used to gove an example
                    of the adequacy of the calibration
                    method in Figure 10.12.

PGS-3167   was made from the GEM –T1
                    normal equations but solved to
                    be of a smaller size -·being
                    complete to deqree and order
                    20 (like GEM-L2) and not 36,
                    which was the truncation limit
                    of GEM-T1 (Figure 8.7).

PGS-3163   was a combination solution combining
                    GEM-T1 with SEASAT altimeter
                    matrices. The altimetry in this
                    field was given a weak weight
                    of 0.1 (Figure 8.5, Figure 10.3.1, and
                    Figure 10.10).

PGS-3164   was the PGS-3163 field, solved
                    giving greater weight of 0.5
                    to the altimetry (Figure 10.11).

SECTION 2.0
THE GEODYN AND SOLVE SYSTEMS

The Cyber 205 computing system was obtained by Goddard Space Flight Center in 1982. An effort was immediately undertaken (and continues today) to improve our principal analysis tools, GEODYN and SOLVE, to efficiently use the Cyber's vector processing capabilities. This section describes the design decisions, status, and most importantly, the enormous benefits which accrued as a result of these software development activities.

2.1 SOFTWARE DESCRIPTION

The primary software tools utilized by the GSFC TOPEX gravity modeling team were the SOLVE program and the GEODYN system of programs.

GEODYN provides state-of-the-art orbit determination and geodetic parameter estimation capabilities [Putney, 1977; Martin et al., 1980, Martin et al., 1987]. Using a fixed-integration-step, high-order Cowell integrator, GEODYN numerically integrates the spacecraft Cartesian state and the force model partial derivatives. The forcing function includes a spherical harmonic representation for Earth gravitation as well as models for point mass lunar, solar and planetary gravitation, solar radiation pressure, Earth atmospheric drag, and dynamical Earth and ocean tides. Observation modeling includes Earth precession and nutation, polar motion and Earth rotation, and tracking stations displacements due to solid tides and ocean loading. Tracking measurement corrections are provided for tropospheric and parallactic refraction, annual and diurnal aberration, antenna axis displacement and spacecraft center of gravity offset. Dynamic data editing is performed as the Bayesian least squares estimator is iterated to solution convergence. Estimable parameters include measurement and timing biases, and tracking

station coordinates, as well as the orbit state and force model parameters in all of the above mentioned models. The normal equations formed within GEODYN may be output to a file for inclusion in large parameter estimations and error analyses.

The SOLVE computer program selectively combines and edits the least squares normal equations formed by the GEODYN Program to form solutions for the gravity field, tracking station coordinates, polar motion, earth rotation, ocean tides and other geodetic parameters. The SOLVE Program provides a highly flexible tool for the computation of the solutions.

This software has evolved over the last 20 years to include the processing of many satellite tracking data types using sophisticated geophysical models. In the past, the research has been heavily constrained by the capabilities of the available computers. Typically, computer runs to create and solve large normal matrices for the solution of geodetic parameters required several CPU hours. As additional geophysical models were added, the increase in the number of estimable parameters was clearly limited by computer resources.

In 1982, the Cyber 205 vector computer was installed at GSFC. For more than a year before the installation, both GEODYN I and SOLVE were upgraded for the Cyber 205. The GEODYN program required some basic redesign to optimally use the vector hardware. This entailed a complete rewrite of the original scalar version of GEODYN, creating the GEODYN II Program. The SOLVE program, which intrinsically dealt with large arrays, was modified in sections to take advantage of the vector architecture.

From the beginning of this activity, considerable effort has been devoted to improve computational efficiencies on the Cyber. For GEODYN II, completely rewriting the software has taken several years. For SOLVE, I/O redesign has become necessary, since in a typical run, I/O time is now twice that of CPU time.

10

2.1.1 Vectorization of SOLVE

The SOLVE [Estes and Major, 1986] program has been vectorized for the Cyber 205. The solution section of the code is now fully vectorized and optimally partitioned for CPU and I/O performance. The CPU usage is so small that the algorithm is now clearly I/O bound. Minimizing the I/O time has led to the utilization of special I/O packages. Large quantities of data are moved simultaneously from different disk packs residing on separate I/O channels when possible.

Typically, many hundreds of matrices, each representing a single orbital arc, are required for a solution. Techniques are employed to limit the amount of data processed by SOLVE at any one time; these include combining several matrices into a single "combined" matrix or C-Matrix. SOLVE is capable of performing this function with the option of eliminating satellite arc dependent parameters through back substitution at the same time. There are two types of parameters that are solved for. Some are satellite specific (e.g., the satellite's initial state vector at some epoch time). These so-called "arc" parameters are seldom the ones of major interest. The "common" parameters include those of geodetic interest that are global in nature. They can be gravity coefficients, earth orientation parameters, tidal terms, etc., and it is the set of values of these parameters alone which normally constitute a solution. The process of combining matrices may be done when summing the normals of individual data sets to form C-matrices or at a later stage, when combining C-Matrices to form a second level of C-Matrices. This affords tremendous data compression and creates a final matrix with the smallest possible number of parameters through the back-substitution of all arc-parameters. When this matrix is inverted by SOLVE, corrections to the total set of common parameters are produced without the added expense of carrying along unnecessary arc parameters.

The SOLVE program has the capability to perform a linear shift on the right-hand side of the normal equations. This may be done during the combining stage so that all parameters converged using different values of the global parameters may be transformed to a common reference. The solution also may be referenced to any set of starting values. Other SOLVE capabilities include dynamical suppression of parameters based on numerical stability, application of weights to individual matrices or C-Matrices when combining, and carrying out a partitioned Cholesky decomposition to optionally compute (a) the parameter solution, (b) the parameter solution plus standard deviations or (c) the parameter solution plus a full variance/covariance matrix, as the user requires.

An example of the reduction in computing time which has been achieved is provided for the full inversion of a 1921 x 1921 matrix. On the IBM 3081 this process took 116 minutes of CPU time and 31 minutes of I/O time. On the Cyber 205 (with four million words of computer memory) the process required only 90 seconds of CPU time and 142 seconds of I/O time. This is a factor of 77 improvement in CPU and a factor of 13 improvement in I/O!

2.1.2 Evolution of GEODYN

The original GEODYN system (GEODYN I) was designed for IBM mainframe computers. In this form, GEODYN I was optimized to take full advantage of its environment. When NASA began the procurement process for a vector computer, it became immediately apparent that a redesign of the GEODYN system was necessary to make a cost-effective utilization of the vector computing environment. Also of great importance was the vastly increased speed achieveable for large parameter solutions if this approach was undertaken. Additionally the GEODYN I software contained a number of outdated approximations which needed to be eliminated in the system redesign.

With these concepts in mind, a two-pronged approach was taken which led to a new and highly efficient GEODYN operating within the vector processing environment.

Because GEODYN's historical computing environment - the IBM 360/95, was to be replaced, a scalar version of GEODYN I for the Cyber 205 computer was created directly from the IBM version. This program has been commonly referred to as Cyber GEODYN I.

In a parallel effort, a totally new GEODYN program was designed to take full advantage of the vector-processing environment. This new program is called GEODYN II and has been developed in such a fashion that those functions which are I/O intensive are performed on the "front-end" to the vector computer and the CPU intensive functions are performed either on the vector computer or on the "front-end" computer at the specification of the user.

These two efforts have permitted a smooth transition of operations from the IBM 360/95 to the Vector Processing Facility at GSFC. Because the GEODYN II system required a development period of about 5 years, the Cyber GEODYN I was used in the interim. A more thorough discussion of the GEODYN II design philosophy and its impact on the TOPEX gravity model effort are presented below.

2.1.2.1 GEODYN II Design Philosophy

There were a number of key considerations that went into the design of the GEODYN II system. They are briefly presented below and individually discussed in the following paragraphs.

o   All data formats were made a uniform 64-bit floating point.

13

o   I/O intensive operations were off-loaded from the vector computer.

o   Observation processing was adapted to vectorization.

o   Interpolation and partial derivative chaining were fully vectorized.

o   Force model evaluations and partial derivatives were vectorized where appropriate.

o   Numerical integration of the orbit was vectorized where possible.

o   Numerical integration of force model partial derivatives was fully vectorized.

o   Formulation of normal equations was fully vectorized.

o   Large parameter solutions exhibit different vectorization problems than routine orbit determination solutions. Therefore capabilities were provided to allow optimization of vectorization based upon the type of problem to be solved.

Figure 2-1 presents the data flow structure of the GEODYN II system. It also indicates the operating environment of the various programs in the system. No explicit references to this figure are made in the following paragraphs, but an awareness of its contents may be useful to the reader.

Transmissions of data between the Cyber 205 vector computer and its "front-end", the Amdahl V7 computer, require data conversions if the data are to be used by both computer systems. These data conversions are
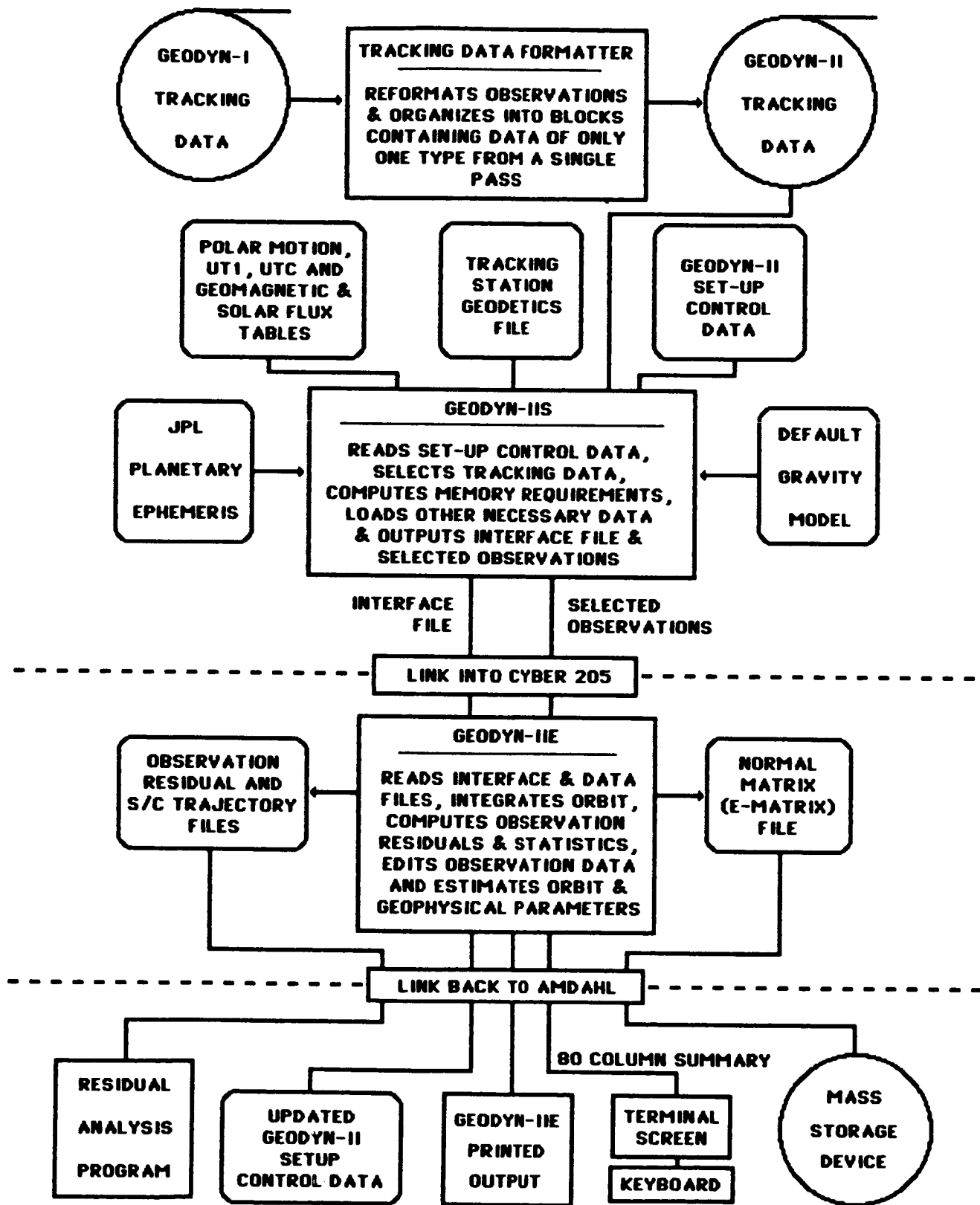
Figure 2.1   GEODYN-II Flow Diagram.

greatly facilitated and performed at a higher speed if the data are all of one FORTRAN variable type. For these reasons, all observation data and all output files from the Cyber 205 exclusively use 64-bit floating point words. The Tracking Data Formatter (TDF) program has been designed as the part of the GEODYN II system that converts all observation data into a common 64-bit floating point format.

The Cyber 205 is well-suited to the performance of operations that take advantage of vector pipeline commands. For this reason the basic input data processing, which is fundamentally serial, is performed on the Amdahl V7 computer by the GEODYN II-S program. This involves reading the various input files and selecting those subsets of data required to perform the numerical computations. The GEODYN II-S program also performs the bookkeeping functions of the system and transmits this information along with the data subsets to the computationally intensive component of the GEODYN II system.

The GEODYN II-E program is the computing engine of the GEODYN II system. This program has been designed in such a fashion that it may be used on both the "IBM type" computer or on the Cyber 205 vector processor. It is in this segment of the system where the CPU intensive operations are performed. GEODYN II-E has been optimized for the vector processing environment, and as a consequence, is most efficient when utilizing the Cyber 205 computer.

Observation processing has been vectorized within the GEODYN II system. This has been made possible by carrying this theme throughout all of the above programs:

> Beginning with the TDF, the observations are organized by measurement type and tracking station into data blocks. Each data block contains observations of only one data type from a single tracking pass. The observations within each block are chronologically

16

ordered and the blocks themselves are chronologically ordered with respect to block start times.

The GEODYN II-S program retains an observation block structure in the data that it selects and passes on to GEODYN II-E. However, at this stage the data blocks may be subdivided to facilitate later processing.

GEODYN II-E processes data blocks by treating each observation identically within the same block. This allows the application of vector operations to the data processing algorithms. It further permits the vector interpolation of orbit and force model dynamical partial derivatives obtained from the numerical integration of the variational equations and the vector chaining of partial derivatives.

The primary time consuming algorithms in the numerical integration of satellite orbits and force model parameters are associated with 1) spherical harmonic evaluation of the Earth's gravitation field, 2) evaluation of variational derivatives, 3) numerical integration of the equations of motion, 4) evaluation of force model partial derivatives, 5) numerical integration of force model variational equations, and 6) the evaluation of other force model perturbations. The relative importance of each of these items depends on the specific circumstances pertaining to each problem. In the typical orbit determination problem items 1-3 will be expected to dominate computation times. When a tide model including 300 pairs of coefficients is evaluated, item 6 will become a very significant factor. Or, if a full gravity field normal matrix is to be calculated, items 4-5 will have substantial impact.

Because all of the above factors enter into the numerical integration problem, a very high level of vectorization is required in these areas. To deal in an efficient manner with these various problems GEODYN II-E has been vectorized in the following fashion:

1) Spherical harmonic evaluation has been fully vectorized including the Legendre polynomial recursions.

2) Spherical harmonic variational derivatives have been fully vectorized.

3) Numerical integration of the equations of motion is fundamentally sequential in nature, however some vectorization has been performed in this area.

4) Force model partial derivatives for terrestrial gravity and Earth and ocean tides have been fully vectorized.

5) Numerical integration of force model partial derivatives has been fully vectorized.

6) Evaluation of Earth and ocean tidal perturbations has been fully vectorized.

For large problems, the greatest speed improvements may be achieved through vectorization of the formation of the normal equations. Computations in this area are linearly proportional to the number of observations and proportional to the square of the number of adjusted parameters. This segment of the code has been fully vectorized in GEODYN II-E.

Problem-oriented intelligent optimization has also been performed within GEODYN II.

For simple orbit determination problems, the number of force model parameters is generally substantially smaller than the number of observations within each data block. Under these circumstances the matrix of partial derivatives is dimensioned such that partial derivative interpolation, chaining and normal summation will be vectorized based on the number of observations in the block.

For solutions with a large number of adjusted parameters, the problem is sufficiently complex that the normal equations for each data arc must be put in a file for later combination with the normal equations of other data arcs. In this situation the matrix of partial derivatives is dimensioned such that the partial derivative interpolation, chaining and normal summation will be vectorized based upon the number of adjusted parameters. Improvements achieved in this area result primarily from linearization of the relationship between computation time and the number of adjusted parameters.

Another problem addressed by GEODYN II occurs when the normal equations become sufficiently large that the program and its arrays no longer fit into computer memory. If left to its own devices the computer's virtual memory paging system will interminably thrash about consuming exorbitant amounts of computer time. For this reason the GEODYN II system has been optimized to partition the matrix summation problem. GEODYN II-E temporarily stores the measurement partial derivatives on disk and forms the normal matrix in the minimum number of segments necessary to allow summation without paging.

2.1.2.2 GEODYN II Benefits

The benefits of this extensive effort to reconstruct GEODYN for the vector processing environment are several:

o   The switch to the normalized Legendre recursion formulation in GEODYN II permits the numerically stable computation of gravitational coefficient accelerations and partial derivatives to degrees in excess of 360.

o   The computation of the Right Ascension of Greenwich is performed more precisely, eliminating annual discontinuities on the order of 100 microns.

o   Precession and nutation are included in the integration of the adjusted force model parameters resulting in more accurate force model partial derivatives.

o   Two-way range is strictly modeled as such, removing errors on the order of one micron for satellites at altitudes of one Earth radius. Errors of much greater magnitude are eliminated for more distant satellites.

o   The JPL DE-200 ephemeris using the Wahr nutations and the year 2000 precession model has been implemented.

o   Spherical harmonic contributions to the variational equations are fully computed automatically whenever normal matrices are output.

o   Time dependent non-conservative forces are now modeled.

and last, but not least,

o   Typical orbit determination runs are 6.5 times faster on the
     Cyber using GEODYN II than on the IBM 3081 using the original
     GEODYN I.

o   Gravity model normal matrix generations are at least 90 times
     faster using GEODYN II on the Cyber than original GEODYN I on
     the IBM 360/95. This factor of 90 is based upon duplication
     within GEODYN II, of the original GEODYN I processing of non-
     altimeter, satellite only, dynamical normals for inclusion in
     the GEM-10B gravity model.

2.1.3 GEODYN II, SOLVE and the TOPEX Gravity Models

The TOPEX gravity modeling effort presented the first large scale
problem to be solved using the GEODYN II system and the Cyber optimized
SOLVE.

From the viewpoint of GEODYN II operations, three classes of
satellite data arcs were used in the TOPEX gravity modeling effort.
These classes were: optical data arcs, laser data arcs, and Doppler data
arcs.   The primary computational performance difference between the
optical and laser data arcs derives from the number of estimated
parameters included in the normal matrices generated. The Doppler data
arcs not only include the greatest number of parameters but also include
nearly an order of magnitude greater number of observations.

Figure 2-2 graphically illustrates the relationship between
GEODYN II running time on the Cyber, the number of adjusted parameters
and the number of observations in a data arc. The numbers shown are
typical for the analysis of both optical and laser data.   Similar
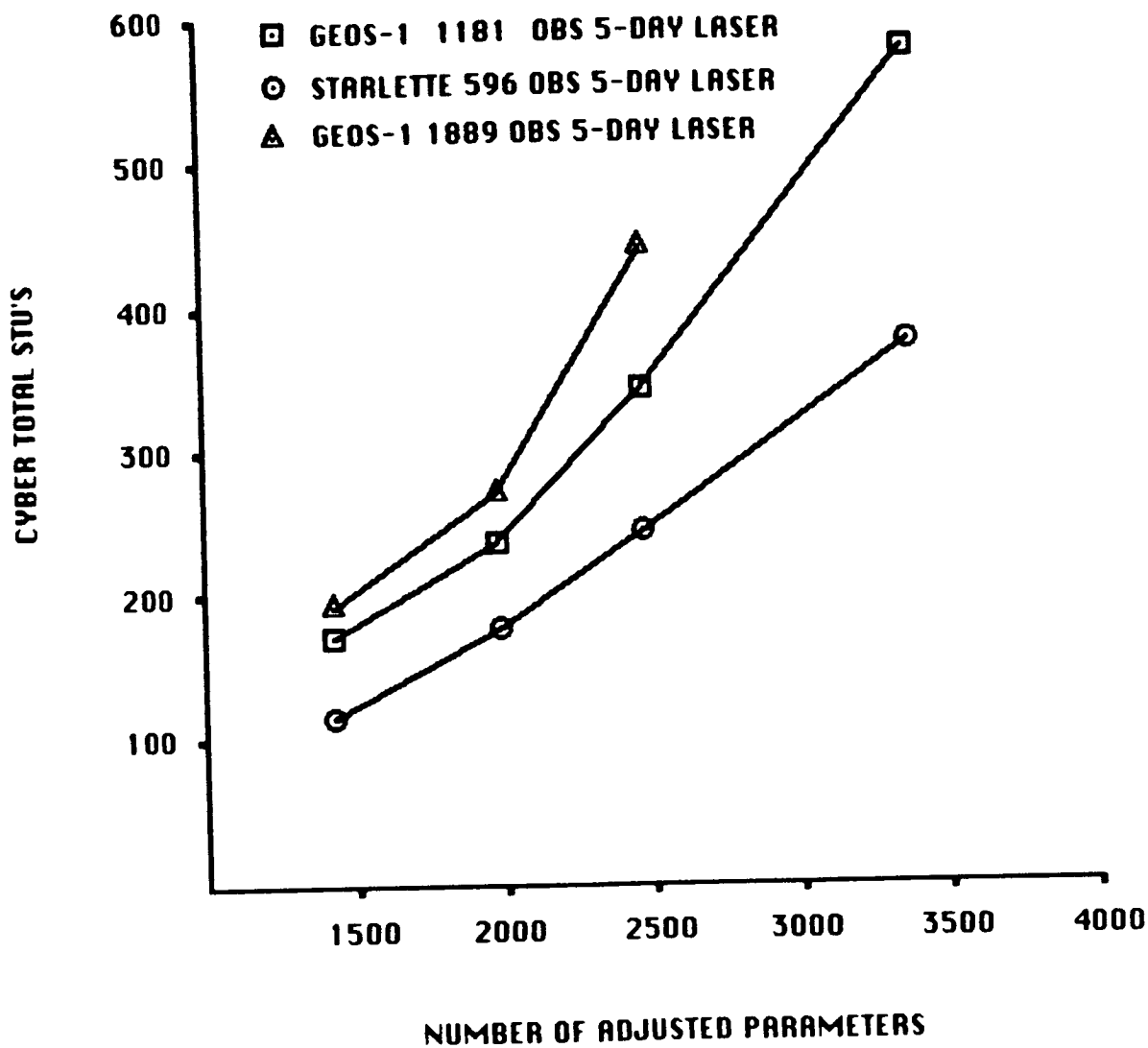
Figure 2.2 Computer Time Required for Generation of Normal Equations by
GEODYN-II.

relationships exist for Doppler processing, with an approximately ten-fold increase in running time associated with the ten-fold increase in weighted observations.

Of particular note in Figure 2-2 is the strong linearity of all profiles as the number of adjusted parameters is increased. This should be compared with the quadratic increase in running time associated with the generation of normal matrices on scalar computers such as the IBM 360/95 and the IBM 3081.

Using a conservative speed-increase factor of 90 for GEODYN II on the Cyber versus the original GEODYN I on the IBM 360/95 (which is comparable in speed to the IBM 3081), the following estimates merit consideration.

o   Cyber 205 computer time required to generate 580 normal matrices of 2000 parameters and 1380 observations should be 44 hours.

o   IBM 360/95 computer time required to generate 580 normal matrices of 2000 parameters and 1380 observations should be 3,960 hours.

Using a factor of 6.5 speed increase for GEODYN II on the Cyber versus the original GEODYN I on the IBM 3081, estimates of the resources to converge each of the data arcs used in the gravity model determination are as follows:

o   Cyber 205 computer time required to converge 580 satellite data arcs, using 12 iterations each, should be 178 hours.

o   IBM 3081 computer time required to converge 580 satellite data arcs, using 12 iterations each, should be 1156 hours.

Using that same factor of 6.5, the following are estimates of the resources required to converge 720 data arcs used to evaluate the test gravity model solutions.

o   Cyber 205 computer time required to converge 720 satellite data arcs, using 6 iterations each should be 110 hours.

o   IBM 3081 computer time required to converge 720 satellite data arcs, using 6 iterations each should be 718 hours.

Translated into other terms, the projected resource requirements for the convergence and formation of 580 normal matrices and the testing of gravity model solutions would require the exclusive utilization of an IBM 3081 computer by the project for the period of nine full months.

This same computational burden, when placed on the Cyber 205 computer using the GEODYN II system, constitutes less than five percent of the annual resource allocation of the computer.

In fact the total computer resource budget for this TOPEX gravity model effort was only 500 hours of Cyber 205 time spent over a period of approximately one year. This figure also includes the computer resources used by SOLVE to combine the 580 normal matrices, remove all arc parameters through back-substitution, and produce some 120 test gravity fields. Such a concentrated effort to produce these TOPEX gravity models would not have been logistically possible using the original GEODYN I and SOLVE even with a dedicated IBM 3081 computer.

2.2 OPERATIONS

With thousands of arcs to be processed by a dozen individuals at GSFC, the operation of the gravity field modelling effort was standardized as much as possible.

This was achieved in several ways. Each satellite was given a two character abbreviation and a three digit number so that required data sets and matrix numbers could be related to the satellite automatically. Generic setups were created to provide common control language and common model constants for ease of operation and quality control of input data streams. Naming conventions were defined for satellite observation data sets. The summary page output of the GEODYN program was modified to include more summary information. The normal equations were numbered to provide satellite and arc information as well as version number (see Figure 2-3). An on-line file was created to provide a reservoir of information for sharing and documenting the status of arcs completed and for combining arcs in the solution.

The actual task of arc processing and matrix generation was divided into subtasks by satellite and data type. After the processing for an arc had been completed, matrix numbers and mass storage cartridge and backup tape location was stored in an on-line data file.

The job submission was done on the Amdahl V-7, which is the front-end for the Cyber 205. It has an MVS operating system with the TSO interactive capability. TSO command files, or CLISTs, were created for the job submittal. Typically, the submittal of any of the job steps in the GEODYN or SOLVE program required the typing of only one line of controlling input containing the epoch date of the data arc, the satellite identifier, and the type of processing to be performed. The CLISTs, given this information, filled in the required data sets and

25

E MATRIX   USSSTDDDDDDER   13 DIGITS
                                                            (USUALLY 12)
                            EXAMPLE: 460176022701

                            VERSION 1 GEOS-3
                              LASER DATE 760227

LEVEL 1
C MATRIX   SSSTVAACCC   10 DIGITS
(CONTAINS ARC
 PARAMETER)   EXAMPLE: 2403110205

                            BE-B OPTICAL VERSION 1
                              10 ARCS CARTRIDGE 205

LEVEL 2
C MATRIX   TTSSSAAVV - ONE SATELLITE   9 DIGITS

                            EXAMPLE: 112601201

                            LASER BE-C 12 ARCS VERSION 1

(NO ARC PARAMETERS)   TTBBAAAVV - MULTIPLE SATELLITES 9 DIGITS

                            EXAMPLE: 110412001

                            LASER 4 SATELLITES 120 ARCS
                              VERSION 1

WHERE:

AA OR AAA = NO. OF ARCS   SSS = SATELLITE NUMBER
        BB = NO. OF SATELLITES   TT = DATA TYPE ENTERED TWICE
       CCC = CARTRIDGE NUMBER   VER OR VV OR V = VERSION NUMBER
    DDDDDD = DATE

Figure 2.3   Matrix Numbering Scheme.

submitted the runs. In addition, various types of output were collected for further processing, documentation or continuation of the arc processing. This process automation has proven invaluable throughout the TOPEX gravity modeling project.

Data management for the normal equations was a nontrivial problem. A 2400 parameter matrix requires 2.9 million 8-byte words. Consequently, only 6 matrices fit onto a 6250-bits-per-inch magnetic tape. The storage of 1000 matrices requires 166 tapes. Consequently 332 tapes were required to maintain the minimal two copies that prudence demanded. The matrices to be used were stored on the mass storage device attached to the Amdahl V-7 computer. Cartridges were used to store the individual normal equations, and the combined normal equations. Typically, six normal equations were output from the GEODYN program onto a mass storage cartridge. These six were combined to form a Level 1 C-Matrix. This combined matrix was stored on the mass storage device as well. The arc parameters (state, drag, solar radiation, biases etc.) were maintained through the Level 1 C-Matrix. When 6 C-Matrices were completed they were combined into a Level 2 C-Matrix. At this point the arc parameters were eliminated from the matrix. The aim was to produce a single matrix from each satellite with a single data type. This would allow weighting of matrices in the solutions by satellite and data type. Some satellite data sets could also be combined, since they would be handled alike. This was true of the optical and some of the laser satellites. The record keeping and numbering/naming conventions are vital in such a large data management problem. It was important that the matrix number indicate the satellite or number of satellites, combined matrix level, version number, and the number of arcs or date of arc. Figure 2-3 shows how the different levels of combined matrices were numbered to maintain control of the data problem. In addition, combining matrices requires a fair amount of computer time. Therefore, it was necessary that a normal matrix compression occur at each successive level so that a sufficiently small

number of matrices would be created to permit a good turnaround of experimental solutions.

These operational concepts have paid off in providing a high degree of quality control, offering flexibility to the analyst in preparing arcs for inclusion in the gravity computation, and allowing control of the overall model and in the use of constants. The GSFC TOPEX gravity modeling project has benefitted immensely from this effort.

SECTION 3.0

REFERENCE FRAME

3.1 INTRODUCTION

A uniform series for connecting the Conventional Inertial Reference System (CIRS) realized by the orbital dynamics, with the Conventional Terrestrial System (CTRS) realized by the global network of tracking stations was a requirement for our new gravity solution. This was one of the preliminary activities undertaken for the development of the TOPEX field. A desirable technical constraint on the origin of these series requires that it be as close as possible to the average pole of the mid-70's to mid-80's interval. This required a redefinition of the origin to coincide with the LAGEOS estimated 1979-84 six-year average pole. The major characteristics of the new series are its uniformity, its new origin, and its consistency with other conventional models used in the transformation CIRS <=> CTRS, namely the nutation model (Wahr's) and the precession model (Lieske's).

3.2 DESCRIPTION OF THE CONTRIBUTING DATA

The polar motion and UT1-UTC data available to us were as follows:

(1) the somewhat poorly documented but well maintained file of polar motion values contained in GEODYN I,

(2) two series based on BIH data (Feissel, private communication),

(3) the series resulting from the LAGEOS SL6 solution.

The source(s) for the first data set is not clear, especially for the earliest years. The BIH series were obtained from the BIH Circular D data set with additional corrections to reference them to the IAU 1980 nutation theory (Wahr,1979) and contained some weak Vondrak smoothing to remove periodicities shorter than 35 days. The third and last set of data, that obtained by GSFC from LAGEOS, was used as the basis for unifying the series. This set was adopted for it is more consistent with the rest of the mathematical model than any other. Details about the periods covered by each data set are given in Table 3.1. The BIH series are shown in Figure 3.1.

3.3 DISCREPANCIES BETWEEN DATA SETS

The discrepancies reconciled here were different for each of the data sets, even though for the most part, they all amount to a different origin of the local frame in which the pole coordinates are reported. As a first step we compared each of the above with the SL6 series. The origin of the BIH 1967-85 series could be easily and rigorously related to that of SL6 since the two series overlapped for a considerable time interval. The six year period (1979-84) was selected as the most appropriate for determining the transformation parameters between the two series for several reasons. First, this period is where the LAGEOS-determined polar motion is the strongest due to the robustness of the tracking data set. Second it covers most of the period over which very accurate tracking data are available for analysis under this project. A six year period was selected to properly average both the annual as well as the Chandlerian cycles of the polar motion.

Table 3.1

POLAR MOTION
AND EARTH ROTATION SERIES

● SELECTED DATA FOR POLAR MOTION

SOURCE	*PERIOD*
- OLD GEODYN FILE	58 09 18 - 61 12 31
- BIH CIRCULAR D (OLD SYSTEM)	62 01 05 - 66 12 30
- BIH CIRCULAR D (NEW SYSTEM)	67 01 04 - 78 12 27
- LAGEOS SOLUTION SL-6	79 01 01 - 84 12 30

● EARTH ROTATION SERIES

- OLD GEODYN FILE	58 09 18 - 61 12 31
- BIH CIRCULAR D	62 01 05 - 84 12 30

● MAJOR DISCREPANCY

THE REFERENCE FRAME DIFFERENCE BETWEEN THE
BIH CIRCULAR D SERIES AND THE LAGEOS SL-6 SERIES.
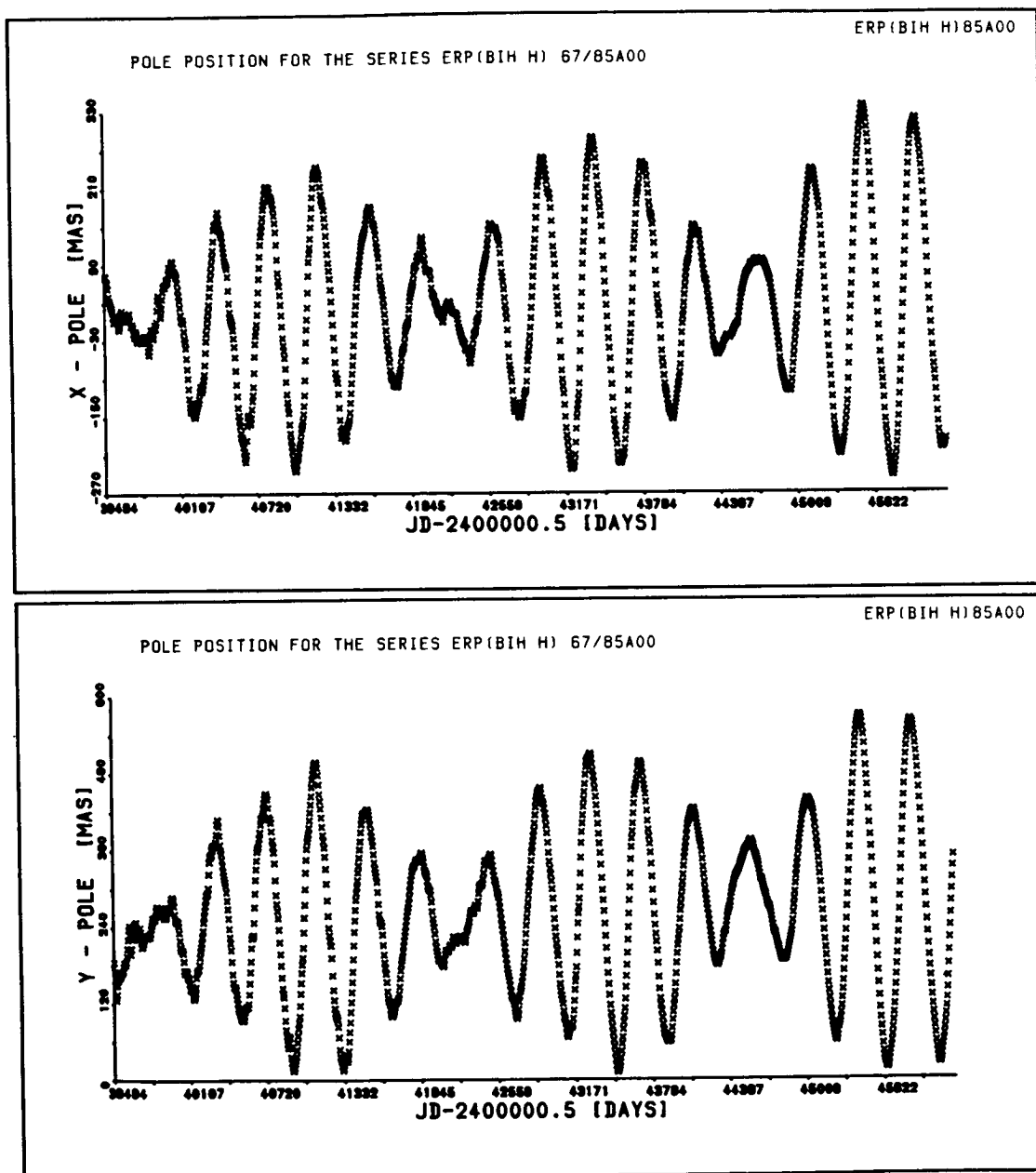
Figure 3.1   BIH Polar Motion.

3.4   MATHEMATICAL FORMULATION

The general theory on which we based our reference frame trans-
formations is detailed in the recommendations report made by COTES
(IAG/IAU Joint Working Group on the Establishment and Maintenance of a
Conventional Terrestrial Reference System) to the MERIT Steering
Committee (CSTG Bulletin, June 9, 1982). Since the LAGEOS-derived Earth
Rotation variations (UT1-UTC) do not provide a continuous uniform series
we limited our analysis to that of the polar motion series. We thereby
adopted the BIH-provided UT1-UTC series with no changes whatsoever. A
general picture of the geometry and notation utilized in this analysis
is shown in Figure 3.2. With the third rotation eliminated by virtue of
the fact that the two Earth Rotation series are identical, the mathe-
matical model relating the x_p, y_p discrepancies to the systematic
transformation parameters is as follows:

THE MERIT/COTES WORKING GROUP MODEL

$$\Delta y = \alpha_1 \cos \theta + \alpha_2 \sin \theta - \beta_1 \qquad\qquad (3.1)$$

$$\Delta x = -\alpha_1 \sin \theta + \alpha_2 \cos \theta - \beta_2$$

where:

α_1, α_2:   implied inertial frame misalignment

β_1, β_2:   implied terrestrial frame misalignment

θ :   Greenwich Mean Sidereal Angle
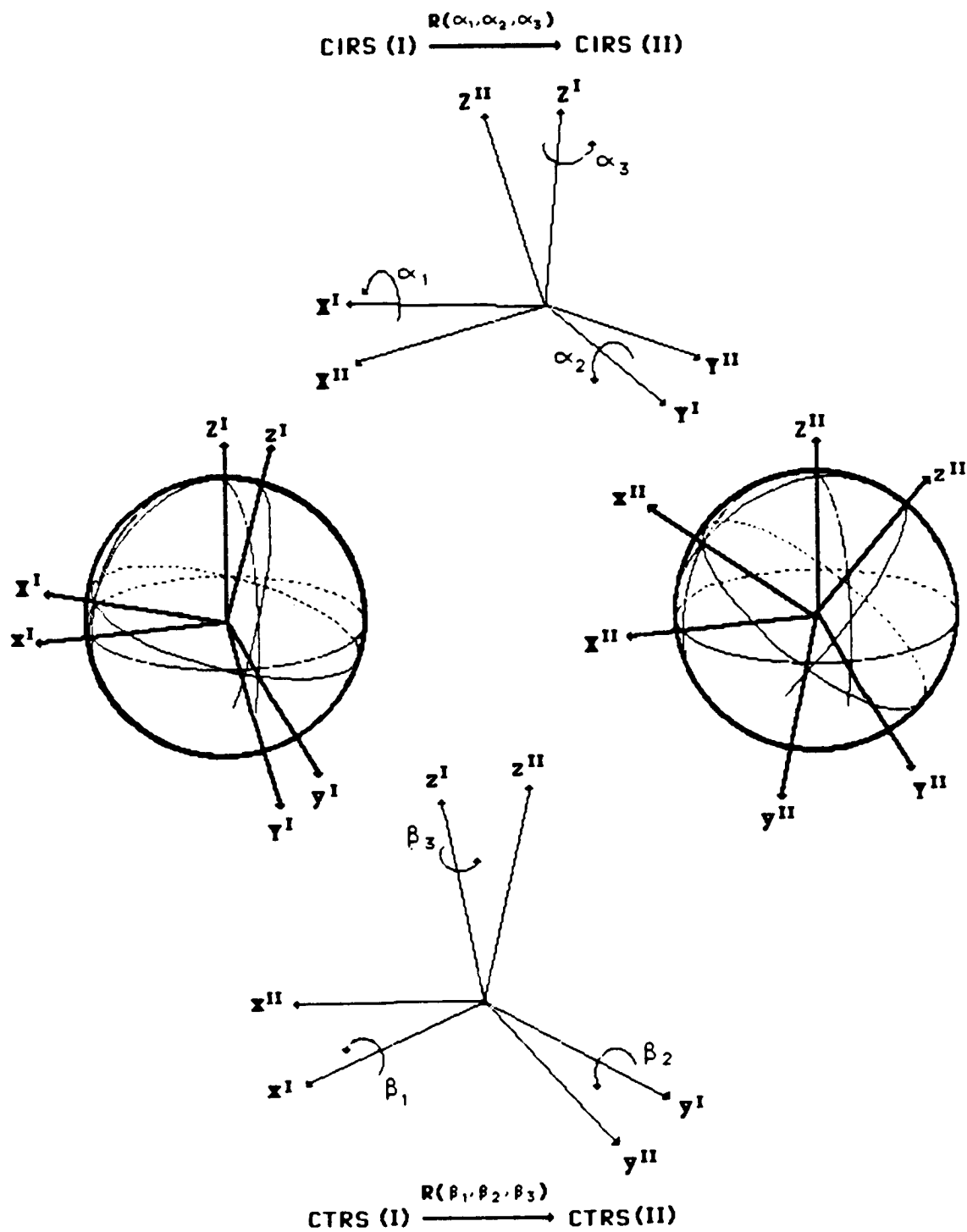
Figure 3.2   Geometry for Coordinate Transformations.

Application of this model to the selected 6-year BIH-SL6 polar motion discrepancies resulted in the determination of the misalignment angles listed in Table 3.2. These parameters were used to transform all of the BIH polar motion series from 1962 to the end of 1978 into the SL6 reference frame. The average values of the x_p, y_p listed in this table were used to define the new origin of the local plane coordinate system to which the coordinates of the pole refer. The reason for this is apparent after a discussion of the dynamic polar motion. Since this origin coincides with the Z-axis of our terrestrial system of reference, we have, in effect, redefined that axis as well. To be consistent therefore we must apply the appropriate rotations to the station coordinates to make them compatible with this new Z-axis. The geometry and the relationship of these coordinate systems at the pole are shown in Figure 3.3. The redefinition of this origin was realized for this new polar motion series through a simple subtraction of the above average values. In the case of the station coordinates we must apply these two rotations about the X-axis (y_p) and Y-axis (x_p). Since the angles are small, the cosines are basically equal to one and the sines can be approximated by the angles in radians. The transformation equations then are:

$$X_T = X_S - \bar{x}_p Z_S$$

$$Y_T = Y_S + \bar{y}_p Z_S \qquad\qquad (3.2)$$

$$Z_T = Z_S + \bar{x}_p X_S - \bar{y}_p Y_S$$

where the subscript S stands for the SL6 coordinates and the T for the new frame for TOPEX.

TABLE 3 2

BIH (1979–84) TO LAGEOS (SL–6) POLAR MOTION SERIES TRANSFORMATION PARAMETERS

$$\beta_1 = 1.46 \pm 0.3 \text{ mas}$$

$$\beta_2 = -3.80 \pm 0.3 \text{ mas}$$

$$\alpha_1 = -0.22 \pm 0.3 \text{ mas}$$

$$\alpha_2 = 0.62 \pm 0.3 \text{ mas}$$

$$\text{RMS } (\Delta x) : 6.5 \text{ mas}$$

$$\text{RMS } (\Delta y) : 6.2 \text{ mas}$$

SIX YEAR AVERAGE

$$x = 38.2 \pm 0.9$$

$$y = 280.3 \pm 2.2$$
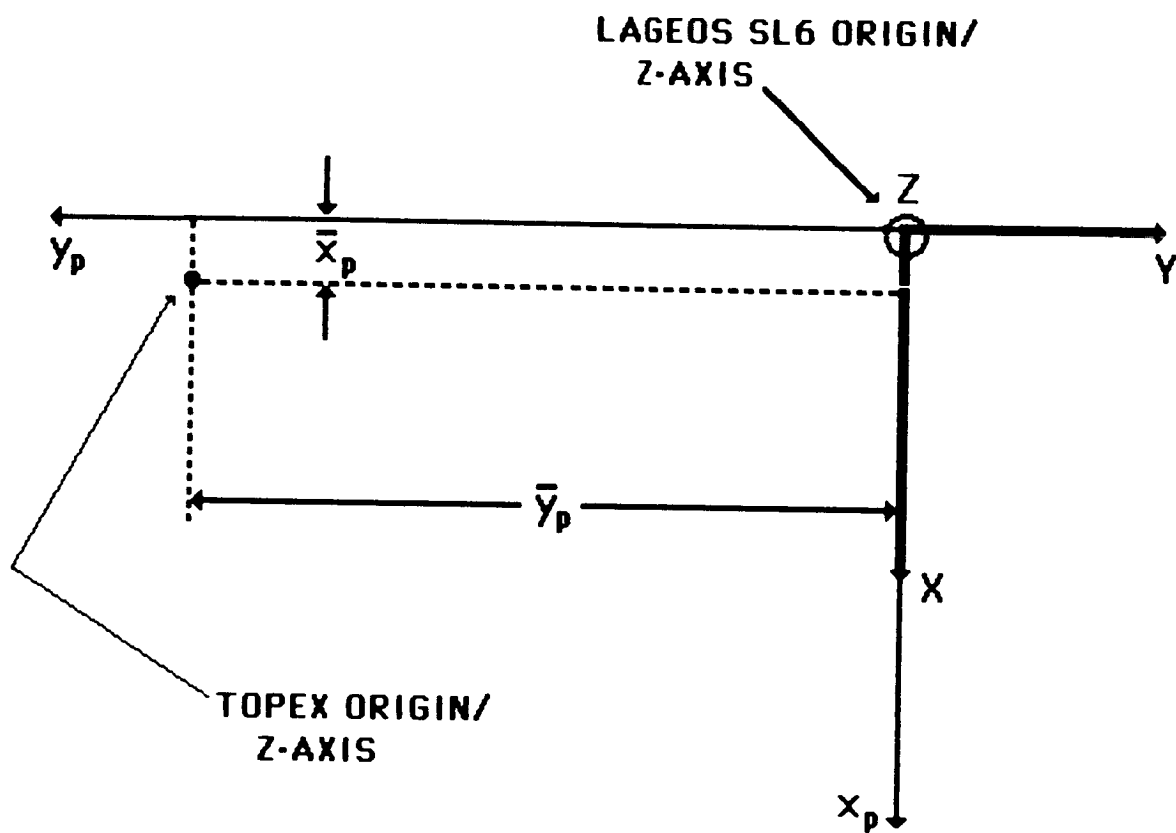
Figure 3.3   Relationship of Coordinate System Origins.

3.5   DYNAMIC POLAR MOTION

The non-rigidity of our planet is clearly manifested in the temporal variability of the Earth's moments of inertia in response to both rotational and tidal deformations. The Earth's axis of figure, which is the principal axis of angular momentum, exhibits two periodic motions. There is daily motion with an amplitude that can reach 60 meters due to the Earth's response to the tidal deformation. The tides are modeled elsewhere and therefore this motion is accounted for. The much smaller motion, with a period similar to that of the Chandlerian wobble, is the Earth's response to the rotational deformation. The geometry of the motions involved is depicted in Figure 3.4.

Most of the theories developed so far [Gaposchkin,1972], [Lambeck,1971 and 1972], [McClure, 1973] concluded that this motion is proportional to the main wobble. The proportionality factor when the geopotential is referenced on the CTRS is about 1/3 and depends on the Earth's elastic properties. Because our capability to determine $C(2,1)$ and $S(2,1)$ is of higher accuracy than our knowledge of the Earth's elasticity parameters, it is only prudent to parameterize this factor. It is well known [Heiskanen and Moritz, 1967] that the orientation of the axis of figure with respect to some arbitrary frame of reference is reflected in the values of the second degree, order one, harmonics of the spherical harmonic expansion of the gravitational field of the body $(C,S(2,1))$. Based on the equations given in [ibid.] relating the moments of inertia to the $C(2,1)$ and $S(2,1)$ harmonics (through $C(2,0)$), we can derive a general formulation which accounts for the temporal variations of the figure axis through the application of proportional variations of the $C,S(2,1)$ harmonics. Denoting this proportionality factor by k (to be determined), the resulting model is:

38

Figure 3.4   Dynamic Polar Motion Model.

$$C_{2,1}(t) = \hat{C}_{2,1}(t_o) + \dot{C}_{2,1}(t-t_o) + kx_p(t) \hat{C}_{2,0}$$

$$\text{(3.3)}$$

$$S_{2,1}(t) = \hat{S}_{2,1}(t_o) + \dot{S}_{2,1}(t-t_o) - ky_p(t) \hat{C}_{2,0}$$

where the harmonics with the carets refer to the value of these harmonics relative to the CTRS at the initial epoch, t_o. It should be clear that the periodic part, which is represented by the last term, will average out in each Chandler cycle; any mean offsets in the polar motion series cause there to be a need for nonzero first terms. The center of the polar motion migrates slowly, and after some time, accummulates as an offset. To the extent that this offset becomes much larger than that of the periodic part, the second term is included to compensate for this future secular motion. If we were to reference our gravitational expansion to a CTRS whose third axis coincides with the average wobble center at t_o, then the first terms are identically equal to zero. Over a short period of time (several years) the second term is negligible; and as argued above, the third term will average out if we analyze data over full Chandler cycles.

Our current software does not completely model this effect. Plans to implement it have been developed. Therefore with the current SL6 coordinate system very close to that of BIH, the average pole for the recent years (which contain the most accurate and more important tracking data) would be about 10 meters off at an azimuth of about 270 degrees. The first term in the above model therefore would be nonzero and very significant. By redefining the origin and the Z-axis of our CTRS we have avoided these implications and at the same time, we can still use the available software. Additionally, when the full model is implemented we lose nothing since we can always apply it with the initial harmonics at t_o equal to zero.

3.6 SUMMARY

The methodology used for creating a uniform series for the coordinates of the pole over the period Sep. 18, 1958 through Dec. 30, 1984 based on series provided primarily by the BIH and the LAGEOS SL6 system has been presented. The resulting series realizes a modified SL6 CTRS, modified in the sense that its Z-axis and thus the origin of the local plane system to which the pole coordinates x_p, y_p refer, coincide with the axis through the center of the 1979-84 six-year wobble. This deviation from the SL6 CTRS makes it possible to set $C(2,1)$ and $S(2,1)$ identically equal to zero with no further modeling for the dynamic polar motion and still claim a model accuracy which is only slightly inferior to the ideal model described herein.

SECTION 4.0
A PRIORI CONSTANTS ADOPTED IN THE GENERATION
OF THE TOPEX GRAVITY MODEL

The constants that were adopted and used in the development of the a priori TOPEX gravity model delineate the physical parameters within which the solution exists. These constants were chosen after considerable thought and debate. This brief chapter describes the adopted parameters and updates a similar monograph found in Marsh and Tapley (1985). The constants and procedures are listed by parameter type in the following section on common parameters. By common parameters it is meant parameters which are not satellite dependent (e.g. parameters regarding the Earth).

4.1 COMMON PARAMETERS

4.1.1 Earth Tides

A total of eight tidal harmonics were used from Wahr's frequency dependent model (Wahr, 1979), providing the a priori standard. All other solid earth tides were modeled through a closed formula for their combined 2nd degree tidal potential using $k_2 = 0.30$ and a zero phase lag. Partials were included for each of the specific frequency-dependent solid earth tidal terms, as well k_2, ε_2 and k_3, to add some flexibility in our tidal analysis (see Section 7.1 for a complete description of the earth tide modeling).

4.1.2 Ocean Tides

The a priori ocean tide model was developed by Christodoulidis, et al. (1986b) in which 600 individual terms representing 32 major and

minor tides were calculated from point admittances. For diurnal and semi-diurnal constituents, the tidal expansion was carried out in spherical harmonics to degree 6 for both the prograde and retrograde parts of that expansion. For long period tides only prograde terms were used. The a priori terms were predicted from admittances over each band using the values and errors found in the Schwiderski (NSWC) oceanographic models. Details on the algorithm can be found elsewhere (Section 7.1) in this document. Partials were computed for the 6 prograde terms giving long period orbital perturbations for each of 12 tidal frequencies.

4.1.3 Tidal Deformations

The Love and Shida numbers h_2 and ℓ_2 had, as a priori values, the values adopted for the MERIT Campaign standards, (Melbourne et al., 1983); $h_2 = .609$, $\ell_2 = .0852$. Partials were included for h_2 and ℓ_2.

4.1.4 Earth Parameters

The a priori value adopted for the product of the gravitational constant and the Earth's mass, GM, was 398600.436 km^3/s^2. The speed of light adopted was set at 299792.458 km/s. The semi-major axis of the Earth was set at 6378137m. The Earth's flattening chosen as 1/298.257. These values are consistent with the adopted laser tracking station coordinates used as a priori values for the orbital recoveries.

4.1.5 Polar Motion and A1-UT1

In conjunction with a more consistent definition of the geometric and gravimetric reference frames, a zero-mean set of polar motions has been adopted. Partials have been calculated for average five-day polar

motion and earth rotation values. Details regarding the a priori values used for this zero-mean set of polar coordinates can be found elsewhere in this document.

4.1.6 Station Coordinates

A priori station coordinate files were constructed based upon the global laser station coordinate solution SL-6. The MERIT adopted reference longitude for the laser station at McDonald, TX, was implemented and the coordinates were rotated to comply with the zero mean pole definition mentioned before. Station parameter partials were computed for further analysis and quality checks. Further details on this subject are presented in Section 6.

4.1.7 Third Body Effects

Gravitational potential perturbations have been modeled for all of the planets except Pluto.

4.1.8 Z-Axis Definition

The Z-reference for the gravity field is provided by the instantaneous spin axis of the Wahr model.

4.1.9 Coordinate System

The J2000 reference epoch and associated precession constants as adopted by the IAU have been utilized throughout. The nutation model used is that of Wahr.

4.1.10 Relativity

Relativistic effects were not applied.

4.1.11 A Priori Gravity Modeling

An a priori gravity model is neccessary in order to converge the orbits and to construct the matrices required for a linear differential correction to form a new gravity solution. Four gravity models were used in this regard. The LAGEOS data were prepared by using the GEM-L2' model of Lerch et al (1982). The prime denotes that the model (in spherical harmonic form) was obtained through a new solution which contained all of the original GEM-L2 data but now constrained the $C(2,1)$ and $S(2,1)$ coefficients to zero. Justification for this constraint is discussed in detail in Section 3. The STARLETTE data were prepared by using the PGS-1331' model; a model that has been tailored for STARLETTE analysis (Marsh et al, 1985). The SEASAT data were prepared by using the PGS-S4' model; a model that has also been tailored for SEASAT analysis (Lerch et al, 1982). All other satellites contributing in the solution were prepared by using the GEM-10B' model (Lerch et al, 1981) which is GSFC's preferred general gravity model. Note that all the models mentioned here have been resolved constraining the $C(2,1)$ and $S(2,1)$ coefficients to have zero values (as denoted by the primes). The adoption of several gravity models means that differing a priori parameters were used with different data sets. This approach was adopted after conducting the following study.

4.1.11.1   Selection of an A Priori Gravity Model: General Vs. Several Tailored Fields

The question of which gravitational field should be chosen as the _a priori_ model was investigated.   The central concern was whether adopting one model or several specialized models, or even some new "ad hoc" ones, would be better for the linearization of the observation equations.   This question was of concern because of the known properties of general and "tailored" fields.   Tailored models fit the data from one specific satellite orbit very well.   However, the individual coefficients in these models can be at times, geophysically unrealistic.   The general models, on the other hand, have the best set of coefficients overall, but they may poorly model a specific "lumped harmonic" on an important satellite.   The result is larger data residuals and a less accurate orbit.

One approach implies the linearization of _all_ equations with _one_ single set of starting values prior to a series of iterative linear adjustments, which is correct for the Gauss-Newton method implemented in our orbit and field estimation programs. However, a modification of this approach could provide quicker convergence in the particular problem at hand.   This second approach was to use "tailor-made" fields, adjusted to each of the main data sets (of which fields several are already available from previous projects) in order to ensure that the computed orbits, along which the linearized equations and residuals are calculated, are as close to the true orbits as possible. This latter approach seeks to minimize the non-linearities associated with mis-modeling the orbit's evolution.   This implies using different fields as _a priori_. All of these various "starting points" are made approximately compatible with the single field chosen for actual improvement, by way of linear transformations (or "shifts") in the right-hand sides of the normal equations.   A question which required answering was whether non-linear aspects of the problem could adversely affect these transformations. Nevertheless, it is important to note that in preparation for the normal

equation generation, the use of "tailored fields" improved upon our ability to eliminate spurious data due to tighter editing than is possible when using a single, more general model.

The main purpose here was to select a procedure that was likely to converge to the correct solution (within the accuracy allowed by the data). In order to clarify which of the two methods, the "unique starting field" or the "multiple, tailored fields," was likely to satisfy our needs best, a number of small-scale simulations of the problem were carried out. The idea was to reproduce the main characteristics of the adjustment for either approach in a reasonably inexpensive way. A more complete description of the results of the simulations is given in the next section. These simulations had the respective properties of tailored and global models. In the a priori tailored fields, some potential coefficients adjusted to provide accurate orbits were clearly geophysically unrealistic. On the other hand, the general a priori model did not fit the simulated data for a particular arc nearly as well as the corresponding tailored model.

If the problem was sufficiently close to being perfectly linear, either method should give virtually the same results, in which case the choice becomes trivial from a theoretical point of view. (There are practical operational differences even in this case.) This would happen if the non-linear problem had such a well-behaved geometry in a neighborhood of the actual solution, that in it, the hypersurface defined by each normal equation could be regarded as flat in this neighborhood, and all the different "starting fields" fell within this region. As shown in the following section, this seems to have been the situation in the cases simulated.

48

4.1.11.2 Simulations for Geopotential Solution Using Tailor-Made vs General A Priori Models

A. Simulations Design

A set of 21 spherical harmonic coefficients were recovered using simulated laser data on 3 satellites with 13th order resonance. Data from a simulated global set of laser stations were employed for the normal equations using one 9-day arc on each satellite. The geopotential model used to simulate the observations consisted of the 21 coefficients to be recovered plus a base model complete through degree and order 4 with values obtained from GEM-9. The general a priori model contained 21 perturbed GEM-9 coefficients. When it was used in the orbital recovery, only the state parameters were solved for on each arc. The tailor-made model had the same perturbed coefficients but each arc permitted certain geopotential coefficients to adjust (i.e., tailor the field) for each satellite individually. These coefficients were then "shifted" to the common values of the general a priori model before solving the normals. The state parameters consisted of six orbital elements plus two drag parameters $(C_D, \dot{C}_D)$ for each of the three satellite arcs. Two cases involving different data quality were considered. One case had 5 cm Gaussian random noise applied to the range observations and the other case had perfect data, that is, with no noise applied.

B. Coefficient Terms Recovered

The 21 coefficient terms of the spherical harmonics that were recovered in the solution consisted of:

Zonals	Tesserals	Resonant Tesserals
C(3,0)	CS(2,2)	CS(15,13)
C(4,0)	CS(10,4)	CS(17,13)
C(7,0)	CS(19,17)	CS(19,13)
C(16,0)	CS(25,23)	CS(27,13)
C(17,0)		

Lumped Coefficients Solved by Satellite for Tailored Model

To "tailor" each individual satellite's model, lumped coefficient terms were solved for on individual arcs. These were:

C(16,0), C(17,0), CS(27,13)

Starting Values of Coefficients (A Priori)

Except for the base 4x4 terms, the a priori model (starting values) was GEM-9 $\pm 3\sigma$ where the σ values represent the published errors in the GEM-9 field. Since C,S(25,23) was not recovered in GEM-9 the σ value was computed from Kaula's rule ($10^{-5}/\ell^2$ for ℓ=25). The coefficients C(16,0), C(17,0), and CS(27,13) were solved for on the individual satellite arcs to obtain a priori values for the tailored models, and the true values of these terms from GEM-9 were used as the a priori for the general model. Notice, for example, in Table D the very large adjustment made on C(23,13) to tailor a local gravity model to fit the data on 5BN-2. The same is true for the C,S(23,13) adjustments for ANNA. But note that, although these coefficient adjustments were large when "tailoring" the satellite-specific fields, these tailored models fit the simulated data many times better than the constant a priori field. In the constant a priori field, no coefficient errors were greater than 3σ. The "tailored" model for 5BN.2 had a coefficient error for C(23,13) of nearly 50σ. (See Section D for comparisons.)

C. Satellite Orbital Characteristics

Satellite	a	e	I	Mean Motion (rev/day)	Primary Resonant Period (days)	Drag (C_D=2) m/day^2
DI-D	7622 km	.0848	39.5°	13.05	8.4	70
ANNA	7501	.0082	50.1°	13.37	4.8	4
5BN-2	7462	.0058	89.9°	13.46	2.4	10

D.   A Priori Satellite Arc Residuals and Lumped Coefficients

		A Priori Residuals	
Satellite	No. of Observations (±5 cm noise)	Tailor Model rms	General Model rms
DI-D	6937	110 cm	383 cm
ANNA	6124	133	730
5BN-2	3637	192	725

Adjusted Tailored Model Lumped Coefficients	Coefficient Units 10^{-9}			Correct Answer:
	DI-D	ANNA	5BN-2	GEM-9
C(16,0)	- 5.4	- 7.8	- 18.5	- 8.5
C(17,0)	19.2	14.5	- 7.8	16.2
C(23,13)	-12.8	28.7	-202.2	- 7.7
S(23,13)	-18.9	75.9	- 78.4	-10.7

E.   Recovery of Geopotential

The normal equations were solved using both the tailor-made a priori model and the general a priori model.   Errors in the solutions of the 21 geopotential coefficients were plotted for comparison of the two methods. An ideal TOPEX accuracy goal of 1/4 the errors in the GEM-9 model (i.e., 25% of GEM-9's uncertainties) was also plotted to show the significance of the differences between the solutions of each method. Both cases of simulation, with noise on the data (Figure 4.2) and without noise (Figure 4.3) were plotted.   The following additional information has been plotted in Figure 4.1: (a) the general a priori starting values (GEM-9±3σ), (b) the standard deviations (error estimate) of the recovered coefficients for the case where noise was applied to the data, and (c) the Topex accuracy goal of 1/4 GEM-9 error σ's for comparison.   A log scale was used since over 6 orders of magnitude are seen in the plots.
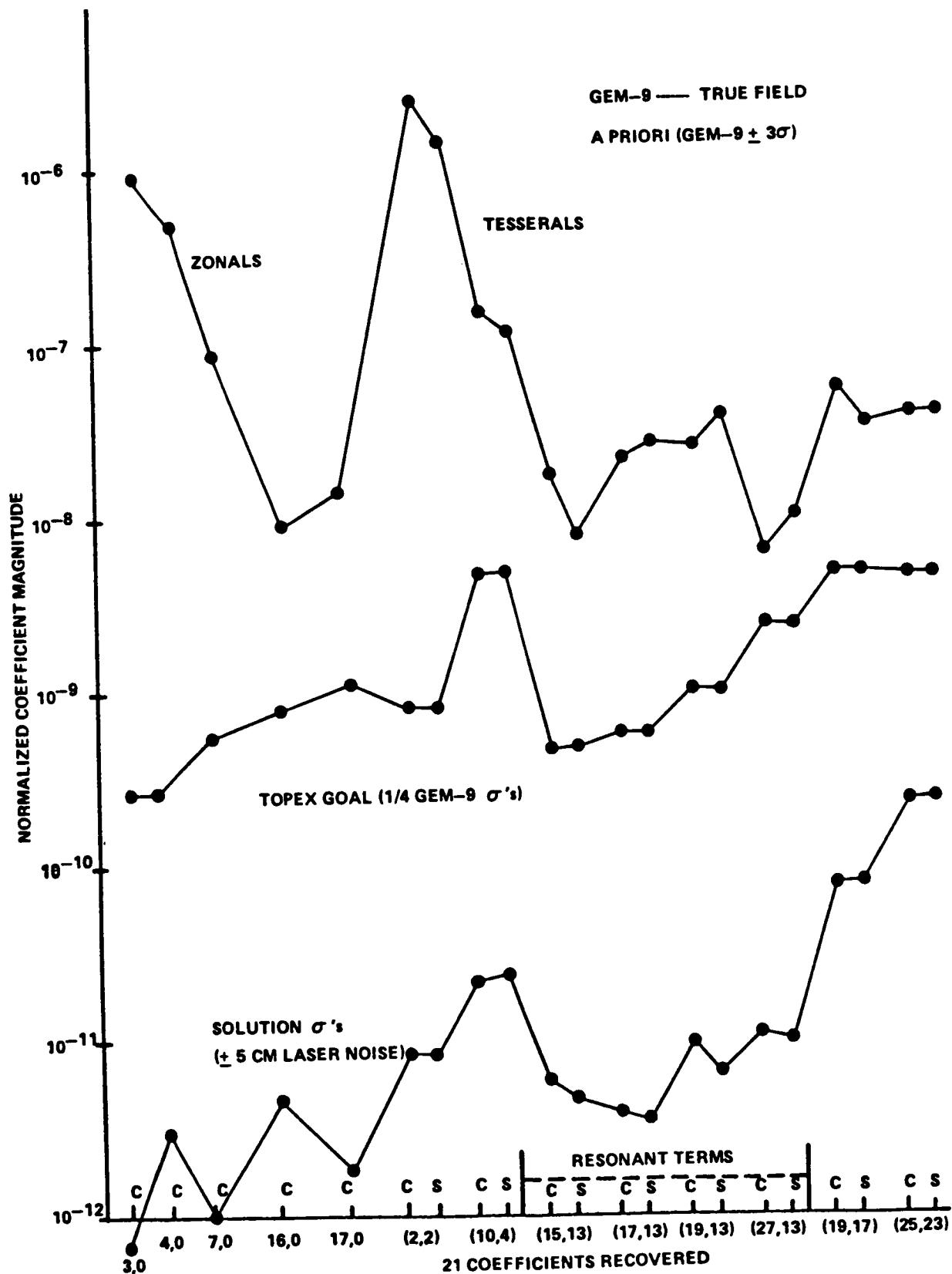
Figure 4.1 Geopotential Simulation Information.

F.   Summary and Conclusions

In Figure 4.2 (with noise applied to the data) the errors are approximately the same for the two methods except for the C(7,0) value. Moreover, these differences are small and based upon the TOPEX goal, there is not a significant difference between the two methods. The main feature of these errors (Figure 4.3) is that the general model (with smaller errors for most of the zonal terms but with larger errors for most of the other terms) has a larger spread in the errors than the tailored model which gives a much more consistent error. These errors are much less significant when compared to the TOPEX goal than the previous set of errors of Figure 4.2 where noise was applied to the data.

The solutions were compared through post-solution fits to the simulated range observations on DI-D using the "true" data (no noise). The rms of the residuals gave the following results:

Model	RMS
General	.116 cm
"Tailored"	.025 cm

The conclusion of this simulation is that the tailored model gives slightly better results (especially in the perfect data case) but the improvement seen is sufficiently small that, considering the goals of TOPEX, or the present state-of-the-art, either method may be used.
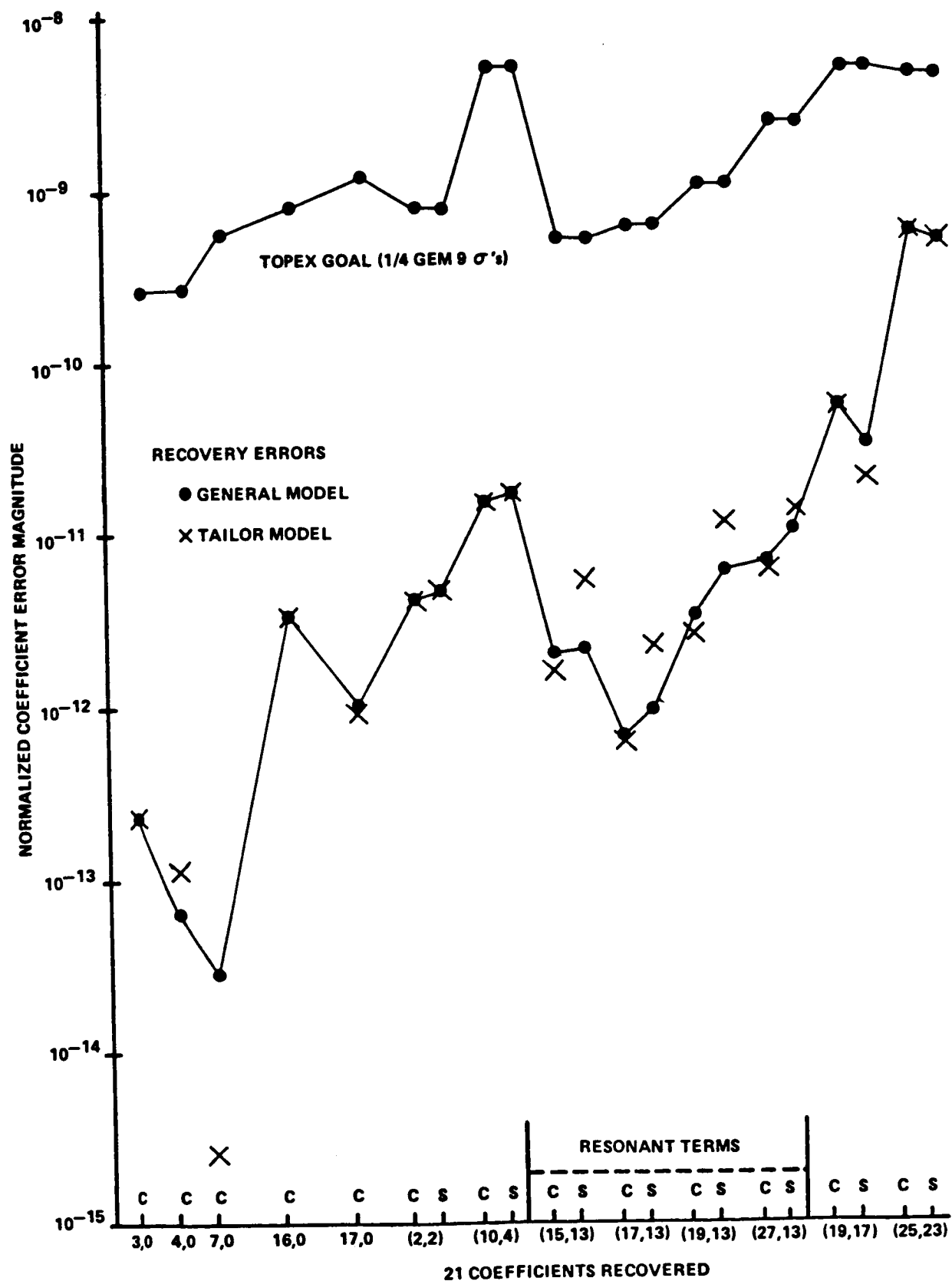
Figure 4.2   Gravity Recovery from Noise.
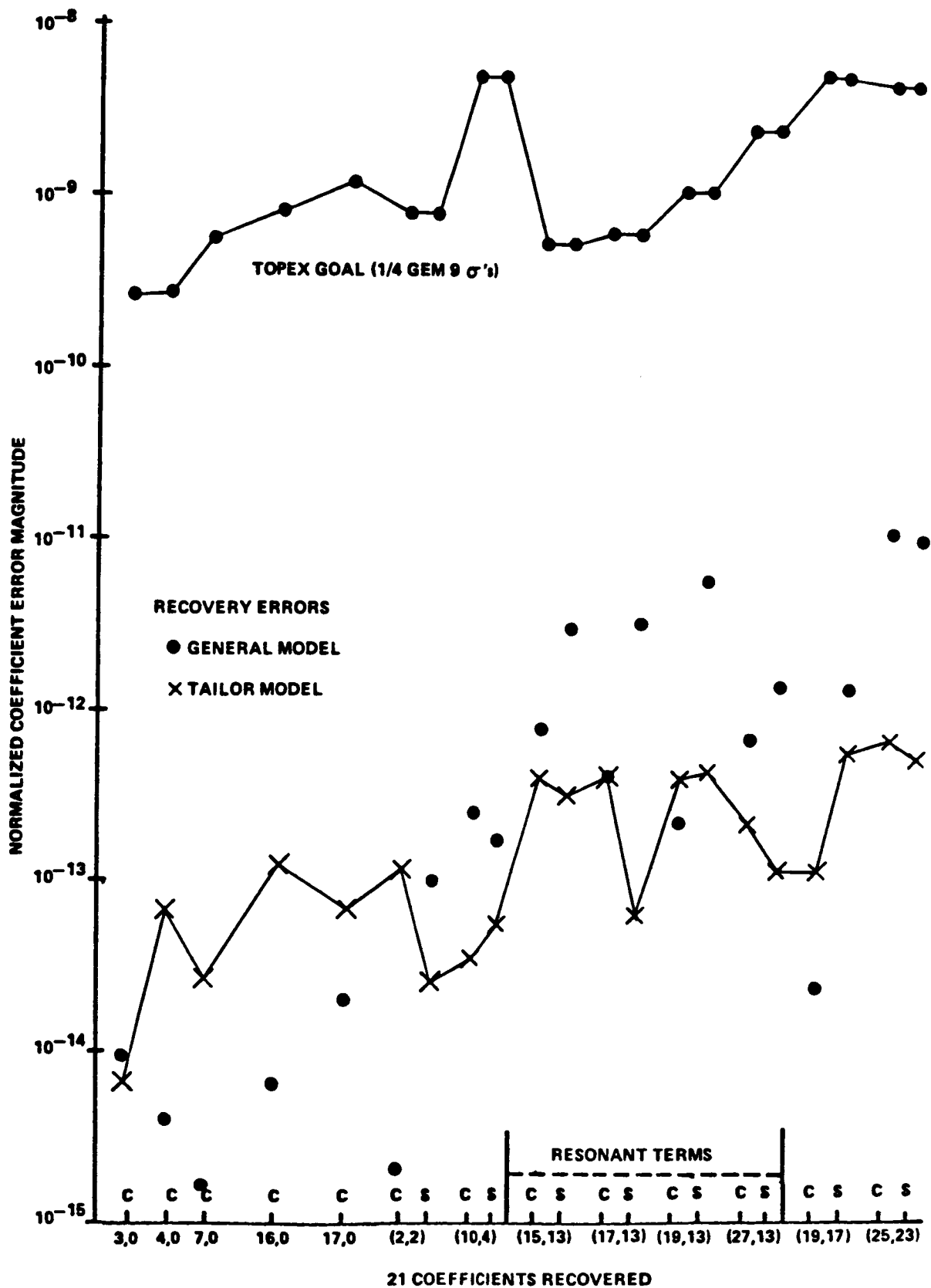
Figure 4.3   Gravity Recovery without Noise.

G.   Interpretation of Results and Future Investigation

Even though the simulation shows that the difference in the results between the two approaches is not clearly significant, it is interesting to interpret the difference.   First, it is clear that non-linear effects in the system cause the different geopotential results.   An explanation for the improved results of the tailored approach is that some non-linear effects in the residuals are removed with the lumped (tailored) coefficients in the iteration used to converge the orbit.   These effects remain filtered-out when a linear shift is made to adjust the tailored coefficients to the common values of the general model.

The approach using the general model as well as that using the tailored model may both benefit from the adjustment of additional orbit parameters.   This is evident in the present results, where the drag parameters apparently are removing non-linear effects from the residuals. in the process of converging the orbits.   Both cases, tailored vs. general a priori models, have obtained better geopotential results with the application of drag parameters as compared to results where drag was not applied.

The present simulation is quite simplified since most of the gravity field was considered perfectly known in the recovery of the 21 coefficients and of those adjusting, 40% were 13th order resonant terms.   Yet, this work is important since in practice both methods have been employed in the recovery of past geopotential models.   We however felt safe in concluding that there were no inherent ill-effects in using "tailored" models to reduce the data and shift the resulting normals to a common base in the final solution.   Since this approach had the benefit of improving our data editing and orbit convergence activities, it was adopted in the development of GEM-T1.

On the other hand, it was not necessary to compute tailored models for each satellite. We were able to adopt an approach of using available tailored fields for certain satellite analyses, and a general model elsewhere.

One should exercise caution before accepting our conclusions as completely general. We have not attempted to assess the impact of using a truly poor model as a priori. Furthermore, the effects of non-linearity becomes more severe in the solution as the matrix conditioning degrades. Hence this simulation would have been more conclusive if a more complete set of coefficients were employed in the solution instead of the simplified subset actually used. However, the present results provided a basis for additional insight into the choice of an a priori model, and revealed little significant problem with the approach we ultimately adopted.

SECTION 5.0
TRACKING DATA

The earliest satellite tracking systems were quite crude by today's standards. Camera images and Minitrack interferometric tracking yield satellite single-point positioning of from 10 to 100 meters. Although the observations themselves were somewhat imprecise, a large group of satellites having diverse orbital characteristics were tracked by these systems. Therefore, these observations (especially those obtained on twenty or so different orbits by a globally deployed network of Baker-Nunn and MOTS cameras) have formed the basis for earlier gravity modeling activities at GSFC and elsewhere.

In the early and mid-1970's electronic tracking of considerably higher precision than that obtained by cameras became the routine method for locating operational satellites. The main operational tracking network for NASA became the Unified S-Band Electronic Network. These electronic tracking systems acquired data in all weather conditions but provided data of significantly lesser precision than that produced by the early laser technologies of this era.

Laser systems are currently the most accurate and advanced means of precision satellite tracking. These ranging systems have substantially evolved and have undergone nearly a ten-fold improvement in system precision every three years of the last decade. The evolution of laser systems typify the progress which has been made in monitoring the motion of near-earth satellites and has resulted in much more stringent demands for geopotential models capable of utilizing data which now are accurate to a few centimeters. The only limitation found with the lasers is their dependence on weather and the somewhat restricted number of satellites which carried corner cubes enabling them to be tracked by ground laser systems. Historically, there are ten satellites which have been tracked by NASA's laser systems.

The parallel capability of S-Band and laser tracking provided flexibility within NASA's operational environment. The laser network provided NASA with the means of obtaining high quality data on geodetic missions which required precision rather than mere operational orbital accuracies. Satellite missions with less stringent orbit determination requirements were supported by the S-Band Network.

The routine tracking obtained by the S-Band Network has been utilized in past GSFC gravity solutions. The S-band stations operationally tracked using a single frequency. Ionospheric refraction effects are significant in S-band average range-rate observations. These data have not been used within GEM-T1 pending the implementation of either a reliable general ionospheric refraction model or some method for deleting data significantly corrupted by this effect.

5.1   DATA SELECTION

There are perhaps sixty satellites which received sufficient tracking to warrant their consideration for inclusion in the GSFC gravity modeling activities. The TOPEX orbit determination requirements are such that a four-fold improvement over existing field accuracies is necessary. Such an improvement can only be accomplished with greatly improved data handling and data validation directed at existing data sets, particularly the older ones. Therefore some manageable framework for selecting, qualifying and processing those data which were deemed most important was developed as a preliminary step in the creation of GEM-T1.

One of the first tasks was a selection of the most important data sets upon which a "satellite-only" field could be computed. The sixty objects which had geodetic quality data sets and orbits which were reasonably free of large perturbations due to air drag were evaluated

according to certain criteria: (a) the quality, quantity and global distribution of their tracking data sets, (b) the uniqueness of orbital perturbations on the satellite (d) the similiarity of the orbit to that anticipated for TOPEX (e) the distribution of the data set over the satellite's apsidal period and (f) the sensitivity of the satellite's orbit to present weaknesses in existing gravity models.

The satellites which were considered are described in Table 5.1 which also shows their orbital characteristics. The satellite physical dimensions, shape and weight are also given in Table 5.1. Based upon an evaluation scheme detailed in (Marsh and Born, 1985) the ranking of the satellite data sets can be found in Table 5.2. GEM-T1 has been computed from seventeen of the top thirty ranked data sets. Almost all objects rated in the top ten have been utilized. To achieve a better sampling of inclinations, six satellites of low inclination were selected (see Section 5.2.8). Future models containing additional orbits, altimetry, surface gravity and satellite-tracking-satellite data are being planned.

In all, 17 satellites were included in the GEM-T1 solution. A data summary for the GEM-T1 solution is presented in Table 5.3. Table 5.4 describes the orbital characteristics of the satellites used in the formation of GEM-T1. The distribution of the selected satellite's orbital characteristics are shown in Figure 5.1.a. The temporal distribution of the data used is summarized in Figure 5.1.b. As is obvious from the summaries in Table 5.3, precise laser tracking played a dominant role in defining the GEM-T1 gravity and tidal models. The LAGEOS and STARLETTE laser satellites especially, played a central role in both the tidal and gravity field recoveries. These satellites are completely passive orbiting objects whose sole functions are to serve as space-based laser targets. Both satellites are extremely dense spheres (area to mass ratios of .00069 and .00096 m^2 kg^{-1} respectively) covered by laser corner cubes and are in orbits designed to minimize non-conservative forcing effects. LAGEOS orbits at nearly an earth radius

TABLE 5.1

SATELLITE CHARACTERISTICS FOR GEOPOTENTIAL IMPROVEMENT

NAME	DATE	AREA	MASS	SHAPE	$\dot{\omega}$	PR HI	AP HI	ECC	INCL
TELSTAR	621115	0.581	77.0	sphere	1.986	955.89	5649.96	0.2426	44.80
GEOS-1	651116	1.23	172.5	oct. Sphere	0.659	1107.54	2276.53	0.0725	59.37
TIROS-9	660115	0.6	138.0	cylinder	- 2.165	706.10	2572.67	0.1166	96.40
SECOR-5	651201	0.288	18.0	sphere	- 0.792	1140.15	2446.97	0.0801	69.23
OVI-2	661028	0.697	22.7	cyl.hemis.	4.839	414.80	3467.11	0.1835	144.27
ECHO-1RB	600920	0.23	23.0	cylinder	2.976	1505.89	1702.09	0.0123	47.23
BE-C	660405	1.139	52.6	octagon	5.158	945.07	1321.12	0.0250	41.19
DI-D	670219	0.697	22.7	cylinder	5.372	595.89	1888.31	0.0848	39.46
DI-C	670224	0.697	22.7	cylinder	5.913	586.62	1359.39	0.0526	40.00
ANNA-1B	640229	0.657	158.8	spheroid	2.970	1076.81	1181.81	0.0070	50.13
GEOS-2	680310	1.23	211.8	oct.pyramid	- 1.621	1092.09	1600.23	0.0330	105.79
OSCAR-7	660422	1.25	50.0	cylinder	- 2.934	876.40	1222.86	0.0233	89.70
5BN-2	650426	1.139	61.0	octagon	- 2.862	1096.16	1133.10	0.0025	89.95
COURIER-1B	670127	1.327	230.0	sphere	8.230	963.38	1225.28	0.0175	28.33
GRS	650623	0.889	99.3	cylinder	3.501	415.54	1309.79	0.0618	49.76
TRANSIT-4A	610902	0.897	79.0	cylinder	- 0.694	902.89	1015.66	0.0077	66.83
BE-B	670316	1.139	52.6	octagon	- 2.543	889.08	1087.64	0.0135	79.69
OGO-2	660521	4.645	486.9	box	- 3.050	428.22	1512.96	0.0739	87.37
INJUN-1	610916	0.19	22.0	sphere cyl.	- 0.6927	888.40	1007.86	0.0082	66.80
AGENA-RB	640615	28.0	1000.0	cylinder	- 1.276	929.08	934.80	0.0004	69.90
MIDAS-4	641110	84.5	1600.0	cylinder	- 0.980	3490.52	3752.47	0.0131	95.83
VANGUARD-2RB	660128	1.275	68.0	cylinder	5.273	572.15	3285.55	0.1634	32.89
VANGUARD-2	600505	1.275	23.0	sphere	5.256	573.94	3302.49	0.1641	32.90
VANGUARD-3	600115	3.0	68.0	roc.-sph.rod	4.859	513.84	3754.57	0.1904	33.35
ALOU-2	690721	1.0	145.0	oblate sph.	- 1.906	507.65	2946.21	0.1505	79.82
LANSAT-1	720801	7.030	816.0	conc	- 2.728	924.20	938.78	0.0010	99.12
PEOLE	710202	1.539	70.0	sphere	13.121	520.93	745.25	0.0160	15.00
SAS	710103	2.041	143.0	cylinder	14.914	522.09	563.62	0.0030	3.04
VANGUARD-1	581204	0.080	1.47	sphere	4.421	652.11	3947.09	0.1900	34.25
EXPLORER-7	671205	1.014	41.5	double cone	3.417	562.75	1080.22	0.0360	50.31
TIROS-1RB	671106	2.168	24.0	cylinder	4.143	691.50	734.04	0.0030	48.39
AO4	661107	2.168	24.0	cylinder	- 3.012	614.92	856.79	0.0170	98.69
RELAY-1	630101	1.883	78.0	oct.prism	1.213	1325.31	7436.43	0.2840	47.49
TELSTAR-2	630602	2.54	79.4	spheroid	1.217	969.98	10808.11	0.4010	42.73
MIDAS-7	630803	42.412	2000.0	cylinder	- 1.001	3670.26	3730.72	0.0030	88.41
SECOR-1	640204	0.496	18.0	rect.box	- 1.271	922.92	952.11	0.0020	69.89
LCS-1	650605	7.1	34.0	sphere	3.623	2710.42	2875.39	0.0090	32.11
NIMBUS-2	660606	7.03	414.0	cone	- 2.348	1105.93	1181.12	0.0050	100.35
EXPLORER-39	770407	42.084	9.3	sphere	- 2.170	687.19	2170.52	0.0950	80.66
LANDSAT-2	750202	7.03	953.0	cone	- 2.729	926.32	940.90	0.0010	99.09
LANDSAT-3	780403	7.03	960.0	cone	- 2.730	914.89	929.46	0.0010	99.14
LANDSAT-4	810915	13.935	1496.86	cone	- 3.099	705.29	705.43	0.0001	98.20
NIMBUS-6	750705	7.03	827.0	cone	- 2.429	1098.47	1108.94	0.0007	99.96
NIMBUS-7	781106	9.935	832.0	cone	- 2.666	959.37	969.63	0.0007	99.29
HEAO-1	770901	43.731	2720.0	cylinder	12.835	433.68	447.31	0.0010	22.76
HEAO-3	791002	43.731	2720.0	cylinder	6.222	494.37	508.11	0.0010	43.61
SMM	800303	28.903	2315.0	cylinder	10.570	568.83	571.61	0.0020	28.51
SME	810701	19.97	437.0	cylinder	- 3.435	531.27	535.41	0.0003	97.55
STARLETTE	750527	0.045	47.25	sphere	3.296	812.19	1114.80	0.0206	49.83
LAGEOS	790812	0.2827	411.0	sphere	- 0.214	5834.25	5944.82	0.0045	109.84
GEOS-3	750531	1.4365	345.909	oct.pyramid	- 0.349	841.10	857.55	0.0011	114.98
SEASAT	780921	25.31	2213.6	cylinder	- 1.722	812.00	818.59	0.0005	108.01
EXPLORER-38	680801	4.58	190.0	tub.cross	0.152	5855.43	5865.21	0.0004	120.64

Table 5.2
FINAL SATELLITE SELECTION RANKING

NAME	INCL	ACU	GLB	PAS	TOTL DATA	UNI	ACL	TOP SIMLY	GRV SENS	APSD COVR	TOTAL SCORE
SME	97.6	8.	4.	4.	9.	7.	-35.	4.	3.	7.	-4.
EXP39	80.7	7.	4.	3.	7.	3.	-25.	8.	1.	3.	-2.
OVI2	144.3	7.	4.	13.	8.	7.	-25.	0.	2.	3.	0.
SAS	3.0	2.	1.	2.	2.	15.	-25.	4.	4.	3.	3.
ADR	98.7	7.	3.	2.	6.	3.	-12.	4.	2.	7.	4.
VAN1	34.3	7.	4.	2.	6.	5.	-7.	4.	-1.	2.	4.
HEAO1	22.8	8.	6.	8.	12.	13.	-25.	0.	7.	7.	10.
VAN2	32.9	7.	6.	2.	6.	5.	-10.	4.	2.	7.	14.
TIRIR	48.4	7.	4.	3.	6.	12.	-12.	4.	3.	2.	17.
VAN3	33.4	7.	6.	2.	6.	5.	-10.	6.	2.	7.	17.
SEC1	69.9	7.	3.	3.	6.	5.	-2.	8.	2.	2.	17.
EXPL7	50.3	7.	3.	3.	6.	5.	-7.	6.	3.	6.	19.
TEL2	42.7	8.	5.	3.	6.	4.	-3.	8.	0.	7.	19.
EXP38	120.6	7.	3.	4.	6.	12.	-1.	8.	0.	0.	20.
HEAO3	43.6	7.	4.	5.	9.	5.	-15.	4.	4.	7.	21.
OSCR7	89.7	8.	5.	5.	11.	5.	-2.	6.	2.	3.	22.
LAND4	98.2	8.	3.	5.	10.	15.	-9.	0.	5.	7.	22.
PEOLE	15.0	10.	5.	5.	11.	8.	-15.	4.	2.	7.	24.
LAND3	99.1	8.	5.	3.	8.	3.	-3.	8.	2.	5.	24.
MUJN1	66.8	7.	5.	5.	8.	5.	-2.	6.	2.	7.	24.
GRS	49.8	7.	5.	3.	11.	5.	-5.	4.	3.	2.	24.
LAND1	99.1	8.	5.	5.	6.	5.	-2.	12.	-2.	2.	25.
SEC5	69.2	7.	3.	2.	9.	5.	-1.	4.	2.	7.	25.
VN2R	32.9	8.	6.	3.	11.	5.	-2.	4.	2.	7.	25.
LAND2	99.1	8.	5.	3.	7.	12.	-7.	4.	-1.	7.	25.
OGO2	87.4	7.	4.	3.	2.	7.	-1.	10.	-1.	6.	26.
TIR9	96.4	2.	5.	2.	11.	8.	-2.	5.	2.	7.	26.
SBN2	90.0	7.	5.	5.	11.	3.	-3.	6.	-1.	7.	26.
HIMB2	100.4	8.	5.	3.	8.	3.	-2.	8.	-2.	7.	26.
NMB7	99.3	7.	5.	4.	11.	12.	-10.	3.	0.	4.	27.
TRM4A	66.8	10.	4.	6.	9.	12.	-4.	6.	-1.	7.	27.
AGEMR	69.9	7.	6.	12.	11.	7.	-1.	8.	2.	3.	27.
D1C	40.0	10.	4.	4.	6.	12.	-6.	6.	0.	4.	27.
LCS1	32.1	12.	6.	2.	17.	8.	-4.	6.	2.	7.	28.
MID7	88.4	2.	5.	6.	9.	12.	-2.	8.	0.	6.	29.
NMB6	100.0	7.	6.	4.	16.	8.	-1.	10.	2.	7.	29.
D1D	39.5	10.	5.	3.	12.	12.	-8.	2.	2.	6.	31.
RELY1	47.5	8.	5.	8.	8.	12.	-5.	6.	-1.	7.	31.
SEAST	108.0	7.	5.	4.	15.	12.	-1.	2.	2.	7.	31.
MID4	95.8	12.	4.	3.	15.	5.	-1.	9.	-1.	7.	32.
ALOU2	79.8	7.	5.	8.	20.	5.	-1.	7.	2.	6.	33.
COUR1	28.3	13.	4.	4.	23.	12.	0.	12.	-1.	7.	36.
BEB	79.7	12.	4.	8.	18.	12.	-1.	7.	2.	7.	38.
TEL1	44.8	8.	6.	8.	22.	12.	0.	9.	-1.	6.	41.
SMM	28.5	15.	6.	12.	33.	7.	0.	8.	0.	7.	43.
GEOS1	59.4										44.
STRLT	49.8										47.
GEOS2	105.8										50.
GEOS3	115.0										53.
LAGEOS	109.8										

63

Table 5.3

DATA UTILIZED IN PRELIMINARY
TOPEX GRAVITY MODEL: 1986

SATELLITE	DATA TYPE	NUMBER OF NORMAL MATRICES	NUMBER OF OBSERVATIONS
LAGEOS	LASER	58	144527
STARLETTE		46	57356
GEOS-1		48	71287
GEOS-2		28	26613
GEOS-3		36	42407
BE-C		39	64240
SEASAT		14	14923
D1-C		4	7455
D1-D		6	11487
PEOLE		6	4113
SUB-TOTAL - LASER		285	444,408
SEASAT	DOPPLER	15	138042
OSCAR-14		13	63098
SUB-TOTAL - DOPPLER		28	201,140
GEOS-1	CAMERA	43	60750
GEOS-2		46	61403
ANNA		30	4463
TELSTAR		30	3962
BE-C		50	7501
BE-B		20	1739
COURIER 1B		10	2476
VANGUARD-2RB		10	686
VANGUARD-2		10	1299
D1-C		10	2712
D1-D		9	6111
PEOLE		6	38
SUB-TOTAL - CAMERA		273	153,140
TOTAL		580*	798,688

*PEOLE arcs contained both optical and laser data.

64

TABLE 5.4

SATELLITE ORBITAL CHARACTERISTICS

SATELLITE NAME	SATELLITE ID NO.	SEMI-MAJOR AXIS	ECC	INCL. (DEG.)	DATA* TYPE
ANNA-1B	620601	7501.	.0082	50.12	O
BE-B	640841	7354.	.0135	79.69	O
BE-C	650321	7507.	.0257	41.19	L,O
COURIER-1B	600131	7469.	.0161	28.31	O
D1-C	670111	7341.	.0532	39.97	L,O
D1-D	670141	7622.	.0848	39.46	L,O
GEOS-1	650891	8075.	.0719	59.39	L,O
GEOS-2	680021	7711.	.0330	105.79	L,O
GEOS-3	750271	7226.	.0008	114.98	L
LAGEOS	760391	12273.	.0038	109.85	L
OSCAR	670921	7440.	.0029	89.27	D
PEOLE	701091	7006.	.0164	15.01	L,O
SEASAT	780641	7170.	.0021	108.02	D,L
STARLETTE	750101	7331.	.0204	49.80	L
TELESTAR-1	620291	9669.	.2429	44.79	O
VANGUARD-2RB	590012	8496.	.1832	32.92	O
VANGUARD-2	590011	8298.	.1641	32.89	O

* D = Doppler
  L = Laser
  O = Optical
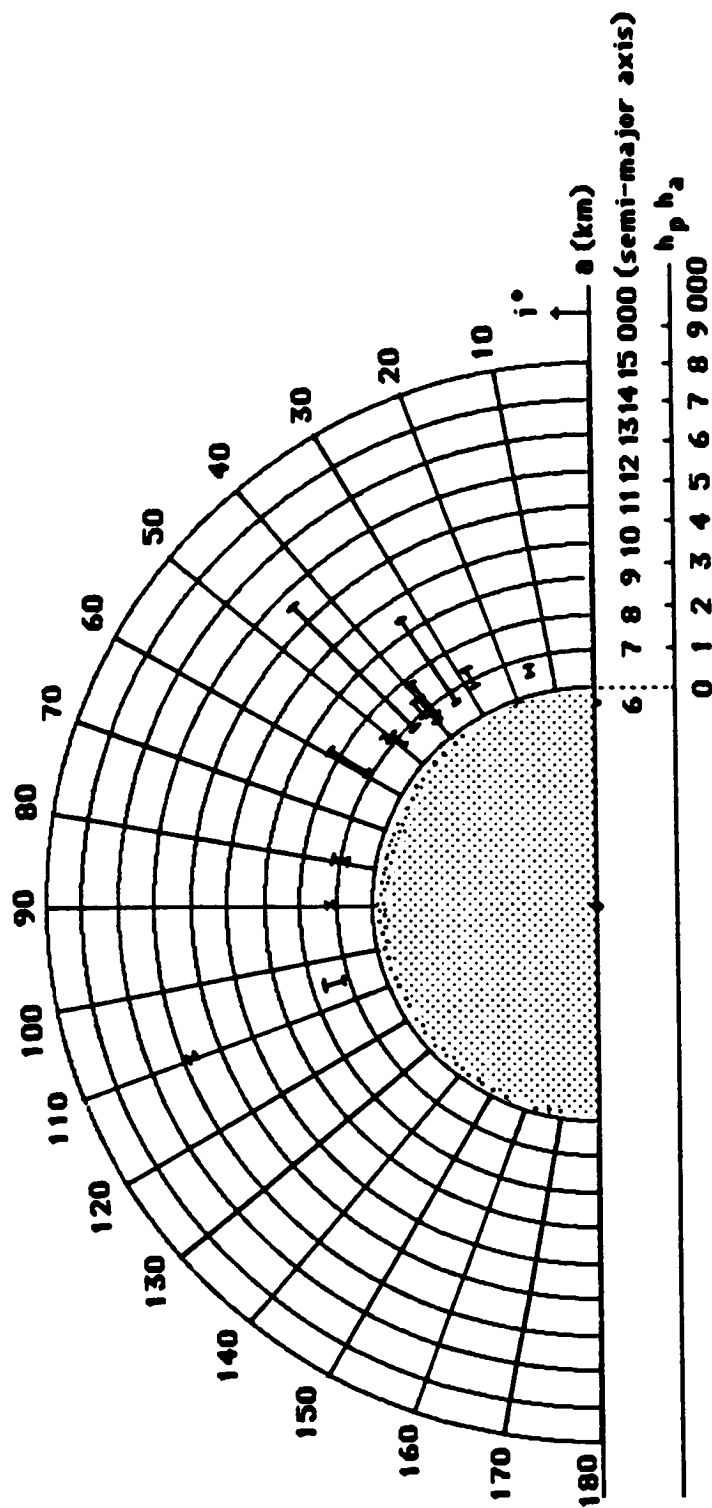
Figure 5.1a. Orbital Characteristics of the GEM-T1 Satellites.
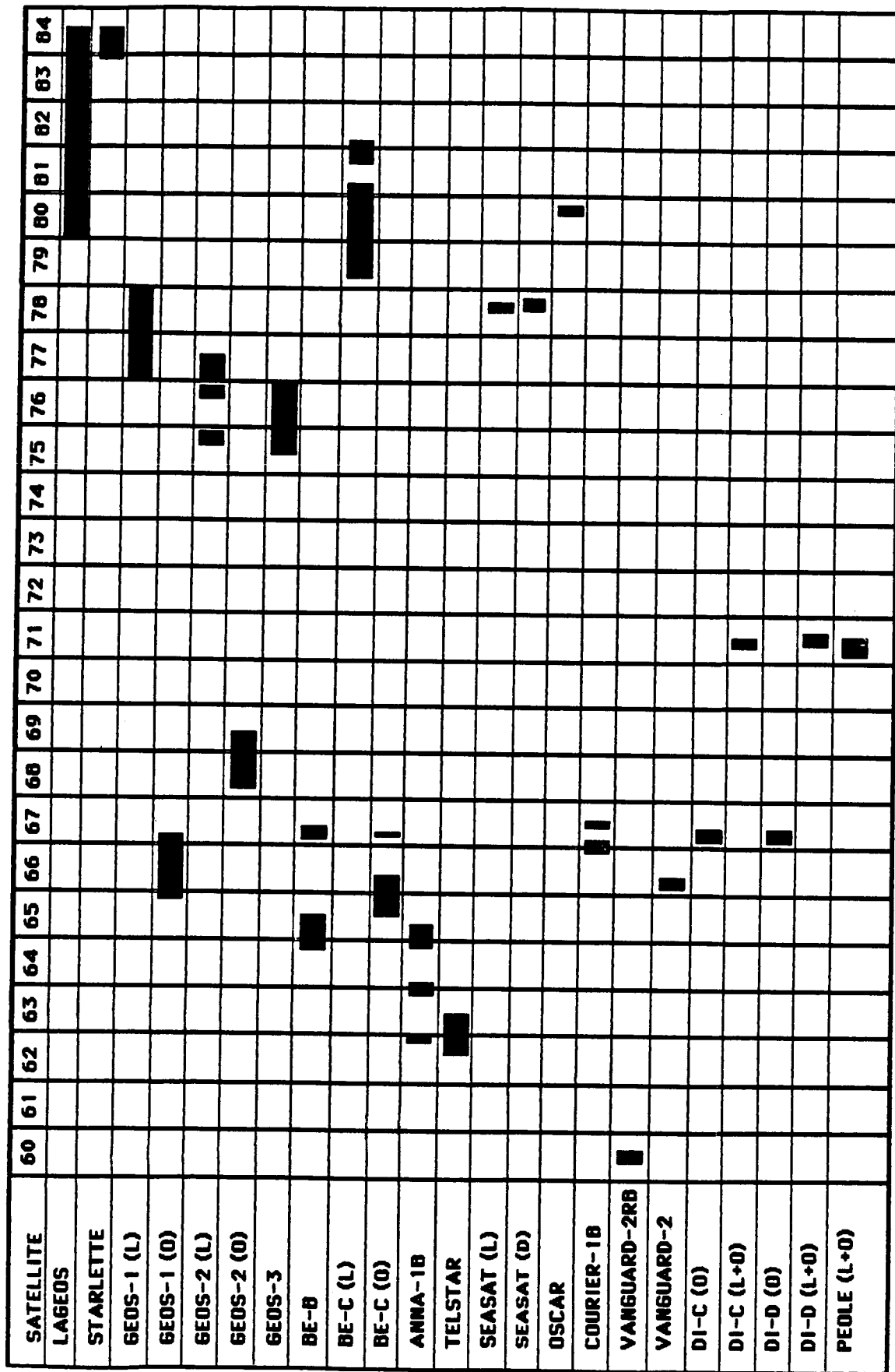
Figure 5.1b. Time Line of Satellite Tracking.

above the earth, and senses only the longest wavelength gravity and tidal effects. STARLETTE, orbiting at a much lower altitude of about 1000 km, experiences a rich spectrum of tidal and gravity perturbations and is highly complementary to LAGEOS for the separation of long and short wavelength gravity and tidal terms. Both of these satellites are tracked on a high priority basis by a global network of laser tracking stations and have extensive observation sets which have been supported by NASA's Crustal Dynamics Project activities, Project MERIT, and the WEGENER Campaign.

The following sub-sections as reported by the individual analysis managers, describe the data analysis activities which were undertaken for the high-priority satellites utilized in forming GEM-T1.

5.2.1 Analysis of SEASAT Doppler and Laser Data

SEASAT was launched on June 28, 1978. The SEASAT satellite is of major significance because it has four distinct data types; S-Band, laser, Doppler and altimetry.

The nominal orbit parameters used in processing the SEASAT Doppler and laser arcs are listed in Table 5.2.1a.

Orbit computations using the PGS-S4' gravity model in the GSFC GEODYN-2 computer program have been performed on 14 arcs of both Doppler and laser data covering the span from July 27, 1978 to October 11, 1978. These arcs were of 6-day duration with the exception of those arcs between August 8 and September 17, which were shortened or lengthened due to maneuvers during this period (Table 5.2.1b). In the computation of the orbital solution for each Doppler arc, the six orbital elements, daily atmospheric drag coefficients (C_D), and a single solar radiation pressure coefficient (C_R) were determined. Pass-by-pass measurement biases were also determined for each station in the solution.

The Doppler data in the SEASAT orbital solutions were pre-edited by passing the residuals from the initial orbits through a residual edit analysis program. This program produced delete cards for passes of data that exceeded the maximum RMS value of 1.5 cm/sec, fell below an elevation cutoff of 5° and/or has a maximum timing bias of 5 ms. Passes with less than 5 data points were also edited. The program also produced the initial measurement bias values for input into GEODYN-2.

The laser orbits were computed by constraining the converged Doppler orbits and passing them through the laser data. Solar radiation pressure and the daily atmospheric drag parameters were also constrained at their Doppler determined values. This was done to permit proper combination of laser and Doppler orbital arcs with flexibility remaining for defining the relative weight of Doppler vs. laser observations. The nominal weighting sigma used on the Doppler data was 1 cm/sec for all stations. A sigma of 1 meter was used for all of the laser stations except 7833 (KOOTWIJK), which had a sigma of 2 meters applied. For the laser orbits, Kootwijk was sampled at every 2nd observation and the GSFC lasers were sampled at every 3rd observation. Stations 7804 (SAFLAS), 7842 (GRASSE) and 7834 (WETTZEL) were deleted from the solutions.

An estimate of the "true" noise was 0.6 cm/sec for the Doppler data and 10 cm for the laser data. The overall RMS of fit obtained for the Doppler orbits was about 0.75 cm/sec and 1.23 meters for the laser orbits (Table 5.2.1c and 5.2.1d) based on the a priori PGS-S4 gravity model.

5.2.2 Analysis of OSCAR Doppler Data

The OSCAR-14 satellite, launched in 1967, is one of the U.S. Navy navigation satellites. Data for this satellite were obtained as part of the MEDOC Campaign, an international Doppler data program. The data is

Table 5.2.1a

NOMINAL ORBIT PARAMETERS FOR SEASAT

AREA:	25.31 m^2
MASS:	2213.6 kg
ECCENTRICITY:	0.001
INCLINATION:	108°
PERIGEE HEIGHT:	7171 km
APOGEE HEIGHT:	7183 km
PERIOD:	100 minutes

Table 5.2.1b

SEASAT PRECISION ORBITS

ARC NO.	START YYMMDD HHMM	STOP YYMMDD HHMM
1	780727 0000	780802 0000
2	780802 0000	780808 0000
3	780808 0000	780815 0730
4	780815 0743	780818 0748
5	780818 0749	780823 0921
6	780823 0922	780826 0927
7	780826 0928	780901 0000
8	780901 0000	780905 0000
9	780905 0000	780910 0105
10	780910 0123	780917 0000
11	780917 0000	780923 0000
12	780923 0000	780929 0000
13	780929 0000	781005 0000
14	781005 0000	781011 0000

LAUNCHED: JUNE 28, 1978   FAILED: OCTOBER 10, 1978

HEIGHT: 800 km ALTITUDE   INCLINATION: 108^{0}

Figure 5.2.1.   SEASAT

72
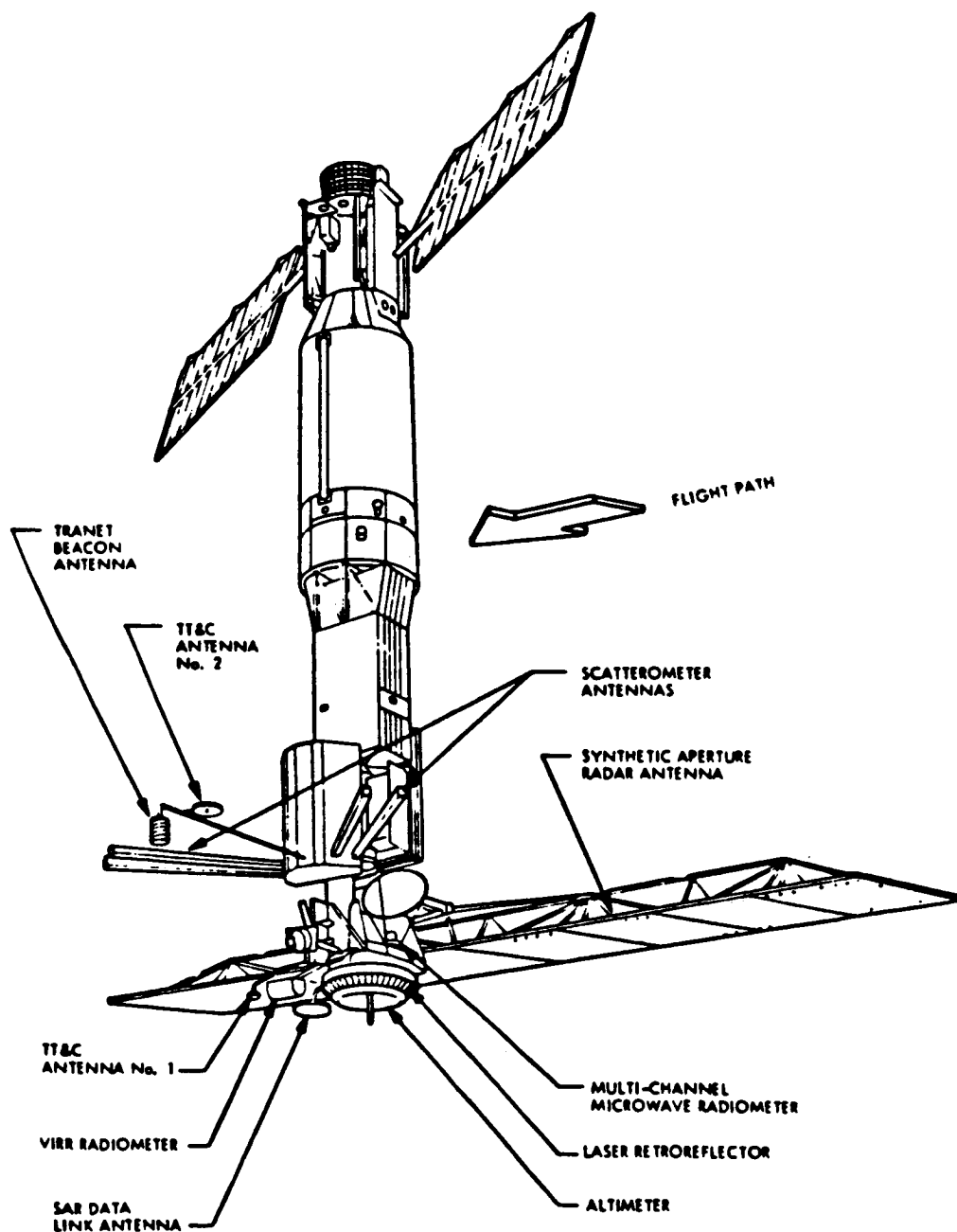
Table 5.2.1c

EMAT SUMMARY FOR SEASAT DOPPLER

EPOCH	NUMBER OF OBSERVATIONS	WEIGHTED RMS (cm/sec)	NUMBER OF STATIONS	ARGUMENT OF PERIGEE (AT EPOCH)
780721	7100	1.7822	35	180.573
780727	14860	.7318	35	193.017
780802	13511	.7135	35	153.474
780808	15203	.7662	34	116.081
780815	6041	.6708	34	146.012
780818	6723	.7109	34	141.374
780823	5369	.6704	33	124.192
780826	10808	.7030	33	51.376
780901	7369	.7058	34	99.272
780905	8453	.8914	34	292.590
780910	10404	.7498	34	115.672
780917	9592	.7399	33	93.448
780923	8934	.7483	33	122.805
781005	6982	.7656	32	56.247

73

Table 5.2.1d

EMAT SUMMARY FOR SEASAT LASER

EPOCH	NUMBER OF OBSERVATIONS	WEIGHTED RMS (m)	NUMBER OF STATIONS	ARGUMENT OF PERIGEE (AT EPOCH)
780727	676	1.4265	8	193.018
780802	986	1.3541	8	153.474
780808	1522	1.1539	8	116.082
780815	424	1.3371	4	146.013
780818	483	.9859	3	141.375
780823	355	.6760	4	124.193
780826	1129	.8644	5	51.377
780901	627	1.0067	4	99.273
780905	664	2.0218	9	292.591
780910	1289	1.7256	10	115.672
780917	1725	1.2234	10	93.449
780923	1785	1.3231	9	122.806
780929	1915	1.7240	9	281.185
781005	1343	1.8012	9	56.248

of particular importance because the satellite is in a polar orbit giving complete global sampling of the gravity field. This is the first time a strong polar orbit has been incorporated into the determination of GSFC gravity fields.

The nominal orbit parameters used in processing OSCAR-14 data were as follows:

Area:	25 m^2
Mass:	1000 kg
Eccentricity:	.004
Inclination:	89°
Perigee Height:	1040 km
Apogee Height:	1085 km
Period:	106 minutes

Orbit computations for OSCAR-14 utilized the GEM-10B' gravity model. Thirteen 7-day arcs were analyzed using the GSFC GEODYN-2 computer program. The data coverage was from August 1, 1980 through October 24, 1980 (Table 5.2.2a). Computation of orbital solutions for these arcs included the adjustment of the six orbital elements, daily atmospheric drag parameters (C_D), a single solar radiation pressure coefficient (C_R), and observation biases for each pass. Timing biases were computed for SHANGHAI (743) and PURPLE MT. (7185). Data from GRAZ (425) were deleted from the solution. The sigma on all the data was nominally 1 cm/sec.

An estimate of the "true" noise for the Doppler data was ~1.2 cm/sec, largely due to the large variety of receivers which tracked. The overall RMS obtained for the OSCAR-14 orbits was about 1.59 cm/sec (Table 5.2.2b).

Table 5.2.2a

<u>OSCAR-14 PRECISION ORBITS</u>

ARC NO.	START YYMMDD	STOP YYMMDD
1	800801	800808
2	800808	800815
3	800815	800822
4	800822	800829
5	800829	800905
6	800905	800912
7	800912	800919
8	800919	800926
9	800926	801003
10	801003	801010
11	801010	801017
12	801017	801024
13	801024	801031

Table 5.2.2b

EMAT SUMMARY FOR OSCAR 14

EPOCH	NUMBER OF OBSERVATIONS	WEIGHTED RMS (m)	NUMBER OF STATIONS	ARGUMENT OF PERIGEE (AT EPOCH)
800801	5867	1.4677	16	357.420
800808	5559	1.3992	16	337.814
800815	6227	1.4702	17	336.019
800822	5635	1.5358	17	277.827
800829	5812	1.5332	18	273.059
800905	5944	1.5991	17	240.671
800912	5993	1.6518	17	209.115
800919	6015	1.6174	16	187.183
800926	4519	1.5773	18	187.551
801003	5500	1.5881	17	136.816
801010	2251	1.8217	13	140.581
801017	1881	1.6457	10	119.267
801024	1895	1.7754	9	97.921

5.2.3 Analysis of GEOS-1 Laser Ranging Data

GEOS-1 laser data from the period January 20, 1977 to December 14, 1978 have been chosen for analysis. This period spans more than one cycle of the argument of perigee, thus providing good temporal coverage. The data involves both SAO and NASA stations.

The first step in the procedure was to catalog the data and divide it into 5-day arcs, eliminating those time periods with little or no coverage. Attention was given to the number of passes and the number of stations involved in any 5-day period. A total of 104 arcs survived this scrutiny. Tables 5.2.3a and 5.2.3b provide summaries of the satellite's orbit and the tracking data.

The NASA data was provided at a frequency of one measurement/sec, with one measurement/7.5 sec for the SAO data. It was decided to select every third NASA observation and every SAO observation to get a more even balance in the data weighting. Using estimates of the position and velocity vectors of the satellite, nominal values for air drag, solar radiation pressure and solid earth tidal parameters, an ocean tide model, and the GEM-10B′ gravity field, the arcs were converged. In the convergence process, the position and velocity vectors, air drag and solar radiation pressure parameters were adjusted for each arc. The purpose of the convergence is twofold: (1) to obtain more accurate position and velocity vectors preparatory to the creation of the matrix of normal equations ("E"-matrix) to be used in the gravity field solution, and (2) to identify and delete nonreliable measurements and/or passes. One air drag coefficient (C_D) for each day of a 5-day arc and one solar radiation pressure (C_R) coefficient for the whole arc were solved for. A total of 101 arcs survived this procedure.

Table 5.2.3a

ORBITAL DATA FOR GEOS-1

Semi-major axis:	8080 km
Eccentricity:	.07
Inclination:	59°.4
Perigee Height:	1135 km
Apogee Height:	2270 km
Year of Launch:	1965
Area:	1.23 m^2
Mass:	172.5 kg
Period:	120 minutes
Period of Arg. of Perigee:	540 days

Table 5.2.3b

<u>TRACKING DATA SUMMARY</u>

- SATELLITE: GEOS-1

- TIME PERIOD: 1/20/77 - 12/14/78

- DATA: SAO + NASA LASER

- ARC LENGTH: 5 DAYS

- NO. ARCS (INCL. NASA):   101 (58)

- NO. OBSERVATIONS: 129,371

Table 5.2.3c

SUMMARY OF GEOS-1 ORBITS

ARC EPOCH YYMMDD	NO. OBS.	RMS (m)
770120	838	0.886
126	904	0.721
207	724	0.821
213	752	0.848
311	616	0.850
321	1169	0.744
329	978	0.463
403	1303	0.816
408	1359	0.658
413	1589	1.088
418	1061	0.890
423	1649	0.794
* 428	2084	0.801
* 503	1778	0.717
508	1525	0.771
* 524	1085	0.933
* 603	1520	0.782
* 608	1830	0.949
613	1331	1.345
* 618	1245	0.714
* 623	1637	1.073
* 628	1240	0.788
703	1235	1.025
708	1255	1.141
* 713	1238	0.836
718	1095	1.077
* 723	704	0.655
729	1512	0.959
803	1728	1.326
808	1513	1.063
818	1151	0.828
* 825	1614	1.081
* 830	1364	1.153
* 904	1739	1.189
916	1661	1.458
921	2343	1.106
928	1804	1.452
* 1003	908	0.652
* 1008	1207	1.707
* 1013	1647	1.507
* 1024	1706	1.424
* 1029	1598	1.340

*Includes NASA data

81

Table 5.2.3c *cont.*

	ARC EPOCH YYMMDD	NO. OBS.	RMS (m)
	771103	1195	1.815
*	1110	1295	0.742
*	1116	1359	1.137
	1126	961	0.859
	1201	1089	0.649
	1211	1114	0.915
	1216	801	0.876
	780123	1196	0.804
	201	1075	0.880
*	209	1039	0.798
*	217	1280	0.868
*	222	1644	0.783
*	308	864	0.806
*	314	985	0.754
*	322	827	0.767
*	330	885	0.821
*	404	942	0.804
	413	894	0.761
	419	940	0.681
	424	1465	0.937
	429	960	1.010
	504	1313	0.815
	509	1810	0.932
*	514	1049	0.838
*	520	1065	0.789
	528	1092	0.871
	602	1443	0.860
	607	1700	0.982
*	613	1533	0.841
*	625	1478	0.949
*	630	1329	0.805
*	705	1670	1.199
*	710	1440	0.928
*	715	1212	0.697
*	720	938	0.997
*	725	632	0.773
	730	1329	0.925
	804	1318	1.112
*	809	742	0.933
*	820	683	0.852
*	825	771	0.793
*	830	961	0.488
*	906	789	0.529
*	919	1770	0.718

*Includes NASA data

Table 5.2.3c *cont.*

	ARC EPOCH YYMMDD	NO. OBS.	RMS (m)
*	780924	1315	0.793
*	929	1468	0.908
*	1004	1620	1.044
*	1009	1975	0.579
*	1014	1890	0.969
*	1019	1189	0.807
*	1024	2034	0.701
*	1029	1278	0.826
*	1105	1169	0.967
*	1110	1227	0.709
	1115	1380	0.753
*	1120	1571	0.973
*	1125	865	0.658
*	1204	1362	1.019
*	1209	912	0.843

Average rms = 0.912 m   *Includes NASA data

Finally, one E-matrix (matrix of normal equations) was prepared for each arc. RMS of fit values for the arcs provide an indication of the overall fit to the data. They are presented in Table 5.2.3c

The RMS values ranged from 0.4 m to 1.8 m, with an average of 0.91 m. This is quite good, considering the vintage of the data. The GEOS-1 laser data provided an important contribution to the determination of the Earth's gravity field.

5.2.4 GEOS-3 Analysis of Laser Ranging Data

The Geodynamics Earth and Ocean Satellite, GEOS-3, was launched on April 9, 1975. The satellite characteristics and the nominal orbital parameters are the following:

Area:	1.4365 m^2
Mass:	345.909 kg
Eccentricity:	0.00114
Inclination:	115°
Perigee Height:	840 km
Apogee Height:	860 km
Orbital Period:	102 minutes
Argument of Perigee Period:	1039 days

The available data were obtained by both NASA and SAO laser tracking stations during the years 1975 and 1976. It is distributed as follows:

1975:	196916 meas.
1976:	193405 meas.
Total:	389421 meas. (SAO: 18%)

Past experience at GSFC indicates that a 5 to 7 day arc length is optimum for the analysis of data acquired on geodetic satellites at 800 to 1000 km orbit heights. This time span provides strong gravitational information without excessive contamination from nonconservative force effects such as atmospheric drag and solar radiation pressure. A 5-day arc for GEOS-3 covers approximately the period of the effect produced by the resonant 14th order coefficients of the Earth's gravitational field. This effect can reach magnitudes of 150 meters in the along-track component. The gravitational field used in the computations was the GEM-10B' model complete to degree and order 36, derived from satellite tracking data, surface gravity and altimetry. The atmospheric density was that of the Jacchia 1971 model.

Forty-eight arcs covering the time period from May, 1975 to December, 1976, have been analyzed using the GEODYN Program. The editing applied to the data consisted of several stages. There was a preliminary selection based on existing knowledge concerning the quality of the data obtained by different stations at different times. The internal consistency of the data was checked on a pass by pass basis. Finally, the dynamic editing inherent in GEODYN was applied also.

The atmospheric drag model formulation allowed the estimation of a daily drag coefficient (C_D), and the force model for the solar radiation pressure incorporated a single coefficient C_R for every 5-day arc. The solid earth tidal effects were modeled after Wahr's formulation, the ocean tides force model used a spherical harmonics approach due to D. Christodoulidis, et al. (1986b): the long wavelength components of approximately 600 constituents were used in the calculations and the coefficients of about 60 are actually estimated when computing a solution.

The trajectory generated using these estimated parameters was used to compute an RMS value for each 5-day arc, which provided an

Table 5.2.4a

GEOS-3 ORBIT DETERMINATION RESULTS

ARC EPOCH	NO. OF MEAS.	RMS (METERS)
750519	356	0.510
750524	435	0.273
750614	910	0.559
750619	662	0.679
750629	926	0.633
750709	1120	0.757
750724	796	0.469
750729	876	0.363
750828	1705	0.596
750902	1240	0.459
750907	1501	0.527
750929	336	0.571
751118	537	0.613
751123	488	0.593
751216	1333	0.485
760108	903	1.542
760113	1533	1.454
760205	1219	1.202
760210	2078	1.237
760217	1450	0.809
760222	1184	0.869
760227	1801	1.300
760404	1009	1.487
760409	1217	1.282
760417	1178	1.186
760422	1112	1.380
760427	2307	1.443
760502	1866	1.391
760507	1193	1.079
760523	1010	1.218
760601	1003	1.231
760606	974	1.374
760614	900	1.465
760621	804	1.319
760913	848	1.480
761004	1641	1.309
761009	1085	1.432
761018	878	0.904
761023	1031	1.145
761028	1072	1.641
761102	810	1.547
761107	1634	1.126
761112	984	0.965
761117	1394	1.369
761122	1527	1.386
761127	955	1.294
761202	610	1.383
761207	839	1.306
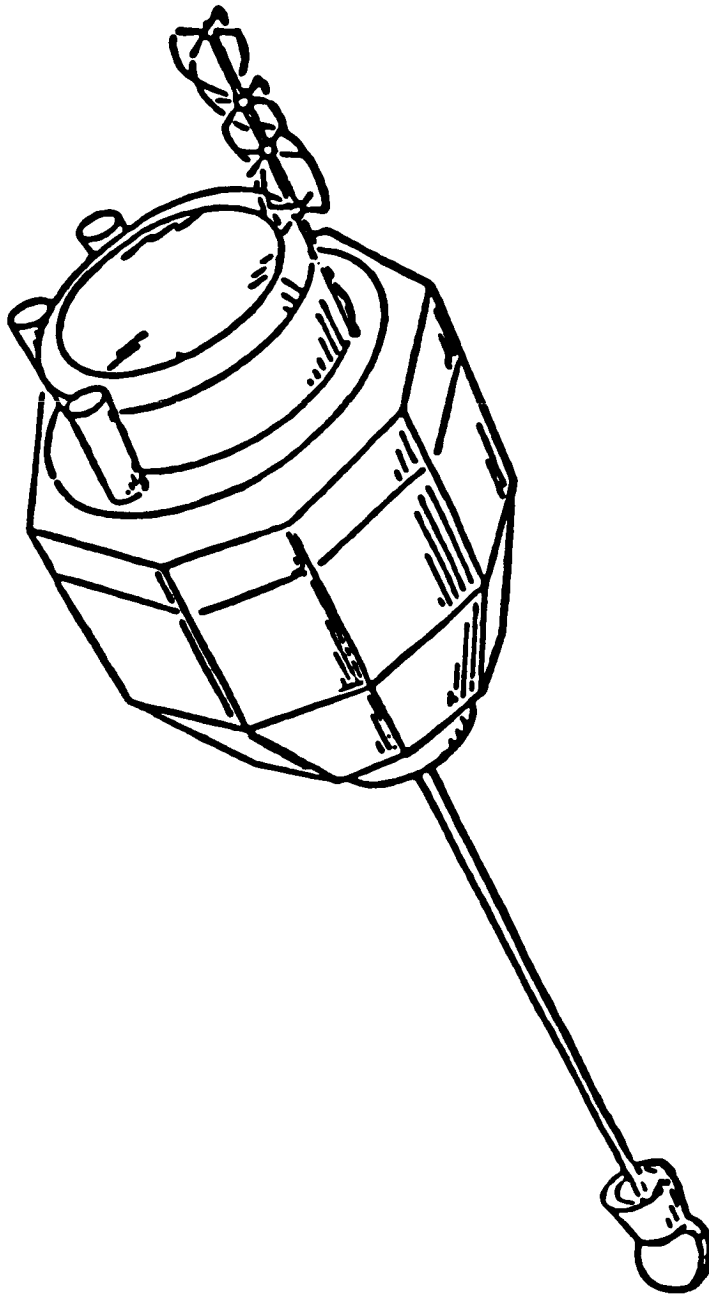
Figure 5.2.4a. GEOS-3 Spacecraft.

● : NASA stations   S : SAO stations
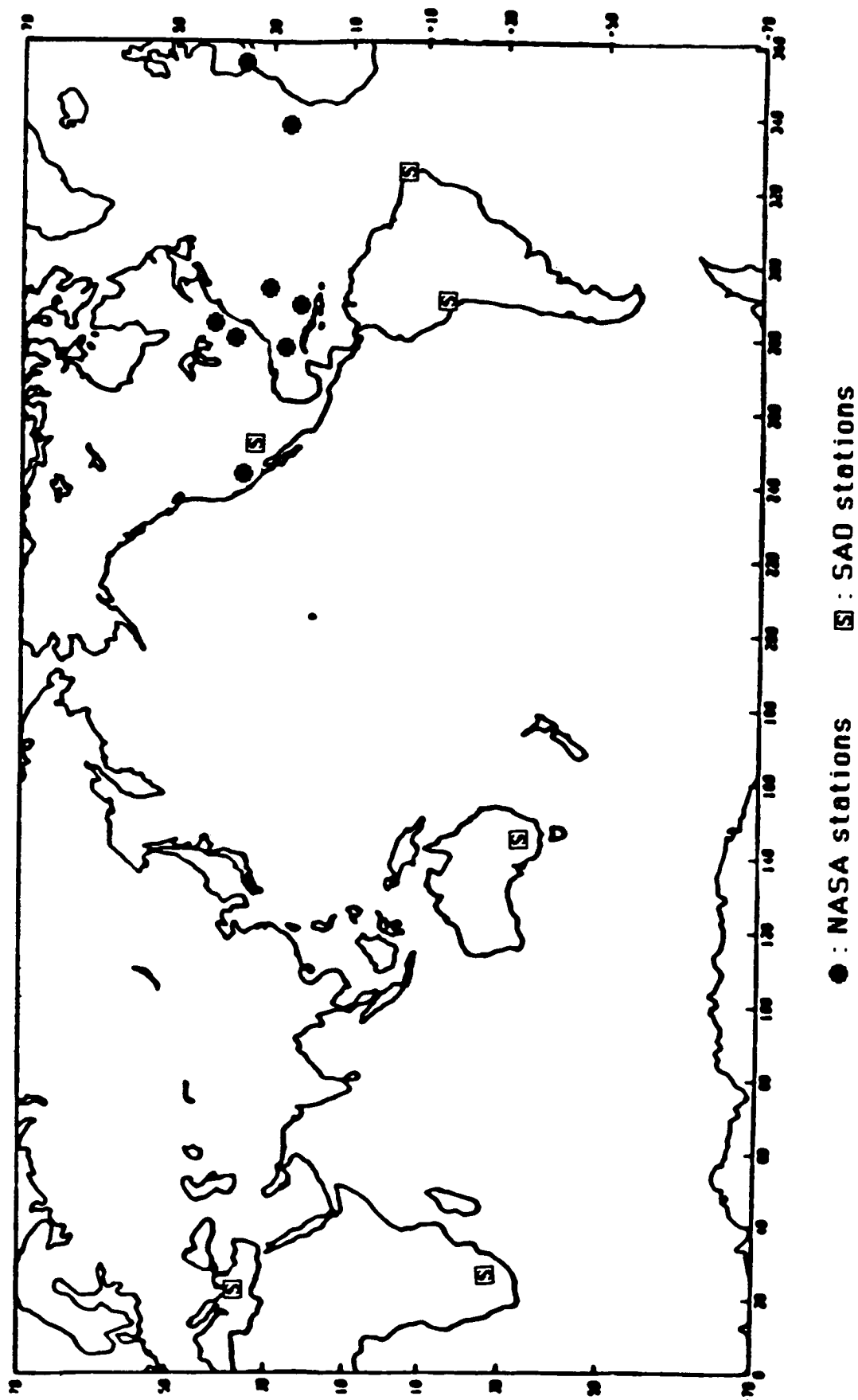
Figure 5.2.4b. Position of Stations Used in Tracking GEOS-1 and GEOS-3.

indication of the overall fit to the data for each arc. The results are given in Table 5.2.4a below. The converged arcs were used to compute the normal equations.

The higher RMS values in the 1976 arcs are due to the presence of data from the SAO stations, which are less accurate than the NASA stations. The SAO stations provide a global coverage which would be lacking with the use of NASA data alone.

5.2.5 Analysis of STARLETTE Laser Ranging Data

This section documents the various stages of the data reduction effort in connection with the STARLETTE laser ranging data set. The data which fulfilled the editing criteria were subsequently used to form the normal equations contributing to the estimation of the TOPEX model parameters.

STARLETTE is a geodetic satellite launched by the French Space Agency in 1975. Information on its size, shape, mass and orbital characteristics is given in Table 5.2.5a. The STARLETTE data used in this effort consist of a set of raw ranges sampled in such a way that each station has about one range per six seconds (whenever available). Based on previous experience we decided that this procedure produced results similar to those obtained using normal points. The laborious process of forming normal points was thus avoided. We have only completed the analysis of the data covering the first eight months of 1984, with much more data being available.

These data that have been selected for analysis cover the January 1984 through August 1984 period. Table 5.2.5b shows the amount of tracking available for analysis from each station. The breakdown in terms of passes and individual ranges per station gives a rough

Table 5.2.5a

ORBITAL AND PHYSICAL CHARACTERISTICS
OF STARLETTE (7501001)

APOGEE HEIGHT	1105 km
PERIGEE HEIGHT	810 km
ECCENTRICITY	0.02
INCLINATION	49°.8
PERIOD	104 min.
ASCENDING NODE RATE	-3.94 °/day
ARGUMENT OF PERIGEE RATE	3.30 °/day
AREA	0.04524 m^2
MASS	47.250 kg
SHAPE	SPHERE
RADIUS	12 cm
ONBOARD INSTRUMENTATION	RETROREFLECTORS

indication of the varying repetition rates in this network. Based on prior experience with STARLETTE and considering the quality of our a priori models, a 5-day nominal arc length was choosen. The data were edited using the GEODYN-II software package appended with editing programs to perform post-fit residual analysis on station-by-station and pass-by-pass basis. Table 5.2.5c gives a summary of the constants and models used in the dynamical orbit determination process. The residual analysis package was invaluable in locating data problems and eliminating outliers. The philosophy here was to edit data points that looked suspect where documentation was lacking for curable station problems. Given the abundance of data, this process was beneficial in creating a stable and bias-free set of tracking data. Figure 5.2.5a shows a residual plot where one can clearly see an edited outlier and a number of residuals of questionable quality. The latter had to be edited manually and the whole process repeated until it converged. To give an insight into what was achieved through this process, we have included Tables 5.2.5d and 5.2.5e which show the apriori model fits and those based on our first generation TOPEX model, the PGS-T2. The improvement is highly significant. Table 5.2.5f gives a summary of the statistics by station based again on the same set of data and the same models as the previous two tables. We have analyzed forty-six 5-day arcs covering a period from January 1984 through August 1984. These arcs sample 2.2 periods of the argument of perigee and 2.6 periods of the ascending node. We chose to start the editing process with the more recent data since this period is characterized by intense tracking due to the ongoing (at the time) MERIT campaign. The large amount of data and the participation of new tracking stations for which we had no prior performance records on any satellite made the editing effort more complicated and tedious, but at the same time more important.

Starting with the "raw" data fits at the 1-2 meters level the editing process resulted in a very significant reduction to about 60 cm which was the typical RMS fit at the "normal- equation-forming" stage. A

Table 5.2.5b

STARLETTE DATA CATALOG

JANUARY 1983 - AUGUST 1984

SUMMARY BY STATIONS

LOCATION	NAME	NUMBER	PASSES	POINTS
POTSDAM, DDR	POTSDM	1181	59	1271
SAN DIEGO, CA.	ML0306	7062	3	30
AUSTRALIA	ML0502	7090	64	3649
GREENBELT, MD.	ML0501	7102	1	5
GREENBELT, MD.	ML0702	7105	105	5499
QUINCY, CA.	ML0802	7109	288	18247
MONUMENT PEAK,CA	ML0402	7110	270	12059
PLATTEVILLE, CO.	ML0201	7112	208	8589
HUAHINE, FR.POL.	ML0101	7121	41	1033
MAZATLN, MEXICO	ML0601	7122	54	2733
MAUII, HAWAII	HOLLAS	7210	37	1441
METSAHOVI, FINN.	FINLAS	7805	12	209
HELWAN, EGYPT	HELWAN	7831	12	376
KOOTWIJK,HOLLAND	KOOLAS	7833	32	419
WETTZELL, FRG	WETZEL	7834	50	1602
GRASSE, FRANCE	GRASSE	7835	7	111
SIMOSATO, JAPAN	SHOLAS	7838	124	4690
GRAZ, AUSTRIA	GRAZ	7839	106	3665
HERSTMONCEUX, UK	RGO	7840	56	1609
AREQUIPA, PERU	ARELAS	7907	939	44344
MATERA, ITALY	MATERA	7939	289	15089
DIONYSOS, GREECE	DIOLAS	7940	6	81
ZIMMERWALD, SWIZ		7810	29	691

```
TOTAL NO. OF PASSES =   2792
TOTAL NO. OF OBSERVATIONS =   127442
```

Table 5.2.5c

DATA REDUCTION MODEL
FOR
STARLETTE DATA EDITING

GENERAL PARAMETERS

GM	$3.98600436 \times 10^{14}$ m^3/s^2
SPEED OF LIGHT	299792458.0 m/s
a_e	6378137.0 m
$1/f$	298.257
JPL EPHEMERIDES	DE-200/LE-200
ATMOSPHERIC DENSITY MODEL	JACCHIA 1971

GLOBAL PARAMETERS

GEOPOTENTIAL	PGS1331'(36 x 36)
TIDES	APRIORI TOPEX MODEL
POLAR MOTION & EARTH ROTATION	APRIORI TOPEX SERIES
STATION POSITIONS	LAGEOS SL6 SOLUTION

ARC PARAMETERS

STATE VECTOR	6
DRAG COEFFICIENT	1
SOLAR RADIATION COEFFICIENT	1
MEASUREMENT BIASES	NONE

STATION MATERA1   MEASUREMENT TYPE: RANGE   MIDPOINT TIME (YYMMDD HHMMSS): (840115 222258)

ITER	NUSED	BASE RMS	NEW RMS	BIAS	SIGMA	TIME BIAS	TIME BIAS SIGMA
1	76	4.630	4.422	-0.998508	0.114723	0.200471	0.024592
2	75	0.674	0.306	-0.482160	0.115527	0.077130	0.024806
3	75	0.674	0.306	-0.482160	0.115527	0.077130	0.024806

MBIAS 79394101 51   -0.4821605 840115221714.02840115222842.

DELETE79394101 51   840115221924.0109   840115221924.0129
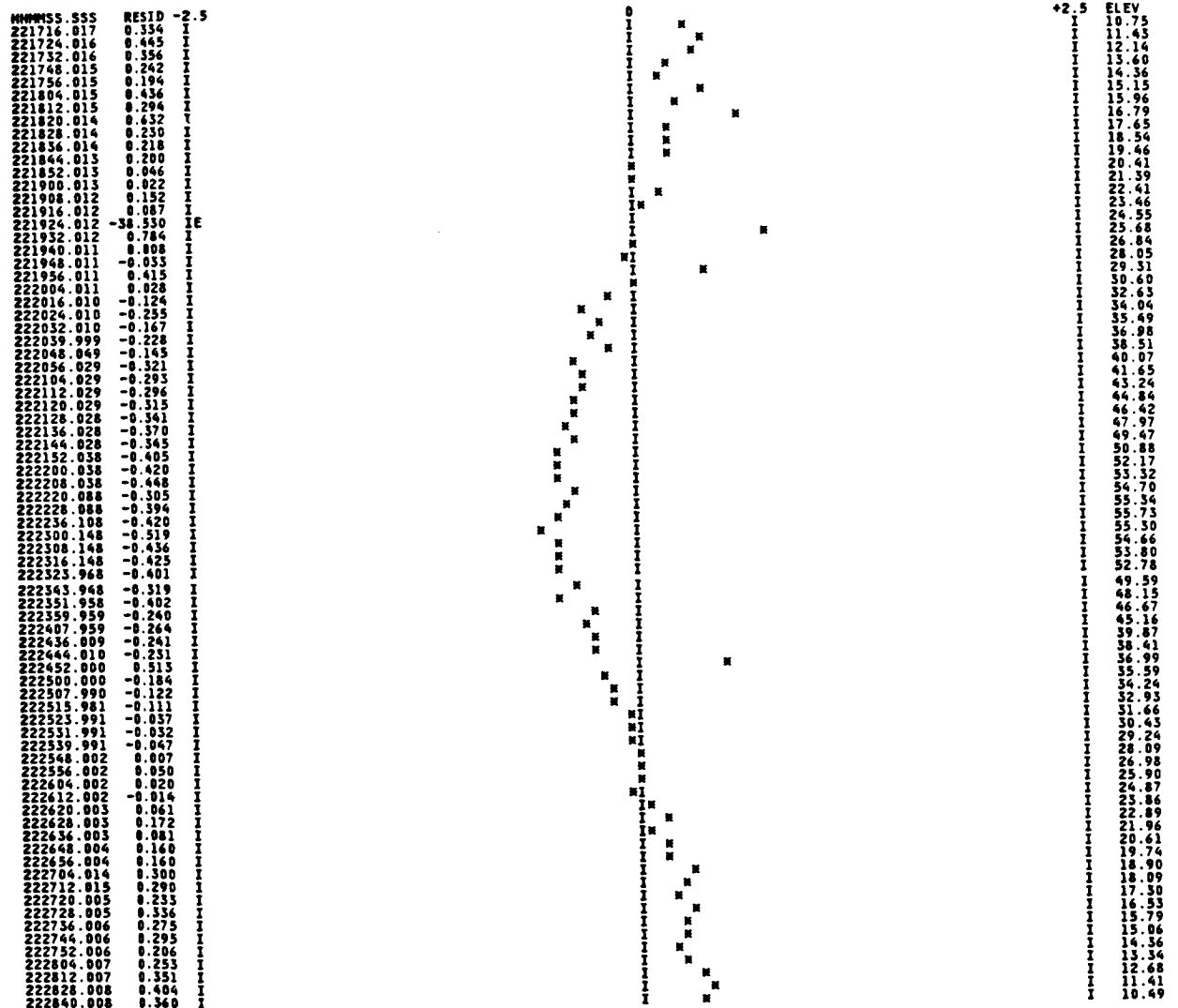
Figure 5.2.5a. Example of Residual Analysis Package Diagnostic Plot from Starlette: Matera Residuals Plotted Versus Time.

94

Table 5.2.5d. Example of Residual Analysis for Starlette Laser Passes During Period
of January 3 to 7, 1984:   Statistics Based on Apriori Model (Pgs 1331')

STANAM	ISTA	MTYPE	YYMMDD	HHMMSS	NPTS	ITER	USED	BIAS	SIGMA	T. BIAS	SIGMA	FIT RMS	BASE RMS	MAXEL
GRAZ1	78393401	RANGE	840103	12643	33	3	33	-2.041	0.178	0.539	0.080	0.157	2.211	42.6
GRAZ1	78393401	RANGE	840105	20521	46	3	46	-0.329	0.148	0.223	0.043	0.088	0.863	80.8
GRAZ1	78393401	RANGE	840105	35558	10	3	10	0.131	0.965	0.897	0.383	0.046	0.417	67.6
GRAZ1	78393401	RANGE	840106	3600	39	3	39	0.397	0.161	0.147	0.063	0.044	0.582	45.3
GRAZ1	78393401	RANGE	840106	22454	56	3	56	0.390	0.134	-0.083	0.040	0.091	0.486	81.8
GRAZ1	78393401	RANGE	840106	41448	25	3	25	0.039	0.206	-0.273	0.063	0.045	0.923	71.6
GRAZ1	78393401	RANGE	840107	5416	9	3	9	-0.048	0.821	0.337	0.388	0.049	0.861	66.0

TOTAL POINTS THIS STATION: 218
RMS OF UNADJUSTED DATA: 1.048
RMS OF ADJUSTED DATA: 0.089

STANAM	ISTA	MTYPE	YYMMDD	HHMMSS	NPTS	ITER	USED	BIAS	SIGMA	T. BIAS	SIGMA	FIT RMS	BASE RMS	MAXEL
LAGU1102	71100402	RANGE	840107	74440	16	3	16	1.157	0.324	0.178	0.078	0.274	0.993	50.6
LAGU1102	71100402	RANGE	840107	93513	34	3	34	-1.209	0.341	0.309	0.106	0.043	0.630	36.2

TOTAL POINTS THIS STATION: 50
RMS OF UNADJUSTED DATA: 0.743
RMS OF ADJUSTED DATA: 0.153

STANAM	ISTA	MTYPE	YYMMDD	HHMMSS	NPTS	ITER	USED	BIAS	SIGMA	T. BIAS	SIGMA	FIT RMS	BASE RMS	MAXEL
MATERA1	79394101	RANGE	840103	50554	81	6	77	0.153	0.114	-0.020	0.030	0.097	0.199	39.4
MATERA1	79394101	RANGE	840104	33518	64	5	61	0.585	0.129	0.087	0.033	0.219	0.684	39.2

TOTAL POINTS THIS STATION: 138
RMS OF UNADJUSTED DATA: 0.474
RMS OF ADJUSTED DATA: 0.161

STANAM	ISTA	MTYPE	YYMMDD	HHMMSS	NPTS	ITER	USED	BIAS	SIGMA	T. BIAS	SIGMA	FIT RMS	BASE RMS	MAXEL
PLATVL1	71120201	RANGE	840105	104850	40	4	38	-1.100	0.208	-0.002	0.059	0.118	1.140	41.0

TOTAL POINTS THIS STATION: 38
RMS OF UNADJUSTED DATA: 1.140
RMS OF ADJUSTED DATA: 0.118

STANAM	ISTA	MTYPE	YYMMDD	HHMMSS	NPTS	ITER	USED	BIAS	SIGMA	T. BIAS	SIGMA	FIT RMS	BASE RMS	MAXEL
QUIN1092	71090802	RANGE	840105	85703	31	3	31	0.259	0.439	-0.062	0.125	0.026	0.114	38.8
QUIN1092	71090802	RANGE	840106	91659	39	3	39	1.688	0.649	-0.349	0.147	0.065	0.444	60.5

TOTAL POINTS THIS STATION: 70
RMS OF UNADJUSTED DATA: 0.336
RMS OF ADJUSTED DATA: 0.051

STANAM	ISTA	MTYPE	YYMMDD	HHMMSS	NPTS	ITER	USED	BIAS	SIGMA	T. BIAS	SIGMA	FIT RMS	BASE RMS	MAXEL
SIMOSATA	78383601	RANGE	840105	231608	9	3	9	0.649	3.752	0.673	0.795	0.120	4.333	46.5

TOTAL POINTS THIS STATION: 9
RMS OF UNADJUSTED DATA: 4.333
RMS OF ADJUSTED DATA: 0.120

STANAM	ISTA	MTYPE	YYMMDD	HHMMSS	NPTS	ITER	USED	BIAS	SIGMA	T. BIAS	SIGMA	FIT RMS	BASE RMS	MAXEL
YARAG1	70900501	RANGE	840105	154412	72	3	72	0.178	0.118	-0.057	0.026	0.063	0.317	65.0
YARAG1	70900501	RANGE	840106	121436	54	7	49	-0.097	0.144	0.095	0.039	0.020	0.380	40.4

TOTAL POINTS THIS STATION: 121
RMS OF UNADJUSTED DATA: 0.341
RMS OF ADJUSTED DATA: 0.050

TOTAL POINTS INPUT= 658
TOTAL USED= 644
TOTAL EL CUT= 0
TOTAL OTHER EDITS= 14

NUMBER OF PASSES PROCESSED= 17
NUMBER DELETED ENTIRELY= 0

RMS OF UNADJUSTED DATA: 0.877
RMS OF ADJUSTED DATA: 0.108

C-3

Table 5.2.5e. Post Fit Residual Analysis for Starlette Laser Passes During Period of January 3 to 7, 1984: Statistics Based on Pgs–T2.

STANAM	ISTA	MTYPE	YYMMDD	HHMMSS	NPTS	ITER	USED	BIAS	SIGMA	T. BIAS	SIGMA	FIT RMS	BASE RMS	MAXEL
GRAZ1	78393401	RANGE	840103	12643	33	2	33	-0.087	0.178	0.104	0.080	0.049	0.242	42.6
GRAZ1	78393401	RANGE	840105	20521	46	2	46	-0.397	0.148	-0.041	0.043	0.080	0.428	80.8
GRAZ1	78393401	RANGE	840105	35558	10	2	10	0.115	0.960	-0.038	0.381	0.046	0.064	67.6
GRAZ1	78393401	RANGE	840106	3600	39	2	39	0.024	0.161	-0.122	0.063	0.028	0.320	45.3
GRAZ1	78393401	RANGE	840106	22454	56	2	56	-0.092	0.134	-0.019	0.040	0.047	0.126	81.8
GRAZ1	78393401	RANGE	840106	41448	25	2	25	-0.199	0.206	-0.103	0.063	0.069	0.454	71.6
GRAZ1	78393401	RANGE	840107	5416	9	2	9	-0.303	0.818	-0.056	0.386	0.049	0.233	64.0

TOTAL POINTS THIS STATION: 218
RMS OF UNADJUSTED DATA: 0.302
RMS OF ADJUSTED DATA: 0.055

STANAM	ISTA	MTYPE	YYMMDD	HHMMSS	NPTS	ITER	USED	BIAS	SIGMA	T. BIAS	SIGMA	FIT RMS	BASE RMS	MAXEL
LAGU1102	71100402	RANGE	840107	74440	16	2	16	-0.231	0.324	-0.001	0.078	0.094	0.262	50.6
LAGU1102	71100402	RANGE	840107	93513	34	2	34	-0.042	0.341	-0.026	0.106	0.036	0.130	36.2

TOTAL POINTS THIS STATION: 50
RMS OF UNADJUSTED DATA: 0.177
RMS OF ADJUSTED DATA: 0.059

STANAM	ISTA	MTYPE	YYMMDD	HHMMSS	NPTS	ITER	USED	BIAS	SIGMA	T. BIAS	SIGMA	FIT RMS	BASE RMS	MAXEL
MATERA1	79394101	RANGE	840103	50540	76	2	76	0.158	0.115	-0.018	0.030	0.095	0.201	39.4
MATERA1	79394101	RANGE	840104	33518	61	3	60	0.136	0.130	0.023	0.033	0.118	0.196	39.2

TOTAL POINTS THIS STATION: 136
RMS OF UNADJUSTED DATA: 0.198
RMS OF ADJUSTED DATA: 0.105

STANAM	ISTA	MTYPE	YYMMDD	HHMMSS	NPTS	ITER	USED	BIAS	SIGMA	T. BIAS	SIGMA	FIT RMS	BASE RMS	MAXEL
PLATVL1	71120201	RANGE	840105	104855	38	2	38	-0.237	0.208	0.084	0.059	0.073	0.254	41.0

TOTAL POINTS THIS STATION: 38
RMS OF UNADJUSTED DATA: 0.254
RMS OF ADJUSTED DATA: 0.073

STANAM	ISTA	MTYPE	YYMMDD	HHMMSS	NPTS	ITER	USED	BIAS	SIGMA	T. BIAS	SIGMA	FIT RMS	BASE RMS	MAXEL
QUIN1092	71090802	RANGE	840105	85703	31	2	31	0.103	0.438	0.058	0.125	0.026	0.312	38.8
QUIN1092	71090802	RANGE	840106	91659	39	2	39	0.270	0.648	-0.035	0.147	0.032	0.135	60.5

TOTAL POINTS THIS STATION: 70
RMS OF UNADJUSTED DATA: 0.227
RMS OF ADJUSTED DATA: 0.029

STANAM	ISTA	MTYPE	YYMMDD	HHMMSS	NPTS	ITER	USED	BIAS	SIGMA	T. BIAS	SIGMA	FIT RMS	BASE RMS	MAXEL
SIMOSATA	78383601	RANGE	840105	231608	9	2	9	-0.656	3.303	-0.364	0.743	0.117	2.691	46.3

TOTAL POINTS THIS STATION: 9
RMS OF UNADJUSTED DATA: 2.691
RMS OF ADJUSTED DATA: 0.117

STANAM	ISTA	MTYPE	YYMMDD	HHMMSS	NPTS	ITER	USED	BIAS	SIGMA	T. BIAS	SIGMA	FIT RMS	BASE RMS	MAXEL
YARAG1	70900501	RANGE	840105	134412	72	2	72	-0.031	0.118	-0.015	0.026	0.040	0.088	65.0
YARAG1	70900501	RANGE	840106	121436	53	2	53	-0.158	0.138	0.046	0.038	0.047	0.252	40.4

TOTAL POINTS THIS STATION: 125
RMS OF UNADJUSTED DATA: 0.175
RMS OF ADJUSTED DATA: 0.043

TOTAL POINTS INPUT= 647
TOTAL USED= 646
TOTAL EL CUT= 0
TOTAL OTHER EDITS= 1

NUMBER OF PASSES PROCESSED= 17
NUMBER DELETED ENTIRELY= 0

RMS OF UNADJUSTED DATA: 0.367
RMS OF ADJUSTED DATA: 0.067

Table 5.2.5f

STARLETTE RESIDUAL STATISTICS SUMMARY

APRIORI MODEL (PGS 1331')

STANAM	ISTA	MTYPE	YYMMDD	HHMMSS	NPTS	ITER	USED	BIAS	SIGMA	T. BIAS	SIGMA	FIT RMS	BASE RMS	MAXEL
GRAZ1	78393401	RANGE	840103	12643	33	3	33	-2.041	0.178	0.539	0.080	0.157	2.211	42.6
GRAZ1	78393401	RANGE	840105	20521	46	3	46	-0.329	0.148	0.223	0.043	0.088	0.883	80.8
GRAZ1	78393401	RANGE	840105	35558	10	3	10	0.131	0.965	0.097	0.383	0.046	0.417	67.6
GRAZ1	78393401	RANGE	840106	3600	39	3	39	0.397	0.161	0.147	0.063	0.044	0.582	45.3
GRAZ1	78393401	RANGE	840106	22454	56	3	56	0.390	0.134	-0.083	0.040	0.091	0.486	81.8
GRAZ1	78393401	RANGE	840106	41448	25	3	25	0.039	0.206	-0.273	0.063	0.045	0.923	71.6
GRAZ1	78393401	RANGE	840107	5416	9	3	9	-0.048	0.821	0.337	0.388	0.049	0.861	64.0
LAGU1102	71100402	RANGE	840107	74440	16	3	16	1.157	0.324	0.178	0.078	0.276	0.993	50.6
LAGU1102	71100402	RANGE	840107	93513	34	3	34	-1.209	0.341	0.309	0.106	0.043	0.630	36.2
MATERA1	79394101	RANGE	840103	50554	81	6	77	0.153	0.114	-0.020	0.030	0.097	0.199	39.4
MATERA1	79394101	RANGE	840104	33518	64	5	61	0.585	0.129	0.087	0.033	0.219	0.684	39.2
PLATVL1	71120201	RANGE	840105	104850	40	4	38	-1.100	0.208	-0.002	0.059	0.118	1.140	41.0
QUIN1092	71090802	RANGE	840105	85703	31	3	31	0.259	0.439	-0.062	0.125	0.026	0.114	38.8
QUIN1092	71090802	RANGE	840106	91659	39	3	39	1.688	0.649	-0.349	0.147	0.065	0.444	60.5
SIMOSATA	78383601	RANGE	840105	231608	9	3	9	0.649	3.752	0.673	0.795	0.120	4.333	46.3
YARAG1	70900501	RANGE	840105	134412	72	3	72	0.178	0.118	-0.057	0.026	0.063	0.317	65.0
YARAG1	70900501	RANGE	840106	121436	54	7	49	-0.097	0.144	0.095	0.039	0.020	0.380	40.4

TOPEX MODEL PGS - T2

STANAM	ISTA	MTYPE	YYMMDD	HHMMSS	NPTS	ITER	USED	BIAS	SIGMA	T. BIAS	SIGMA	FIT RMS	BASE RMS	MAXEL
GRAZ1	78393401	RANGE	840103	12643	33	2	33	-0.087	0.178	0.104	0.080	0.049	0.242	42.6
GRAZ1	78393401	RANGE	840105	20521	46	2	46	-0.397	0.148	-0.041	0.043	0.080	0.428	80.8
GRAZ1	78393401	RANGE	840105	35558	10	2	10	0.115	0.960	-0.038	0.381	0.046	0.064	67.6
GRAZ1	78393401	RANGE	840106	3600	39	2	39	0.024	0.161	-0.122	0.063	0.028	0.320	45.3
GRAZ1	78393401	RANGE	840106	22454	56	2	56	-0.092	0.134	-0.019	0.040	0.047	0.126	81.8
GRAZ1	78393401	RANGE	840106	41448	25	2	25	-0.199	0.206	-0.103	0.063	0.069	0.454	71.6
GRAZ1	78393401	RANGE	840107	5416	9	2	9	-0.303	0.818	-0.056	0.386	0.049	0.233	64.0
LAGU1102	71100402	RANGE	840107	74440	16	2	16	-0.231	0.324	-0.001	0.078	0.094	0.262	50.6
LAGU1102	71100402	RANGE	840107	93513	34	2	34	-0.042	0.341	-0.026	0.106	0.036	0.130	36.2
MATERA1	79394101	RANGE	840103	50540	76	2	76	0.158	0.115	-0.018	0.030	0.095	0.201	39.4
MATERA1	79394101	RANGE	840104	33518	61	2	60	0.156	0.130	0.023	0.033	0.118	0.196	39.2
PLATVL1	71120201	RANGE	840105	104855	38	2	38	-0.237	0.208	0.084	0.059	0.073	0.254	41.0
QUIN1092	71090802	RANGE	840105	85703	31	2	31	0.103	0.434	0.058	0.125	0.026	0.312	38.8
QUIN1092	71090802	RANGE	840106	91659	39	2	39	0.278	0.648	-0.035	0.147	0.032	0.135	60.5
SIMOSATA	78383601	RANGE	840105	231608	9	2	9	-0.656	3.503	-0.364	0.743	0.117	2.691	46.3
YARAG1	70900501	RANGE	840105	134412	72	2	72	-0.031	0.118	-0.015	0.026	0.040	0.088	65.0
YARAG1	70900501	RANGE	840106	121436	53	2	53	-0.158	0.138	0.046	0.058	0.047	0.252	40.4

detailed picture of the individual 5-day arc normal equations is shown in Table 5.2.5g. The STARLETTE normal equations allowed for the adjustment of geopotential harmonics, the selected subset of tidal coefficients, the Earth orientation parameters, the station positions, and the orbital arc parameters. The 46 matrices were subsequently combined (after the elimination of the arc parameters) into a single matrix, the STARLETTE C-mat. This allowed for an easier combination and weighting of the data. The RMS of fit values from Table 5.2.5g are shown pictorially in Figure 5.2.5b.

Forty six five-day arcs of recent (1984) STARLETTE laser ranging data have been analyzed. The resulting normal equations have contributed in the determination of the latest interim TOPEX model, GEM-T1. Extensive data editing and a general overhauling of the physical and mathematical models used in this analysis resulted in a remarkably improved performance of these data. This is very encouraging in light of the fact that the altitude of STARLETTE is relatively low and its orbit is strongly influenced by gravity and tidal perturbations. Its sensitivity to these forces however, coupled with the robustness of the edited data set and STARLETTE's orbital similarities with TOPEX make its contribution to the solution a very important one.

5.2.6 Analysis of LAGEOS Laser Ranging Observations

The utilization of Satellite Laser Ranging for monitoring the earth's motions (both tectonic and rotational) has been greatly enhanced by the May, 1976 launch of the LAGEOS satellite. LAGEOS stands for the LAser GEOdynamics Satellite and is the first NASA satellite to be launched exclusively to serve as a space-based laser target. The nominal orbital characteristics for LAGEOS are described in Table 5.2.6a. The high altitude of the LAGEOS orbit reduces errors arising from short-wavelength gravity, tidal and drag effects, leaving a strong

Table 5.2.5g

EMAT SUMMARY FOR STARLETTE

EPOCH	NUMBER OF OBSERVATIONS	WEIGHTED RMS (m)	NUMBER OF STATIONS	ARGUMENT OF PERIGEE (AT EPOCH)
840102	633	.5736	7	328.219
840107	682	.5172	9	343.032
840112	1043	.6436	10	1.779
840117	1012	.7107	10	17.217
840122	2270	.4651	9	32.676
840127	958	.4331	10	50.280
840201	847	.3903	7	64.865
840206	1499	.5625	8	83.486
840211	398	.6710	6	97.697
840216	338	.4215	5	113.218
840221	502	.8665	8	129.760
840226	841	.7439	7	144.077
840302	451	.8990	5	162.843
840312	716	.6586	5	194.533
840317	741	.4125	6	212.022
840322	1289	.6363	9	227.683
840327	1971	.5744	8	247.627
840401	2069	.5924	7	262.668
840406	2212	.5219	6	279.917
840411	3084	.5851	8	297.023
840416	827	.6289	8	312.347
840421	1437	.6480	7	332.052
840426	893	.8068	9	347.073
840501	619	.5879	5	4.323
840506	874	.8000	4	20.754
840511	905	.7750	4	36.110
840516	574	.6051	8	54.741
840521	2250	.7150	8	68.645
840526	1437	.7178	8	85.147
840531	2012	.6031	8	100.373
840605	1279	.5656	11	115.013
840610	2160	.7684	10	133.685
840615	2323	.5638	12	148.093
840620	1480	.5611	9	165.902
840625	3451	.6866	10	181.369
840630	1429	.4409	8	197.607
840705	1197	.6200	7	216.576
840710	550	.4866	5	231.370
840715	486	.5503	5	249.614
840720	824	.7427	4	265.374
840725	350	.4617	3	281.668
840730	754	.4867	5	301.339
840804	749	.6397	6	316.584
840809	921	.5161	7	335.486
840814	1170	.5073	8	350.581
840819	2849	.4891	8	7.096
46 EMRTS	57356	.6120		

STARLETTE E-MAT SUMMARY
WEIGHTED RMS
(APRIORI)
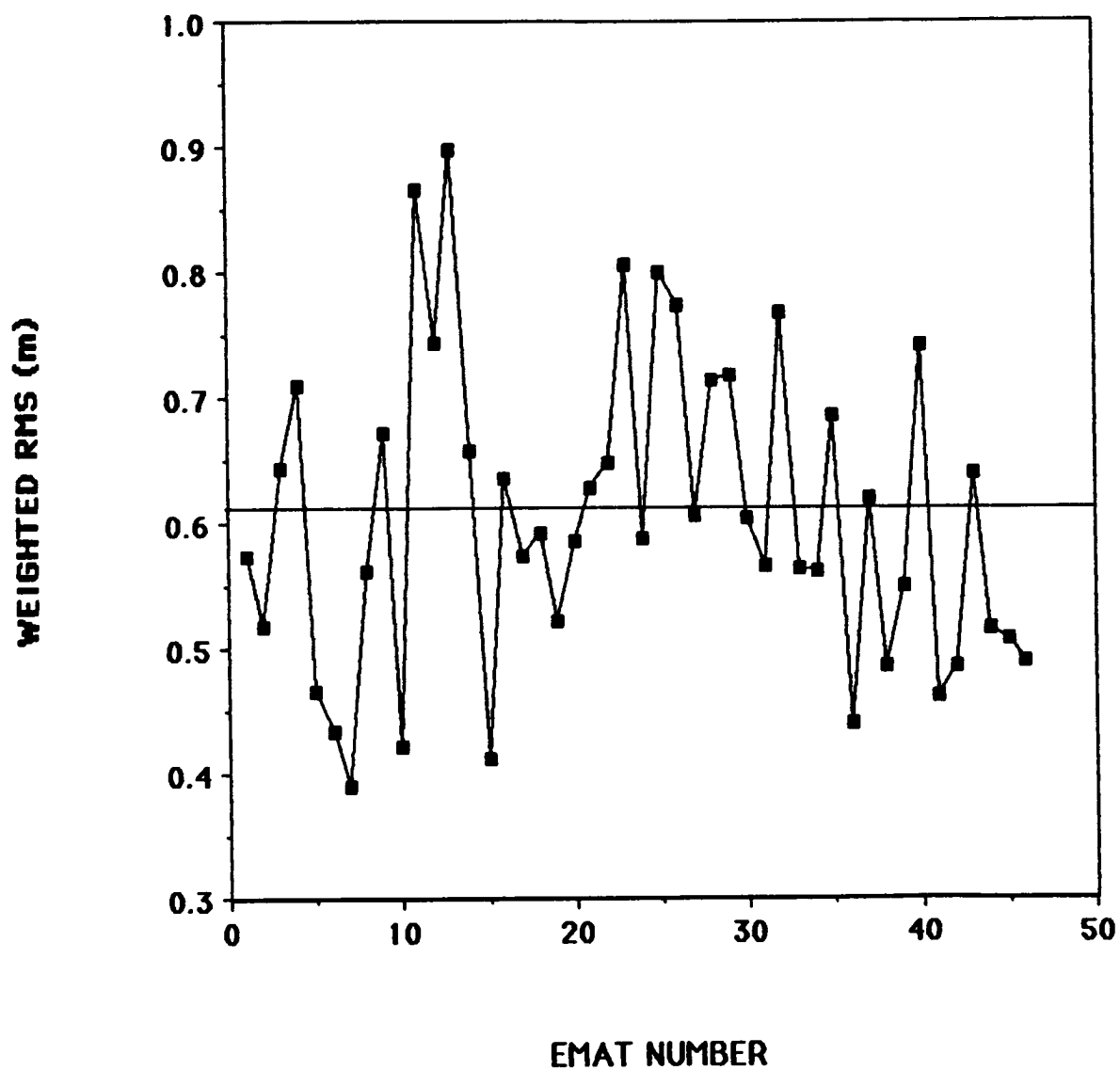
Figure 5.2.5b. STARLETTE E-MAT Summary.

signal for the longest wavelength portion of the gravitional field. Furthermore, by being extremely dense and having a perfectly spherical shape (see figure 5.2.6a), LAGEOS also minimizes errors arising from non- conservative forces like solar radiation pressure and albedo re- radiation. Therefore, LAGEOS is an ideal satellite for improving the determination of the long wavelength gravity field. A significant distinction of LAGEOS over previous laser satellite missions is the extensive international cooperation which has occured to enhance global laser coverage. There is now a worldwide network of third generation laser stations which is tracking LAGEOS as their highest priority target. These constitute the largest and best distributed set of laser observations which have ever been collected. In our present analysis, 5 years of laser data acquired on LAGEOS have been used in the GEM-T1 solution. These ranges have been condensed into laser "normal-points" at two minute intervals. The time span selected contains the most outstanding set of these data encompassing the years 1980 through to the end of 1984. The NASA mobile laser systems were first deployed in late 1979 so early data sets are somewhat unsatisfactory. The additional data from 1985, which is now available, will be added to the solution over the next year. It is desirable to have at least six years of these observations in our gravity solutions. Six years of tracking is somewhat important because it corresponds to the beat period of the two dominant polar motion terms, that of the annual and Chandler periods. And LAGEOS data make a strong contribution to the definition of the pole obtained within our solution. The LAGEOS data were reduced in monthly arc lengths with a solar radiation pressure and along track acceleration parameter allowed to adjust along with the epoch state elements. These observations were carefully edited, and post-processing analysis of these data indicate RMS of fits for monthly arcs of between 4.5 to 10 cm. A summary of the LAGEOS arcs used to generate the normal equations is presented in Table 5.2.6b.
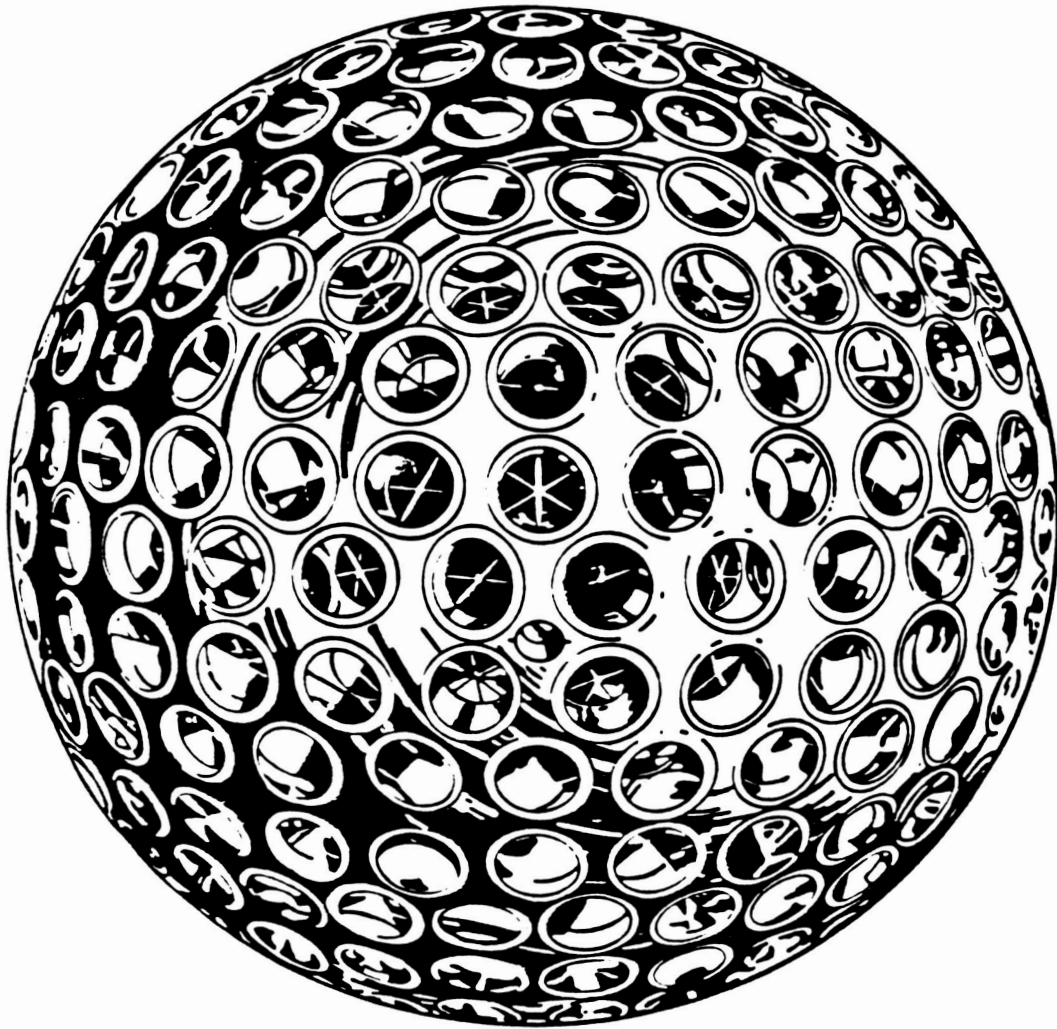
Figure 5.2.6. LAGEOS Satellite.

Table 5.2.6a

LAGEOS
(LASER GEODYNAMICS SATELLITE)

Launch: May 4, 1976

Spacecraft: Spherical, 60 cm diameter
406.965 kg
426 laser retro-reflectors, 3.8 cm diameter

Orbit:

Semi-major axis	12265 km
Inclination	109.8 degrees
Eccentricity	0.004
Perigee height	5858 km
Apogee height	5958 km
Node rate	+0.343 deg/day
Perigee rate	-0.214 deg/day
Semi-major axis rate	-1.1 mm/day

Table 5.2.6b

EMAT SUMMARY FOR LAGEOS

EPOCH	NUMBER OF OBSERVATIONS	WEIGHTED RMS (m)	NUMBER OF STATIONS	ARGUMENT OF PERIGEE (AT EPOCH)
791230	1455	.2065	13	345.174
800129	2319	.2210	14	338.042
800228	2639	.2475	14	330.814
800329	2231	.2228	14	321.579
800428	1543	.2396	10	311.512
800528	1926	.2336	9	313.865
800702	1801	.2241	13	297.302
800801	3187	.2237	13	290.785
800831	3496	.1934	16	287.046
800930	3336	.2088	18	281.014
801030	2751	.2191	14	271.071
801129	1413	.2022	11	260.453
801229	794	.1736	8	255.325
810128	1287	.1784	9	253.457
810227	2739	.1787	13	240.940
810329	1943	.1913	11	232.084
810428	1884	.2057	9	226.531
810528	1944	.2512	11	221.412
810627	2187	.2555	12	217.269
810727	2168	.1948	13	201.207
810826	2821	.2065	14	199.978
810925	3143	.2308	16	194.745
811025	1972	.2095	12	188.166
811124	1573	.2126	12	181.017
811224	1314	.3018	12	168.490
820123	1878	.2427	12	172.349
820222	1883	.2125	15	162.371
820329	1926	.2007	12	153.177
820428	3084	.2055	12	148.207
820602	2488	.1811	11	142.263
820702	2980	.2022	11	134.020
820801	2027	.2197	13	126.356
820831	2720	.2154	14	127.720
820930	3596	.1788	15	118.145
821030	1938	.1604	12	110.051
821129	2041	.1788	11	104.642
821229	1699	.1990	11	101.347

LAGEOS *CONTD....*

EPOCH	NUMBER OF OBSERVATIONS	WEIGHTED RMS (m)	NUMBER OF STATIONS	ARGUMENT OF PERIGEE (AT EPOCH)
830128	1494	.2204	12	97.008
830227	2010	.2378	14	87.259
830329	2187	.2079	14	79.935
830428	2405	.2180	13	79.208
830627	1920	.1511	8	64.706
830727	2751	.1796	8	57.853
830831	2520	.1425	11	54.654
830930	3761	.1760	17	48.845
831030	3177	.2306	17	36.054
831229	2729	.2583	17	30.879
840128	2425	.2172	16	23.527
840227	2437	.2519	22	16.220
840329	3817	.2267	20	9.126
840428	4129	.2554	22	1.119
840528	4541	.2468	20	3.869
840627	4372	.2724	19	349.233
840801	4857	.2617	22	344.696
840831	4611	.2408	21	338.433

LAGEOS E-MAT SUMMARY
WEIGHTED RMS
(APRIORI)
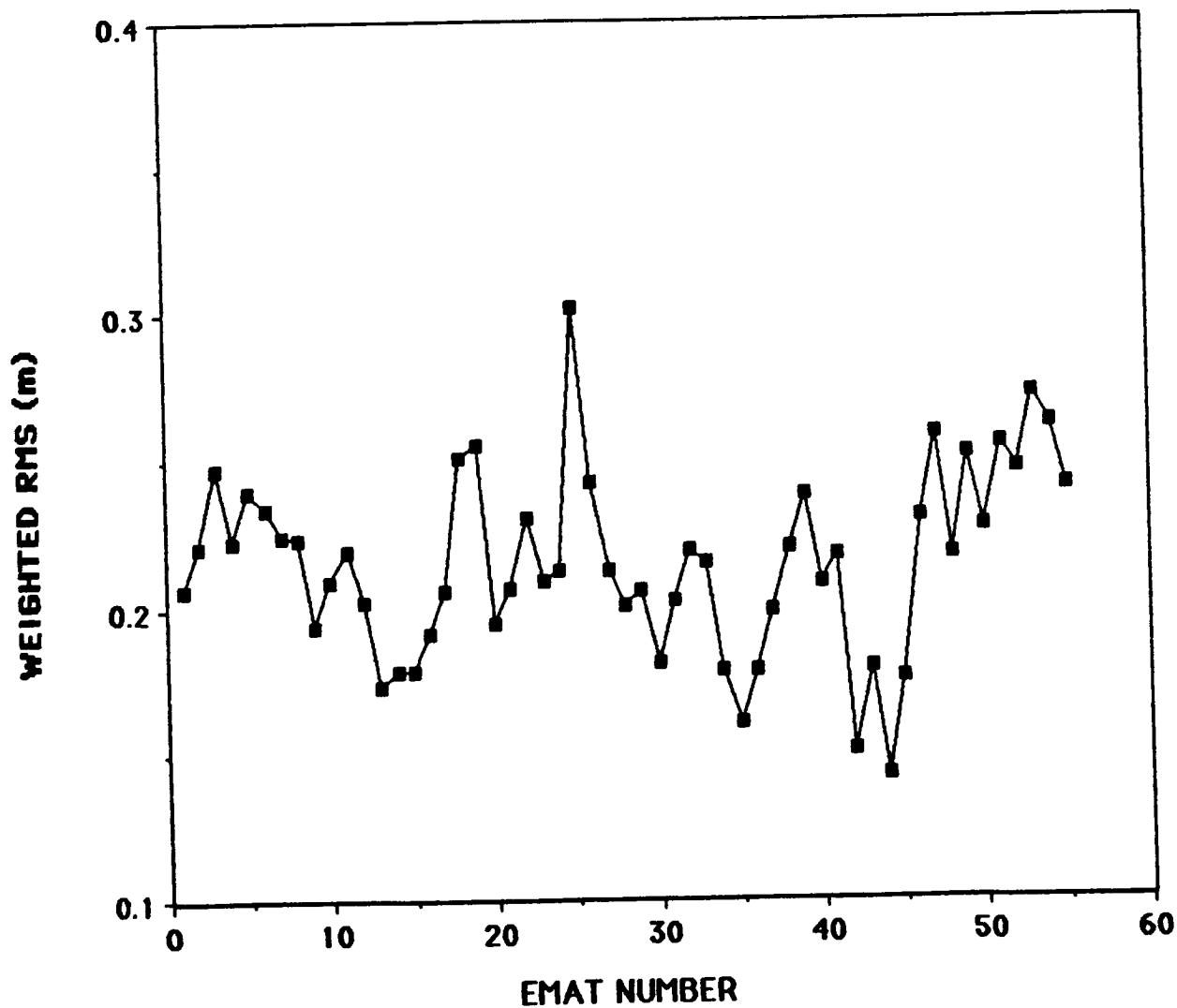
Figure 5.2.6b. LAGEOS E-MAT Summary.

5.2.7 Analysis of GEOS-2 Laser Tracking Data

The GEOS-2 satellite was launched on April 28, 1968. This satellite was one of the earliest geodetic missions initiated by NASA and served several purposes. First and foremost, GEOS-2 carried flashing lamps which allowed it to be photographed (as was GEOS-1) by a globally distributed network of optical observatories. The National Geodetic Satellite Program had an objective to unify the world's tracking datums to the 5 to 10 m level of uncertainty with respect to the geocenter. This was to be accomplished through an accurate reduction of these satellite photographic positions for use in solutions (both geometric and dynamic) of camera locations within a global reference system. It was an analysis of these early observations (NASA, 1977; Marsh et al, 1973) which satisfied the NGSP objectives. Of secondary interest was the calibration of NASA's Minitrack Network. Cameras were located at all of the worldwide Minitrack installations and the direction cosines obtained by these electronic fences were calibrated against those simultaneous right ascension and declination measurements acquired photographically. Fortunately, GEOS-2 also carried corner cubes and served as a target of opportunity for early laser ranging experiments.

The characteristics of the GEOS-2 orbit are given in Table 5.2.7a. GEOS-2 was intermittently tracked on a low priority basis by the lasers for much of the 1970's. Tracking apparently ceased in the middle of 1977. We thereby had a sparse data set to utilize for gravity modeling investigations from third generation laser systems which started to appear in the 1975 timeframe. Consequently, after an evaluation of data catalogues, we found only a limited number of possible arcs for GEOS-2. To have a reasonably large sample, we were forced to use the 1975 SAO data although these systems were not upgraded until late 1975 to early 1976. Some of the earlier 1975 SAO data was found to have range biases which were seen to be a function of range. The SAO

data taken during 1975 were heavily edited, but a subset of them were found to be satisfactory for inclusion in our GEM-T1 solution.

Five day arc lengths were used in the GEOS-2 data reduction and normal equation solutions. In these arcs, a drag parameter per day, a solar radiation coefficient per arc and the orbital state were all permitted to adjust. The normal equations for 28 of these arcs were generated and are summarized in Table 5.2.7b. Note that even when including SAO lasers in many of the 1975 arcs, only 3 or 4 stations were tracking over this time period.

Table 5.2.7a

Orbital Characteristics of GEOS-2

Apogee Height	1569 km
Perigee Height	1077 km
Eccentricity	0.03
Inclination	105.8 degrees
Anomalistic Period	112.1 minutes

5.2.8 Analysis of Optical and Low Inclination Satellite Observations

The optical observations acquired by a global network of predominantly SAO Baker Nunn observatories were the state-of-the-art in satellite tracking throughout the 1960's. A reasonable data set was acquired for over 60 satellites, rocket bodies, fragments, and space-borne balloons of this era. These observations provided the data base for the first comprehensive satellite-based gravity solution, that of the Smithsonian Astrophysical Observatory in 1966. Surprisingly, these observations are still making important contributions to the gravity solution even though they have an observational noise which is four orders of magnitude greater than that which is obtained by the best laser tracking of the 1980's.

Table 5.2.7b

EMAT SUMMARY FOR GEOS-2

EPOCH	NUMBER OF OBSERVATIONS	WEIGHTED RMS (m)	NUMBER OF STATIONS	ARGUMENT OF PERIGEE (AT EPOCH)
750708	595	1.3994	4	55.162
750803	638	1.6999	3	14.673
750815	472	1.0250	3	354.021
750825	732	.8124	5	337.992
750901	416	1.0606	4	327.452
750906	573	.6148	5	319.665
750915	357	1.5540	5	301.713
750923	785	1.8013	5	289.163
751006	475	1.4644	4	268.194
751021	923	1.1042	4	244.037
751027	1351	2.1442	6	233.716
751102	1204	2.0522	6	223.079
760829	544	1.4113	5	95.276
760927	894	2.0713	5	49.825
761009	1435	1.6547	4	33.373
761019	1184	1.7588	7	17.469
761025	1389	1.9487	7	7.638
761103	1418	1.9838	6	349.358
761108	1364	1.0963	7	341.704
761115	1475	1.2160	7	331.432
770120	701	1.5675	5	222.343
770320	784	1.4755	6	125.612
770403	1412	1.2887	6	103.939
770409	1277	1.5900	5	95.076
770425	1040	1.4304	3	70.440
770430	881	1.1608	3	59.898
770607	1196	1.2060	6	1.945
770613	1098	1.6737	4	351.478

The reason for this importance is found in the diversity of objects which have been optically tracked. Any given satellite orbit samples the earth's gravity field in a way which causes it to sense certain perturbative frequencies. Each of these perturbations may be mathematically described as some linear combination of the spherical harmonics used to represent the gravity field. These sums (or "lumped-harmonics") can be very accurately determined although they are satellite specific. Past experience has shown that data analyzed on many orbits over a wide range of inclinations and mean motions yield a sufficiently large set of "lumped harmonics" to permit an accurate deconvolution of this signal into well determined individual spherical harmonic coefficients comprising a global gravity model. The optical satellites continue to play an important role in filling in the inclination gaps found within the data sets available from other tracking systems. In point of fact, the optical satellites are one of the best sources of gravity information for low inclination objects. Results will be discussed later showing the very important role these observations have in resolving accurate values for the zonal harmonic terms (m=0 coefficients). Initially, six optically tracked satellites, only one of which was exclusively camera tracked, were selected for inclusion in the gravity solution. These satellites were : ANNA-1B, TELESTAR-1, BE-B, BE-C, GEOS-1 and GEOS-2. TELESTAR-1 is solely an optical satellite. While tracking data for them exists from other systems, only optical data for ANNA-1B and BE-B have been used at present to obtain GEM-T1. ANNA-1B's Doppler tracking and the very limited laser data taken on BE-B are yet to be used. Both of the GEOS satellites flew flashing lamps which permitted unlimited nighttime visibility for observing instruments. The flashing lamp data sets from the two GEOS were much more robust than those from the other four satellites. These other satellites were passively observed, requiring solar illumination of the objects against a dark sky. Therefore, data collection was restricted to the dusk period or before dawn.

A summary of the data, RMS of fit, perigee coverage and number of stations found in each of the optical arcs are shown in tables 5.2.8a through 5.2.8f. These data comprised the total optical data set found in the PGS-T2 field (Marsh et al, 1986) which is a precursor of GEM-T1.

The optical data have a precision of approximately two seconds of arc. The weighted observation residuals (whose RMS values are given in Tables 5.2.8a to 5.2.8f) were calculated as:

declination: $$\Delta\delta_W = \frac{\Delta\delta}{2}$$

right ascension: $$\Delta\alpha_W = \left| \frac{\Delta\alpha}{2} \right| \cos\delta$$

where

$\Delta\delta$, $\Delta\alpha$ are the observation residuals in declination and right ascension from the orbital fit, and

$\Delta\delta_W$, $\Delta\alpha_W$ are their corresponding weighted residuals.

Figure 5.2.8a presents the uncertainties for the PGS-T2 field obtained from a scaled covariance of the solution. These values can be compared to figure 5.2.8b which is a similiar result from the GEM-L2 field. What is strikingly different between the two sets of uncertainties is the degradation of the accuracy for the zonal harmonics within PGS-T2. This degradation is confirmed when the values for the zonals are compared to those found in GEM-L2. The (PGS-T2) minus (GEM-L2) zonal harmonic differences are many times greater than the uncertainty in the GEM-L2 determination of these terms (see Figure 5.2.8c). Therefore, we concluded that an inadequate coverage of orbital inclinations was used in obtaining PGS-T2 with significiant information being absent from low inclination objects.

ERRORS X 10⁹ — rendered as $\text{ERRORS} \times 10^{9}$

DEGREE	RMS	ORDER 0	1	2	3	4	5	6	7	8	9	10	11	12	13	14	15	16	17	18	19	20	21	22	23	24	25	26	27	28	29	30	31	32	33	34	35	36
2	1	1	2	1																																		
3	1	0	1	1	1																																	
4	2	3	3	3	3	3																																
5	3	3	4	4	3	3	3																															
6	4	6	6	5	5	5	5	3																														
7	6	8	7	6	7	6	6	5	3																													
8	7	12	13	11	9	9	8	8	7	3																												
9	9	14	12	13	11	11	9	9	8	6	5																											
10	10	16	17	15	12	12	11	11	10	10	8	5																										
11	11	17	16	18	14	14	13	13	12	11	10	8	5																									
12	12	18	18	19	17	16	15	15	13	12	11	10	9	2																								
13	11	17	17	18	18	17	15	14	13	13	11	10	10	10	1																							
14	11	16	16	17	17	16	14	13	13	12	11	11	11	11	10	2																						
15	10	14	15	16	16	15	13	12	12	12	11	11	11	11	11	11	3																					
16	10	13	14	15	15	14	12	11	11	11	10	10	11	11	12	11	11	5																				
17	10	11	13	14	14	13	11	10	11	10	10	10	10	10	10	8	9	7	6																			
18	9	10	12	13	13	12	10	10	10	10	9	9	9	9	8	7	6	6	6	7																		
19	9	10	11	12	12	11	10	9	9	9	9	9	8	8	7	7	6	6	6	7	10																	
20	9	9	11	11	11	11	9	9	9	9	8	8	7	7	7	7	6	6	6	7	8	13																
21	8	9	10	11	11	10	9	8	8	8	7	7	7	7	7	6	6	7	7	8	10	11	11															
22	8	8	10	10	10	10	9	8	8	7	7	7	7	6	6	6	6	6	7	8	9	11	12															
23	7	7	9	9	9	9	8	7	7	7	6	6	6	6	6	5	6	6	7	7	10	10	11															
24	7	7	8	8	8	8	7	7	7	6	6	6	6	6	5	5	6	6	7	8	11	11																
25	7	6	8	8	8	8	7	6	6	6	6	5	5	5	5	5	5	6	6	8	8																	
26	7	6	7	7	7	7	6	6	6	6	5	5	5	5	5	5	5	5	7	7																		
27	6	6	7	7	7	7	6	6	6	5	5	5	5	5	4	5	3																					
28	6	5	6	6	6	6	5	5	5	5	4	4	4	4	5	5																						
29	6	5	6	6	6	6	5	5	5	4	4	4	3	3	3																							
30	5	5	6	6	6	6	5	5	4	4	4	5	4																									
31	5	5	6	6	6	6	5	5	4	4	5	5																										
32	5	5	6	6	6	6	5	5	4	5	5																											
33	5	5	6	6	6	6	5	6	6	6	5																											
34	5	5	6	6	6	6	6	6	6	5																												
35	5	5	6	6	6	6	6	5	5																													
36	5	5	5	5	5	5	5																															
RMS		10	10	11	11	11	10	9	9	8	8	7	6	5	4	4	5	6	6	7	7	7	7	6	6	6	6	5	4	4	5	5	6	6	6	6	6	5

Figure 5.2.8a. Estimated Errors for PGS–T2 Coefficients.

112

ERRORS X 10⁹

Figure 5.2.8b. Estimated Errors for GEM-L2 Coefficients.

RMS	DEGREE	0	1	2	3	4	5	6	7	8	9	10	11	12	13	14	15	16	17
1	2	1	1	2															
3	3	4	3	2	4														
3	4	4	4	6	3	5													
6	5	6	6	6	7	9	5												
5	6	7	8	11	6	8	3	6											
9	7	9	7	10	13	10	9	4	9										
8	8	8	11	16	18	7	7	11	8	9									
13	9	12	12	14	14	12	14	8	10	6	10								
11	10	10	15	21	22	18	17	14	9	9	11	15							
15	11	15	16	17	19	17	15	12	13	11	10	5							
13	12	11	17	20	20	19	14	17	11	12	11	11							
15	13	14	18	17	20	18	16	15	11	13	6								
15	14	14	15	15	18	20	18	14	15	14									
14	15	13	18	18	16	16	18	15	14	14									
13	16	14	15	19	19	19	17	15	15										
14	17	12	17	15	15	18	18	14	14										
14	18	14	15	18	17	18	18	15	14										
13	19	12	16	16	16	17	17	14	13										
13	20	12	15	16	15	16	16												
11	21	11	14	15	13														
11	22	11	13	13															
9	23																		
11	24																		
12	25																		
6	26																		
9	27																7	11	
7	28																1	7	
8	29																7		
2	30																		2

ORDER: 0 1 2 3 4 5 6 7 8 9 10 11 12 13 14 15 16 17 18 19 20 21 22 23 24 25 26 27 28

RMS: 4 11 14 15 15 15 14 12 13 11 11 6 4 6 9 13 14 13 17 0 0 0 0 0 6 9 5

Figure 5.2.8c. Zonal Coefficients.

114

Table 5.2.8a

ANNA-1B OPTICAL 7-DAYS ARCS

NO.	EPOCH	NO. OF OBS.	WEIGHTED RMS ARCSEC/2	NO. OF STATIONS	ARGUMENT OF PERIGEE (AT EPOCH)
1	621101	157	1.294	9	207.7
2	621115	126	1.413	10	248.1
3	621122	154	1.212	6	274.3
4	621129	158	1.221	9	294.2
5	621213	258	1.201	10	343.6
6	621220	262	1.155	11	358.1
7	631107	64	1.149	4	228.4
8	631114	98	1.109	10	245.9
9	631121	78	1.479	9	269.3
10	631128	36	1.028	6	295.7
11	631205	118	1.293	7	316.6
12	631212	183	1.360	8	336.0
13	631219	232	1.577	7	3.2
14	631226	56	1.173	6	17.5
15	640102	36	0.940	4	39.8
16	640110	56	0.875	9	65.9
17	640117	82	1.226	8	75.2
18	651128	162	1.017	11	294.9
19	660116	130	0.905	6	85.4
20	660123	102	1.076	6	101.1
21	660130	120	1.122	7	119.9
22	660215	184	0.994	7	163.3
23	660222	250	1.063	6	188.8
24	660301	96	1.169	4	206.9
25	660308	147	0.899	6	227.9
26	660315	318	1.132	6	255.4
27	660329	132	1.311	7	297.7
28	660410	264	1.079	7	325.4
AVERAGE		148	1.160	7	
TOTAL		4151			

Table 5.2.8b

BE-B 7-DAYS ARCS

NO.	EPOCH	NO. OF OBS.	WEIGHTED RMS ARCSEC/2	NO. OF STATIONS	ARGUMENT OF PERIGEE (AT EPOCH)
1	641026	38	1.427	8	104.7
2	641102	60	1.309	11	85.3
3	641109	38	1.021	3	74.8
4	650112	52	1.173	6	266.7
5	650203	32	1.139	4	213.1
6	650323	54	1.005	9	92.0
7	650406	30	1.329	6	59.4
8	650415	46	1.555	8	41.2
9	650424	30	1.300	6	14.7
10	650613	50	1.357	5	242.7
11	650627	40	1.166	8	196.1
12	650716	30	1.451	8	149.2
13	670226	211	1.181	9	100.2
14	670305	56	1.258	4	88.8
15	670312	128	0.909	6	65.7
16	670319	228	1.109	6	52.6
17	670507	60	1.148	4	284.8
18	670514	154	1.461	5	269.2
19	670521	232	1.064	12	245.7
20	670528	170	0.983	8	233.4
AVERAGE		87	1.217	7	
TOTAL		1739			

Table 5.2.8c

BE-C OPTICAL 7-DAYS ARCS

NO.	EPOCH	NO. OF OBS.	WEIGHTED RMS ARCSEC/2	NO. OF STATIONS	ARGUMENT OF PERIGEE (AT EPOCH)
1	650619	64	1.381	4	327.6
2	650626	56	0.998	6	1.5
3	650703	52	1.326	7	38.7
4	650710	56	1.113	8	73.9
5	650717	94	1.104	9	109.0
6	650724	155	1.225	9	145.3
7	650731	80	1.080	11	180.3
8	650807	48	1.079	10	217.7
9	650814	62	0.871	8	253.7
10	650821	74	0.983	9	135.8
11	650828	50	1.190	5	237.9
12	650904	38	1.124	7	4.8
13	650911	66	1.002	9	38.9
14	650918	64	0.848	8	77.4
15	650925	58	1.084	11	109.2
16	651002	38	1.188	5	147.5
17	651009	42	1.220	9	182.1
18	651016	66	1.164	9	218.9
19	651023	54	1.200	9	255.7
20	651030	56	0.965	8	293.3
21	651106	68	1.346	4	329.0
22	651113	58	0.940	8	6.0
23	651120	38	1.155	6	41.4
24	651127	34	1.060	9	77.5
25	651210	48	1.114	7	142.5
26	651217	32	0.865	8	179.8
27	651225	54	1.337	9	219.2
28	660101	73	1.079	9	258.7
29	660108	92	0.970	7	293.7
30	660115	67	0.983	6	331.4
31	660301	216	1.107	9	201.5
32	660308	301	0.985	10	238.2
33	660315	374	0.957	9	275.6
34	660322	544	0.897	6	311.4
35	660329	269	1.096	7	349.5
36	660405	235	0.992	7	24.2
37	660412	274	0.854	9	60.7
38	660419	299	0.994	8	95.7
39	660426	346	1.051	8	130.9
40	660503	210	1.145	9	167.8
41	660510	270	0.986	9	201.9
42	660517	257	0.858	9	241.4
43	660524	189	0.886	7	275.9
44	670312	185	1.089	9	346.0
45	670319	327	1.090	9	23.5
46	670326	207	1.062	7	57.8
47	670402	472	1.116	8	94.0
48	670410	235	1.173	10	135.7
49	670417	250	1.187	10	169.4
50	670424	204	1.074	8	206.4
AVERAGE		150	1.071	8	
TOTAL		7501			

Table 5.2.8d

GEOS-1 OPTICAL 7-DAYS ARCS

NO.	EPOCH	NO. OF OBS.	WEIGHTED RMS ARCSEC/2	NO. OF STATIONS	ARGUMENT OF PERIGEE (AT EPOCH)
1	651108	244	0.920	9	150.5
2	651115	331	1.051	10	154.7
3	651122	1692	0.727	17	159.9
4	651129	883	0.785	22	164.4
5	651213	1177	0.829	22	173.5
6	651220	1426	1.001	25	177.3
7	651227	1291	1.126	30	182.2
8	660103	769	1.231	24	187.5
9	660110	1524	1.036	29	191.4
10	660117	1722	0.980	26	196.0
11	660124	1296	0.862	27	200.9
12	660131	838	0.961	22	205.2
13	660207	364	0.901	18	209.4
14	660214	773	0.954	21	214.8
15	660221	1249	0.836	25	218.6
16	660228	967	0.889	26	223.7
17	660307	1506	1.038	36	228.8
18	660314	2673	0.823	30	232.9
19	660404	1781	0.865	30	246.6
20	660411	1879	0.805	30	250.8
21	660425	2034	0.778	31	260.6
22	660502	2079	0.771	28	265.0
23	660509	1471	0.770	24	270.3
24	660516	743	0.724	17	274.7
25	660523	263	0.649	11	280.0
26	660709	3485	0.780	31	310.5
27	660716	3780	0.857	30	315.6
28	660723	3433	0.781	28	319.9
29	660730	3039	0.792	25	324.5
30	660806	1791	0.688	28	329.7
31	660813	1506	0.667	20	333.9
32	660820	1091	0.704	16	338.2
33	660827	594	0.585	11	343.5
34	660903	702	0.615	15	348.0
35	660922	2218	0.919	9	359.7
36	661006	2378	0.892	22	9.8
37	661013	1721	0.803	24	13.7
38	661020	1446	0.809	24	18.6
39	661115	1141	0.707	14	35.1
40	670226	214	0.987	10	101.9
41	670305	575	0.931	8	106.2
42	670312	375	0.928	11	110.1
43	670319	286	0.971	7	115.1
AVERAGE		1413	0.854	22	
TOTAL		60750			

Table 5.2.8e

GEOS-2 OPTICAL 7-DAYS ARCS

NO.	EPOCH	NO. OF OBS.	WEIGHTED RMS ARCSEC/2	NO. OF STATIONS	ARGUMENT OF PERIGEE (AT EPOCH)
1	680315	1378	0.857	26	67.1
2	680322	1938	0.865	27	53.5
3	680329	1664	0.803	32	44.6
4	680405	1613	0.753	33	34.6
5	680412	1607	0.986	32	21.7
6	680419	2132	1.040	36	11.0
7	680426	1772	0.737	35	357.4
8	680503	1696	0.826	30	347.7
9	680510	1427	0.798	27	338.7
10	680517	1619	0.720	24	324.3
11	680524	1390	0.724	26	313.2
12	680531	1196	0.702	18	301.3
13	680607	2098	0.754	30	289.1
14	680614	2775	0.723	31	279.8
15	680621	2978	0.709	34	266.6
16	680628	417	0.702	17	255.0
17	680719	1712	0.727	30	220.0
18	680814	1172	0.668	15	177.2
19	680828	1220	0.922	30	154.9
20	680904	1793	0.920	29	143.3
21	680911	1242	0.808	29	134.2
22	680918	2863	0.766	35	121.8
23	680925	1650	0.829	28	109.5
24	681002	2007	0.932	29	100.2
25	681009	1954	0.851	30	87.4
26	681016	1254	0.850	29	77.4
27	681023	1616	0.852	29	67.6
28	681116	869	0.832	14	28.5
29	681217	463	0.970	13	336.4
30	690128	729	1.030	9	269.1
31	690204	908	1.099	13	256.0
32	690211	912	0.995	12	244.6
33	690218	579	1.085	9	235.3
34	690225	429	0.969	11	221.3
35	690304	760	0.931	13	210.1
36	690311	908	0.927	13	198.3
37	690318	847	0.851	12	186.9
38	690325	675	0.874	12	178.2
39	690331	861	0.770	19	167.9
40	690407	1068	0.758	22	155.4
41	690414	839	0.762	11	143.3
42	690421	1259	0.816	23	133.5
43	690428	778	0.774	18	121.7
44	690505	1160	0.761	20	110.7
45	690512	491	0.669	9	100.5
46	690519	685	0.778	9	87.4
AVERAGE		1335	0.846	22	
TOTAL		61403			

Table 5.2.8f

TELSTAR-1 OPTICAL 7-DAYS ARCS

NO.	EPOCH	NO. OF OBS.	WEIGHTED RMS ARCSEC/2	NO. OF STATIONS	ARGUMENT OF PERIGEE (AT EPOCH)
1	620713	39	1.096	5	170.1
2	620725	80	1.211	10	193.9
3	620801	74	1.112	7	207.8
4	620808	128	0.989	9	221.8
5	620816	138	1.482	7	237.7
6	620823	106	1.113	7	251.7
7	620830	116	0.936	5	265.5
8	620913	153	1.127	6	293.2
9	620920	105	1.102	7	307.2
10	620927	166	1.043	10	321.2
11	621004	209	1.122	9	335.2
12	621018	154	1.225	11	3.0
13	621025	210	1.171	11	16.9
14	621101	124	1.037	10	30.8
15	621108	94	1.256	7	44.5
16	621115	138	1.187	9	58.5
17	621122	114	1.004	7	72.4
18	621206	68	1.405	9	100.2
19	621213	58	0.898	7	114.1
20	630207	64	1.047	6	225.3
21	630214	147	0.840	10	239.3
22	630221	139	0.965	10	253.2
23	630228	122	0.853	11	267.0
24	630307	129	0.806	7	280.9
25	630314	193	0.783	8	294.7
26	630328	144	1.095	8	322.7
27	630414	118	1.033	10	356.5
28	630421	110	0.767	10	11.0
29	630526	180	0.884	5	79.9
30	630616	342	0.764	12	121.0
AVERAGE		132	1.045	8	
TOTAL		3962			

120

Table 5.2.8g

LOW INCLINATION (I<40°) SATELLITE DATA

FOR GEM-T1

SATELLITE	# OF OBS CAMERA DATA	# OF OBS LASER DATA	# OF ARCS	PERIGEE HEIGHT (KM)	E	I (DEG)
COURIER-1B	2476	----	10	989	.0161	28.3
VANGUARD-2RB	686	----	10	562	.1832	32.9
VANGUARD-2	1299	----	10	562	.1641	32.9
DI-C	2712	----	10	587	.0532	39.9
DI-C	159	7455	4			
DI-D	6111	----	9	589	.0848	39.5
DI-D	146	11487	6			
PEOLE	38	4113	6	515	.0164	15.0

121

Table 5.2.8h

PEOLE LASER+OPTICAL 7-DAYS ARCS

NO.	EPOCH	NO. OF OBS.	WEIGHTED RMS ARCSEC/2	NO. OF STATIONS	ARGUMENT OF PERIGEE (AT EPOCH)
1	710225	736	2.840	4	104.7
2	710304	663	1.730	4	191.6
3	710507	815	1.400	5	324.3
4	710527	1594	2.810	4	220.4
5	710610	104	4.270	1	55.5
6	710623	239	0.680	2	222.3
AVERAGE		692	2.29	3	
TOTAL		4151			

Table 5.2.8i

DI-D OPTICAL 7-DAYS ARCS

NO.	EPOCH	NO. OF OBS.	WEIGHTED RMS ARCSEC/2	NO. OF STATIONS	ARGUMENT OF PERIGEE (AT EPOCH)
1	670219	164	1.138	7	156.2
2	670226	250	1.113	10	194.5
3	670305	432	1.066	7	232.1
4	670312	275	0.957	8	270.1
5	670319	174	1.030	7	308.1
6	670430	1003	0.967	11	173.7
7	670507	1367	1.020	11	211.4
8	670514	1592	0.934	12	249.5
9	670521	854	1.360	14	287.1
AVERAGE		679	1.065	10	
TOTAL		6111			

DI-D LASER + OPTICAL 7-DAYS ARCS

NO.	EPOCH	NO. OF OBS.	WEIGHTED RMS ARCSEC/2	NO. OF STATIONS	ARGUMENT OF PERIGEE (AT EPOCH)
1	710423	3463	1.040	6	108.1
2	710507	1824	1.930	9	183.4
3	710514	2027	0.950	10	221.5
4	710703	1604	1.480	2	132.5
5	710710	2368	1.870	2	169.7
6	710719	347	1.890	4	218.7
AVERAGE		1939	1.530	5	
TOTAL		11633			

Table 5.2.8j

VANGUARD-2 7-DAYS ARCS

NO.	EPOCH	NO. OF OBS.	WEIGHTED RMS ARCSEC/2	NO. OF STATIONS	ARGUMENT OF PERIGEE (AT EPOCH)
1	660202	42	1.121	6	252.4
2	660209	70	0.868	6	290.0
3	660216	136	1.192	8	326.9
4	660223	170	1.039	8	3.8
5	660302	136	1.243	9	41.3
6	660309	163	1.003	9	77.9
7	660316	249	0.885	6	114.9
8	660323	231	1.221	8	152.0
9	660330	64	1.194	8	188.8
10	660407	38	1.165	8	231.3
AVERAGE		130	1.093	8	
TOTAL		1299			

124

Table 5.2.8k

VANGUARD-2RB 7-DAYS ARCS

NO.	EPOCH	NO. OF OBS.	WEIGHTED RMS ARCSEC/2	NO. OF STATIONS	ARGUMENT OF PERIGEE (AT EPOCH)
1	600402	42	1.273	4	357.5
2	600409	30	0.846	2	31.7
3	600417	40	1.643	5	71.3
4	600427	30	1.007	7	120.7
5	600505	74	1.298	5	160.3
6	600512	92	1.427	6	194.6
7	600519	124	1.020	7	229.4
8	600526	94	1.173	8	226.3
9	600608	55	0.920	6	328.6
10	600717	105	1.259	8	0.0
AVERAGE		69	1.187	6	
TOTAL		686			

Table 5.2.81

DI-C OPTICAL 7-DAYS ARCS

NO.	EPOCH	NO. OF OBS.	WEIGHTED RMS ARCSEC/2	NO. OF STATIONS	ARGUMENT OF PERIGEE (AT EPOCH)
1	670220	164	1.061	4	217.9
2	670227	158	1.195	7	259.0
3	670306	300	1.071	10	301.5
4	670313	201	1.049	7	343.6
5	670320	127	0.949	4	24.8
6	670416	244	0.921	8	183.6
7	670423	400	1.055	8	226.7
8	670430	720	1.001	9	267.8
9	670507	196	0.902	9	308.8
10	670514	202	1.003	10	351.9
AVERAGE		271	1.021	8	
TOTAL		2712			

DI-C LASER + OPTICAL 7-DAYS ARCS

NO.	EPOCH	NO. OF OBS.	WEIGHTED RMS ARCSEC/2	NO. OF STATIONS	ARGUMENT OF PERIGEE (AT EPOCH)
1	710401	751	0.780	4	165.6
2	710608	698	1.320	10	213.0
3	710615	3783	2.580	8	255.9
4	710622	2382	2.230	8	297.8
AVERAGE		1903	1.720	7	
TOTAL		7614			

Table 5.2.8m

COURIER-1B 7-DAYS ARCS

NO.	EPOCH	NO. OF OBS.	WEIGHTED RMS ARCSEC/2	NO. OF STATIONS	ARGUMENT OF PERIGEE (AT EPOCH)
1	661224	334	1.130	9	95.5
2	670107	307	1.183	8	211.8
3	670114	368	1.072	8	273.6
4	670121	301	1.087	10	332.1
5	670128	237	1.059	9	27.8
6	670602	97	0.971	5	343.6
7	670609	97	1.150	5	40.5
8	670616	151	1.074	7	94.1
9	670623	258	1.010	7	150.2
10	670708	326	1.244	7	276.6
AVERAGE		248	1.098	8	
TOTAL		2476			

To remedy this situation, data sets of six additional satellites were selected for inclusion in the model. These satellites were COURIER-1B, VANGUARD 2 rocket body, VANGUARD 2, DI-C, DI-D, and PEOLE. The later three of these satellites were tracked by the first generation laser systems in the early 1970's. Tables 5.2.8g through 5.2.9m summarize the data contribution of these low inclination satellites. As it will be discussed later, the inclusion of these data had a dramatic positive impact on the resulting GEM-T1 gravity solution.

5.2.9 Analysis of BE-C Laser Observations

Beacon Explorer-C was launched from Wallops Flight Facility, Wallops Island, Virginia in 1965. The satellite was magnetically stabilized, had reasonably large solar panels and fortunately also carried a ring of laser retro-reflectors. Because of its low inclination, BE-C became a favorite target for early North American crustal motion studies. BE-C at times, was visible to laser sites located in the United States on three to four successive revolutions. Therefore, a large BE-C data set could be acquired in a short time interval enabling short arcs to be utilized in station position determination solutions. To support these studies, the global laser network tracked BE-C often, yielding a reasonably robust data set. However, given this satellite's magnetic stabilization and the location of its corner cubes at its lowest end, BE-C unfortunately was not visible to lasers located beyond the equatorial region of the Southern Hemisphere.

The orbital characteristics for BE-C are presented in Table 5.2.9a. This satellite was studied using 5 day arcs. A drag parameter per day, a solar radiation pressure coefficient and the orbital state vector were adjusted within each arc. In general, the laser data taken on BE-C were quite good, being data from third generation systems which were globally deployed to support the LAGEOS mission. Since this object

128

was and remains a satellite of interest, data from 1979 onwards were sufficient to have this satellite well represented in our gravity modeling solutions. The normal equations generated from BE-C tracking data are shown in Table 5.2.9b. In all, 39 arcs of BE-C laser data were used in the GEM-T1 solution with other additional arcs being available for field testing.

Extensive tests of the drag parameterization on BE-C were performed and are found summarized in Section 7.2.2.

Table 5.2.9a. Orbital Characteristics of BE-C

Semi-Major Axis	7507 km
Apogee Height	1320 km
Perigee Height	940 km
Eccentricity	0.0257
Inclination	41.19 degrees
Mean Motion	13.35 revolutions/day
Beat Period	5.5 days

Table 5.2.9b

EMAT SUMMARY FOR BEC

EPOCH	NUMBER OF OBSERVATIONS	WEIGHTED RMS (m)	NUMBER OF STATIONS	ARGUMENT OF PERIGEE (AT EPOCH)
790320	1153	1.2126	8	18.204
790402	1535	1.7486	8	81.950
790411	2472	1.4003	8	128.830
790417	3596	1.2484	9	161.207
790426	3265	1.1535	8	207.915
790501	1904	1.3096	6	232.713
790512	3136	1.2258	6	291.352
790523	1173	1.4735	4	349.258
790813	614	1.3281	5	51.989
791022	1254	1.1893	8	54.306
791112	1765	1.1033	7	161.403
791202	986	1.4961	9	265.595
791217	1002	1.3430	7	344.681
800115	973	.6662	7	133.182
800122	1022	.7459	10	168.528
800129	2202	1.1481	7	206.047
800205	1710	.9070	7	239.858
800408	1460	1.2113	8	206.400
800505	1551	1.1468	8	349.147
800528	644	2.1713	4	106.631
800602	1197	1.2983	6	131.798
800728	1215	1.5013	8	62.832
800802	1175	2.0744	10	89.221
800915	1683	1.4970	7	99.180
800923	1564	1.5275	10	359.756
801006	1412	1.6996	10	63.421
801013	1419	1.7794	9	101.679
801124	632	1.0837	5	319.695
801201	1010	1.4706	6	355.343
801215	1076	1.2099	7	67.447
810303	1911	1.5659	9	111.785
810317	1760	1.1450	7	181.514
810728	1357	1.3487	7	149.842
810817	1266	1.3525	5	254.153
810924	2039	1.4846	7	92.630
811006	3997	1.4363	8	150.636
811012	2717	1.7980	8	182.613
811019	2258	1.0116	7	221.105
820201	1135	1.2684	6	46.323

SECTION 6.0
DEFINITION OF A PRIORI GEOCENTRIC
TRACKING STATION COORDINATES

In order to compute an improved preliminary gravity field model for the TOPEX mission, the coordinates of all contributing tracking stations must be referred to one unified coordinate system. The reference frame for this work will be briefly described in the course of this section as well as the procedures and transformations required to bring existing station coordinates into a unique system. The existing station coordinates are in a variety of coordinate systems from various solutions made in past years. The coordinate system chosen for the TOPEX work is closely related to GSFC's laser coordinate system, SL-6.

6.1   COORDINATE SYSTEM DEFINITION

The unified coordinate system developed for the a priori station positions needed for the TOPEX gravity model project is based upon the laser coordinate system developed by GSFC from LAGEOS tracking, known as the SL-6 system [for a description of a typical laser coordinate solution, see Smith et al. (1985)]. The longitude definition was adopted from that used in the MERIT campaign [Melbourne, et al. (1983)]. Thus all of the station coordinates that were transformed into the SL-6 system were ultimately rotated by +0.144525 arcsec in longitude to accommodate the McDonald Observatory reference meridian definition. A zero mean pole position was adopted to better model the mean figure and rotation axes, and all station coordinates were rotated further to this zero mean pole origin. This issue is considered in more detail elsewhere in this document. The resulting coordinate frame will be referred to as the TOPEX Coordinate System (TCS). The station coordinates are put in Cartesian form for use in the data-reduction and

the E-matrix generation runs, but, for the purpose of cataloging, the coordinates have also been transformed to geodetic form. The geodetic coordinates refer to an ellipsoid with a semi-major axis of 6378137 m and a flattening of 1/298.257.

6.2 INITIAL STATUS OF STATION COORDINATES

The station positions to be transformed into the TCS exist in a variety of coordinate systems. These include local datum coordinates and dynamically derived coordinates from solutions such as GEM-9 [Lerch et al. (1979)], and GSFC-73 [Marsh et al. (1973)]. The means for determining the transformations is provided by a set of laser sites for which both the SL-6 coordinates and the datum or dynamically determined coordinates are known. Table 6.1 lists the laser sites and their unmodified SL-6 coordinates that were used in this work. The approximate epoch for these stations is 1982.

6.3 THE TRANSFORMATION MODELS

Two transformation models were used to complete this task. The first model utilizes the coordinates for widely distributed laser stations known in both coordinate systems, the SL-6 system and the other coordinate system of interest (e.g., local datum or dynamically determined system) for which we wish to establish a rigorous transformation. The second model employs a simple linear transformation for stations which are in close proximity to one of the laser stations listed in Table 1. By "close proximity", we mean that station separations do not exceed 100 km. Beyond this distance, the errors committed by ignoring scale and rotation parameters can grow rapidly to a size of a few meters. This aspect will be described shortly.

Table 6.1 Laser sites known from the SL6 dynamic solution								
Station		latitude			longitude			ellipsoidal
NAME	no.	d	m	s	d	m	s	height
QUINY	7051	39	58	24.5710	239	3	37.5530	1052.8800
EASTER	7061	-27	8	52.1650	250	36	58.9940	110.5550
SANDIE	7062	32	36	2.6580	243	9	32.7810	981.4700
STALAS	7063	39	1	13.3620	283	10	19.7950	12.1670
GSFCLS	7064	39	1	15.1040	283	10	18.6050	10.1530
BDILAS	7067	32	21	13.7620	295	20	37.927	-30.1170
GRKLAS	7068	21	27	37.7710	288	52	5.0330	-25.7760
RAMLAS	7069	28	13	40.6520	279	23	39.2980	-30.6690
BEARLK	7082	41	56	0.8960	248	34	45.5370	1955.9060
OVRLAS	7084	37	13	55.6560	241	42	15.1130	1171.0190
GOLDLS	7085	35	25	27.9630	243	6	48.9170	958.3230
FTDAVS	7086	30	40	37.3040	255	59	2.4810	1954.3160
YARLAS	7090	-29	02	47.4100	115	20	48.1070	234.2260
HAYLAS	7091	42	37	21.6890	288	30	44.3390	84.9250
KWJLAS	7092	9	23	37.6890	167	28	32.4860	25.7920
SAMLAS	7096	-14	20	7.5170	189	16	30.3570	41.8820
GSF100	7100	39	1	15.4510	283	10	47.6350	3.1100
GSF101	7101	39	1	16.2050	283	10	42.8350	1.3140
GSF102	7102	39	1	14.3800	283	10	18.7920	10.8910
GSF103	7103	39	1	14.6070	283	10	18.7950	10.8330
GSF104	7104	39	1	17.0820	283	10	36.8380	2.8980
GSF105	7105	39	1	14.1640	283	10	20.1580	12.0840
QUILAS	7109	39	58	30.0020	239	03	18.9490	1099.2260
MONLAS	7110	32	53	30.0020	243	34	38.2580	1831.8602
PLALAS	7112	40	10	58.0010	255	16	26.3360	1494.4826
OVRLAS	7114	37	13	57.2120	241	42	22.2150	1170.9230
GOLLAS	7115	35	14	53.9000	243	12	28.9490	1031.5171
MUILAS	7120	20	42	27.3920	203	44	38.1020	3060.6295
HUANIL	7121	-16	44	0.6830	208	57	31.7780	40.1250
MAULAS	7210	20	42	25.9960	203	44	38.6000	3061.2004
FINLAS	7805	60	13	2.2880	24	23	40.2110	71.2110
KOOLAS	7833	52	10	42.2450	5	48	35.1190	86.4620
WETLAS	7834	49	08	41.7770	12	52	40.9670	654.0907
GRALAS	7835	43	45	16.8840	6	55	15.8640	1315.9275
SHOLAS	7838	33	34	39.7210	135	56	13.1890	94.3156
RGOLAS	7840	50	52	2.5610	0	20	9.8620	68.2651
FORLAS	7885	30	40	37.3060	255	59	2.4780	1954.2694
QUILAS	7886	39	58	30.0180	239	3	18.0180	1102.4716
VANLAS	7887	34	33	58.3570	239	29	57.9780	597.2122
HOPLAS	7888	31	41	6.3150	249	7	18.5000	2327.6088
YUMLAS	7894	32	56	20.9340	245	47	48.6070	234.6146
ARELAS	7907	-16	27	56.7010	288	30	24.6030	2485.1860
HOPLAS	7921	31	41	3.2220	249	7	18.8370	2345.8548
NATLAS	7929	-5	55	40.1350	324	50	7.2190	32.4910
MATLAS	7939	40	38	55.7930	16	42	16.6860	528.8756
ORRLAS	7943	-35	37	29.7560	148	57	17.1240	941.8380
ARESAO	9907	-16	27	56.7010	288	30	24.6030	2485.1860
HOPSAO	9921	31	41	3.2220	249	7	18.8370	2345.8548
NATSAO	9929	-5	55	40.1350	324	50	7.2190	32.4910

$a_e = 6378144.11$, $f = 1/298.255$

6.3.1 Seven Parameter Transformation

The seven parameter transformation, also sometimes known as the Bursa/Wolf transformation [Leick & van Gelder (1975)], is a rigorous transformation relating two geodetic coordinate systems when only small rotations are involved. The transformation has the form

$$
\begin{bmatrix} X \\ Y \\ Z \end{bmatrix}_i^{SL6} = \begin{bmatrix} \Delta X \\ \Delta Y \\ \Delta Z \end{bmatrix} + (1 + \Delta L) \begin{bmatrix} 1 & \omega & -\psi \\ -\omega & 1 & \epsilon \\ \psi & -\epsilon & 1 \end{bmatrix} \begin{bmatrix} X \\ Y \\ Z \end{bmatrix}_i^{dat} \tag{6.1}
$$

where

$\begin{bmatrix} X \\ Y \\ Z \end{bmatrix}_i^{dat}$ is the ith station's Cartesian coordinates referred to the local datum (or other coordinate systems, depending on the case),

ω, ψ, and ϵ are small Euler rotations about the Z,Y,X axes respectively,

ΔL is a scale factor, and

$\Delta X, \Delta Y, \Delta Z$ are translations between the local datum (or other coordinate systems) and the SL-6 system.

The seven parameters are determined in a least squares solution by comparing the laser station coordinates in both systems for which the transformation is desired. Further details and a derivation are found in Rapp (1983).

6.3.2 The Linear Translation

The approximate linear translation of the ith station into the SL-6 system is found from

$$\phi_i^{SL6} = \phi_i^{dat} + (\phi_j^{SL6} - \phi_j^{dat})$$

$$\lambda_i^{SL6} = \lambda_i^{dat} + (\lambda_j^{SL6} - \lambda_j^{dat}) \qquad (6.2)$$

$$H_i^{SL6} = H_i^{dat} + (H_j^{SL6} - H_j^{dat})$$

where j denotes the near-by j^{th} laser station having its coordinates known in both coordinate systems (e.g., in SL6 and in the local datum (dat)). Some errors can be expected to arise in this model primarily due to neglecting scale and rotation parameters. This is especially true when stations i and j are relatively far apart. A computation was made to ascertain the size of these errors as a function of distance using the NAD to SL-6 transformation. It was found that errors in longitude grow most rapidly and the magnitude of the error can be as large as 3 meters at a distance of 100 km. The linear method was primarily used to determine older optical and doppler sites in our new system when they were situated near laser tracking stations.

6.4 NUMERICAL RESULTS

This section will highlight the numerical aspects of the transformations used to establish the table of TOPEX a priori station positions. Table 6.2 lists the stations used to determine the transformation parameters relating: NAD 27 to SL-6; GEM-9 to SL-6; and GSFC-73 to GEM-9. The TOPEX a priori station coordinates given here are currently regarded as being the best, but they may be changed when better information becomes available.

137

Table 6.2. Stations used in least-squares determination of the seven parameter transformations. (i.e. solutions from program STC)

nAD 27 → SL-6

7062 : SANDIE	7109 : QUILAS
7069 : RAMLAS	7110 : MONLAS
7082 : BEARLK	7112 : PLALAS
7086 : FTDAVS	7114 : OVRLAS
7091 : HAYLAS	7115 : GOLLAS
7105 : GSF105	7921 : HOPLAS

GEM 9 → SL-6

1038 : 1ORORL	7907 : ARELAS
7063 : STALAS	7921 : HOPLAS
7067 : BDILA1	7929 : NATLAS
7068 : GRKLAS	9012 : 1MAUIO

GSFC-73 → SL-6

9001 : 1ORGAN	9007 : 1QUIPA
9002 : 1OLFAN	9009 : 1CURAC
9004 : 1SPAIN	9011 : 1VILDO
9005 : 1TOKYO	9012 : 1MAUIO
9006 : 1NATAL	9021 : HOPKIN

6.4.1 NAD 27 to SL-6 Transformation

The NAD 27 to SL-6 transformation parameters were determined from 12 stations distributed over the United States as shown in Figure 6.1. These parameters were then used to transform NAD 27 optical and Doppler tracking station coordinates into SL-6. The NAD 27 coordinates were used since the terrestrial coordinates are considered more accurate than coordinates determined from camera and Doppler solutions made in previous years. Small rotations for longitude definition and zero mean pole definition were applied to these stations to complete the transformation into TCS.

6.4.2 GEM-9 to SL-6 Transformation

The GEM-9 to SL-6 transformation parameters were determined from 8 stations distributed around the globe. These parameters were then used to transform tracking stations located around the globe with the exception of stations in Europe. The European stations are discussed in the next paragraph. The GEM-9 to SL-6 transformation was used since the local datum coordinates for most of these stations are not very well known or are of dubious origin. Again, the small rotations for zero mean pole and longitude definition were applied to bring these coordinates into the TCS.

6.4.3 GSFC-73 to GEM-9 Transformation

The GSFC-73 solution was used because a European Datum to SL-6 transformation could not be determined due to insufficiencies in the terrestrial data and because the European GSFC-73 dynamically derived positions are considered more reliable than the GEM-9 dynamically derived positions. It may appear rather odd that the transformation relates GSFC-73 to GEM-9 rather than to SL-6. This was done since a direct GSFC-73 to SL-6 transformation could not be established due to

insufficient data. To get around this problem, a two-step procedure was used. The transformation parameters relating GSFC-73 to GEM-9 were determined from 10 stations distributed globally. The European stations were then transformed into GEM-9 via these parameters, followed by the GEM-9 to SL-6 transformation mentioned in the previous paragraph. Small rotations again were applied, accounting for the zero mean pole and our new longitude definition, to bring these stations into the TCS.

6.4.4 Other Transformations

After some analysis, it became apparent that a few of the stations positions were causing larger than anticipated residuals. The network of S-band tracking stations was one such case. The S-band tracking stations (used to track SEASAT) were transformed into SL-6 by determining the GEM-9 to SL-6 parameters found exclusively from S-band position data known in both systems. Six S-band stations were used to determine these parameters. Thirteen other S-band stations were then transformed via these parameters into the SL-6 system. Likewise, similar rotations as mentioned above were employed to these sites to bring them into the TCS.

6.5 DISCUSSION

6.5.1 Transformation Parameters and Accuracies

The determination of the seven parameters in the transformations were performed in a least-squares based program known as STC (STation Comparison). The transformation parameters relating the coordinate systems described in the previous sections as computed by STC are given in Table 6.3.

140

Table 6.3. Transformation Parameters

parameter	NAD → SL-6	GEM9 → SL-6	GSFC73 → GEM9
$\triangle$X (m)	-31.4805	-0.9451	2.5460
$\triangle$Y (m)	172.5176	-1.7602	2.6820
$\triangle$Z (m)	182.7296	0.8776	-0.2535
$\triangle$L	1.6015E-6	-3.5305E-7	9.0237E-8
ω (")	-0.77841	0.32384	-0.00924
ψ (")	-0.01160	-0.08520	-0.02139
ε (")	-0.31494	0.04528	-0.04434

Table 6.4. Quality of the transformations
(RMS about the mean, see text)

parameter	NAD → SL-6	GEM9 → SL-6	GSFC73 → GEM9
X (m)	3.158	1.404	4.663
Y (m)	2.422	1.133	3.014
Z (m)	2.826	0.469	3.128
Φ (")	0.1161	0.0464	0.1615
λ (")	0.1166	0.0233	0.1080
H (m)	1.784	1.537	3.158

141

The translation parameters in the NAD 27 to SL-6 transformation are large (i.e., tens and hundreds of meters) since NAD 27 is not a center of mass system. The magnitude of the translations is consistent with other investigations reported in Bomford (1980), p. 635 with the exception of the ΔY translation component. The value we determined for ΔY is 15 meters larger than that found by other investigators. The seven parameter determination by STC is highly dependent upon the distribution of stations. As can be noted in Figure 6.1, our determination will be stronger in the western United States. This is the case since the LAGEOS tracking network is concentrated in the more tectonically active west coast. Although the distribution is far from optimal, the resulting transformation has suited our needs and is of adequate precision (to be discussed below).

The other two transformations, GEM-9 to SL-6 and GSFC-73 to GEM-9, have smaller parameters since all three coordinate systems are supposedly center of mass systems. However, significant differences are present which are most likely due in part to differences in the longitude origin of the systems. The ΔZ translational component is at least an order of magnitude smaller than the equatorial plane components, ΔX and ΔY. In the equatorial plane, the SL-6 center of mass falls nearly half-way between the center of mass of the GEM-9 and GSFC-73 coordinate systems.

6.5.2 Precision of the Transformations

The precision of the transformations can be gauged from the RMS scatter of the residuals after the transformation has been made. The RMS scatter is given by

$$\bar{X}_\sigma = \left[\sum_i (\bar{X}_{if} - T(\Delta X, \Delta Y, \Delta Z, \omega, \psi, \epsilon, \Delta L) \, \bar{X}_{ia})^2 \right]^{1/2} \qquad (6.3)$$
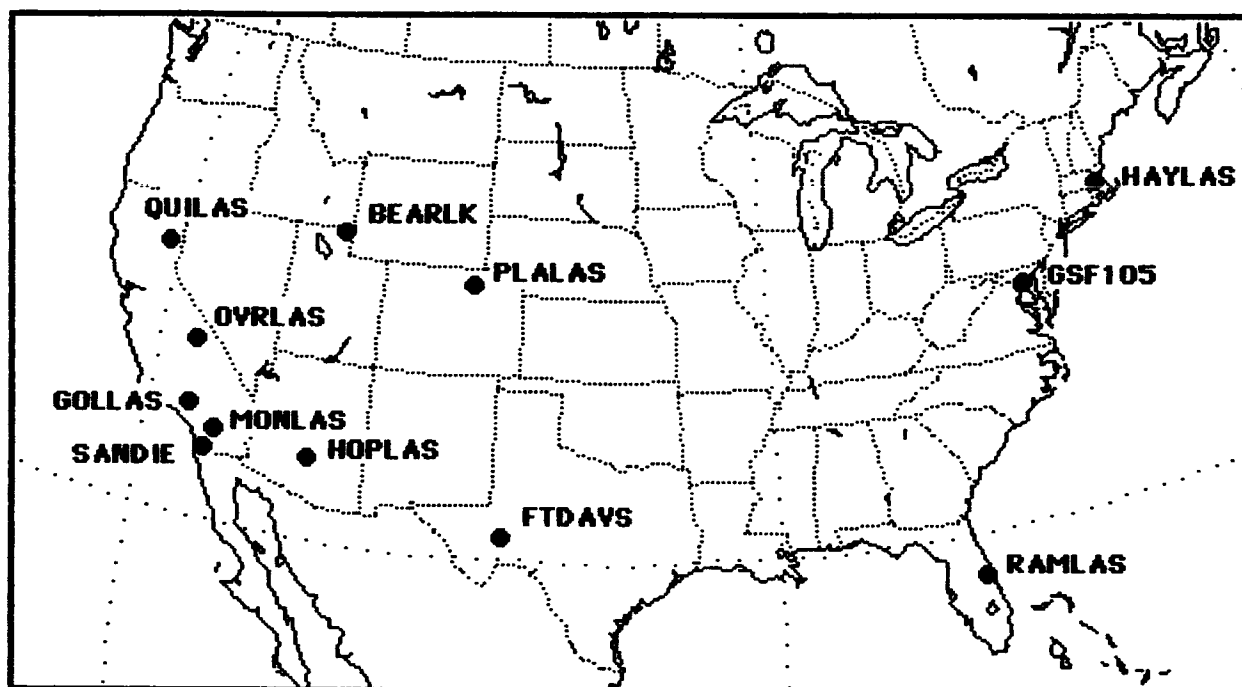
Figure 6.1. Laser Tracking Station Locations used in Determining the Seven Parameter Transformation between NAD 27 and SL-6.

where

$\overline{X}_{if}$ are the known coordinates for tracking station i in the unified coordinate system (e.g., SL-6),

$\overline{X}_{ia}$ are the known coordinates in the a priori coordinate system (e.g., NAD 27, GEM-9, etc.), and

T denotes the seven parameter transformation.

This actually provides a measure of how well the stations that were used to determine the parameters of T agree when T is applied to their a priori coordinates. The RMS quantities for the three transformations described here are given in Table 6.4. It can be seen in Table 6.4 that the GEM-9 to SL-6 transformation is the strongest of the three with residuals averaging in the 1 to 1.5 meter range. The NAD 27 to SL-6 transformation is weaker with residuals in the 2.5 to 3 meter range. Finally, the GSFC-73 to GEM-9 transformation is the weakest with 3.5 to 4 meter residuals. This latter result is not too surprising since the GSFC-73 coordinates are based upon early camera and laser data with a solution accuracy goal of 5 meters. As mentioned earlier, though the uncertainties of the GSFC-73 coordinates may seem large by today's standards, in some cases (especially the European and other remote or abandoned sites), the GSFC-73 coordinates are the best available. GEM-9 used much of the same data, and therefore must share in the resulting station uncertainties.

6.5.3 Error Sources

Errors in the coordinates of the stations in the TCS can be as large as a few meters. This is especially true for stations having their a priori coordinates determined from an early dynamic solution.

144

Stations in this category very likely have limited tracking histories and will never be positioned accurately from available early tracking observations. On the other hand, most of the laser stations coming directly from the SL-6 solution will have their coordinates determined to an accuracy in the sub-decimeter range: This is especially true for stations with robust tracking histories. Stations that have come from the GEM-9 solution have their coordinates known to an accuracy of 1 to 2 meters; again, those stations with strong tracking histories will be better determined.

The seven parameters of the transformations are thus susceptible to errors in the coordinates of the stations in both the a priori and the SL-6 coordinate systems. These coordinate errors will be mapped into the seven parameters directly. In running the STC Program, stations were selected such that 1) good geographical distribution was maintained, and 2) all coordinates (a priori and SL-6) were well determined. The STC Program unfortunately, uses equal weights for the stations when estimating the transformation parameters. For the remaining stations to be transformed, in addition to the transformation parameter uncertainties, the errors of the a priori coordinates map directly into the resulting unified coordinates.

The linear translations suffer from the fact that rotation and scale are not considered. These errors can grow as large as three meters when the stations involved are separated by 100 km. However, only a small number of optical and doppler stations were transformed in this way; all of them had station separations of less than 3 km.

6.5.4 Distortion in the NAD 27 Datum

The STC program provides the residuals for each station's coordinates after the transformation is applied. These residuals, when viewed geographically, can illustrate the relative distortion between two

CONTOUR INTERVAL: 1 meter
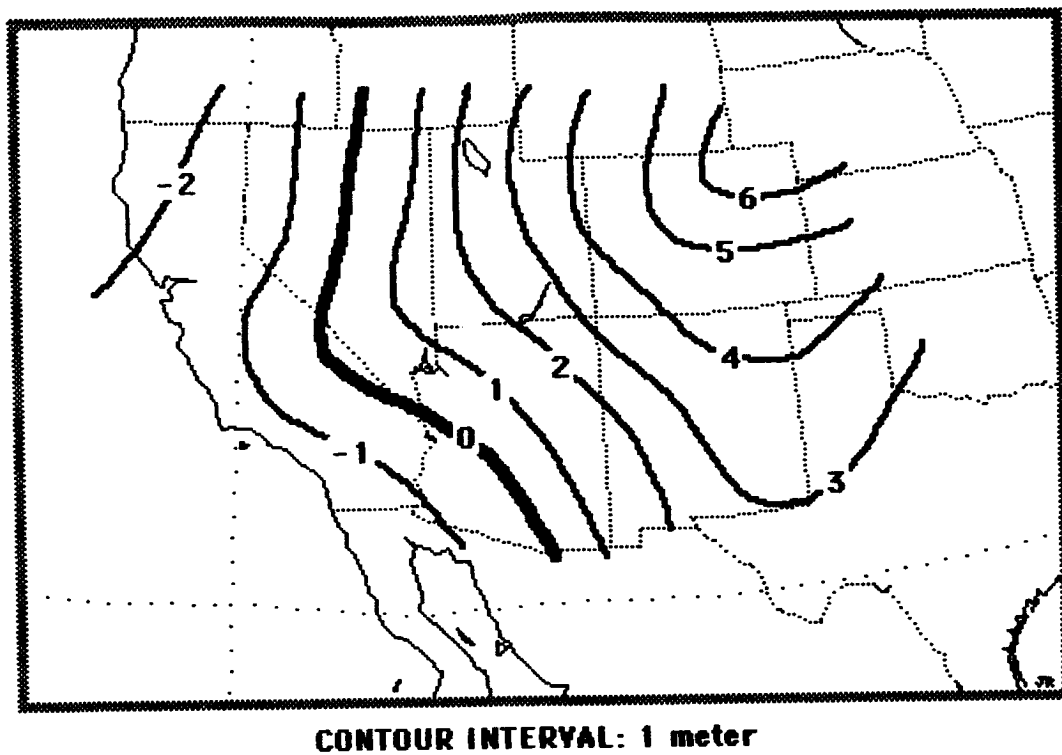
Figure 6.2. Longitude Distortion Based Upon SL-6 vs. NAD.

CONTOUR INTERVAL: 1 meter
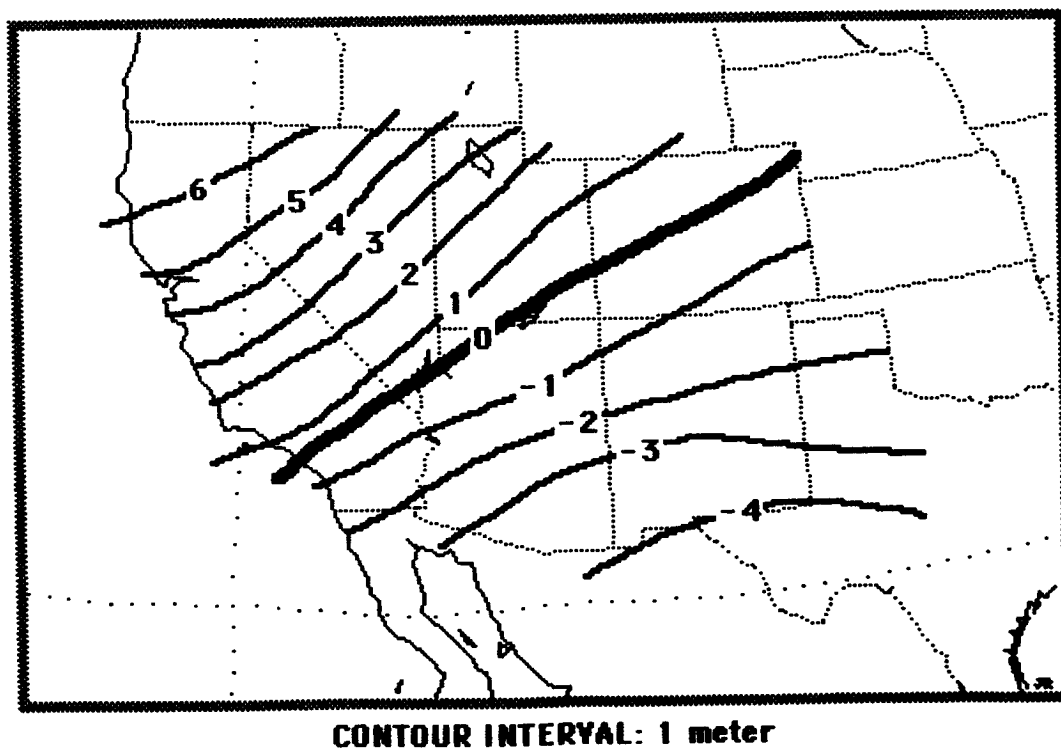
Figure 6.3. Latitude Distortion Based Upon SL-6 vs. NAD.

146

datums. The NAD 27 is a terrestrially determined network established by classical geodetic surveying techniques and adjusted by Gaussian least squares. The distortions of the NAD 27 with respect to SL-6 can be determined by utilizing the more densely distributed stations in the western United States (Figure 6.1). The distortions in longitude and latitude are shown as contour maps in Figures 6.2 and 6.3. Regions of negative distortion indicate areas where NAD 27's longitude or latitude is larger than SL-6's. Leick & Van Gelder (1975) published similar maps comparing NAD 27 to the NWL9D Doppler satellite center of mass system. Their results agree quite well with those of the present analysis.

6.6 SUMMARY OF STATION DEFINITION

Station positions from a variety of sources have been transformed into a unified geocentric coordinate system (the TCS) to aid in the creation of a preliminary gravity field model to support the TOPEX mission. Complete lists of the stations in the TCS system are found in Appendices 1 and 2. Appendix 1 has the currently maintained TOPEX geodetic file which consists primarily of active laser and Doppler sites. Appendix 2 consists of older optical sites, many of which are no longer active. The transformations used are anticipated to yield station coordinates with an accuracy of 2 to 5 meters in all coordinates for the NAD 27 transformed stations, and 3 to 7 meters for the dynamically determined coordinates transformed into the modified SL-6 system. The stations which appeared in Table 1 are assessed to have coordinate uncertainties in the range of a few centimeters since they have been determined in recent laser/dynamic solutions. Error sources have been identified and attempts have been made to eliminate, as best as possible, their effects on the resulting transformed coordinates. NAD 27 distortions have been estimated in a limited region and are in good agreement with previous studies. Maintenance of the station coordinates as a geodetic file is an ongoing project. As new solutions and data become available, this file will be updated. Since the station

147

coordinates come from a variety of sources, an associated epoch cannot be assigned generally. It is planned that as the TCS geodetic file improves, epoch dates can either be assigned to individual stations or the stations will be rotated to a particular epoch using a set of plate motion parameters. The effects of plate motion will continue to grow as tracking histories lengthen in time.

SECTION 7.0

FORCE MODELING

The force model used for the GEM-T1 development consists of the conservative geopotential forces and the non-conservative solar radiation pressure and drag forces. This section describes the specific application of the models and provides the general basis for the details of the modeling.

7.1 POTENTIAL EFFECTS

The geopotential consists of both a static part, which is defined by the unperturbed mass distribution of the Earth, and a dynamic part, commonly known as the tidal potential, which is due to the mass deformation of the Earth caused by the gravitational forces of the Sun and Moon. The force is computed as the gradient of the potential.

7.1.1 Mathematical Formulation of the Potentials

The standard form of the geopotential is given by:

$$U^S = \frac{\mu}{r} \left[1 + \sum_{n=2}^{nmax} \sum_{m=0}^{n} \left[\frac{a_e}{r} \right]^n \bar{P}_{nm}(\sin \phi) \left[\bar{C}_{nm} \cos m\lambda + \bar{S}_{nm} \sin m\lambda \right] \right] \qquad (7.1)$$

where μ is the gravitational constant of the Earth (elsewhere referred to as GM), r is the geocentric satellite distance, ϕ is the satellite geocentric latitude, λ is the satellite east longitude, $\bar{P}_{nm}(\sin \phi)$ are the associated Legendre functions of the first kind, and $\bar{C}_{nm}$ and $\bar{S}_{nm}$ are the geopotential coefficients. The use of the normalized harmonics is

149

indicated by the overbar. The relationship between the normalized and unnormalized functions is

$$\bar{P}_{nm} = \left[\frac{(n-m)! \ (2\ell+1) \ (2-\delta_{om})}{(n+m)!} \right]^{1/2} P_{nm} \qquad (7.2)$$

where δ_{om} is the Kronecker delta, which equals 1 when m is 0 and otherwise equals 0.

The tidal potential adopted consists of the body tide potential and the ocean tide potential. The body tide potential is modeled based on the frequency dependent elastic response of the Wahr Earth model. The ocean tide model is based upon the spherical harmonic expansion of a simple surface density layer model. Both of these potentials may be expressed in the standard form given above, where the coefficients vary with time. However, tidal potentials are more conventionally expressed in terms of amplitude and phase, where the amplitudes are related to either cm of tide height or to the contribution to the elasticity parameter k_2.

The body tide potential is given by

$$U^B = \sum_f A_f \ k_{2,f} \left[\frac{a_e}{r} \right]^3 P_{2m}(\sin \phi) \cos \left(\sigma_f^B + \delta_{2,f} \right) \qquad (7.3)$$

and the ocean tide potential is similarly expressed as

$$U^O = \sum_f \sum_{\ell,q,\pm} K_\ell \ C_{\ell q}^{\pm} \left[\frac{a_e}{r} \right]^{\ell+1} P_{\ell q}(\sin\phi) \cos \left(\sigma_{\ell q,f}^{\pm} + \epsilon_{\ell q,f}^{\pm} \right) \qquad (7.4)$$

150

where

$\underset{f}{\sum}$ indicates summation over all tidal constituents f.

Λ_f is a body tide constant associated with constituent f.

σ_f^B is the angular argument associated with constituent f of the body tide.

$k_{2,f}, \delta_{2,f}$ are the Love number amplitude and phase respectively which describe the body response of the Earth.

m   is the order associated with f and is 0 for the long period tides, 1 for the diurnal tides, and 2 for the semi-diurnal tides.

K_ℓ is an ocean tide constant associated with degree ℓ.

$\sigma_{\ell q,f}^\pm$ is the angular argument associated with the $(\ell,q,\pm)$ subharmonic of the ocean tide generated by constituent f.

$C_{\ell q}^\pm, \epsilon_{\ell q,f}^\pm$ are the amplitude and phase of the $(\ell,q,\pm)$ subharmonic of the ocean tide generated by constituent f.

Each constituent f is associated with an unique frequency. It should be noted that if

$$k_{2,f} \equiv k_2$$

$$\delta_{2,f} \equiv \delta_2 \qquad\qquad (7.5)$$

for all f, then the total body tide potential may be simply computed in the time domain using the potential

151

$$U^B = \sum_d \frac{k_2}{2} \frac{\mu_d \, a_e^2}{r_d^3} \left[\frac{a_e}{r} \right]^3 \left[3 \left[\frac{\overline{r}_d \cdot \overline{r}}{r_d \, r} \right]^2 - 1 \right] \qquad (7.6)$$

where $\overline{r}_d$ is the geocentric vector to the Sun or Moon and μ_d is the gravitational constant of the Sun or Moon. For a frequency dependent model for the Love numbers, most of the variations are concentrated in a single band (the diurnal). It is computationally efficient to use a simple background model and correct terms for which the Love numbers differ significantly from the background reference values. This procedure was adopted.

The tidal constituent f is uniquely identified by the Doodson argument number. Table 7.1 identifies the principal tidal frequencies and gives the (approximate) matching Darwinian symbol for each corresponding Doodson number. The frequencies are based upon the ecliptic element rates. Note that these same frequencies are also present in the ocean tide effects.

7.1.2 The a priori Static Geopotential Models

The a priori models adopted for the GEM-T1 development are:

    GEM-L2'   for   LAGEOS
    PGS-1331'   for   Starlette
    PGS-S4'   for   SEASAT
    GEM-10B'   for   all other satellites

These gravity models were analytically corrected to zero mean pole, modern ellipsoid parameters (a_e=6378137m, f^{-1}=298.257), and the adopted definition of the new speed of light (c=2.99792458x10^8m/sec).

TABLE 7.1

Darwinian Symbol	Doodson's Argument Number	Period (hr)	Description
M_2	255.555	12.42	Principal lunar semidiurnal
S_2	273.555	12.00	Principal solar semidurnal
N_2	245.655	12.66	Larger lunar elliptic semidiurnal
K_2	275.555	11.97	Lunar/Solar semidiurnal
L_2	265.455	12.19	Smaller lunar elliptic
K_1	165.555	23.93	Lunar/Solar diurnal
O_1	145.555	25.82	Principal lunar diurnal
P_1	163.555	24.07	Principal solar diurnal
M_f	075.555	13.66d	Lunar fortnightly
M_m	065.455	27.55d	Lunar monthly
S_{sa}	057.555	188.62d	Solar semi-annual

7.1.3 The a priori Body Tide Model

Table 7.2 gives the Love numbers computed by Wahr (1979), based upon the Earth Model 1066A of Gilbert & Dziewonski (1975). Note that $\delta_{2,f}$ is zero for this elastic model, i.e., the model is free of dissipation. These Love numbers fully characterize the response of the 1066A Earth to the non-loading tide generating potential.

7.1.4 A priori Ocean Tides Models

The response of the oceans to the tide generating potential is a set of constituent tide heights

$$\xi_f(P) = A_f(P) \cos \left(\omega_f - \psi_f(P)\right) \tag{7.7}$$

where ω_f is the angular argument associated with constituent f and $A_f(P)$ and $\psi_f(P)$ are the tidal amplitude and phase respectively at point $\dot{P}$. The amplitudes and phases are computed from numerical solutions of the Laplace Tide Equations. Such solutions involve a high computational burden and presently such models are available for only a limited number of tidal constituents.

The tidal heights are expanded into spherical harmonics by:

$$\xi_f(P) = \sum_{\ell,q,\pm} C^{\pm}_{\ell q,f} \; P_{\ell q}(\sin \phi) \cos \left(\sigma^{\pm}_{\ell q,f} \pm \epsilon^{\pm}_{\ell q,f}\right) \tag{7.8}$$

Given the global tidal heights, the coefficients $C^{\pm}_{\ell q,f}$ and phases $\epsilon^{\pm}_{\ell q,f}$ necessary for the evaluation of the potential can be computed.

154

TABLE 7.2

WAHR LOVE NUMBERS FOR 1077A

Band	Tidal Line	$k_{2,f}$
Long Period	All	.299
Diurnal	145555 (O1)	.298
	163555 (P1)	.287
	165545	.259
	165555 (K1)	.256
	165565	.253
	166554 (PSI)	.466
Semi-Diurnal	All	.302

Observed tide models for 11 major tide constituents in the semidiurnal, diurnal, and long period bands have been computed on a 1° x 1° global grid by E.W. Schwiderski using an integration scheme which incorporates the available deep sea tide gauge data. These tidal constituents should account for over 90% of the total ocean tide amplitude at any point. However, no models are available for the minor tide constituents, which although small in amplitude, can have significant perturbing effects on a satellite's orbit.

Table 7.3 shows the estimated radial perturbation amplitude due to the major ocean tide constituents on the proposed TOPEX orbit and on the GEOS-3 orbit. This analysis was based upon a Kaula-type first order linear orbit perturbation theory. More than half of the constituents have effects which exceed 1 decimeter radially. These terms must be modeled. It is probable that the associated minor tides for some of these also must be modeled if the minor tide response is proportional to the tide raising potential of the major tide.

Figure 7.1 presents a qualitative analysis of 53 satellites, whose tracking data might contribute to an improved geopotential model. A crude estimate of the ocean tide effect is about 10% of the body tide. The 53 satellite orbits were evaluated for their nominal ocean tide perturbations at 230 tidal frequencies. These 53 orbits represent a variety of orbital inclinations and altitudes, and all have reasonable tracking data histories. Figure 7.1 shows the number of satellites having effects over .001 arcsec in the inclination as a function of tidal frequency. Satellites were also included if the principal third degree terms from an ocean tide decomposition produced a perturbation in the orbit eccentricity greater than 1 ppm. In this analysis, the amplitude of the ocean tide coefficients was assumed to be 1 cm. Note that the criterion of 1 ppm perturbation in the eccentricity is equivalent to the criterion of a .001 arcsec perturbation in the inclination.

156

TABLE 7.3   OCEAN TIDE RADIAL PERTURBATION AMPLITUDES ON SATELLITE ORBITS

	Schwiderski Tide Model	Tide Frequency (cycles/Day)	GEOS-3 Amplitude (cm)	TOPEX Amplitude (cm)
LONG-PERIOD	S_{sa}	0.005	10	6
	M_m	0.036	1	1
	M_f	0.073	1	1
DIURNAL	Q_1	0.083	2	2
	O_1	0.930	13	–
	P_1	0.997	24	24
	K_1	1.003	125	116
SEMI-DIURNAL	N_2	1.896	3	2
	M_2	1.932	3	13
	S_2	2.000	29	70
	K_2	2.005	13	13

157
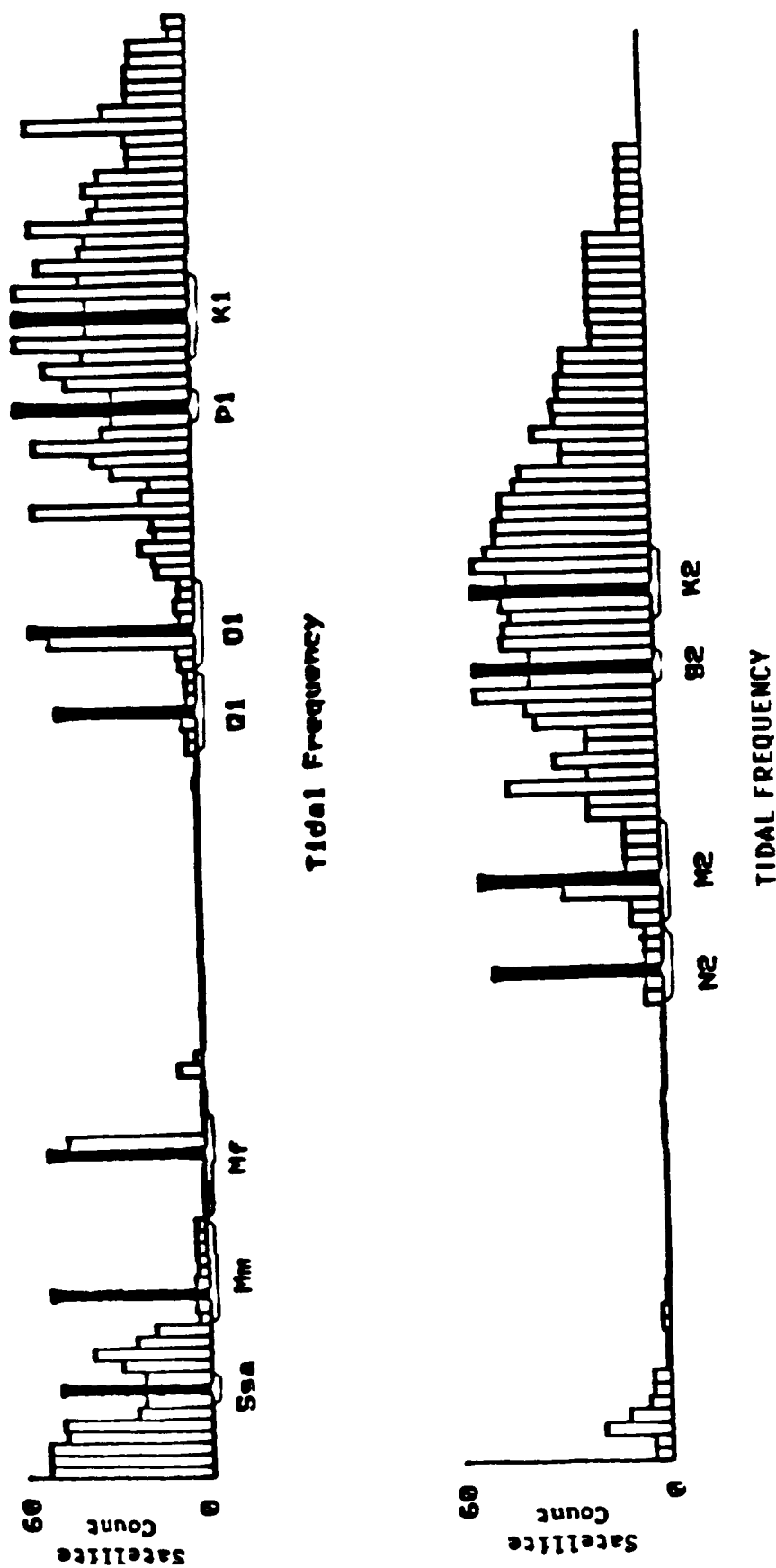
Figure 7.1 Histogram of the Number of Satellites with Strong Sensitivity to Various Tidal Frequencies.

158

This analysis revealed more than 150 possibly significant tidal constituents. A substantial number of these are associated, not with the main tidal frequencies, but with the nearby sideband frequencies. The periodicities of the satellite orbital motion are convolved with those of the tides as seen on the Earth to produce the frequencies seen at the satellite. Some of the sideband terms are closer to exciting orbital resonance than the dominant tidal terms due to their commensurability with orbital frequencies. However, only the low degree and order terms in the spherical harmonic expansion of the tides can have significant potential effects on the satellites because of the attenuation with distance of these effects on orbiting objects. Our fundamental concern is thus with the long wavelength character of the tides.

The most complete set of a priori ocean tides available represents only the main tidal frequencies. A procedure was developed in order to provide estimates and their errors for the sideband terms from existing oceanographic models in order to both perform a quantitative error analysis and to better assess the recoverability of the low degree and order spherical harmonic tidal terms in a true simultaneous solution with the terms of the geopotential. The complete ocean tidal model which was used as a priori is given in Appendix 3.

The procedure is based upon the concept of admittance, as detailed below. Models were derived for some 36 minor tides, which are on a one degree global grid matching that of Schwiderski. These models have also been converted to spherical harmonics for the subsequent satellite studies. The use of the admittance was motivated by the study of Munk and Cartwright (1977).

The tide raising potential at time t and at latitude ϕ and longitude λ is given by

$$\Gamma(\phi,\lambda,t) = \sum_{\beta} \Gamma_\beta(\phi,\lambda,t) = \sum_{\beta} g \, \eta_\beta \, P_{2m}(\sin \phi)\cos[\sigma_\beta t + \chi_\beta + m\lambda] \quad (7.9)$$

where β designates the particular constituent of frequency σ_β and equilibrium tide amplitude η_β. χ_β is the phase constant associated with the ephemerides of the Sun or Moon for the epoch of January 0,1900. The gravitational acceleration at the Earth's surface is represented by g. P_{2m} is the associated Legendre function of degree 2 and order m. The terms for degree greater than 2 are of negligible effect (e.g. Munk and Cartwright,1977). Note that in specifying β, m is also specified.

The response to this perturbing potential is the set of constituent tide heights

$$\xi_\beta(\phi,\lambda,t) = A_\beta(\phi,\lambda) \cos[\sigma_\beta t + \chi_\beta - \psi_\beta(\phi,\lambda)] \qquad (7.10)$$

where $A_\beta(\phi,\lambda)$ and $\psi_\beta(\phi,\lambda)$ are the amplitude and phase respectively. The admittance function relating the complex exponential signal Γ_β' corresponding to the input signal Γ_β with the complex output signal ξ_β' for the constituent β is given by

$$Z_\beta(\phi,\lambda) = \frac{A_\beta}{g \, \eta_\beta \, P_{2m}} e^{-j(\psi_\beta+m\lambda)} \qquad (7.11)$$

These admittances are readily computed from the known tides. If, on the other hand, the admittance is known for constituent β, then one may compute

$$\xi_\beta = R_e[\xi_\beta'] = R_e[Z_\beta \Gamma_\beta'] \qquad (7.12)$$

Thus, if reasonable admittance function descriptions could be obtained from the known tides, the unknown tides could be estimated.

The major tide constituent data, the Schwiderski models (1980a, 1980b), were obtained in the form of a standard NSWC GOTD-1981 tape, i.e. tide values for A_β and ψ_β on a one degree global grid. The rms values of these constituents, computed from their spherical harmonic representation, are tabulated in Table 7.4. Also shown are NSWC's estimated errors for the semidiurnal and diurnal tides and each constituent's equilibrium tide amplitude, η_β. NSWC did not provide us with estimated errors for the long period tides. Nominal errors for the long period band were estimated as being proportionately as well determined relative to the equilibrium tide as M_2, i.e., 12.8%. The model errors are available only in an overall rms sense - the geographic distribution of the estimated errors is not available. Note that there are only four semidiurnal, four diurnal, and three long period tides available.

From the outset, we chose to do separate analyses for the semidiurnal, diurnal, and long period bands so that the range of frequency being represented was more limited. The procedure assumes that the tidal admittance is locally a linear function of frequency, i.e. within each band at each particular ϕ, λ point on the Earth's surface. This linearity assumption was adopted because global nonlinearities are anticipated to be small, and also, for the practical reason that there are only at best four points to interpolate over (or extrapolate from) in each band. The procedure is illustrated in Figure 7.2. Proportionally, there is a much greater span of frequency variation in the long period band than in the diurnal or semidiurnal band. However, only three long period tides are available, so this frequency band cannot be further segmented to reduce the range of interpolation. Also, the NSWC M_m and M_f tides are smaller by a factor of 3 or 4 compared to their equilibrium values. This suggests a conflict with the assumption of linearity of the admittances across the long period tidal band.

TABLE 7.4

NSWC TIDE MODELS

Cumulative RMS Tide Values Summed to Degree 30 and their RMS Errors

Tide Constituent	Equilibrium Tide Amplitude η_β (cm)	NSWC RMS (cm)	NSWC Model Errors (cm & deg)*	
			Amplitude	Phase
M_2	24.2	30.0	3.11	3.72
S_2	11.3	12.2	1.28	4.24
M_2	4.6	6.5	0.51	4.12
K_2	3.1	3.4	0.23	3.13
K_1	14.1	10.9	0.94	9.95
O_1	10.1	7.9	0.57	3.42
P_1	4.7	3.5	0.20	4.14
Q_1	1.9	1.7	0.08	2.41
M_f	4.2	1.0	--	--
M_m	2.2	0.8	--	--
S_{sa}	1.9	1.6	--	--

*From Table of Comparison of Empirical and Modeled Ocean Tides at 195 Island and Deep-Sea Stations (used and not used), E.W. Schwiderski, private communications.
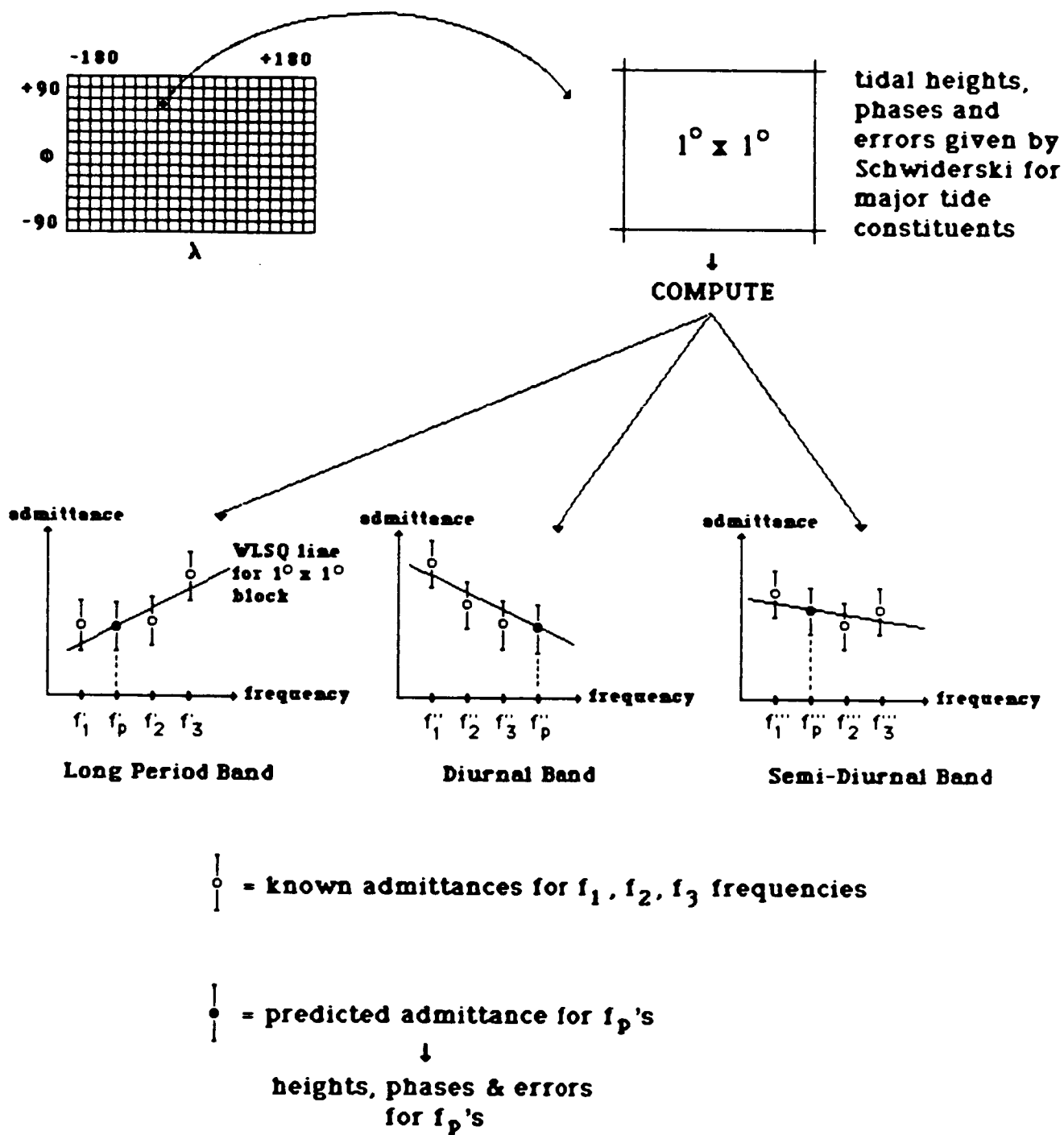
Figure 7.2. Background Tides Model Development.

163

The residuals from the fitting process reflect the disagreement of the NSWC tides with this hypothesis. The fitting process is a least squares linear regression weighting each $A_\beta \cos \psi_\beta$ or $A_\beta \sin \psi_\beta$ according to the specified NSWC estimated errors:

$$\text{weight} = (\delta a^2 + A_\beta^2 \delta \psi^2)^{-1} \tag{7.13}$$

where δa represents the error in $A_\beta(\phi,\lambda)$ and $\delta \psi$ represents the error in $\psi_\beta(\phi,\lambda)$. For the long period tides, we estimated that the error was proportionally the same as for M_2, which is 12.8% of the equilibrium tide amplitude. Because we are dealing with tide models as data, our residuals should be dominated by local nonlinearities in areas such as the Patagonian Shelf and the more global nonlinearities due to the Earth's diurnal resonance. The differential response to solar radiation will be present. These residuals will also reflect nonlinearities in the physical modeling of Schwiderski (1980a, 1980b) and any systematic data errors specific to a particular tide. Clearly, if a nonlinear hypothesis were to be adopted to replace the linear arc based on the admittance concept, a physically justifiable nonlinear model would be essential.

The global amplitudes and phases for the M_2 tide as computed by Schwiderski and our numerical model are compared in Figures 7.3 and 7.4. The models are qualitatively the same, which indicates that, in a global sense, we have not seriously mismodeled this important tide. This is true for all of the semidiurnal and diurnal tides. The upper part of Figure 7.5 shows the global amplitude of the residuals in M_2 (vector magnitude). As expected, local areas such as the Patagonian Shelf dominate the residuals. There are also significant differences in the general area of the Marquesas Islands and the western Atlantic. The lower part of Figure 7.5 shows the percentage relative error, indicating that the error is typically less than 20%. The regions of high relative error, greater than 20%, generally correspond to amphidrome locations

Schwiderski M$_2$ Tide — Amplitude in Cm

Interpolated M$_2$ Tide — Amplitude in Cm.
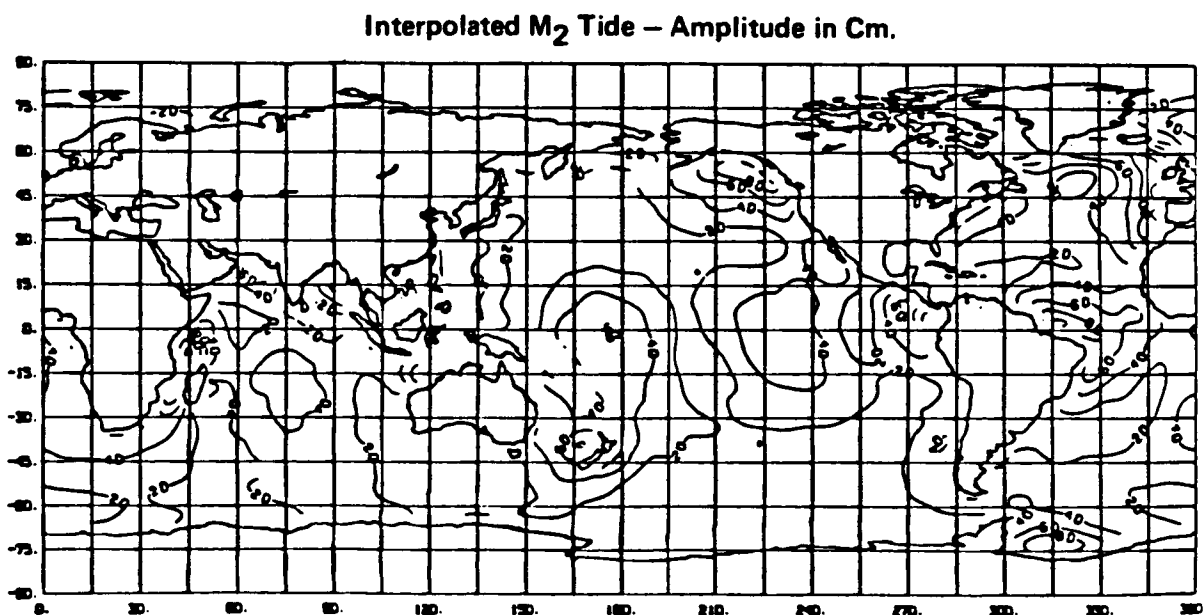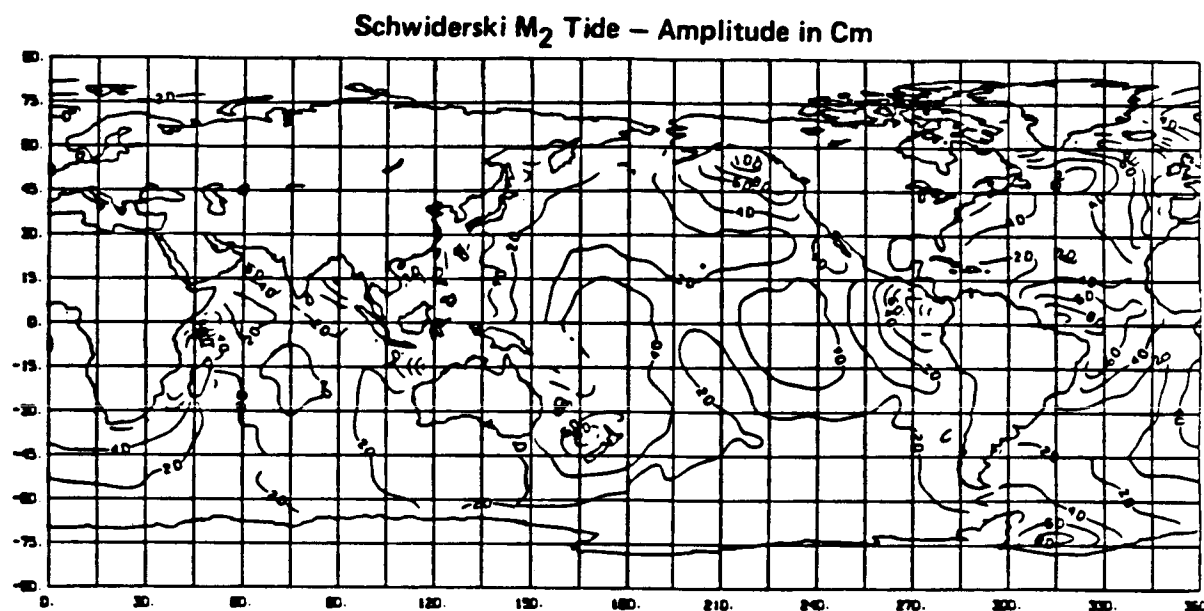
Figure 7.3. Comparison of M$_2$ Tide Amplitudes.

165

Schwiderski M$_2$ Tide — Phases in Deg.
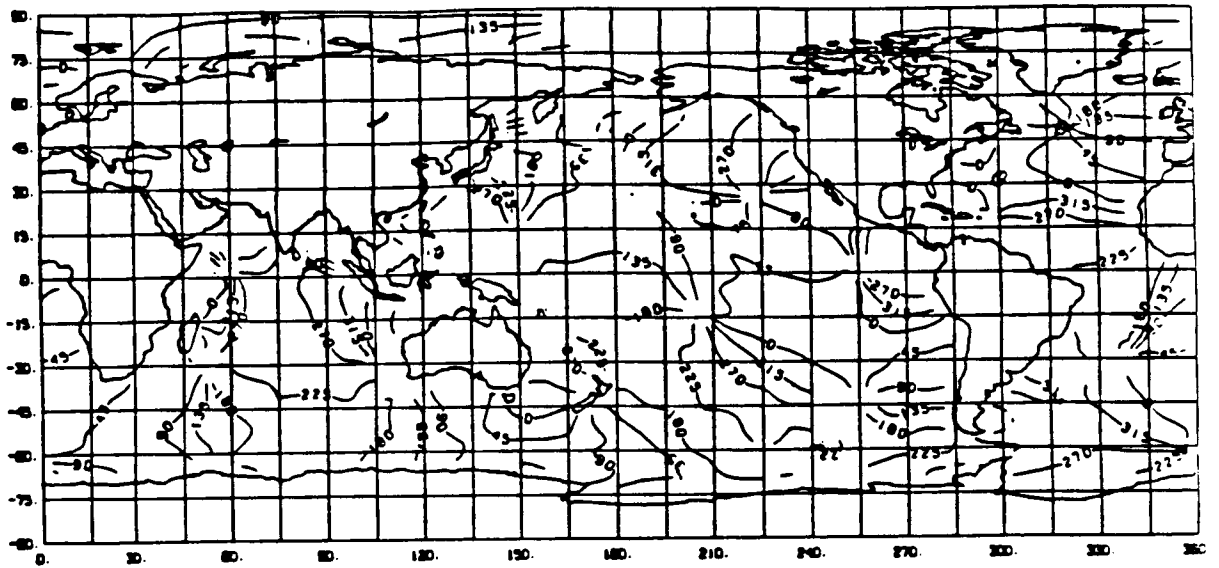
Interpolated M$_2$ Tide — Phases in Deg.
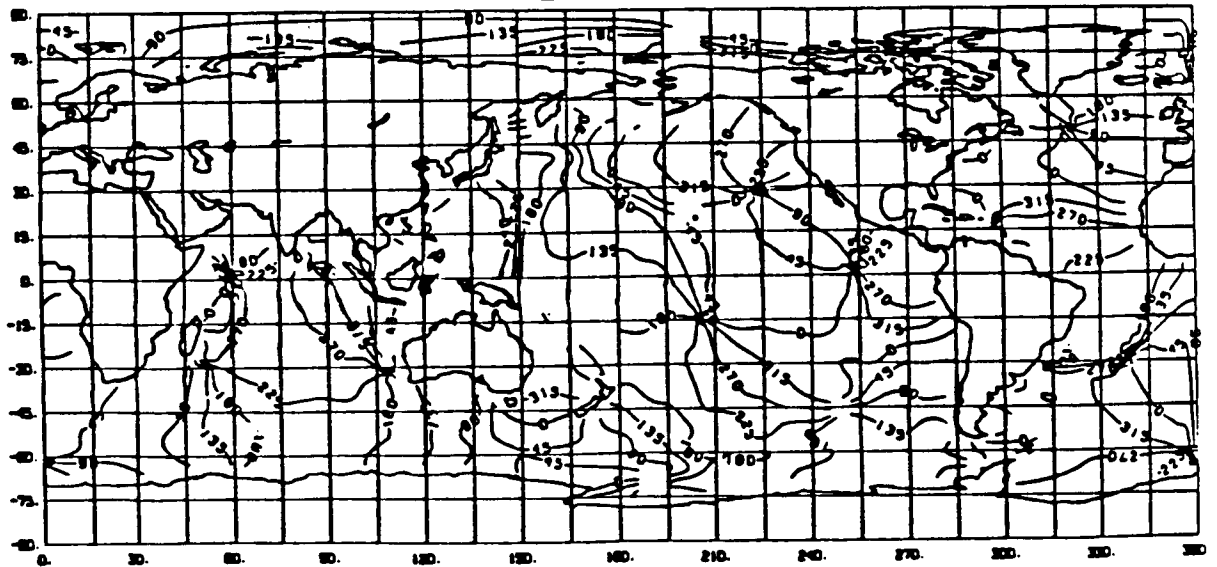
Figure 7.4. Comparison of M$_2$ Tide Phases.

166

Amplitude of Error In Cm

Relative Error in Percent

Figure 7.5. Error in Interpolated M_2 Tide.

167

where the amplitude variability is small. This example is typical of the results we obtained for all of the tides in the diurnal and semidiurnal bands.

Similar comparisons for the long period tides show large regions of high relative error, over 100%, which indicates that our approach has difficulties with the long period tidal band. These difficulties were not unexpected given the substantial frequency range within this band. However, as there are only three major tides available in this band, there is no practical alternative.

Table 7.5 presents the global statistical summary for each of the NSWC tides. The rms of fit in cm shown was computed from the rms admittance. With the exception of O_1 and M_2, the rms global fit in each of the semidiurnal and diurnal bands shows that the linear model disagrees with the NSWC input by approximately the estimated error in NSWC. O_1 and M_2 disagree by a factor of two in this quantity. M_2, the worst case, has a weighted rms disagreement of 7 cm out of a total 30 cm, yet still has an error in power of less than 5%. The fits in the long period band confirm the conclusion that these tides are not adequately modeled with this procedure, in that the weighted rms residual amplitude is on the order of the entire NSWC rms tide amplitude. However, the weighted rms residual amplitude is only twice our 12.8% of the equilibrium tide amplitude. As can be seen in Table 7.4, the NSWC M_m and M_f tide amplitudes are quite different from the equilibrium tide amplitudes.

The standard deviations of unit weight given in Table 7.5 provide the factors by which the NSWC rms amplitude errors need to be adjusted in order to map the weighted residuals into the unit normal distribution. The semidiurnal and diurnal bands are near unity, but the long period band is off by a factor of 2.5. Thus the linear model is not inconsistent with the semidiurnal and diurnal data, but it is

168

TABLE 7.5 SUMMARY OF AMPLITUDES AND ERRORS

Band i	Tide j	Equilibrium Tide Amplitude K_β (cm)	NSWC RMS Ampl. (cm) $\bar{a}_{ij}$	NSWC RMS Ampl. Err. (cm) $\bar{\sigma}_{a_{ij}}$	RMS Residual Mod. Admittance $\bar{\delta M}_{ij}$	RMS Residual Amplitude (cm) $\bar{\delta a}_{ij}$	Stand. Dev. of Unit Wt. $\hat{\sigma}_{o_1}$	Estimated RMS Ampl. Error (cm) $\hat{\sigma}_{o_1} * \bar{\sigma}_{a_{ij}}$
0	S_{sa}	1.9	1.6	0.2*	0.27	0.5	2.5	0.5
	M_m	2.2	0.8	0.3*	0.37	0.8		0.8
	M_f	4.2	1.0	0.5*	0.16	0.7		1.3
1	Q_1	1.9	1.7	0.1	0.05	0.1	1.1	0.1
	O_1	10.1	7.9	0.6	0.12	1.2		0.7
	P_1	4.7	3.5	0.2	0.03	0.2		0.2
	K_1	14.1	10.9	0.9	0.06	0.9		1.0
2	N_2	4.6	6.5	0.5	0.18	0.8	1.3	0.7
	M_2	24.2	30.0	3.1	0.29	7.0		4.0
	S_2	11.3	12.2	1.3	0.13	1.5		1.7
	K_2	3.1	3.4	0.2	0.07	0.2		0.3

*Estimated

inconsistent for the long period tides assuming the projected error estimates for these tides are correct. However, rms fits are still less than 40% of the equilibrium amplitude for these long period tides, and are only about twice the estimated nominal error in these tides.

In addition to computing the unknown tides, we have also computed the associated errors of these tides based on errors which have been corrected to attain unit variance. The error at a point is simply obtained by propagating the covariance matrix associated with each point to the desired frequency.

7.2 ATMOSPHERIC DRAG AND SOLAR RADIATION PRESSURE

The non-conservative forces which are of concern in modeling the evolution of the spacecraft orbit are the forces of atmospheric drag and solar radiation pressure.

7.2.1 Mathematical Formulation of the Models

In GEODYN, the acceleration due to atmospheric drag is

$$\bar{A}_D = - \frac{1}{2} C_D \left| \overline{\frac{A}{M}} \right| \rho_D v_r \bar{v}_r \tag{7.14}$$

where C_D is the satellite drag coefficient, A is the cross-sectional area of the satellite, M is the mass of the satellite, ρ_D is the density of the atmosphere, $\bar{v}_r$ is the velocity vector of the satellite relative to the atmosphere and V_r is its modulus. The atmosphere model is the 1971 Jacchia; the atmosphere is presumed to rotate with the Earth.

The acceleration due to solar radiation pressure is given by

$$\bar{A}_R = -\nu \; C_R \; \left| \overline{\dfrac{A}{M}} \right| \; P_s \; \dfrac{P_s}{R_s^2} \; \hat{r}_s \qquad (7.15)$$

where ν is the eclipse factor accounting for shadowing of the satellite by the body of the Earth, C_R is the satellite radiation pressure coefficient, A and M are as before, P_s is the solar radiation pressure in the vicinity of the Earth, R_s is the distance from the satellite to the sun in AU, and $\hat{r}_s$ is the geocentric unit vector pointing toward the Sun.

Both of these models assume the satellite is a sphere. However, the adjustment of the drag and/or radiation pressure coefficient accommodates much of the model error associated with the spacecraft shape. Errors in the density model are similarly accommodated, but, because the atmosphere varies with time, multiple drag coefficients are often required to accomodate the observed drag variations. GEODYN has the capability to model either the drag or solar pressure effects using piecewise discontinuous coefficients over specified time intervals, and, within each time interval, the coefficient can vary according to

$$C = C_0 + \dot{C} \; (t-t_0) \qquad (7.16)$$

For the present efforts, we are only using this capability with the drag modeling.

7.2.2 Atmospheric Drag Model Testing

Almost all of the satellites used in our analyses are significantly perturbed by drag. Given that there are model errors in both the shape of the spacecraft and in the atmospheric density model, the major

171

question to be answered was how best to parameterize the drag so as to minimize the atmospheric drag error within the orbital solutions. The parameterization options investigated were:

(a) a constant scale parameter, C_D, adjusted once in the arc

(b) a C_D and $\dot{C}_D$ adjusted over the length of the arc, or

(c) solution for several C_D values over specified time intervals, (i.e. once per day) over the arc length.

This investigation was most conveniently performed using the GEODYN I software, as it has variable area modeling capabilities and a selection of atmospheric density models -- specifically both the 65 and 71 Jacchia models (Jacchia, 1965, 1971). The BE-C satellite was used as the basis for this investigation.

The BE-C orbit has received a good deal of attention from its contributions to the San Andreas Fault Experiment and the analysis of laser ranging to determine intersite station distances within California (see for example Smith et al., 1977). Of the set of laser satellites which were used in the creation of GEM-T1, BE-C presented one of the most difficult atmospheric drag modeling problems. It was magnetically stabilized, which caused its in-plane cross-sectional area to vary significantly over each orbital revolution. BE-C also has a somewhat eccentric orbit (e=0.0257) with a perigee height of 940km. A variable cross-section surface area model for BE-C was developed by Safren, 1975. Given that BE-C also has a reasonably strong set of laser ranging data, tests of drag modeling error could be designed using orbit intercomparisons and analysis of along track errors sensed at the observing sites using the real tracking data and resulting orbits directly.

Several five-day arcs were selected. These arcs were chosen so as to represent the full spectrum of tracking available on BE-C. For example, a well tracked arc (epoch of 790417) having a total of 78 passes was used. On the other hand a somewhat weaker arc having only 30 passes (epoch of 800201) was also selected. Table 7.6 shows the geographic distribution of the data found in each of these arcs.

7.2.2.1 Orbit Comparison Results

The representation and solution of drag parameters was tested preliminarily through a series of trajectory comparisons. Each of the approaches ((a) through (c) outlined above where (c) was tried two ways-with a coefficient adjusted every 12hrs. and once per day) was utilized to converge each of the five day arcs. Both the Jacchia 1965 and 1971 models were employed. All of these resulting trajectories were intercompared every minute over their respective 5 day intervals as shown in Table 7.6.

Table 7.6 summarizes the RMS along track trajectory component differences for each of these comparisons as shown in Figure 7.7. In all cases, drag predominantly perturbed the along track component of the orbit, with radial and cross track RMS differences always being less than 0.6m. The data sets and non-drag force models were the same in all orbits with the same epoch. The differences in the trajectories are due to drag modeling differences which can be construed as an estimate of drag model error. The effects of this drag error are to be minimized through the solution of drag scaling parameters. Therefore, where different density models show the greatest agreement, this minimization has been effective. There is also some concern that over-parameterization of the drag effects could result in an aliasing of drag and long period gravity signals. Therefore, it was desirable that the number of degrees of freedom devoted to drag scale parameters be held to a minimum unless strong evidence was present indicating a need for
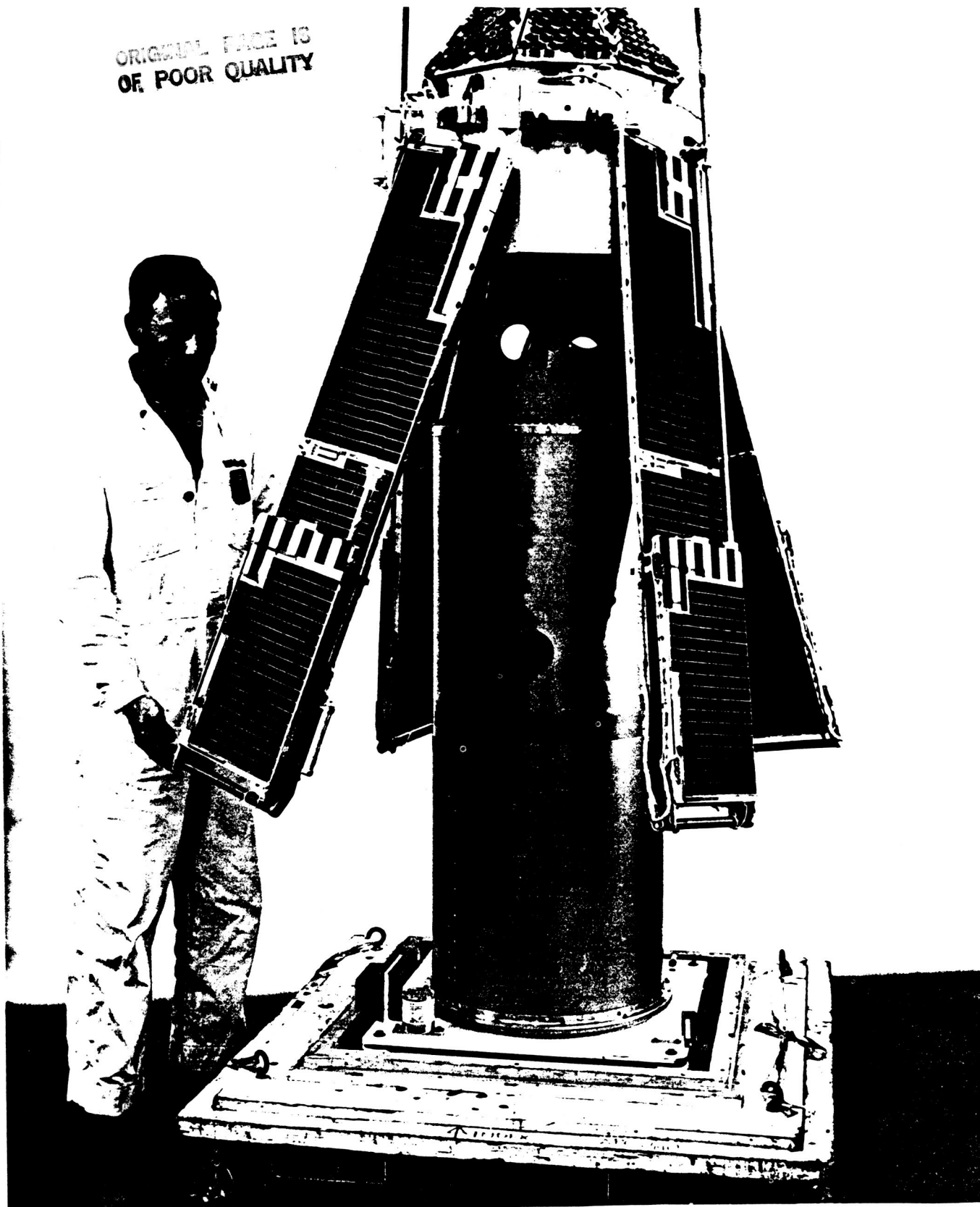
NASA G-65- 6565

Figure 7.6.   BE–C.

174

Table 7 6

BE-C DRAG MODELING ORBITAL COMPARISONS

TEST ARCS: 5 DAY ARC LENGTHS

No. of passes:	790417	800201
W. USA	51	24
E. USA	24	1
S. Am.	3	0
Hawaii	0	5
TOTAL	78	30

790417:   ORBIT COMPARISONS: RMS ALONG TRACK DIFFERENCES (m)

	J71 CD+CDOT	J71 CD/DAY	J71 CD/12H	J65 CD+CDOT	J65 CD/DAY
J71 CD/DAY	3.0				
J71 CD/12H	3.4	0.8			
J65 CD+CDOT	1.6	4.3	4.7		
J65 CD/DAY	3.0	1.2	1.2	4.1	
J65 CD/12H	3.6	1.9	1.4	4.6	1.1

800201:   ORBIT COMPARISONS: RMS ALONG TRACK DIFFERENCES (m)

	J71 CD+CDOT	J71 CD/DAY	J71 CD/12H	J65 CD+CDOT	J65 CD/DAY
J71 CD/DAY	9.3				
J71 CD/12H	9.2	1.5			
J65 CD+CDOT	1.4	8.7	8.5		
J65 CD/DAY	11.5	2.7	2.9	10.7	
J65 CD/12H	11.2	3.1	2.5	10.4	1.5

RMS Cross Track and Radial Differences are all less than 0.6 m
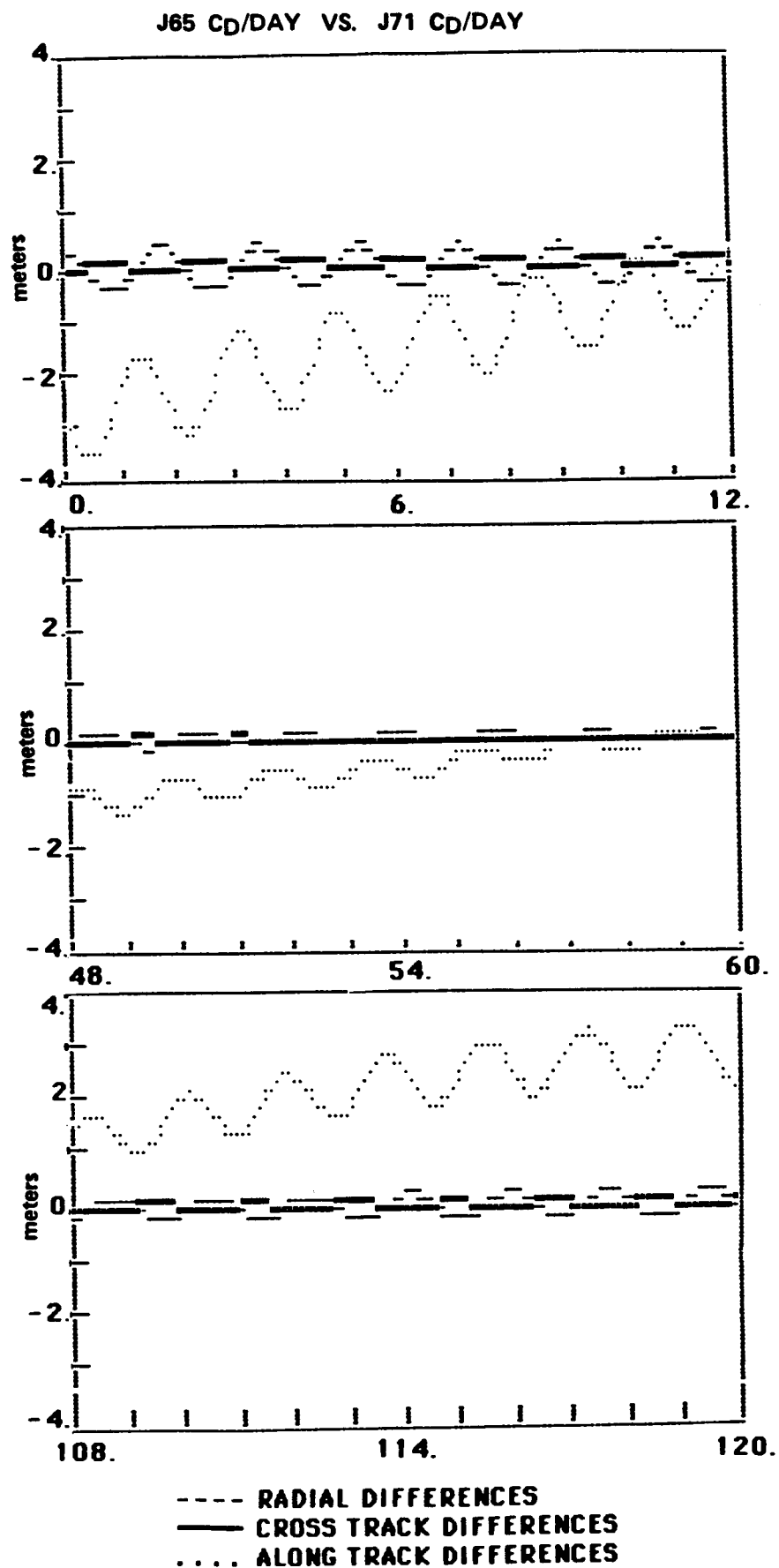
Figure 7.7. Trajectory Differences: BE–C 5 Day Arcs.

additional drag parameters. The drag/day and drag/12hr representations clearly had the best overall performance for reducing drag error and producing the most similiar orbits. This representation yielded results which on the arcs with the strongest tracking showed agreement of better than 2m RMS along track between trajectories calculated using different density models. Even for the weaker second arc, results no worse than 3.1 m RMS were obtained. Since there was no clear improvement to be seen in the C_D/12hr drag parameterization, the C_D/day approach was adopted as the most desirable on the basis of these tests.

These orbits were tested invoking the variable cross-sectional area model and compared with trajectories calculated modeling a constant satellite surface area. No significant improvement was found when the variable area model was utilized. As the variable area modeling was not available in GEODYN II, the data analysis proceeded using constant satellite cross-sectional area values.

7.2.2.2 Evaluation of Apparent Timing Errors

This second approach is based upon analysis of the apparent timing errors seen in each pass of tracking data. As most of the satellite's motion is in its orbital plane, an error in the calculated orbit causes the acquisition time at a station to appear either early or late with respect to the actual observations--these are the so-called apparent "timing errors" which are analyzed. Figure 7.8 presents the apparent timing errors seen in a 5 day arc (epoch 811012) when different parameterizations are employed for the minimization of drag errors.

The intercomparison of the spectra of the timing errors associated with the various types of drag parameterization provided the basis for the evaluation. It is assumed that, if one could completely eliminate drag model errors through some parameterization, then the
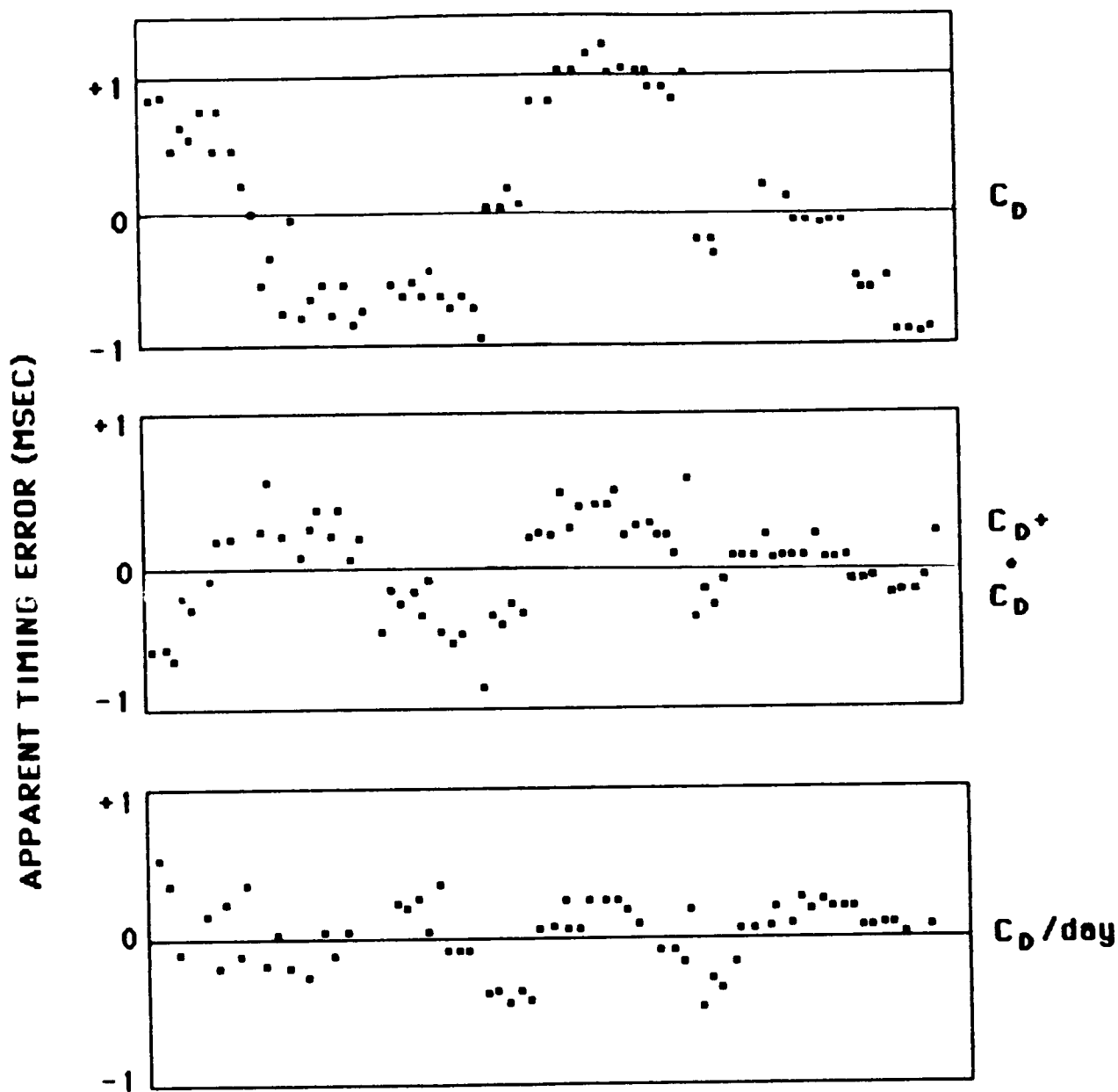
Figure 7.8. Apparent Timing Errors in Laser Passes within a Five Day Arc of BE–C Using Different Representations of Drag Parameterization.

resulting spectra would be unaffected by the density model used. Conversely, if the same representation of drag yielded very different timing error spectra when different density models were used, then it is expected that there would be a strong residual drag related aliasing signal corrupting the computed orbit. Figure 7.9 compares the timing error spectra using different density models for each of the drag parameterizations described above. The difference in the spectra when drag is represented by a C_D and a $\dot{C}_D$ strongly indicates that there is considerable residual drag error left within each of the calculated trajectories. This large error is greatly reduced when a C_D/day or C_D/12hr modeling is used. Other arcs were tested and gave the same strong evidence that a C_D/day coefficient recovery was the most desirable representation requiring a limited set of solution parameters.

7.2.2.3 Conclusions

The BE-C atmospheric drag investigation led to the adoption of the C_D/day parameterization for the orbital data reductions and normal equation generations for the GEM-T1 solution. This representation was used on all near-Earth laser, flashing lamp optical and Doppler satellites. It was not possible to use this approach for the passive optical satellites whose data were too sparse to support daily drag parameter recoveries. LAGEOS and STARLETTE, given their extemely high density and insensitivity to atmospheric drag, required a solution of a single drag parameter for each orbital arc. Table 7.7 summarizes the treatment of the orbital specific parameters by satellite in the analysis and normal equation generation phases of the GEM-T1 investigation.

Further investigations of this nature are planned for future iterations of the gravitational field models. Tests involving the atmospheric model of Barlier (1978) are to be included.

J65 C_D, $\dot{C}_D$ RMS = 3.613 m

J71 C_D, $\dot{C}_D$ RMS = 2.549 m

J65 C_D/DAY   RMS = 1.312 m

J71 C_D/DAY   RMS = 1.566 m

J65 C_D/12 HR   RMS = 1.167 m

J71 C_D/12 HR   RMS = 1.093 m

% power

5   2.5   0.04
             period (days)
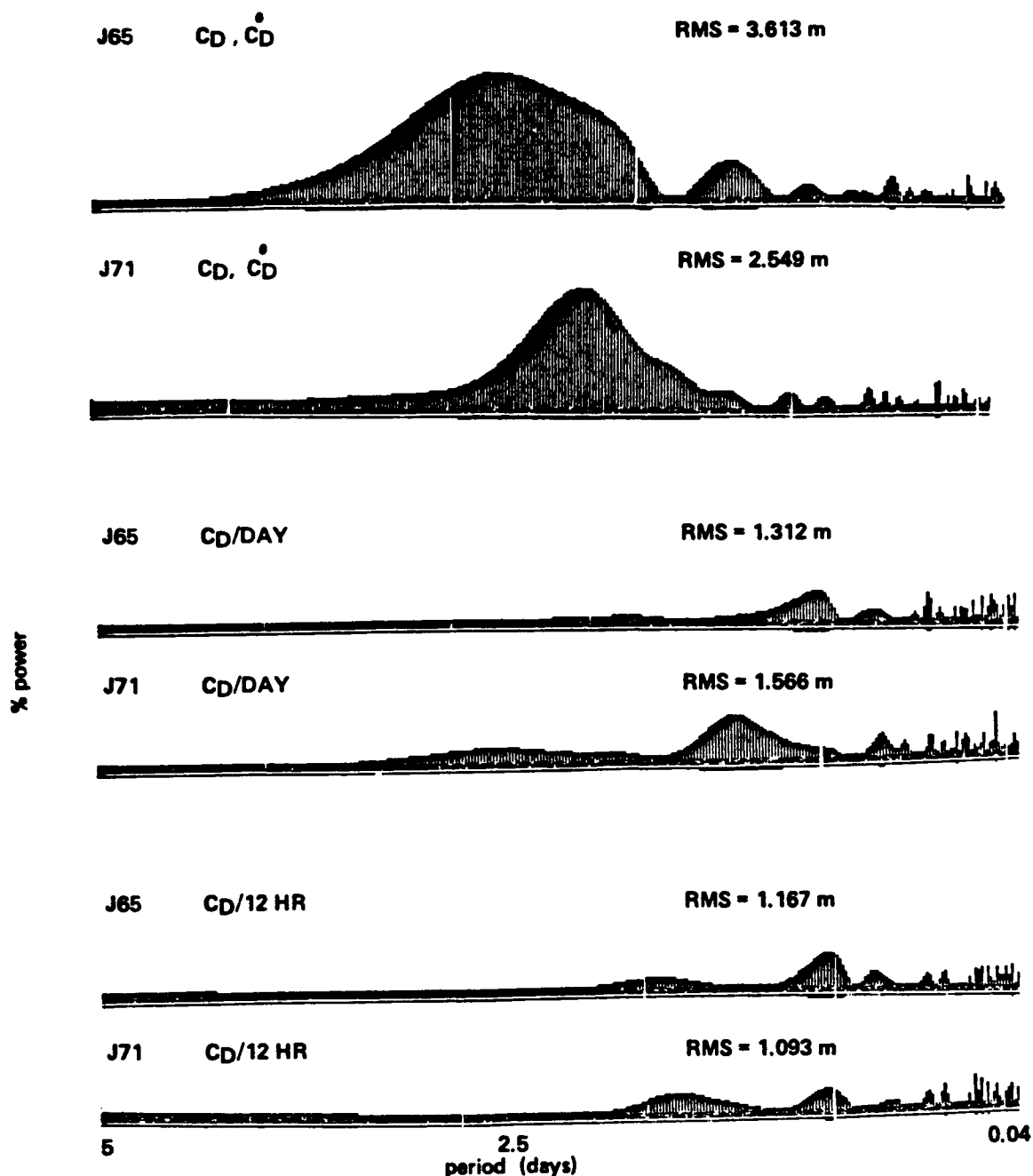
SPECTRUM OF APPARENT STATION TIMING ERRORS FOR A BE-C
FIVE DAY ARC WITH GOOD GLOBAL DATA DISTRIBUTION:

NO. of PASSES:
    S. Am.   16
    W. USA   21
    E. USA   18
    Haw   12

811012 EPOCH :

Figure 7.9. Atmospheric Drag Parameterization Test.

180

Table 7.7

SATELLITE ARC DEPENDENT PARAMETERS USED IN THE DATA ANALYSIS & NORMAL EQUATION GENERATION

SATELLITE	ARC LENGTH	DRAG	SOL. RAD.	ACCEL.
LAGEOS	30^D	-	$C_r , \dot{C}_r$	$a, \dot{a}$
STARLETTE	5^D	C_D	C_r	—
OTHER LASER	5^D	C_D/DAY	$C_r , \dot{C}_r$	—
DOPPLER	$6^D, 7^D$	C_D/DAY	$C_r , \dot{C}_r$	—
FLASHING LAMP	7^D	C_D/DAY	$C_r , \dot{C}_r$	—
PASSIVE OPTICAL	7^D	$C_D , \dot{C}_D$	$C_r , \dot{C}_r$	—

*We have written partial derivatives permitting solution for $\dot{C}_r$ and $\dot{a}$. These parameters have not yet been allowed to adjust from their a priori value of zero.

SECTION 8.0
SOLUTION DESIGN

The design of a comprehensive gravity field solution is complicated by imperfections and incomplete knowledge in the mathematical models used to describe the tracking observations. Therefore, a certain degree of experimentation and testing of preliminary models is necessary. This section describes the method of solution adopted for GEM-T1, and relates how difficult decisions concerning data weighting were made.

8.1   LEAST SQUARES COLLOCATION

The use of a modified least squares method was implemented in recent GEM models (Lerch et al., 1977) to permit a meaningful, stable solution of the satellite field to high degree and order. With the exception of GEM-10B and 10C, all of the post-GEM-7 solutions used this modified form of least squares, which includes a priori information on the power of the field. A general mathematical description of this method follows, with specific details relating to the development of GEM-T1 shown in the next subsection 8.2.

Conventional least squares simply minimizes the observation residuals (noise). However, high correlation between certain high degree and order coefficients in gravity solutions is a persistent problem when large fields are estimated. If uncontrolled, this results in excessively large values for the adjusted coefficients in the conventional least squares solution. By applying constraints in the form of a priori weights for the unknowns we essentially minimize both the signal (e.g., the size of the harmonic coefficients) and the noise (observation residuals) within the solution, thereby preventing an unreasonably powerful gravity solution.

The principle of least squares collocation is to minimize (see Moritz, 1980, Eq. 21.38):

$$Q = s^T K^{-1} s + n^T D^{-1} n \qquad (8.1)$$

with respect to the unknowns y, where

y   -   complete set of solution parameters for the geopotential, stations, earth orientation, tides and the orbit

n   -   adjusted satellite observation residuals

D   -   diagonal matrix for satellite observation residuals whose diagonal elements are the variances of the observations

s   -   signal, which in our application consists of the harmonic (potential) coefficients representing a subset of y, with an expected value of zero

K   -   diagonal matrix, where the diagonal elements are the degree variances per coefficient (see Moritz (ibid) Eqs. 21.23 and 21.52) of the potential.

In principle, there are infinitely many harmonics in the spectrum of the gravitational field, so K would be an infinite matrix. However, at satellite altitude, only a finite number of (lower degree) harmonics perturb orbits to the extent that these perturbations can be observed and separated from the measurement noise. Therefore, for space applications, it is reasonable to make the approximation of assuming that the expansion of the field is finite. This leads to a finite matrix K, which, as is shown, can readily be incorporated into the

adjustment. This is accomplished by adding K^{-1} to the usual normal matrix of Bayesian least squares created by GEODYN, which gives the desired normal matrix for minimizing (8.1). Further consideration on the wisdom of using this type of approximation can be found in Schwarz (1976, 1978) and Moritz (ibid) Chapter 21.

Let s represent the subset of y corresponding to the potential coefficients and x the subset of the other parameters. The y can be partitioned as:

$$y = \begin{bmatrix} x \\ s \end{bmatrix} . \qquad (8.2)$$

Using the linear terms in the Taylor's series expansion of the measured variable (data) d and calling,

$$\ell = d \text{ (observed)} - d \text{ (computed)},$$

one gets

$$\ell = Ax + Bs + n \qquad \begin{array}{l} \text{(where A and B are matrices of} \\ \text{partial derivatives; this is} \\ \text{Eq. (16.1) in Moritz (ibid)).} \end{array} \qquad (8.3)$$

then minimizing Q in (8.1) above gives the normal equations

$$\begin{bmatrix} A^T D^{-1} A & A^T D^{-1} B \\ B^T D^{-1} A & B^T D^{-1} B + K^{-1} \end{bmatrix} \begin{bmatrix} x \\ s \end{bmatrix} = \begin{bmatrix} A^T D^{-1} \ell \\ B^T D^{-1} \ell \end{bmatrix} \qquad (8.4)$$

which are the equations formed and solved with GEODYN and SOLVE, when the elements of K^{-1} are added to the main diagonals of the submatrix $B^T D^{-1} B$ and the a priori values of s are chosen as zero. Moritz (ibid) employs a different formulation of the normal equations to arrive at the expressions needed for specific applications of least squares

collocation. We wish to show that equations (8.4) above are equivalent to those special cases of Moritz's equations that he and others have derived for satellite applications. For this purpose we may write the second matrix row equation of (8.4) as follows:

$$s = (B^T D^{-1} B + K^{-1})^{-1} (B^T D^{-1} \ell - B^T D^{-1} Ax) \qquad (8.5)$$

and by substituting into this equation the matrix identity

$$(B^T D^{-1} B + K^{-1})^{-1} B^T D^{-1} = K B^T (BKB^T + D)^{-1} \qquad (8.6)$$

it follows that

$$s = KB^T (BK B^T + D)^{-1} (\ell - Ax) \qquad (8.7)$$

with

$$x = [A^T (BK B^T + D)^{-1} A] A^T (BKB^T + D)^{-1} \ell.$$

In Moritz ((ibid), Chapter 16), starting from (Eq. 16.1), which is the equivalent of (Eq. 8.3) above, he derives (Eq. 16.37):

$$s = C_{st} \overline{C}^{-1} (\ell - Ax) \quad \text{where, in Moritz's notation,}$$

$$C_{st} = KB^T, \quad \overline{C}^{-1} = (BKB^T + D)^{-1}.$$

186

Hence, in equation (8.7), $(BK\ B^T + D)$ represents Moritz's autocovariance matrix $\bar{C}$, and KB^T is the cross-covariance matrix C_{st}, for a field with a "finite" harmonic expansion.

8.2   STRATEGY FOR DATA WEIGHTING AND FIELD CALIBRATION

As described in the previous section, the solution for high degree gravity coefficients is made reliable through the introduction of least squares collocation.   For simplicity, and to permit a more thorough discussion of data weighting, let (8.1) be rewritten   (see also Moritz (ibid), Chapter 28) as:

$$Q = \bar{f} \sum_{\ell,m} \frac{\bar{C}^2_{\ell,m} + \bar{S}^2_{\ell,m}}{\sigma^2_\ell} + f \sum_t \sum_{obs} \frac{r^2_{it}}{\sigma^2_t} \tag{8.8}$$

where the calibration factors $\bar{f}$ and f compensate for errors in the nominal σ^2_ℓ and σ^2_t, as explained in what follows:

The values of the degree variances per coefficient σ^2_ℓ are based on previous studies (Kaula, 1966), which show that they follow the general approximate rule:

$$\sigma_\ell = 10^{-5}/\ell^2 \tag{8.9}$$

(This means the power spectrum for the signal is referenced here to the ellipsoid instead of a more advanced geoidal model such as that found in contemporary gravity models.   The signal matrix K^{-1} corresponds to the full power of the gravity field and not some correction to an existent model.   In this way, our solution is independent of the coefficient values from earlier gravity models.)

Expression (8.9) has been obtained from the analysis of early sets of surface gravimetry and is known as "Kaula's rule" (1966). In (8.8), r_i is the ith observation tracking residual from the tth homogeneous data subset (e.g. laser ranging on LAGEOS). The weight σ_t^2 given to these observations, is constant for all data in the tth subset* and largely reflects the accuracy of such data as reflected by the residuals seen in the solution.

Two factors, $\bar{f}$ and f are introduced to scale the two terms in (8.1) relative to each other. The $\bar{f}$ parameter, however, is not a free scaling parameter, for if

$$\bar{f} = 2 \qquad\qquad\qquad (8.10)$$

is chosen, it improves Kaula's rule (8.9) so that the signal matrix better reflects the observed power found in contemporary gravity modeling studies (Wagner and Colombo, 1979; Lerch et al., 1979). The f parameter plays an equally important role. The use of data noise alone as a weighting factor in the solution causes the formal estimate of error to be optimistic due to the neglect of unmodeled effects other than noise as solution contaminants. Therefore, f is introduced to scale the least squares normal equations so that the resulting solution has more realistic error estimates, as shown by calibrations using independent data sources (see Section 10). The accuracy of the solution represented by (8.4) is also improved which is most important. In 8.4 D^{-1} is scaled by f and K^{-1} by $\bar{f}$. Iteration on the solution weighting factors f and $\bar{f}$ is generally required to converge on a near optimal answer.

---

* with an occasional variation for a certain station as described in Section 5.

188

The GEM-9 and GEM-L2 solutions were based upon the size of the coefficients and the scaling of the standard errors in GEM-7. We used $\overline{f} = 2$ and $f = 1/10$ in GEM-9 and GEM-L2. Therefore, the noise only formal errors were scaled by $\sqrt{10}$ to yield more realistic error estimates. The accuracy assessments for both GEM-9 and GEM-L2 were re-evaluated in Lerch et al (1985) and proved to be realistic, although for most terms the resulting uncertainties seemed pessimistic by about 30%.

Returning to expression (8.8), both the observation residuals, r_i, and the overall size of the gravity coefficients, $\overline{C}_{\ell,m}$, $\overline{S}_{\ell,m}$ are to be simultaneously minimized. The relationship between the scale factors, f and $\overline{f}$, needs to be chosen prior to the solution, and the weighting for specific data sets, σ_t^2, needs to be established and tested. A natural starting point for scaling the solution is to choose values for f and $\overline{f}$ which were found to be optimal in earlier GEM solutions and then experimentally adjust these parameters. Each σ_t^2 is nominally adopted and improved upon based on experience with the data. The final determination of σ_t^2 must also take into account systematic errors enlarging a specific satellite's residuals due to errors in the modeling of non-conservative forces. Objects experiencing large drag perturbations, for example, are more likely to have larger drag modeling errors. These data sets must be downweighted to some (to be determined) level. The determination of all of these scaling parameters is described below.

If:

N_t is the satellite normal matrix for a given observation type on a specific satellite with a priori weight $W_{ot} = 1/\sigma_{ot}^2$ and scaled weight

$$W_t = \sigma_t^{-2} = w_t \, W_{ot}$$

where w_t is an additional weighting factor for N_t.

189

K^{-1} is the scaled $(\bar{f}=2)$ normal signal matrix for the potential coefficients (diagonal elements only) and is based on the observed power seen in the previous GEM-10B satellite gravity model as shown in (8.10):

$$K_{\ell,m}^{-1} = 1/\sigma_\ell^2 = 2\ell^4 \times 10^{10} \qquad (8.11)$$

Then the combined reduced normal matrix for the gravity solution is given by:

$$C = K^{-1} + f \sum_t W_t M_t \qquad (8.12)$$

(Ordinarily, to reduce the size of the combined normal matrix, M_t is used, and not N_t, where M_t is the reduced satellite normal matrix after back-substitution for the satellite specific orbital parameters.)

Ideally, W_t represents the formal accuracy of the data. In practice, this weight is adjusted to account for the general problem of incomplete information, where there are unmodeled and correlated errors in the observation residuals. W_t therefore is also used to balance the solution, ensuring that satellite residuals with large (systematic) unmodeled errors do not overwhelm it.

The K^{-1} matrix has certain important properties. First, it is unbiased in the sense that it does not favor any single gravity model, as the total field (above some degree and order), and not its adjustment, is minimized. To take an example, suppose a given coefficient does not contribute to the satellite signal. In the final solution, the determined value for this coefficient will be zero with the resulting uncertainty being 100% of its expected power. Although biased towards zero power, this is the best collocation estimate for any coefficient if no satellite information is present for its solution. K^{-1} is applied to terms above a certain degree cutoff. In GEM-T1, this cutoff was degree

5; K^{-1} has not directly been applied to the lowest degree and order terms (i.e., the corresponding diagonal terms in K^{-1} are set equal to zero).

The scaled error covariance for the coefficients is obtained as:

$$\lceil \sigma_{\ell m} \rceil = C^{-1} = [K^{-1} + f \sum_t W_t M_t]^{-1} \tag{8.13}$$

where choosing the overall scale factor of $f=1$ produces errors from the diagonal elements of C^{-1} which are overly optimistic. Therefore, f is adjusted to produce realistic error .estimates for the optimally weighted solution.

Table 8.1 presents a list of the independent data tests used to evaluate the scaling and data weights of the solution. Many of these test results are described more fully in the accuracy and calibration sections of this report. An example of the tests spanning different solutions are shown in Table 8.2. Herein, the factor, f, and certain data weights were varied. Differing results were obtained since $\bar{f}$, as expected, was held constant. Therefore, the relative balance of the K^{-1} and the rest of the normal matrix has been altered. The models which were obtained were tested here using:

o   An estimate of gravity model error for the field truncated respectively at degrees 10, 20 and 36 obtained from intercomparisons with global surface gravimetry (described fully in Section 10);

o   An estimate of complete gravity model error at degree 36 obtained from comparisons with 5 x 5 degree gravity anomaly blocks determined from SEASAT altimetry; and

o   The weighted residual obtained from the models when they are used to predict the longitude acceleration of 10 independently studied 24-hour satellites.

Table 8.2 presents results for a small subset of the testing that the fields undergo, and it shows clearly that experimentally varying the data weights can significantly alter the tested performance of the gravity model solutions. In particular, notice the degradation in field performance which results when f is increased from .02 to .1 as was done in the computation of PGS 3013. This is especially apparent in the test against independent surface gravity data. (PGS 3013 is discussed further in Section 10.2).

The values employed for W_t in (8.13) are also critically evaluated. As shown in Table 8.3, the post-solution RMS of fit of the data using an improved geopotential model can give preliminary values for these parameters.

In an ideal case, the potential coefficient diagonal elements of each satellite's combined normal matrix would reflect the total sensitivity this orbit had to a given gravity harmonic. This ideal case requires complete global coverage and complete orbital information at every point along the orbit (not the incomplete information that a typical tracking observation, for example, a range to the satellite, contains). The sizes of the actual diagonal elements are important when balancing a multi-satellite solution, but the off-diagonal information must also be considered. This is certainly the case when dealing with real (limited) observation histories.

Information obtained through a study of the diagonal elements on the contributions M_t of the individual satellites normal matrices are useful in determining W_t. Figure 8.1 shows the RMS contribution (percentage by degree) for each of the satellite-specific normals to the diagonal elements of the combined normal matrix when the data are weighted using the W_t values finally adopted for GEM-T1. (The four laser data sets from BE-C, GEOS-1, GEOS-2 and GEOS-3 are combined into

TABLE 8.1

DATA AND CRITERIA EMPLOYED FOR EVALUATING AND ADJUSTING WEIGHTS IN SOLUTIONS

- SATELLITE TRACKING DATA ON SELECTED ORBITAL ARCS

- 5° x 5° SET OF SEASAT ALTIMETER DERIVED ANOMALIES

- KAULA ERROR ESTIMATE OF GRAVITY ANOMALY FOR SATELLITE DERIVED MODEL BASED UPON A 5° x 5° SET OF GLOBAL TERRESTIAL GRAVITY ANOMALY DATA

- SATELLITE ACCELERATIONS IN LONGITUDE FOR 24 HR. ORBITS DERIVED BY WAGNER (private communication) FOR TEN SATELLITES TO TEST LOW DEGREE ($\ell \leq 6$) TERMS

- SEASAT ALTIMETER CROSSOVERS

- DIAGONAL TERMS OF WEIGHTED NORMAL EQUATIONS OF EACH SATELLITE OBS. DATA TYPE FOR RELATIVE SENSITIVITY ANALYSIS

- PERCENT REDUCTION OF ERROR VARIANCES OF GRAVITY COEFFICIENTS DUE TO EACH SATELLITE DATA TYPE IN SOLUTION

- CONDITION NUMBERS OF SOLUTION PARAMETERS

- EFFECT ON SOLUTION TESTS BY REMOVAL OF SATELLITE DATA TYPES FROM SOLUTION

C - 3

Table 8.2

TEST RESULTS FOR
EVALUATING AND ADJUSTING
WEIGHTS

MODEL	DESCRIPTION	DATA WEIGHT FACTOR f	KAULA GRAV. ANOM. ERROR (MGAL²) DEG.TRUNCATION			SEASAT ANOM. RESID. MGAL²	24 HR. SAT. ACCEL. RESID. (WEIGHTED)
			10	20	36		
PGS-T2	TOPEX AGU SOL.	.02	2.3	5	8	35	1.7
PGS-3013	5 x DATA WT. OF T2	.10	3.0	13	31	48	1.5
PGS-3016	GEOS-2 DOWN-WEIGHTED IN T2	.02	2.2	4	6	33	1.4
PGS-T3	T2 DATA WITH 3 LOW-INC SATS	.02	1.1	3	5	31	1.4
PGS-3026	2 x DATA WT. OF T3	.04	1.2	4	10	32	1.3
GEM-T1	NEW TOPEX FIELD	.02	1.1	3	5	29	1.3

194

Table 8.3

RELATIVE WEIGHT ESTIMATES
TEST CASE

RMS OF SATELLITE OBSERVATION RESIDUALS FROM TEST FIELD (PGS-T2 TYPE)

$$w_t^* = \sigma_{ot}^2 / RMS_t^2$$

TYPE j (LASER DATA)	APRIORI σ_{oj}	RMS_t	w_t**
LAGEOS	1 m	.1 m	100
STARLETTE	1	.2	25
BE-C	1	.5	4
GEOS-1	1	.7	2
GEOS-2	1	.8	1.6
GEOS-3	1	.7	2
DOPPLER			
OSCAR	1 cm/sec	1.2	0.7
SEASAT	1	.6	2.8

* $w_t = w_t / \sigma_{ot}^2 = 1/RMS_t^2$ where σ_{ot}^2 is the a priori value in the normal equations N_t.

** Because of the relative amounts of data quantity and other factors, further adjustment is considered for relative weighting.

one matrix labeled "4-LASER-SATS" in Figure 8.1). The diagonal elements per se tell an incomplete story. STARLETTE seems to contribute a disproportionately large amount of information to the solution based on Figure 8.1. However, when the individual satellites are evaluated in terms of their specific contribution to the reduction of the error degree-variances within the combined solution (looking at the aposteriori variance-covariance matrix), one sees (Figure 8.2) that the 4-LASER and LAGEOS data now control the solution for low degree terms through degree 13, and STARLETTE is no longer dominant. The impact of optical observations on the solution is nearly completely lost in Figure 8.1, showing an insignificant contribution to the solution's diagonal elements. However, as shown in Figure 8.2, the optical data makes significant contributions to the solution (which must be through off-diagonal conditioning) for the resonance (m=11 through 15) and zonal (m=0) orders. Generally, it is desirable to obtain a solution which has significant contributions from many satellite data sets (as is evidenced in Figure 8.2), for this tends to average-out satellite-specific error sources. Summing up: the data weights used in GEM-T1 (Figure 8.2) have been selected in an attempt to assure a balanced multi-satellite solution.

The diagonal elements can also be used diagnostically. A study of the diagonal elements of the four-laser satellites (which were combined to form a single matrix), revealed an anomaly for GEOS-2. This is shown in Figure 8.3. The diagonal elements for this satellite's contribution were originally too large. A physical explanation for this effect was not found through a study of the magnitude of first-order gravity perturbation estimates for this satellite. Therefore an error in our processing of the normal equations from this satellite was investigated. A software problem in the back-substitution of the orbital parameters, when a priori weights were introduced on the drag parameters, was uncovered and corrected in GEM-T1. The PGS-T2 model contained this erroneous treatment of the GEOS-2 matrices and was also
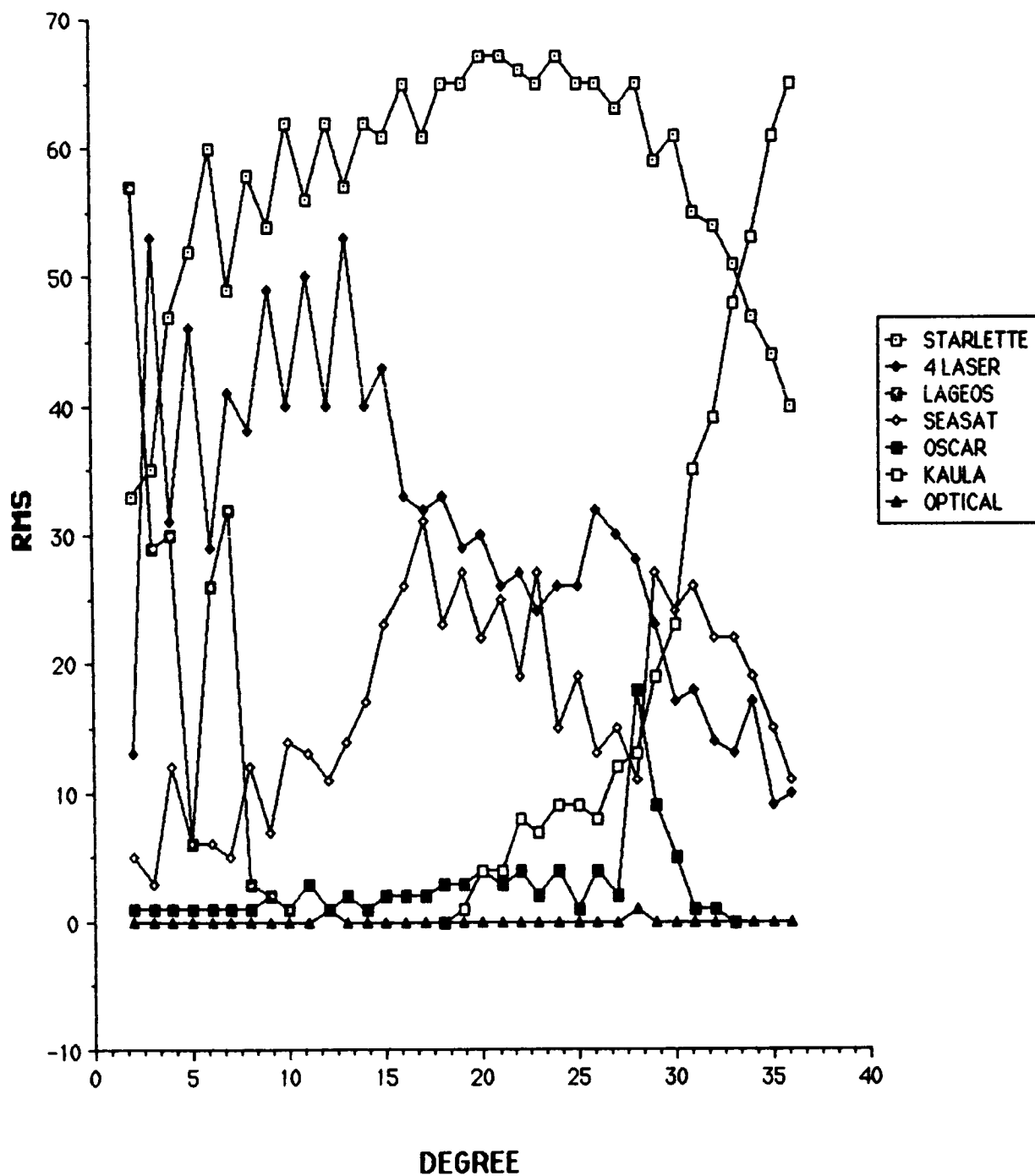
Figure 8.1.   RMS of Percentages of Ratios of Diagonals Per Degree
Comparing Major Data Types in PGS--T2.
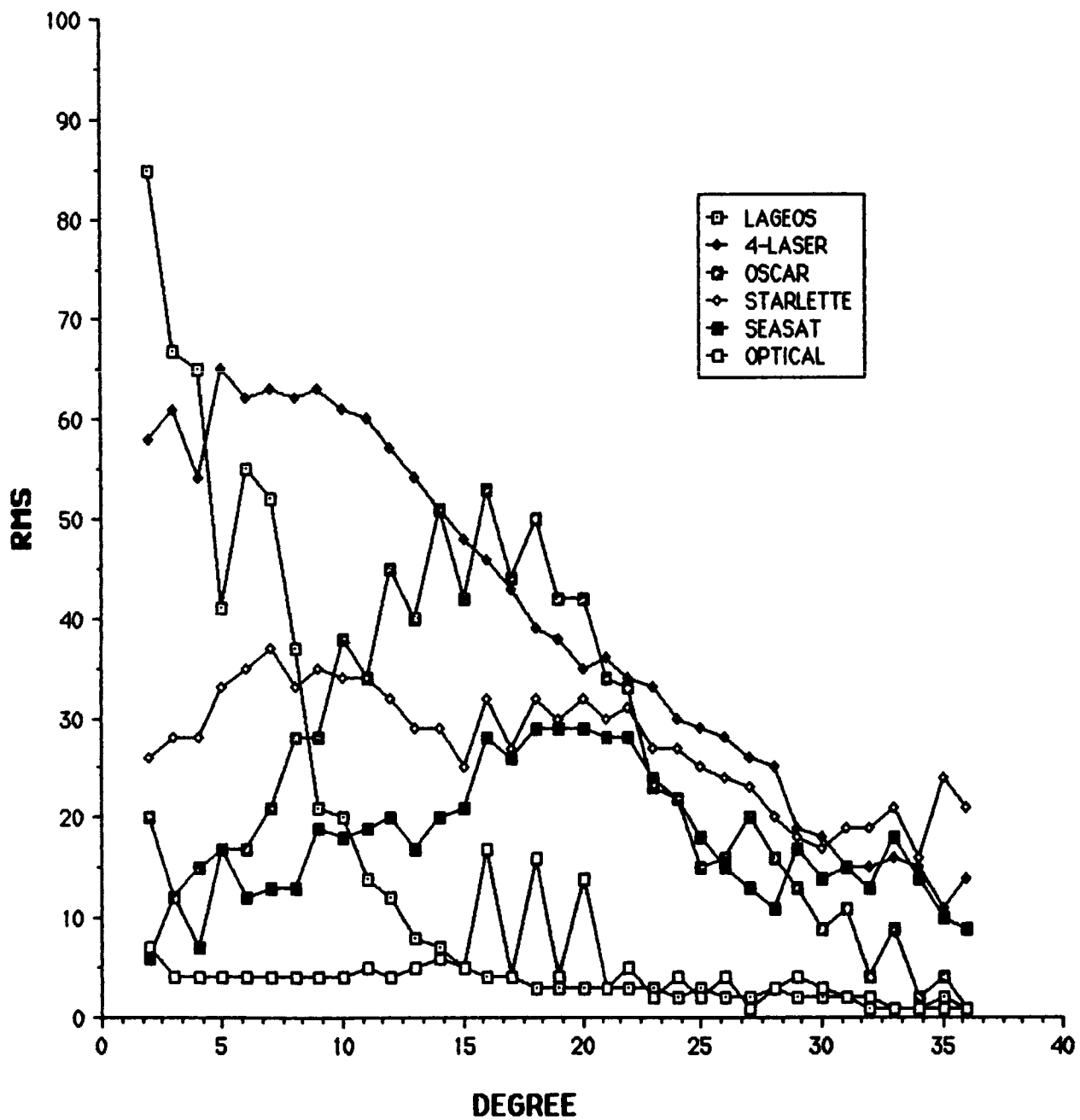
Figure 8.2.   Percent Reduction of Error Variances Due to Major Data Types in Solution.

OF 4-LAS DATA IN COMPARISON WITH PGS-T2
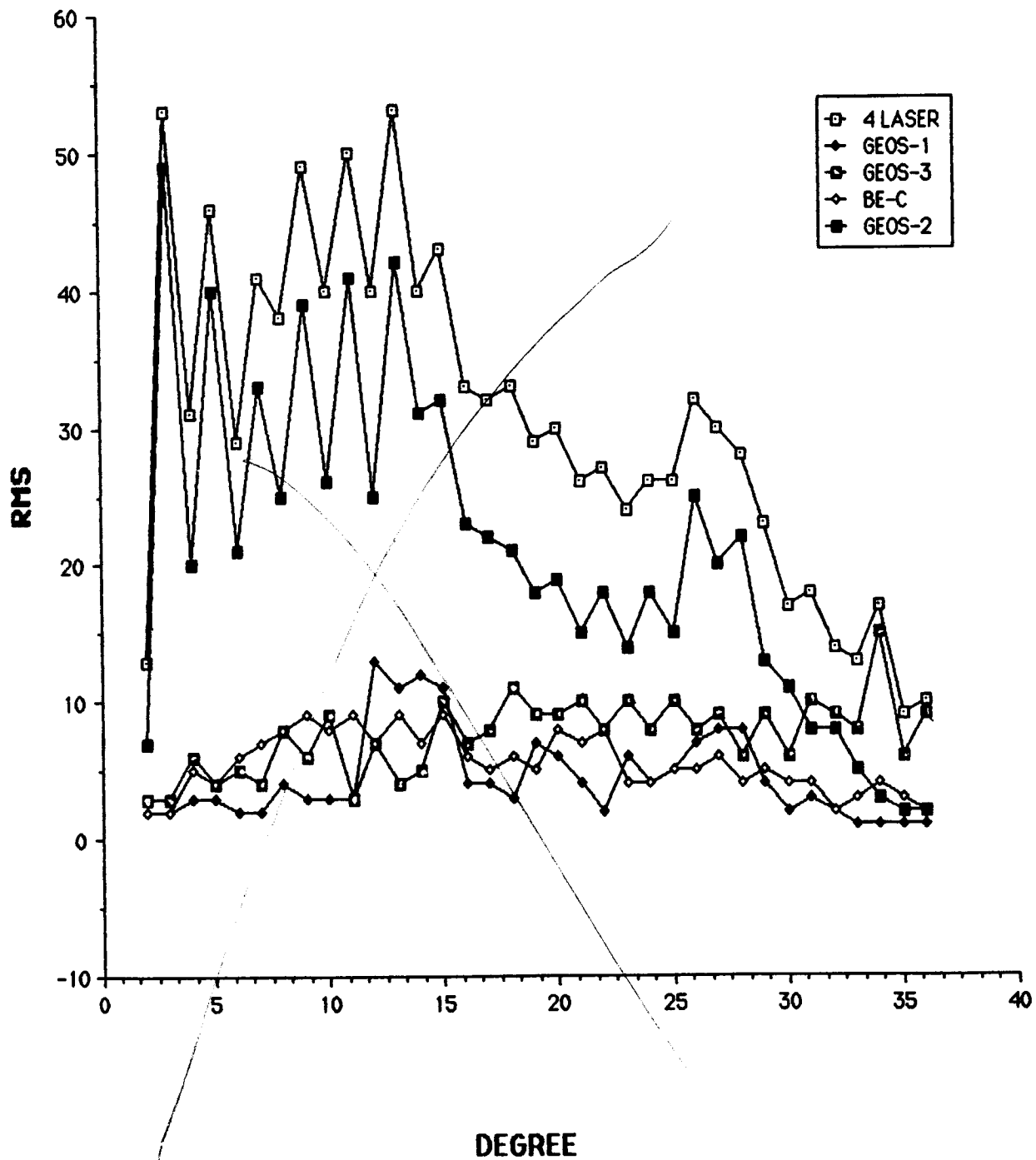
Figure 8.3.   RMS of Percentages of Ratios of Diagonals Per Degree.
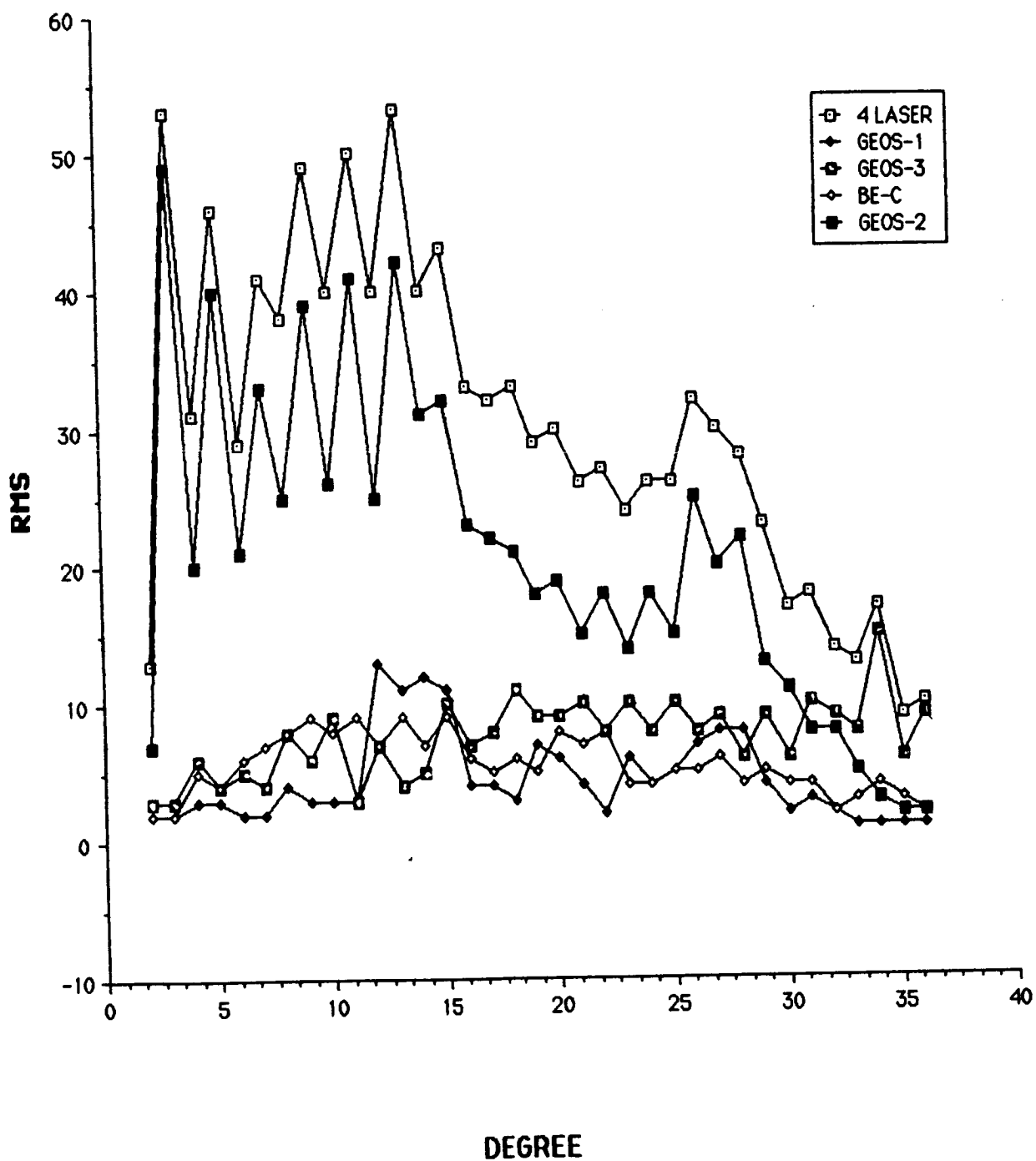
Figure 8.3.   RMS of Percentages of Ratios of Diagonals Per Degree
Comparing the 4 Laser Satellite Contributions Within
PGS–T2.

TOTAL DATA			GEM-T1 RELATIVE WEIGHTS (w_t)	
SAT	**ARCS**	**OBS**	**PGS-T2**	**GEM-T1**
LAGEOS	58	144529	40	40
STARLETTE	46	57356	10	10
4-LAS*	151	204547	1	1*
SEASAT LASER	14	14923	1	1
SEASAT DOPPLER	14	129604	1	1
OSCAR DOPPLER	13	63098	1	0.75
6-OPT*	219	139818	5	5*
LOW INC (OPT)*	49	4461	--	5*
LOW INC (LAS)*	16	23055	--	1*
WEIGHT MULTIPLYING FACTOR (f)			.02	.02
KAULA WT. $(10^{-5}/\varrho^2)$			2	2

*GEM-T1 ADDITIONAL SCALE FACTOR (w_t)

4-LAS	**ARCS**	**OBS**	**w_t**	**LOW INCLIN**	**ARCS**	**OBS**	**w_t**
GEOS-1	48	71287	1.13	COURIER-1B (OPT)	10	2476	2.00
GEOS-2	28	26613	.75	VANGUARD-2RB (OPT)	10	686	2.00
GEOS-3	36	42407	.75	VANGUARD-2 (OPT)	10	1299	2.00
BE-C	39	64240	1.50				
				DI-C (OPT)	10	2712	.75
6-OPT				DI-C (LAS/	4	7455	.75
				OPT)		159	
BE-B	20	1739	2.0				
BE-C	50	7501	1.3	DI-D (OPT)	9	6111	.50
GEOS-1	43	60750	.5	DI-D (LAS/	6	11487	.75
GEOS-2	46	61403	.5	OPT)		146	
ANNA-1B	30	4463	2.0				
TELSTAR	30	3962	2.0	PEOLE (LAS)	6	4113	.75
ALTIM							
SEASAT	8	14093					

DATA ERRORS (σ) FOR WEIGHT = 1	
DATA	**σ (A PRIORI)**
LASER	1 m
DOPPLER	1 cm/sec
OPTICAL	2 arc seconds
ALTIM	1 m

Figure 8.4.   GEM-T1 TOPEX Data and Weighting.

sensitivity to resolve every coefficient to this degree. Therefore, an external estimate of the size of the coefficients was used as a constraint to stabilize the solution. There is an important benefit in solving for a complete 36 X 36 field. We have found that aliasing in the middle degrees of the model has been avoided through this relatively high degree and order solution. And the destabilizing lack of sensitivity to a subset of the coefficients is compensated through the application of least squares collocation, which keeps coefficient errors within less than 100% of the size of the coefficients predicted from independent gravimetry. However, there are certain problems in carrying out such a large solution that need to be discussed.

Firstly, the application of Kaula's rule as a constraint is equivalent to introducing a set of additional observations of the coefficients where their expected values are all zero, with a scaled version of Kaula's power estimate used as a variance on these "observations". This rule represents a mild use of _a priori_ information on the determination of low degree terms, constraining the coefficient only to the approximate power spectrum of gravimetry. However, because some sensitivity is lacking for high degree terms, this collocation constraint has caused the coefficients in GEM-T1 above degree 25 to have less power than the "true" gravity field. And at degree 36, GEM-T1 power is about 1/3 to 1/2 of that seen in fields which used altimetry and surface gravity. While this is troublesome, it should be noted that if no adjustment is made of these high degree terms (i.e., the harmonic model is truncated at a lower degree cutoff) then these terms would be absolutely constrained to zero (as are all terms above the field limits). Hence, with least squares collocation there is a gradual decay in the power spectrum instead of a sharp drop to zero at the point of truncation within the field. In this sense, collocation can be viewed as permitting more power in the solved for short wavelength gravity field, for the model, although constrained, can be extended to much higher degree through the use of this technique.

Altimetry and surface gravimetry provide strong sensitivity to harmonics up to degree 360 and higher in the gravity model. Eventual use of this data in future solutions will overcome the shortcomings of GEM-T1, where a total reliance on satellite data, due to attenuation, causes incomplete resolution of all higher degree gravity terms. Figure 8.5 presents a comparison of the degree variances found in GEM-T1 with those in GEM-10B. GEM-10B is a comprehensive model which used GEOS-3 altimetry and surface gravity data and therefore did not require any form of constraint on the size of the coefficients. The lack of high-degree power for the GEM-T1 model is evident. Interestingly, when preliminary altimetry data sets are even weakly introduced into GEM-T1, (forming PGS3163), the power is much closer to the level seen in GEM-10B (see Figure 8.5). PGS3163 is discussed further in the Calibration Section (Section 10) of this report.

We also believe that the use of Kaula's rule as a constraint may have altered the high-degree terms' covariances, indicating less cross-correlation among these coefficients than is truly found in the overall orbital signal sampled by our selection of satellites. Therefore, calibrations using objects passing through deep resonance may be biased if the full covariance of GEM-T1 is utilized.

However, tests against independent altimeter data show there is valuable information in GEM-T1 above degree 25 and although the coefficients are small, they do improve the orbital fits obtained by this field. Therefore, this 36 degree level of truncation was adopted for GEM-T1. Plans for future efforts are to merge the GEM-T1 database with other observations obtained by altimetric, satellite-to-satellite tracking, and surface gravity data sources. These more comprehensive solutions will be free of the constraint imposed on the GEM-T1 "satellite-only" model. In spite of some limitations, the GEM-T1 solution is a very accurate model at long and intermediate wavelengths, as shown in the next paragraph.
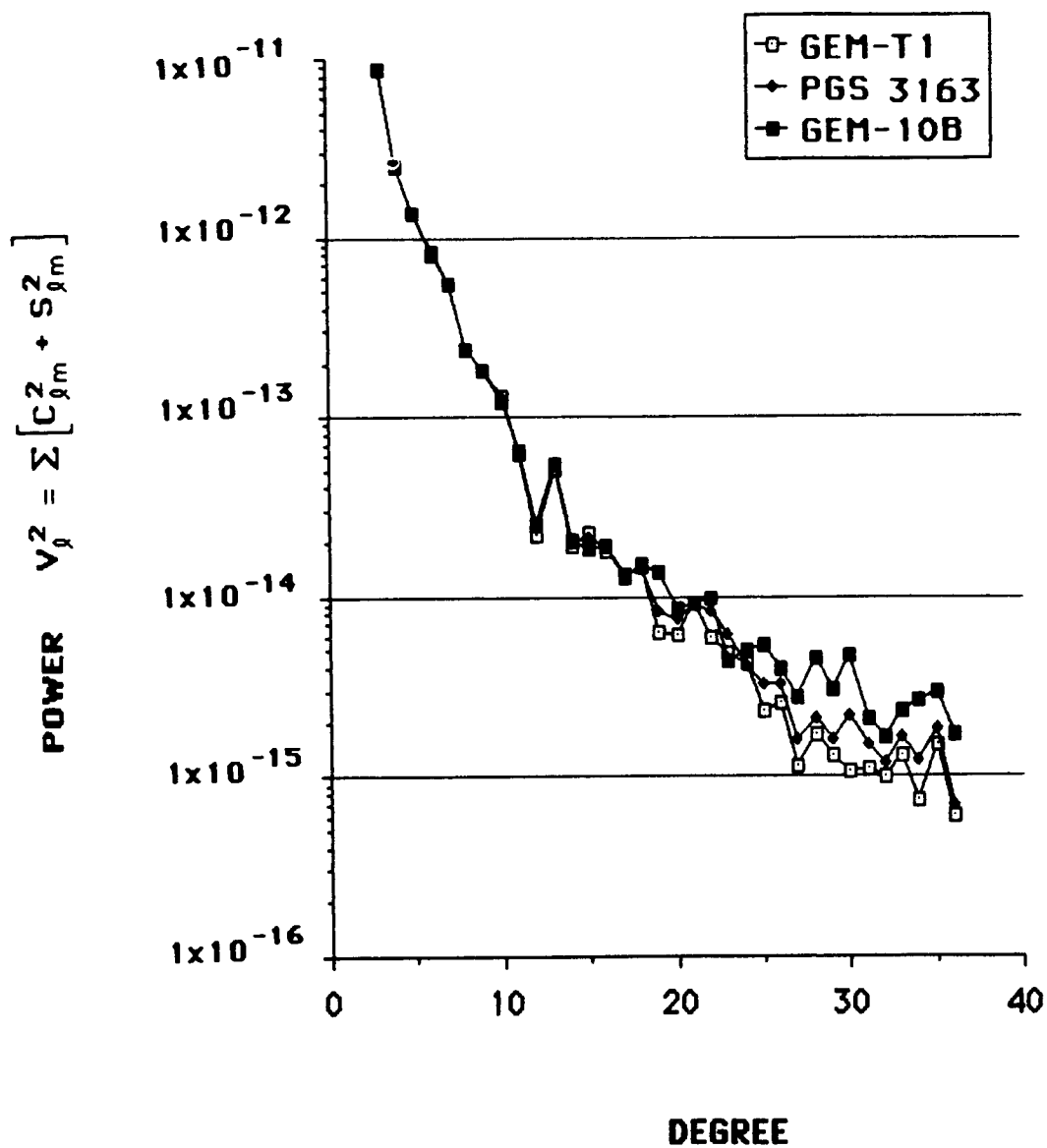
Figure 8.5. Degree Variance Comparison for Recent Models.

An experiment was conducted showing the effect on the GEM-T1 solution of removing the collocation term $\bar{f}K^{-1}$. This was accomplished by setting $\bar{f}=0$. Figure 8.6 compares this test model and GEM-T1 with independent 5°x5° gravity anomalies derived from SEASAT altimetry (Rapp, 1983a) at different levels of field truncation. In the case of the test field, the ordinary least squares method (with $\bar{f}=0$) could not be successfully solved beyond degree 25. The comparison in Figure 8.6 shows that a gravity solution which lacks collocation rapidly becomes unreliable above degree 18, with an excessively large power spectrum found for terms beyond this point.

Although GEM-T1 has a weak power spectrum for its terms beyond degree 25, there are strong benefits achieved in solving for a complete 36 x 36 model and using a least squares collocation approach. This is demonstrated in Figure 8.7 where GEM-T1 has been solved only complete to degree 20 x 20 (yielding PGS-3167) which is the same size as the earlier GSFC GEM-L2 (Lerch et al., 1983) solution. The same gravity anomaly comparison as described in the previous paragraph shows little improvement of PGS-3167 over that of GEM-L2, and clearly inferior field performance compared to what has been achieved in GEM-T1.

The addition of the Cyber 205 computer allowed evaluation and solution of larger gravity models with a consistent reduction and formation of normal matrices for all data sets which was not possible during earlier times. This factor greatly contributed to the development of a complete 36x36 model. GEM-T1 was the result. Previously, this 36x36 option could not be explored due to the enormous computer resources which would have been required.
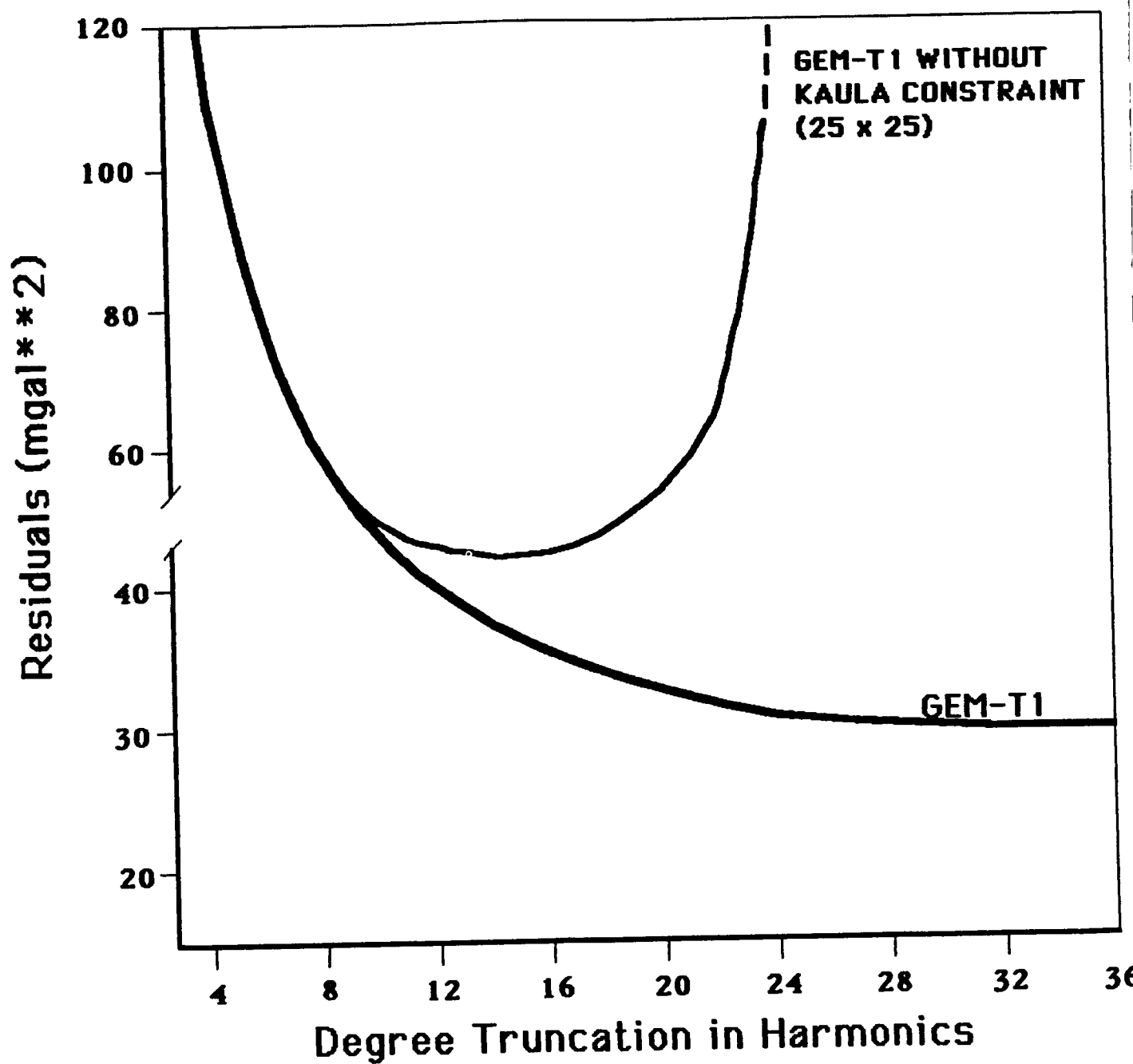
Figure 8.6.   Gravity Model Comparison with 1114 5° x 5° SEASAT Gravity Anomalies: GEM-T1 With and Without Collocation.
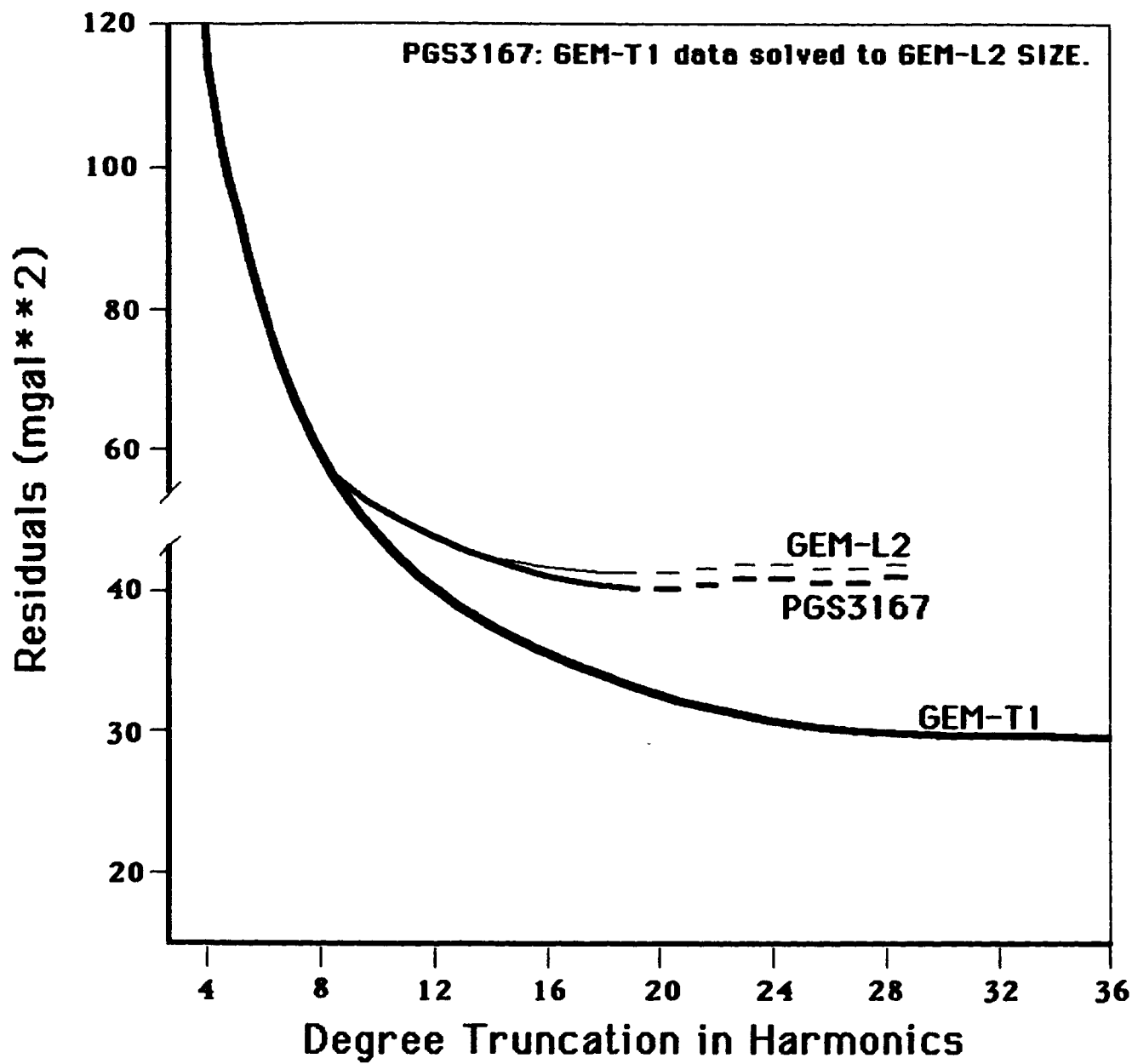
Figure 8.7. Gravity Model Comparison With 1114 5° x 5° SEASAT Gravity Anomalies: GEM-T1 Solved to 20 x 20.

SECTION 9.0

THE GEM-T1 SOLUTION RESULTS

9.1 THE GRAVITY MODEL

Table 9-1 presents the coefficient values which were obtained for the GEM-T1 gravity model. The model is complete to degree and order 36, and has been obtained from a data set consisting exclusively of ground based satellite tracking. To stabilize the coefficient adjustment (see Section 8), a mild constraint on the the size of the coefficients was used to eliminate unstable adjustment of correlated high degree terms. This model is more complete than previous GSFC "satellite-only" models, which in the past were only solved completely to degree 20, with isolated higher degree resonant and zonal terms (GEM-9:Lerch et al, 1979; GEM-L2: Lerch et al, 1982). The remainder of this document discusses the GEM-T1 parameters and their calibrated accuracies in detail. An extensive error analysis to establish field uncertainty is described in Sections 10 and 11. A contour map of the GEM-T1 geoid is presented in Figure 9.0. The geoid was computed using the potential coefficients of Table 9.1 in Brun's formula (Heiskanen and Moritz, 1967, p. 85).

9.2 OCEAN TIDE SOLUTION

With the advent of centimeter level satellite geodesy and geodynamics, it has become necessary to accurately model the deformation of the earth and its oceans due to tides, i.e., the temporal variations of the geopotential, in order to obtain accurate estimates of the static geopotential coefficients. This is in part because the data distribution in time and space cannot be selected so that the effects of these temporal variations average out.

Table 9.1
GEM-T1 NORMALIZED COEFFICIENTS
UNITS OF 10^{-6}

ZONALS

INDEX N	VALUE	INDEX N	VALUE	INDEX N	VALUE	INDEX N	VALUE	INDEX N	VALUE
2 0	-484.1649906	3 0	0.9572375	4 0	0.5387322	5 0	0.0687802	6 0	-0.1481004
7 0	0.0905337	8 0	0.0459023	9 0	0.0283764	10 0	0.0572211	11 0	-0.0512619
12 0	0.0320806	13 0	0.0422319	14 0	-0.0197327	15 0	0.0018731	16 0	-0.0093772
17 0	0.0203968	18 0	0.0112912	19 0	-0.0046084	20 0	0.0153150	21 0	0.0097754
22 0	-0.0048440	23 0	-0.0241260	24 0	-0.0009556	25 0	0.0068867	26 0	0.0018391
27 0	0.0041234	28 0	-0.0058541	29 0	-0.0039091	30 0	-0.0002749	31 0	0.0051154
32 0	0.0000819	33 0	0.0022286	34 0	-0.0024803	35 0	-0.0012731	36 0	0.0007396

SECTORIALS AND TESSERALS

INDEX N	M	VALUE C	VALUE S	INDEX N	M	VALUE C	VALUE S	INDEX N	M	VALUE C	VALUE S
2	2	2.4389280	-1.3998397	3	2	0.9035491	-0.6204198	3	3	0.7209866	1.4131694
3	1	2.0297737	0.2495946	4	2	0.3470021	0.6640304	4	3	0.9909779	-0.2006215
4	1	-0.5334272	-0.4751189	5	2	0.6557902	-0.3234056	5	3	-0.4482036	-0.2151363
4	4	-0.1900348	0.3084595	5	5	0.1777563	-0.6660281	6	3	0.0619709	0.0046430
5	1	-0.0589503	-0.0955435	6	2	0.0516096	-0.3749956	6	6	0.0090593	-0.2363344
5	4	-0.2948236	0.0524087	6	5	-0.2657650	-0.5377472	7	3	0.2507429	-0.2091639
6	1	-0.0813751	0.0238900	7	2	0.3177108	0.0916083	7	6	-0.3578527	0.1509175
6	4	-0.0927975	-0.4733069	7	5	0.0034750	0.0196519	8	3	-0.0199664	-0.0869367
7	1	0.2770971	0.0978177	8	2	0.0703801	0.0684494	8	6	-0.0664178	0.3128323
7	4	-0.2737404	-0.1220207	8	5	-0.0249335	0.0853003				
7	7	0.0015976	0.0220013	8	8	-0.1188827	0.1223320				
8	1	0.0288561	0.0547223								
8	4	-0.2460639	0.0677453								
8	7	0.0704248	0.0748626								

Table 9.1
GEM-T1 NORMALIZED COEFFICIENTS (continued)
UNITS OF 10^{-6}

SECTORIALS AND TESSERALS

INDEX N	M	C VALUE	S VALUE	INDEX N	M	C VALUE	S VALUE	INDEX N	M	C VALUE	S VALUE
9	1	0.1480447	0.0245251	9	2	0.0311365	-0.0323882	9	3	-0.1553742	-0.0840158
9	4	-0.0128303	0.0232637	9	5	-0.0141122	-0.0600627	9	6	-0.0705263	0.2166285
9	7	-0.1186233	-0.1005510	9	8	0.1844954	-0.0018494	9	9	-0.0555457	0.0975889
10	1	0.0769655	-0.1381110	10	2	-0.0805212	-0.0513356	10	3	0.0013119	-0.1614824
10	4	-0.0973123	-0.0693825	10	5	-0.0504401	-0.0438269	10	6	-0.0347366	-0.0777189
10	7	-0.0097468	-0.0042901	10	8	0.0437468	-0.0924808	10	9	0.1281797	-0.0481860
10	10	0.0945596	-0.0201041								
11	1	0.0095019	-0.0278111	11	2	0.0090541	-0.0992414	11	3	-0.0288895	-0.1324963
11	4	-0.0332108	-0.0700036	11	5	0.0459086	0.0552848	11	6	0.0084723	0.0242910
11	7	-0.0096093	-0.0918891	11	8	-0.0063530	0.0225827	11	9	-0.0387774	0.0402849
11	10	-0.0520582	-0.0176126	11	11	0.0543322	-0.0547288				
12	1	-0.0492610	-0.0496520	12	2	0.0076400	0.0349183	12	3	0.0324198	0.0179438
12	4	-0.0653020	-0.0030125	12	5	0.0306040	-0.0014745	12	6	0.0013881	0.0458322
12	7	-0.0126975	0.0348291	12	8	-0.0212177	0.0169046	12	9	0.0469380	0.0132223
12	10	-0.0091273	0.0316782	12	11	0.0054143	-0.0095228	12	12	-0.0035280	-0.0117964
13	1	-0.0540617	0.0434555	13	2	0.0534361	-0.0575844	13	3	-0.0140259	0.0836615
13	4	-0.0088182	-0.0003732	13	5	0.0596176	0.0574460	13	6	-0.0223869	-0.0118360
13	7	0.0035736	-0.0066171	13	8	-0.0122964	-0.0110925	13	9	0.0203827	0.0457820
13	10	-0.0433028	-0.0803383	13	11	-0.0401906	0.0055015	13	12	-0.0280059	0.0864102
13	13	-0.0615483	0.0682661								
14	1	-0.0187462	0.0232244	14	2	-0.0348122	-0.0060681	14	3	0.0369311	0.0224222
14	4	-0.0088329	0.0018783	14	5	0.0227952	-0.0116078	14	6	-0.0031868	0.0065119
14	7	0.0374843	-0.0043588	14	8	-0.0329416	-0.0131814	14	9	0.0371609	0.0179332
14	10	0.0369953	-0.0027966	14	11	0.0080835	-0.0413614	14	12	0.0089681	-0.0320668
14	13	0.0315333	0.0446234	14	14	-0.0505657	-0.0063741				
15	1	0.0082868	0.0142124	15	2	-0.0216258	-0.0364425	15	3	0.0446271	0.0265447
15	4	-0.0443760	0.0126416	15	5	-0.0160742	0.0108864	15	6	0.0272318	-0.0517077
15	7	0.0667130	0.0114545	15	8	-0.0406660	0.0247325	15	9	-0.0134441	0.0410187
15	10	0.0095928	0.0160812	15	11	0.0017171	0.0289322	15	12	-0.0283317	0.0124872
15	13	-0.0281051	-0.0049829	15	14	0.0061707	-0.0256132	15	15	-0.0180948	-0.0080854

211

Table 9.1
GEM-T1 NORMALIZED COEFFICIENTS (continued)
UNITS OF 10⁻⁶

$$\text{UNITS OF } 10^{-6}$$

SECTORIALS AND TESSERALS

INDEX N	M	C VALUE	S VALUE	INDEX N	M	C VALUE	S VALUE	INDEX N	M	C VALUE	S VALUE
16	1	0.0317099	0.0173493	16	2	-0.0156437	0.0245431	16	3	-0.0320841	-0.0450272
16	4	0.0365123	0.0438559	16	5	-0.0077242	-0.0016773	16	6	0.0179949	-0.0267835
16	7	-0.0030511	-0.0090737	16	8	-0.0134376	0.0022804	16	9	-0.0165750	-0.0509825
16	10	-0.0104171	0.0066056	16	11	0.0140156	-0.0064368	16	12	0.0208803	0.0057370
16	13	0.0307754	0.0006134	16	14	-0.0191226	-0.0382895	16	15	-0.0125321	-0.0322958
16	16	-0.0324114	-0.0043686								
17	1	-0.0309381	-0.0268459	17	2	-0.0057800	0.0171247	17	3	0.0101214	0.0098939
17	4	0.0125878	0.0312242	17	5	-0.0111472	-0.0056031	17	6	0.0002920	-0.0304166
17	7	0.0229520	-0.0119809	17	8	0.0311564	0.0087750	17	9	-0.0032015	-0.0343246
17	10	0.0021050	0.0201193	17	11	-0.0171108	0.0175019	17	12	-0.0342734	0.0172570
17	13	0.0169075	0.0201122	17	14	-0.0133370	0.0117613	17	15	0.0049435	0.0057493
17	16	-0.0290683	0.0018848	17	17	-0.0383106	-0.0206234				
18	1	-0.0002253	-0.0456055	18	2	0.0084083	0.0168428	18	3	-0.0010020	-0.0070483
18	4	0.0434167	0.0060924	18	5	0.0017426	0.0211276	18	6	0.0311991	-0.0085569
18	7	-0.0077957	0.0067159	18	8	0.0457191	0.0004305	18	9	-0.0135216	-0.0192446
18	10	0.0090063	-0.0108619	18	11	-0.0127989	-0.0005971	18	12	-0.0261819	-0.0165262
18	13	-0.0065815	0.0351551	18	14	-0.0092828	-0.0109400	18	15	-0.0377619	-0.0198247
18	16	0.0097880	0.0050024	18	17	0.0061142	0.0087663	18	18	-0.0044492	-0.0050647
19	1	-0.0115942	0.0053764	19	2	0.0084369	-0.0104744	19	3	0.0014391	0.0141955
19	4	0.0025699	0.0076747	19	5	-0.0024457	0.0173789	19	6	-0.0062545	0.0039169
19	7	0.0051443	-0.0016620	19	8	-0.0148626	-0.0113273	19	9	0.0017566	0.0086593
19	10	-0.0353538	-0.0026556	19	11	0.0164804	-0.0134748	19	12	0.0032037	-0.0043292
19	13	-0.0060894	-0.0291709	19	14	-0.0051227	-0.0126448	19	15	-0.0183164	-0.0127675
19	16	-0.0199047	-0.0119326	19	17	0.0279459	-0.0108837	19	18	0.0216467	-0.0031131
19	19	0.0064638	0.0104244								
20	1	0.0145119	-0.0212711	20	2	0.0198772	0.0032259	20	3	0.0082691	0.0137151
20	4	-0.0017951	0.0008281	20	5	-0.0104182	0.0003034	20	6	0.0127607	0.0009662
20	7	-0.0077913	0.0048958	20	8	-0.0020109	-0.0012912	20	9	0.0228121	0.0072350
20	10	-0.0224201	-0.0080926	20	11	0.0113787	-0.0239305	20	12	-0.0040581	0.0172980
20	13	0.0266491	0.0048913	20	14	0.0103228	-0.0117620	20	15	-0.0227306	-0.0004135
20	16	-0.0106685	0.0016919	20	17	0.0042934	-0.0089776	20	18	0.0105771	-0.0013024
20	19	-0.0070980	0.0084586	20	20	0.0017085	-0.0135051				

Table 9.1
GEM-T1 NORMALIZED COEFFICIENTS (continued)
UNITS OF 10⁻⁶

SECTORIALS AND TESSERALS

INDEX N	M	VALUE C	S	INDEX N	M	VALUE C	S	INDEX N	M	C	VALUE S
21	1	-0.0153942	0.0174459	21	2	0.0009874	-0.0026067	21	3	0.0019941	0.0226923
21	4	-0.0002550	0.0069894	21	5	0.0177593	-0.0158911	21	6	0.0042146	-0.0083501
21	7	-0.0122279	-0.0014058	21	8	-0.0181008	0.0025208	21	9	0.0173205	-0.0093913
21	10	-0.0036543	0.0018356	21	11	-0.0092806	-0.0367834	21	12	0.0028236	0.0127066
21	13	-0.0181694	0.0159969	21	14	0.0187760	0.0086994	21	15	0.0166205	0.0149837
21	16	-0.0087331	-0.0051553	21	17	-0.0067459	0.0008396	21	18	0.0168304	-0.0065691
21	19	-0.0209515	0.0158790	21	20	-0.0190411	0.0185361	21	21	0.0024775	-0.0068510
22	1	0.0083946	-0.0147250	22	2	-0.0142925	0.0020958	22	3	0.0067253	-0.0080913
22	4	-0.0094462	0.0167100	22	5	-0.0046335	-0.0001257	22	6	0.0146261	-0.0024348
22	7	0.0127538	0.0013042	22	8	-0.0098173	-0.0068267	22	9	0.0125106	-0.0094816
22	10	0.0050062	0.0203830	22	11	-0.0093740	-0.0183775	22	12	0.0074377	-0.0078426
22	13	-0.0169455	0.0178453	22	14	0.0087280	0.0102407	22	15	0.0279373	0.0031033
22	16	0.0000892	-0.0049265	22	17	0.0138079	-0.0111258	22	18	0.0070311	0.0102955
22	19	0.0066210	-0.0046952	22	20	-0.0133152	0.0147789	22	21	-0.0132244	0.0075983
22	22	-0.0014623	0.0047182								
23	1	0.0008657	0.0145970	23	2	-0.0005313	-0.0017780	23	3	-0.0045642	-0.0119458
23	4	-0.0103336	-0.0016696	23	5	0.0019941	-0.0079407	23	6	0.0099988	0.0049568
23	7	-0.0023282	0.0026452	23	8	0.0042209	-0.0067954	23	9	-0.0040274	-0.0103916
23	10	0.0199758	-0.0037585	23	11	0.0038490	0.0136794	23	12	0.0215777	-0.0166812
23	13	-0.0104578	-0.0075112	23	14	0.0046108	-0.0032727	23	15	0.0177318	-0.0022813
23	16	-0.0049029	0.0117671	23	17	-0.0072125	-0.0066031	23	18	-0.0019056	-0.0063023
23	19	-0.0086827	-0.0074916	23	20	0.0172248	-0.0090475	23	21	0.0108195	0.0076428
23	22	-0.0009034	-0.0021445	23	23	0.0008446	-0.0002030				
24	1	0.0081178	-0.0291987	24	2	-0.0058515	0.0052022	24	3	0.0069148	-0.0105925
24	4	0.0060580	0.0181145	24	5	0.0140838	-0.0079805	24	6	-0.0003055	-0.0006641
24	7	-0.0025113	0.0050662	24	8	-0.0024330	-0.0075574	24	9	-0.0038940	0.0014302
24	10	0.0173535	-0.0092954	24	11	0.0127396	0.0121180	24	12	0.0123406	-0.0095152
24	13	-0.0036235	0.0003824	24	14	0.0186436	0.0014570	24	15	0.0098097	-0.0135286
24	16	-0.0004908	-0.0062766	24	17	-0.0084625	0.0018817	24	18	0.0043072	-0.0050725
24	19	0.0005274	-0.0150179	24	20	-0.0060619	-0.0003298	24	21	0.0105744	0.0011197
24	22	-0.0017322	-0.0013033	24	23	-0.0021435	-0.0090055	24	24	0.0023438	-0.0012129

213

Table 9.1
GEM-T1 NORMALIZED COEFFICIENTS (continued)
UNITS OF 10^{-6}

SECTORIALS AND TESSERALS

INDEX N	M	VALUE C	S	INDEX N	M	VALUE C	S	INDEX N	M	VALUE C	S
25	1	0.0037145	0.0043498	25	2	0.0037220	0.0052068	25	3	-0.0032642	-0.0031087
25	4	0.0063503	-0.0015335	25	5	-0.0024585	-0.0023514	25	6	0.0059358	-0.0067430
25	7	0.0002632	-0.0034596	25	8	0.0014256	-0.0041241	25	9	-0.0060297	-0.0098442
25	10	0.0056907	-0.0044669	25	11	0.0055793	-0.0012766	25	12	-0.0055425	0.0110100
25	13	0.0073795	-0.0151883	25	14	-0.0219418	0.0132058	25	15	-0.0019899	-0.0022710
25	16	0.0030419	-0.0127972	25	17	-0.0083083	0.0005500	25	18	-0.0013004	-0.0106697
25	19	0.0091802	-0.0021317	25	20	-0.0037315	-0.0066217	25	21	0.0053968	-0.0031404
25	22	-0.0018741	-0.0017578	25	23	0.0045743	-0.0024633	25	24	0.0036065	-0.0038584
25	25	0.0049455	0.0040141								
26	1	0.0049741	-0.0172518	26	2	-0.0052887	0.0002522	26	3	-0.0002621	-0.0037215
26	4	0.0053222	0.0048968	26	5	0.0043007	0.0106472	26	6	0.0085388	0.0031968
26	7	0.0054524	-0.0025831	26	8	0.0030889	-0.0021407	26	9	-0.0025191	-0.0006592
26	10	-0.0048370	0.0016645	26	11	0.0032045	0.0050467	26	12	-0.0196457	-0.0054338
26	13	0.0027230	0.0014151	26	14	0.0039290	0.0056350	26	15	-0.0113797	-0.0047010
26	16	0.0058241	-0.0007199	26	17	-0.0048890	0.0082820	26	18	-0.0090148	0.0075516
26	19	0.0016260	0.0091610	26	20	0.0094830	-0.0109488	26	21	-0.0003907	-0.0024147
26	22	0.0109119	0.0082488	26	23	0.0023537	0.0089516	26	24	-0.0013736	0.0121837
26	25	-0.0039876		26	26	0.0034281	-0.0042690				
27	1	0.0005230	0.0066113	27	2	0.0102174	0.0028223	27	3	0.0051035	-0.0018585
27	4	0.0029164	0.0006401	27	5	0.0015884	0.0037103	27	6	0.0017746	-0.0021342
27	7	0.0069279	0.0028217	27	8	-0.0041794	-0.0044059	27	9	0.0003990	-0.0021553
27	10	0.0083100	0.0060112	27	11	-0.0011883	-0.0030951	27	12	-0.0004228	-0.0017182
27	13	-0.0059813	0.0041287	27	14	0.0119702	0.0066379	27	15	-0.0043373	-0.0001002
27	16	0.0065849	-0.0041072	27	17	0.0055505	0.0015914	27	18	0.0051898	0.0059394
27	19	0.0009254	-0.0062305	27	20	0.0029525	0.0030106	27	21	0.0020712	-0.0045432
27	22	-0.0001430	0.0029341	27	23	-0.0053881	-0.0027372	27	24	-0.0019361	0.0026238
27	25	0.0118014	0.0031453	27	26	-0.0050080	0.0040035	27	27	0.0068945	0.0034538

Table 9.1

GEM-T1 NORMALIZED COEFFICIENTS (continued)
UNITS OF 10^{-6}

SECTORIALS AND TESSERALS

INDEX N	M	VALUE C	S	INDEX N	M	VALUE C	S	INDEX N	M	VALUE C	S
28	1	0.0065294	-0.0100251	28	2	-0.0084276	-0.0115524	28	3	-0.0002646	0.0011662
28	4	0.0028786	-0.0024855	28	5	0.0029222	-0.0002361	28	6	-0.0083296	0.0020029
28	7	-0.0046459	-0.0015444	28	8	-0.0005655	-0.0031778	28	9	0.0029414	-0.0030550
28	10	-0.0072826	-0.0012046	28	11	0.0006214	-0.0008290	28	12	0.0004024	0.0024269
28	13	0.0000983	0.0035308	28	14	-0.0021064	-0.0065025	28	15	-0.0082106	0.0053751
28	16	-0.0083073	-0.0076860	28	17	0.0045201	-0.0042606	28	18	0.0003645	-0.0008295
28	19	-0.0044182	-0.0138003	28	20	-0.0009805	0.0011271	28	21	0.0024900	-0.0002697
28	22	-0.0048465	0.0005118	28	23	-0.0026403	0.0063891	28	24	0.0068762	-0.0150841
28	25	0.0011295	-0.0048096	28	26	0.0034421	0.0016811	28	27	-0.0099247	-0.0013336
28	28	0.0067689	0.0019493								
29	1	0.0034699	0.0024176	29	2	0.0094632	-0.0043311	29	3	-0.0043864	-0.0017609
29	4	-0.0063641	-0.0007289	29	5	-0.0034464	0.0035422	29	6	-0.0029960	-0.0024663
29	7	0.0011830	-0.0072940	29	8	-0.0064245	0.0025406	29	9	-0.0016394	0.0024790
29	10	0.0000602	0.0060144	29	11	-0.0093226	0.0004548	29	12	-0.0008339	-0.0049254
29	13	-0.0011458	-0.0019753	29	14	0.0051525	0.0019409	29	15	0.0012718	-0.0024918
29	16	-0.0021980	-0.0055327	29	17	-0.0045708	-0.0027849	29	18	-0.0020095	-0.0001378
29	19	-0.0021920	0.0015059	29	20	-0.0047996	0.0031625	29	21	-0.0093986	-0.0059494
29	22	0.0096562	0.0044395	29	23	-0.0050118	-0.0000780	29	24	-0.0025342	-0.0037024
29	25	0.0083057	0.0036286	29	26	-0.0062584	-0.0036878	29	27	-0.0074725	-0.0021507
29	28	0.0103226	-0.0019625	29	29	0.0086366	0.0031601				
30	1	-0.0016171	-0.0090886	30	2	-0.0040515	-0.0053645	30	3	-0.0016075	0.0014770
30	4	-0.0021102	-0.0039250	30	5	0.0033916	0.0006983	30	6	-0.0032177	0.0041679
30	7	-0.0001720	0.0001291	30	8	-0.0029536	0.0005720	30	9	0.0037915	-0.0039351
30	10	0.0012265	-0.0010402	30	11	0.0016207	0.0050752	30	12	0.0028146	-0.0034240
30	13	0.0146742	-0.0000192	30	14	-0.0000327	-0.0025522	30	15	0.0003035	-0.0092780
30	16	0.0006189	0.0056597	30	17	0.0010057	-0.0015438	30	18	-0.0074518	0.0008530
30	19	-0.0056266	-0.0026384	30	20	-0.0000276	0.0035666	30	21	-0.0025120	-0.0030982
30	22	0.0032458	-0.0055410	30	23	-0.0015833	-0.0053377	30	24	-0.0019206	-0.0000377
30	25	0.0088475	-0.0056062	30	26	-0.0032087	0.0081399	30	27	-0.0015075	0.0078152
30	28	0.0089658	0.0051589	30	29	0.0048227	0.0001240	30	30		-0.0004221

215

Table 9.1
GEM-T1 NORMALIZED COEFFICIENTS (continued)
UNITS OF 10⁻⁶

SECTORIALS AND TESSERALS

INDEX N	M	VALUE C	S	INDEX N	M	VALUE C	S	INDEX N	M	VALUE C	S
31	1	0.0051782	0.0023829	31	2	0.0066008	0.0008362	31	3	-0.0018668	-0.0040769
31	4	-0.0049509	-0.0016392	31	5	0.0009096	0.0014649	31	6	-0.0005622	0.0007667
31	7	0.0014817	-0.0017479	31	8	-0.0000872	-0.0011845	31	9	-0.0038941	-0.0017016
31	10	0.0025178	-0.0037447	31	11	-0.0016631	0.0058521	31	12	0.0001491	0.0046159
31	13	0.0056871	0.0013250	31	14	-0.0072828	0.0012481	31	15	-0.0004541	-0.0043732
31	16	-0.0045141	0.0048013	31	17	-0.0059335	0.0025686	31	18	0.0025645	0.0008491
31	19	0.0020172	0.0028162	31	20	-0.0018947	0.0005595	31	21	0.0023358	0.0035767
31	22	-0.0062664	0.0057325	31	23	0.0095047	0.0056544	31	24	-0.0038298	-0.0019101
31	25	-0.0077449	-0.0002757	31	26	-0.0046923	-0.0003639	31	27	-0.0069960	0.0122525
31	28	-0.0003428	0.0017261	31	29	-0.0054215	-0.0059502	31	30	-0.0024527	0.0084230
31	31	-0.0002319	-0.0000737								
32	1	-0.0091529	-0.0092451	32	2	0.0018649	0.0043749	32	3	-0.0006663	0.0029992
32	4	0.0020179	-0.0033825	32	5	0.0000480	-0.0027949	32	6	-0.0038310	0.0002190
32	7	-0.0030832	0.0018611	32	8	-0.0008818	0.0033226	32	9	0.0019461	0.0007681
32	10	0.0008308	0.0019507	32	11	-0.0024010	-0.0006463	32	12	-0.0017118	0.0041940
32	13	0.0072556	-0.0002229	32	14	0.0046569	0.0069216	32	15	0.0039107	-0.0049375
32	16	0.0029187	0.0041010	32	17	0.0036602	0.0018909	32	18	0.0022105	0.0014795
32	19	0.0030881	0.0015146	32	20	-0.0015881	0.0014199	32	21	0.0011690	0.0058848
32	22	-0.0046595	-0.0007455	32	23	0.0038573	-0.0047759	32	24	0.0065905	0.0053251
32	25	-0.0131730	0.0077043	32	26	-0.0010511	0.0015337	32	27	-0.0030949	-0.0030221
32	28	0.0015717	0.0023530	32	29	-0.0033428	-0.0025024	32	30	0.0082893	0.0016713
32	31	-0.0007616	-0.0027125	32	32	0.0007277	0.0005068				
33	1	0.0012672	0.0021258	33	2	-0.0010231	0.0009548	33	3	-0.0017027	-0.0028776
33	4	-0.0002362	0.0003938	33	5	-0.0005132	0.0032353	33	6	0.0013824	-0.0012542
33	7	-0.0000405	-0.0017756	33	8	-0.0000823	0.0015750	33	9	0.0052939	-0.0018691
33	10	-0.0002341	0.0009449	33	11	0.0055568	-0.0004803	33	12	0.0052208	0.0041268
33	13	0.0036684	0.0067767	33	14	0.0092319	0.0025099	33	15	-0.0030055	0.0021726
33	16	-0.0003879	0.0019724	33	17	-0.0021426	0.0030432	33	18	0.0008702	-0.0012393
33	19	0.0016796	0.0002369	33	20	0.0020822	-0.0007525	33	21	0.0007319	-0.0008394
33	22	-0.0040992	0.0010974	33	23	-0.0006277	-0.0043975	33	24	0.0039903	-0.0004821
33	25	-0.0012628	-0.0048224	33	26	-0.0081343	0.0055386	33	27	-0.0103323	0.0021297
33	28	-0.0108851	0.0018952	33	29	-0.0213209	0.0001932	33	30	0.0025217	-0.0134935
33	31	0.0001745	0.0011566	33	32	0.0024100	-0.0000219	33	33	-0.0002676	-0.0003603

Table 9.1

GEM-T1 NORMALIZED COEFFICIENTS (continued)
UNITS OF 10^{-6}

SECTORIALS AND TESSERALS

INDEX N	M	VALUE C	S
34	1	-0.0015608	-0.0091011
34	4	0.0028502	-0.0018773
34	7	0.0023148	-0.0001028
34	10	-0.0014879	-0.0000093
34	13	-0.0080803	0.0012768
34	16	0.0011337	-0.0026578
34	19	0.0005953	-0.0010032
34	22	0.0008294	0.0004221
34	25	0.0062516	0.0082080
34	28	0.0045502	-0.0081979
34	31	0.0023534	-0.0022983
34	34	-0.0002093	-0.0006039
35	1	0.0019069	0.0020110
35	4	0.0027442	0.0014864
35	7	0.0000748	0.0015282
35	10	-0.0014313	-0.0008354
35	13	0.0011849	0.0044812
35	16	0.0001314	-0.0013369
35	19	-0.0029031	0.0005932
35	22	-0.0000159	0.0033003
35	25	0.0033892	0.0015231
35	28	-0.0108936	0.0233542
35	31	0.0013305	0.0010339
35	34	-0.0005168	0.0001237
36	1	0.0028774	-0.0058408
36	4	0.0013157	-0.0001181
36	7	0.0001662	-0.0004199
36	10	-0.0003570	0.0004671
36	13	0.0007685	0.0037948
36	16	0.0013405	-0.0020055
36	19	-0.0002562	0.0006695
36	22	0.0005732	0.0006864
36	25	0.0000270	0.0086477
36	28	-0.0069480	0.0056619
36	31	-0.0035516	0.0013604
36	34	0.0008324	0.0017560

INDEX N	M	VALUE C	S
34	2	0.0035817	0.0051783
34	5	-0.0012952	0.0000401
34	8	0.0007083	-0.0007860
34	11	0.0012406	-0.0038325
34	14	-0.0010431	-0.0002878
34	17	-0.0003626	0.0025764
34	20	0.0008917	-0.0003975
34	23	-0.0009300	-0.0021403
34	26	0.0010816	-0.0090061
34	29	-0.0038113	-0.0044842
34	32	-0.0008166	0.0011610
35	2	-0.0025529	0.0010277
35	5	-0.0002351	-0.0007374
35	8	0.0002679	-0.0001772
35	11	0.0006785	-0.0036583
35	14	-0.0004836	0.0001238
35	17	0.0033863	-0.0024391
35	20	-0.0007745	-0.0008763
35	23	-0.0023783	-0.0015551
35	26	0.0015231	-0.0001412
35	29	0.0143438	-0.0031532
35	32	0.0081878	0.0005664
35	35	0.0039791	-0.0001450
36	2	0.0001790	0.0012922
36	5	-0.0011798	0.0003403
36	8	0.0010487	0.0005378
36	11	0.0005880	0.0007308
36	14	-0.0048384	0.0040665
36	17	0.0021679	-0.0008490
36	20	0.0009128	0.0008661
36	23	0.0012168	0.0005518
36	26	0.0084469	0.0110849
36	29	-0.0013415	-0.0024474
36	32	-0.0008804	0.0003000
36	35	0.0002152	-0.0007347

INDEX N	M	VALUE C	S
34	3	-0.0005145	0.0022065
34	6	0.0005808	-0.0003220
34	9	0.0012660	0.0015093
34	12	0.0004550	0.0024876
34	15	0.0007643	0.0030005
34	18	-0.0027232	-0.0000869
34	21	-0.0013743	-0.0006590
34	24	0.0067267	-0.0008511
34	27	0.0068974	-0.0005442
34	30	-0.0061161	0.0000268
34	33	0.0010234	0.0013813
35	3	0.0006733	0.0006861
35	6	0.0008304	-0.0014752
35	9	0.0010826	-0.0020731
35	12	0.0014841	0.0020619
35	15	0.0002609	0.0028304
35	18	0.0015003	0.0005937
35	21	0.0013843	0.0027357
35	24	0.0025277	0.0021953
35	27	0.0027787	0.0191290
35	30	0.0037128	-0.0028852
35	33	-0.0002881	0.0016655
36	3	-0.0008129	-0.0013852
36	6	-0.0005757	0.0008988
36	9	-0.0003170	0.0005484
36	12	-0.0002182	-0.0016068
36	15	0.0018223	0.0018634
36	18	-0.0007411	0.0005306
36	21	0.0006589	-0.0021175
36	24	-0.0101912	-0.0014201
36	27	-0.0015551	0.0042305
36	30	-0.0023972	-0.0020261
36	33	0.0001484	-0.0026170
36	36		0.0004197

217

GEOID HEIGHTS

REFERRED TO GRS-80 ELLIPSOID
$a_e = 6378137$ m $1/f = 298.257$

Figure 9.0.   The GEM-T1 Geoid.

218

The artificial satellites suitable for geopotential recovery are sensitive to the low degree and order harmonics in the global spherical harmonic expansions of the tides. In fact, these satellites form a sensitive measurement system for monitoring these effects. (Table 9.2 shows the periods of the principal long period tidal perturbations on the orbits for the major satellites used in GEM-T1. The diurnal and semidiurnal bands are particularly variable in frequency relative to the corresponding periodicities of the tides on the Earth's surface since the satellite's nodal precession and not the earth's rotation makes the largest contribution to these periodicities.)

The approach we have used in the development of GEM-T1 is to recover the relevant tidal parameters directly in the simultaneous least squares data reduction process along with the other geodetic and geodynamic parameters. The rationale for this approach is dictated largely by the present uncertainty of these tidal coefficients which are known only to about 10% of their values. This approach was demonstrated with great success in single satellite analyses using STARLETTE (Williamson and Marsh, 1985; Marsh et al., 1985) and LAGEOS (Christodoulidis et al., 1986a).

The a priori values for the ocean tides were derived as detailed in Section 7.1.4. The body tides were held fixed according to the Wahr values as given in Section 7.1.3 and the adopted precession and nutation are the IAU 1980 models. Because the body tides are not separable from the ocean tides, only the ocean tides were adjusted. The ocean tides recovered actually represent a determination of the total temporal variations of the geopotential exterior to the Earth's atmosphere in the presence of a fixed solid earth tidal model.

Table 9.3 summarizes the ocean tidal terms which were modeled or adjusted in the GEM-T1 solution. Due to the altitudes of the satellites, the background model is only required to degree 6. Coefficients associated with the primary tidal terms were adjusted. This restriction of
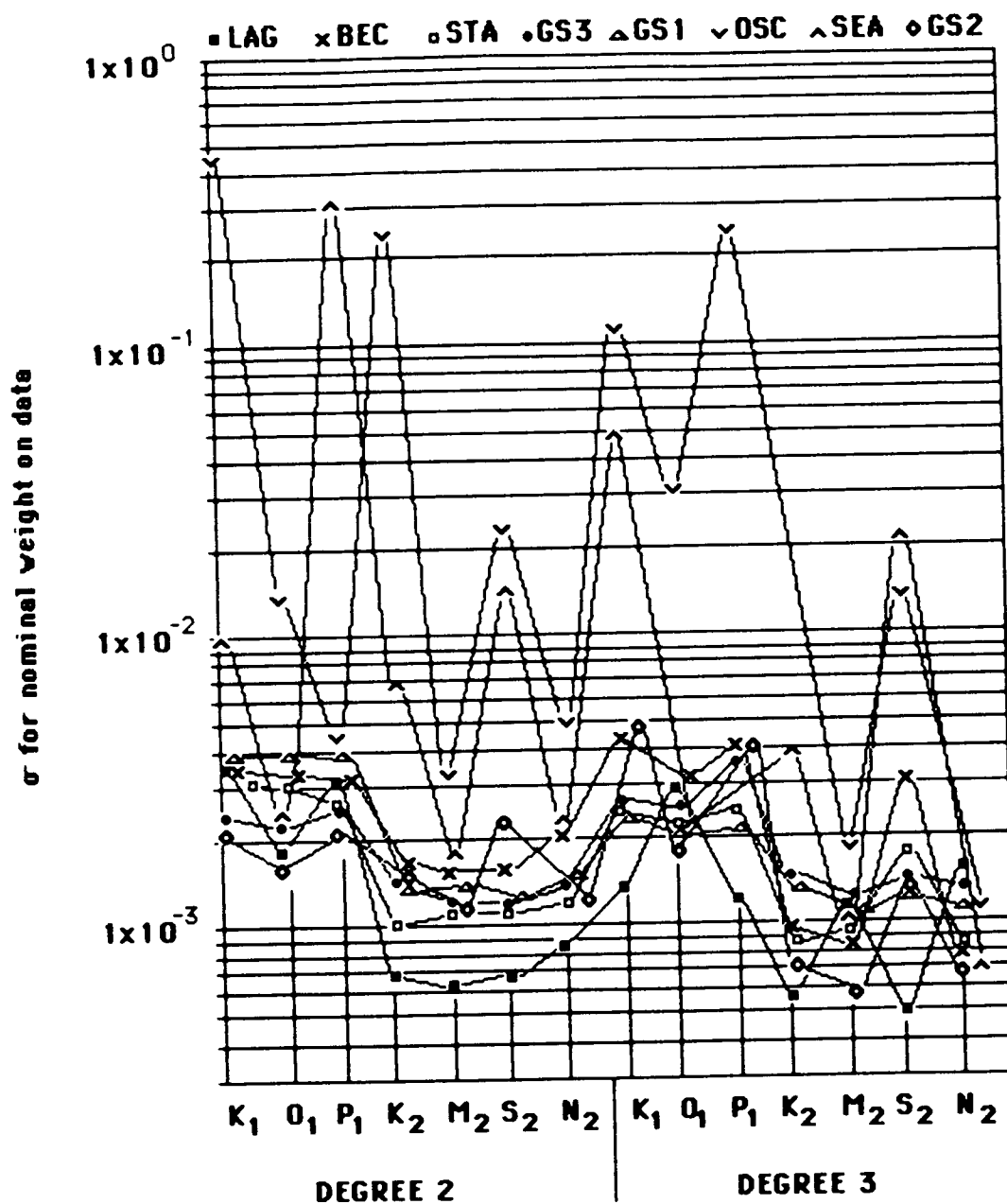
Figure 9.1. Satellite Tidal Sensitivities from Single Satellite Solutions for 5 x 5 Gravity Coefficients and 2nd and 3rd Degree Tidal Terms.

Table 9.2

PERIODS (DAYS) OF PRINCIPAL LONG PERIOD SATELLITE PERTURBATIONS DUE TO SOLID EARTH AND OCEAN TIDES FOR 12 MAJOR TIDE CONSTITUENTS

	056.5545	057.5555	065.4555	075.5555	145.5555	163.5555	165.5555	245.6555	255.5555	272.5565	273.5555	275.5555
SATELLITE	S_a	S_{sa}	M_m	M_f	O_1	P_1	K_1	N_2	M_2	T_2	S_2	K_2
LAGEOS	365	183	27.6	13.7	13.8	221	1050	9.20	14.0	159	280	524
STARLETTE	365	183	27.6	13.7	11.9	60.8	91.0	7.61	10.5	33.1	36.4	45.5
GEOS-1	365	183	27.6	13.7	12.6	85.4	160	8.20	11.7	48.3	55.7	80.2
GEOS-2	365	183	27.6	13.7	14.4	629	257	9.83	15.3	2250	436	129
GEOS-3	365	183	27.6	13.7	15.2	482	132	10.6	17.2	145	104	66.2
BE-B	365	183	27.6	13.7	13.1	118	332	8.66	12.6	70.2	87.0	166
BE-C	365	183	27.6	13.7	11.8	57.9	84.8	7.51	10.3	31.5	34.4	42.4
SEASAT	365	183	27.6	13.7	14.8	7130	178	10.2	16.1	331	174	89.0
TELSTAR-1	365	183	27.6	13.7	12.8	93.9	193	8.34	12.0	53.9	63.2	96.7
ANNA	365	183	27.6	13.7	12.0	64.4	99.4	7.71	10.7	35.3	39.1	49.7
OSCAR	365	183	27.6	13.7	13.6	180	11700	9.12	13.6	119	177	5830

Table 9.3

OCEAN TIDE MODELING
FOR
GRAVITY RECOVERY

• LONG PERIOD TIDES •

Doodson No.	Darwin Name	Modeled	Adjusted
056.554	S_a	deg. 2→6	deg. 2
057.555	S_{sa}	prograde	deg. 2
058.554		only	none
065.455	M_m		deg. 2
075.555	M_f		deg. 2
075.565			none

• DIURNAL •

Doodson No.	Darwin Name	Modeled	Adjusted
135.655	Q_1	deg. 2→6	none
145.545		prograde	none
145.555	O_1	and	deg. 2, 3, 4
155.455		retrograde	none
155.655	M_1		none
162.556	PI_1		none
163.555	P_1		deg. 2, 3, 4
164.556	S_1		none
165.545			none
165.555	K_1		deg. 2, 3, 4
165.565			none
166.554			none
167.555			none
175.455	S_1		none
185.555	OO_1		none

• SEMI-DIURNAL •

Doodson No.	Darwin Name	Modeled	Adjusted
245.655	N_2	deg. 2→6	deg. 2, 3, 4, 5
255.545		prograde	none
255.555	M_2	and	deg. 2, 3, 4, 5
265.455	L_2	retrograde	none
271.557			none
272.556	T_2		deg. 2, 3, 4, 5
273.555	S_2		deg. 2, 3, 4, 5
274.554	R_2		none
275.555	K_2		deg. 2, 3, 4, 5
285.455			none
295.555			none

adjusting the coefficients of the primary terms was adopted because of computer limitations. The background tidal terms are less significant in their orbital perturbations than those from the primary terms, and errors in these terms are not expected to be of consequence now that they are somewhat reliably modeled (we estimate 10 to 20% uncertainty).

Tables 9.4 through 9.7 present the recovered ocean tidal coefficients by degree. The values shown for the coefficient and phase uncertainties were obtained from the covariance analysis which produced the properly calibrated gravity coefficients as described in Section 10. These uncertainties are believed to give realistic estimates for the error in the total exterior tidal potential. Tables 9.4 to 9.7 also compare our GEM-T1 ocean tide coefficients with those obtained from the Schwiderski and Parke models, which were conventionally obtained by solution of the Laplace Tidal Equations using deep ocean tide guage data. The variation seen between the two oceanographic tidal solutions is often larger than the uncertainty in our recovered solution. Generally the satellite results are in reasonable agreement with the Schwiderski and Parke models. A more complete discussion of the GEM-T1 tidal solution is found in Christodoulidis et al., 1987.

A limited test was performed to assess the relative contribution of each of the major satellites in the solution to the tide coefficient recovery. Figure 9.1 shows the relative standard deviations of the second and third degree diurnal and semidiurnal tides from solutions based on individual satellites. Each test solution included the adjustment of a (5x5) gravity model simultaneously with the second and third degree tidal terms. The weights in these solutions were 1 meter on range and 1 cm/sec on range-rate. LAGEOS dominates the second degree semidiurnal recovery, and the polar OSCAR Doppler satellite is not strongly contributing to the solution. Otherwise, the individual satellites contribute nearly equally to within a factor of two or three.

Table 9.4

VALUES FOR DYNAMICALLY ESTIMATED 2ND DEGREE TIDES COMPARED TO OCEANOGRAPHIC DETERMINATIONS

	$C^{+}_{2m,f}$ AMPLITUDE (cm)			$\varepsilon^{+}_{2m,f}$ PHASE (deg)		
	OBSERVED	OCEANOGRAPHIC		OBSERVED	OCEANOGRAPHIC	
TIDE (f)	SATELLITE	SCHWIDERSKI	PARKE	SATELLITE	SCHWIDERSKI	PARKE
LONG PERIOD (m = 0)						
M_m	.36 ± .50	1.06	---	274.10 ± 76.60	258.9	---
S_a	2.44 ± .77	---	---	31.03 ± 18.75	---	---
M_f	1.80 ± .41	1.70	---	245.35 ± 13.08	252.0	---
S_{sa}	1.68 ± .72	1.24	---	223.12 ± 26.44	221.6	---
DIURNAL (m = 1)						
K_1	2.61 ± .23	2.82	2.46	328.50 ± 5.02	315.1	312.0
O_1	2.69 ± .17	2.42	1.88	318.53 ± 3.63	313.7	309.0
P_1	0.81 ± .23	0.90	0.76	296.83 ± 16.07	313.9	311.7
SEMI-DIURNAL (m = 2)						
K_2	0.31 ± .05	0.26	---	302.14 ± 9.79	315.11	---
M_2	3.26 ± .05	2.96	3.38	320.93 ± 0.92	310.6	313.1
S_2	0.80 ± .05*	0.93	0.88	301.93 ± 3.73*	314.0	300.8
N_2	0.70 ± .07	0.65	0.58	334.01 ± 5.52	321.8	324.5
T_2	0.09 ± .05	---	---	19.76 ± 34.80	---	---

*combined ocean/atmospheric effect

Table 9.5

<table>
<tr><td colspan="7" align="center">VALUES FOR DYNAMICALLY ESTIMATED
3RD DEGREE TIDES
COMPARED TO OCEANOGRAPHIC DETERMINATIONS</td></tr>
<tr><td></td><td colspan="3" align="center">$C^+_{3m,f}$
AMPLITUDE (cm)</td><td colspan="3" align="center">$\varepsilon^+_{3m,f}$
PHASE (deg)</td></tr>
<tr><td></td><td>OBSERVED</td><td colspan="2" align="center">OCEANOGRAPHIC</td><td>OBSERVED</td><td colspan="2" align="center">OCEANOGRAPHIC</td></tr>
<tr><td>TIDE (f)</td><td>SATELLITE</td><td>SCHWIDERSKI</td><td>PARKE</td><td>SATELLITE</td><td>SCHWIDERSKI</td><td>PARKE</td></tr>
<tr><td colspan="7">DIURNAL (m = 1)</td></tr>
<tr><td>K_1</td><td>0.57 ± .10</td><td>0.89</td><td>1.04</td><td>58.96 ± 10.38</td><td>33.7</td><td>16.2</td></tr>
<tr><td>O_1</td><td>1.73 ± .21</td><td>1.31</td><td>1.54</td><td>77.59 ± 6.85</td><td>83.6</td><td>74.9</td></tr>
<tr><td>P_1</td><td>0.33 ± .10</td><td>0.29</td><td>0.36</td><td>2.09 ± 18.14</td><td>39.9</td><td>33.8</td></tr>
<tr><td colspan="7">SEMI-DIURNAL (m = 2)</td></tr>
<tr><td>K_2</td><td>0.51 ± .04</td><td>0.09</td><td>---</td><td>206.35 ± 4.88</td><td>195.0</td><td>---</td></tr>
<tr><td>M_2</td><td>0.20 ± .08</td><td>0.36</td><td>0.39</td><td>152.39 ± 22.28</td><td>168.6</td><td>219.7</td></tr>
<tr><td>S_2</td><td>0.38 ± .04</td><td>0.26</td><td>0.48</td><td>237.37 ± 6.14</td><td>201.9</td><td>222.5</td></tr>
<tr><td>N_2</td><td>0.10 ± .09</td><td>0.11</td><td>0.12</td><td>84.93 ± 51.64</td><td>171.9</td><td>174.5</td></tr>
<tr><td>T_2</td><td>0.15 ± .04</td><td>---</td><td>---</td><td>214.52 ± 16.02</td><td>---</td><td>---</td></tr>
</table>

Table 9.6

VALUES FOR DYNAMICALLY ESTIMATED 4TH DEGREE TIDES COMPARED TO OCEANOGRAPHIC DETERMINATIONS

	AMPLITUDE (cm) $C^+_{4m,f}$			PHASE (deg) $\varepsilon^+_{4m,f}$		
	OBSERVED SATELLITE	OCEANOGRAPHIC SCHWIDERSKI	OCEANOGRAPHIC PARKE	OBSERVED SATELLITE	OCEANOGRAPHIC SCHWIDERSKI	OCEANOGRAPHIC PARKE
TIDE (f)						
DIURNAL (m = 1)						
K_1	2.62 ± .34	1.91	1.72	254.42 ± 9.24	254.2	241.2
O_1	1.83 ± .32	1.43	1.46	283.38 ± 9.57	276.3	267.2
P_1	0.35 ± .32	0.63	0.57	234.91 ± 52.62	258.3	253.6
SEMI-DIURNAL (m = 2)						
K_2	0.19 ± .07	0.11	---	75.96 ± 21.23	103.5	---
M_2	0.93 ± .07	1.01	1.29	127.41 ± 4.61	124.7	120.3
S_2	0.41 ± .07	0.21	0.19	86.53 ± 11.18	141.8	125.4
N_2	0.17 ± .08	0.37	0.39	137.28 ± 25.62	103.0	84.8
T_2	0.07 ± .08	---	---	46.02 ± 65.50	---	---

227

Table 9.7

VALUES FOR DYNAMICALLY ESTIMATED 5TH DEGREE TIDES COMPARED TO OCEANOGRAPHIC DETERMINATIONS

$C_{5m,f}^+$

AMPLITUDE (cm)

$\varepsilon_{5m,f}^+$

PHASE (deg)

TIDE (f)	OBSERVED SATELLITE	OCEANOGRAPHIC		OBSERVED SATELLITE	OCEANOGRAPHIC	
		SCHWIDERSKI	PARKE		SCHWIDERSKI	PARKE
SEMI-DIURNAL (m = 2)						
K$_2$	0.10 ± .05	0.04	---	56.10 ± 31.38	0.41	---
M$_2$	0.28 ± .06	0.28	0.25	17.62 ± 12.02	356.60	15.9
S$_2$	0.21 ± .06	0.14	0.12	34.42 ± 17.97	3.77	30.1
N$_2$	0.11 ± .06	0.08	0.05	3.56 ± 31.76	5.03	352.3
T$_2$	0.14 ± .06	---	---	39.03 ± 23.96	---	---

9.3   STATION COORDINATE SOLUTIONS AND COMPARISONS

9.3.1 Introduction

As has been discussed for some time, geopotential modeling has been the dominant source of error in previous station coordinate solutions (Smith et al, 1979). More recently, these uncertainties have been diminishing with the collection of more tracking data and the recovery of refined gravity models. In Smith et al (1985), the uncertainties in the geopotential model (GEM-L2) were estimated to have a degrading effect of less than 5 cm in the coordinate solutions. The development of the improved TOPEX gravity model offers an opportunity to compute new coordinate solutions whereby many of the uncertainties associated with the geopotential model have been further minimized. As part of these efforts, better models for describing tides, polar motion, and non-conservative forces have been developed thereby minimizing uncertainties arising from these parameters. This section restricts itself to preliminary solutions for station coordinates and an assessment of the quality of station positioning which has been achieved.

9.3.2 GEM-T1 STATIONS

The GEM-T1 solution was made holding the station coordinates fixed in the TCS system at the values described in Section 6. However, with the arrival of GEM-T1 force modeling, two solutions have been performed and tested against the a priori values. These solutions included:

*   Doppler station coordinates from a combination of SEASAT and OSCAR data and

*   A laser solution from 5 years of LAGEOS observations.

The laser solution used the GEM-T1 gravity and tide models. The Doppler solution used an earlier GEM-T1 model which contained GEM T1's entire doppler data set but was otherwise incomplete.

9.3.3 Laser Station Solutions

We will concern ourselves, for the moment, with the laser network. A solution for coordinates for stations tracking LAGEOS has been computed utilizing the SOLVE software package. This solution incorporates five years of LAGEOS tracking data and also solves for polar motion, A1-UT1, GM, and the Love numbers h_2, ℓ_2. The GEM-T1 gravity model was used in this solution. This coordinate solution is equivalent to a first iteration using a new gravity model and is not equivalent to making a simultaneous solution for station positions and gravity field.   This means that part of the a priori coordinate uncertainties may possibly have been absorbed in the adjustment for the gravity field (i.e. the computation for GEM-T1) since the gravity field and the station positions may be, in some way, correlated.

To test for the internal consistency of the solution, the solved for coordinates were compared to the a priori set of coordinates in the TOPEX geodetic file. This comparison (as well as those that follow) was performed using software which determines the seven parameter transformation between the two sets of coordinates in a least squares algorithm. This is the same software used in creating the geodetic file (see Section 6 on Station Coordinates).

Within the transformation parameters, the translational components provide an internal check of the stability of the origin of the coordinate system. For the LAGEOS solution, these parameters reveal an encouraging picture.   The results discussed here are summarized in

230

TABLE 9.8

SEVEN PARAMETER COMPARISONS BETWEEN STATION COORDINATE SOLUTIONS

PARAMETER	LASER: NEW vs. A PRIORI	DOPPLER: NEW vs. A PRIORI	DOPPLER : NEW vs. PTGF-2
ΔX	0.26 cm	11.64 cm	-24 cm
ΔY	1.46 cm	4.16 cm	-5 cm
ΔZ	-2.54 cm	-93.89 cm	-4 cm
scale	0.005 ppm	0.011 ppm	
omega	0.23 mas	30.7 mas	
psi	-1.48 mas	-10.5 mas	
epsilon	-1.11 mas	1.86 mas	
RMS X	5.42 cm	55.58 cm	131 cm
RMS Y	4.40 cm	63.30 cm	114 cm
RMS Z	4.23 cm	54.66 cm	59 cm
stations	43	35	28

Table 9.8 along with results from the Doppler solutions. The 2.5 cm
value (and less) for the origin translation implies that the coordinate
system and reference frame were properly maintained in the development
of the TOPEX gravity model effort. The rotational elements of the
transformation provide information regarding mismodeling of the axes
definition. The values for these rotations are at the milli-arc second
level.

Differences in cartesian and geodetic coordinates can be analyzed
after the transformation has been made. With these differences, aber-
rant stations can be isolated easily and the RMS value of all of the
differences allows an assessment of the consistency between the two sets
of coordinates. Upon removing a small set of weakly determined stations,
a 43 station comparison was made. The RMS value of the differences for
these 43 stations is 5 cm or less for each Cartesian coordinate. Thus
one can conclude that the a priori positions (the SL-6 values) for the
LAGEOS tracking stations were well determined and that, in general,
these positions are known relatively to better than 5 cm in any
direction.

9.3.4 Doppler Station Solutions

The Doppler results are not as encouraging as the laser results.
The GSFC group has computed a set of solutions for Doppler station
coordinates based on the complete SEASAT and OSCAR tracking data. The
station coordinates from this solution are thought to be among the best
available and are given in Table 9.9. The University of Texas Center
for Space Research has also made a similar solution based on one of
their preliminary TOPEX gravity models.

First, we will discuss the comparison results for the GSFC
SEASAT/OSCAR solution with the a priori station coordinates in the TOPEX
geodetic file. Referring again to Table 9.8, it can be noted that the

Table 9.9 Doppler Station coordinates based upon PGS-T2' gravity field.

name	num.	X	Y	Z	latitude dd mm ss.ssss			longitude ddd mm ss.ssss			height
SJEDOP	8	4083913.573800	-4209803.360600	-2499113.610600	-23	12	2.9371	314	7	49.3604	612.9718
MCMDOP	19	-1310714.327500	310460.178800	-6213366.135200	-77	50	51.7210	166	40	27.5393	-13.3333
MAHDOP	20	3602881.466600	5238221.052500	-515942.091700	-4	40	14.4561	55	28	46.4214	554.4624
UCLDOP	21	4027833.675100	307023.119300	4919537.009200	50	47	54.9566	4	21	32.2662	158.6962
SMGDOP	22	-3088047.766000	5333058.457000	1638810.773500	14	59	16.0794	120	4	21.0223	56.5049
GWMDOP	23	-5059776.901400	3591211.911800	1472781.612500	13	26	22.8662	144	38	4.2254	95.4591
TAFDOP	24	-6100051.346100	-997193.869001	-1568316.457900	-14	19	45.3816	189	17	3.0985	45.7365
MSADOP	27	-3857199.252000	3108663.581400	4004043.602400	39	8	6.5598	141	8	0.0168	122.0553
PRTDOP	105	5051979.361600	2725636.047000	-2774471.714200	-25	56	48.6545	28	20	51.6482	1607.9857
VIRDOP	107	1090139.925300	-4842520.544000	3991980.602100	38	59	43.7271	282	41	12.6026	85.1699
STFDOP	112	-3942239.972800	3468854.894100	-3608206.038100	-34	40	26.4843	138	39	17.3286	36.9684
NMXDOP	113	-1556216.300000	-5169444.400000	3387248.800000	32	16	43.9534	253	14	45.7268	1183.4922
ANCDOP	114	-2656164.814100	-1544366.619100	5570654.124900	61	17	0.4266	210	10	29.5907	76.3954
BSEDOP	116	4004965.181300	-96560.012500	4946540.225700	51	11	4.5330	358	37	7.9032	125.3628
TULDOP	118	539846.322900	-1388555.012600	6180979.992300	76	32	9.0740	291	14	42.8136	68.8087
ALTDOP	127	-3850349.491000	397642.607500	5052347.981900	52	43	41.8761	174	6	13.3734	73.0156
OTTDOP	128	1091450.648500	-4351284.681200	4518703.573000	45	23	59.8860	284	4	52.3730	47.3492
TEXDOP	192	-740293.468700	-5457073.249600	3207243.561400	30	23	1.1022	262	16	28.3874	218.3548
FLODOP	641	4522403.122800	898011.711900	4392485.926100	43	48	13.6560	11	13	51.9826	147.7314
ACSDOP	68	6119385.149700	-1571426.518600	-871690.023200	-7	54	28.1648	345	35	52.5543	46.1535
KWJDOP	214	-6160998.307900	1339621.205200	960416.180000	8	43	6.9609	167	43	58.0634	36.7855
QUIDOP	121	1280855.854900	-6250961.221400	-10806.752400	0	5	51.6884	281	34	47.7330	2711.3358
SHIDOP	123	6104424.398300	-611087.365300	-1740830.800000	-15	56	34.8304	354	17	0.2890	604.1717
HONDOP	188	-5511608.514600	-2226970.834300	2303885.073100	21	18	52.5097	202	0	4.3898	19.9707
STODOP	280	1743940.076400	-5022701.153800	-3512034.477600	-33	37	26.0465	289	8	51.3386	449.1890
CALDOP	414	-1659604.047400	-3676718.989500	4925497.766500	50	52	17.0968	245	42	23.2188	1247.6164
NAPDOP	448	-4923683.766500	270897.300000	-4031783.343900	-39	27	31.6075	176	51	2.8991	19.1794
EASDOP	730	-1888663.201600	-5355677.966300	-2893871.401500	-27	9	30.4475	250	34	29.8560	49.7576
TVEDOP	793	-5037686.183500	3301866.756900	-2090791.616000	-19	15	43.8999	146	45	28.2094	66.2392
BGKDOP	800	-1139090.620500	6089775.302400	1510692.144300	13	47	32.9671	100	35	41.0243	-13.2719
DGCDOP	939	1915631.941000	6030276.444000	-801057.498700	-7	15	49.0991	72	22	35.6174	-57.5421
LAJDOP	966	4432069.311200	-2268085.806300	3973469.226100	38	46	51.2986	332	53	56.9995	131.8420
BDADOP	967	2293703.881200	-4883222.108500	3390597.138100	32	19	16.9383	295	9	35.8834	-5.3777
PERDOP	968	-2353565.897200	4877202.957400	-3358334.837400	-31	58	39.4718	115	45	37.1351	13.5722
CNIDOP	970	5384988.497500	-1576475.750800	3023842.298400	28	28	54.4718	343	40	56.6697	625.9310
UKIDOP	1960	-2713391.978100	-4144609.641000	4004304.375500	39	8	16.1970	236	47	16.9567	169.9827

Semi-major axis: 6378137.00   Flattening: 1/298.257

center of mass offset between the two sets of coordinates is quite small in the equatorial plane but the magnitude of the axial displacement in the Z direction is nearly -1 meter. This result is similar to that observed in earlier, and unfortunately unreported, GSFC studies dealing with laser tracking sites determined in similar coordinate systems. In the earlier work, a pair of solutions for laser coordinates was made, one based on the SL-6 system and the other based on a coordinate system associated with the PGS-S4 gravity model. The earlier station comparison between these two sets of coordinates showed, as does our station comparison, this -1m Z coordinate offset. Since our a priori stations are based on the SL-6 system, it seems that in the adjustment for the Doppler stations, the stations are adjusting towards those computed in the PGS-S4 based solution. The scale parameter is at the 11 parts per billion level, this slight scale change is most likely attributable to the adjustment of GM. The RMS of the differences between the transformed coordinates is at the 60 cm level (an order of magnitude worse than the lasers). A portion of the RMS disagreement is attributable to errors in the Doppler tracking systems and in part due to the larger SEASAT orbit errors.

A comparison of the GSFC SEASAT/OSCAR solution has been made with a similar solution by University of Texas utilizing their PTGF-2 gravity model (the comparison was provided courtesy of C.K. Shum). This comparison is also summarized in Table 9.8. The translational components of the seven parameter transformation are of the same magnitude as those seen in the previous discussion except that the ΔZ shift is now quite small. Thus, the adjusted Doppler station coordinates in both the GSFC and UT solutions appear to agree well with regard to the coordinate system origin. By the same token, the RMS differences of the positions after transformation are on the 0.5 to 1.5 m level. This leads one to conclude that the station positions are still not resolvable to a level below 50 cm with Doppler data.

The causes for the poor resolution at the Doppler sites are still being studied at this time. The RMS differences after transformation are consistent with the formal uncertainties of 20 to 50 cm observed in the Doppler solution. Modeling the Doppler data as one way average range-rate with pass by pass measurement bias adjustments is the major reason that the solution is formally weak. Additional areas of investigation to improve the determination of the Doppler sites include a re-assessment of editing procedures and re-evaluation of deficiencies in the measurement model, among others. If ten centimeter positioning is expected from TOPEX Doppler tracking, these issues must be resolved.

9.3.5 Summary

The preliminary station solutions basically demonstrate two general conclusions. First, the laser sites in general are very well determined in the a priori geodetic file. Second, the Doppler station coordinates have an uncertainty of 50cm to 1m at some sites. The laser station result comes as no surprise since the a priori laser site positions were determined in a dynamic solution (SL-6) made at GSFC which is very similar in character to the TOPEX laser solution. We note, in conclusion, that we are currently capable of obtaining with the LAGEOS laser data more than an order of magnitude better station location accuracy than with Doppler data.

9.4 EVALUATION OF THE ADJUSTED EARTH ORIENTATION PARAMETERS

9.4.1 Introduction

Accurate determination of the coordinates of the pole requires a robust, accurate and uniformly distributed set of tracking data. Satellites with minimal short periodic perturbations due to the Earth's gravity field are always preferred in this task (e.g. LAGEOS).

Considering the data on which our gravity solution is based and taking into account the above, we decided at present to adjust the pole positions during the 1980-84 period. During this period alone the a priori Earth Orientation Parameters (EOP) can be possibly improved in a combined solution.

9.4.2 The 1980-84 Solution

The a priori polar motion series for the 1980-84 period are shown in Figure 9.2; the series that was simultaneously estimated with the GEM-T1 field is shown in Figure 9.3 . Since we have kept the station positions fixed to their a priori values, we do not expect any large adjustments. This is clearly evident from the two figures. Within each 30-day arc of LAGEOS, a single value for A1-UT1 is held unadjusted to define the longitude of this satellite arc. This presents problems when the quality of the overall solution is to be assessed. The fact that our estimates of Earth rotation are recovered discontinuously from one 30-day interval to the next was overcome by the following procedure. The length of day variation series (LODR) were interpolated using cubic splines to determine the missing (constrained) values (i.e., those held fixed at the a priori values). Once this was done we formed a continuous A.1-UT1R series adopting only a starting value from BIH. Subsequently, the A.1-UT1R series were smoothed using a Vondrak filter with $\varepsilon = 10^{-6}$. This effectively suppresses periods below fifty to sixty days. The smoothed LODR series were obtained from the smoothed A.1-UT1R series by forward differencing. Both the a priori and estimated (smooth) series of Earth rotation (A.1-UT1R) and length of day variation (LODR) are shown in Figure 9.4. The next step was to remove the strong periodicities from the signals so that the underlying detailed structure could be revealed.
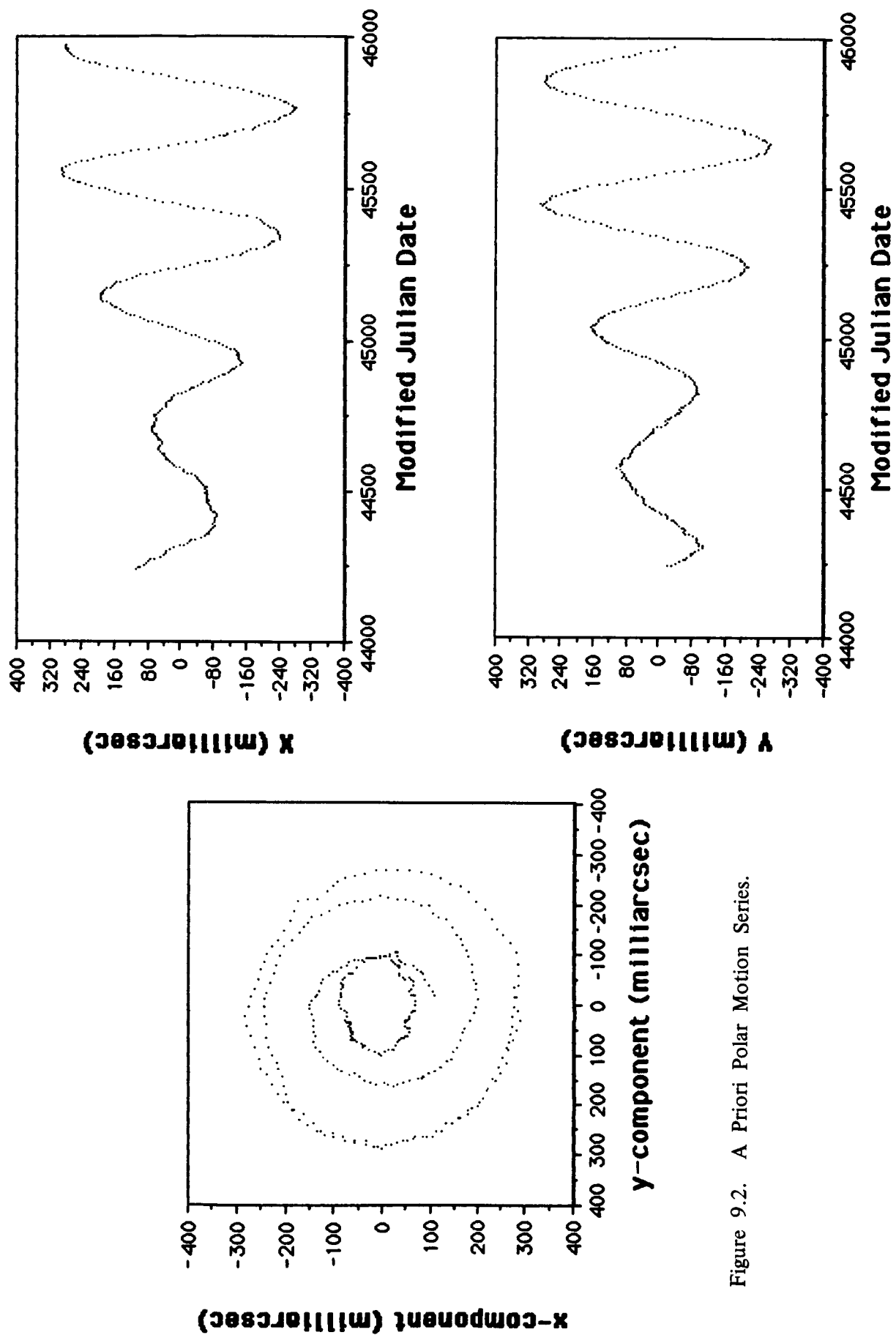
Figure 9.2.   A Priori Polar Motion Series.

237
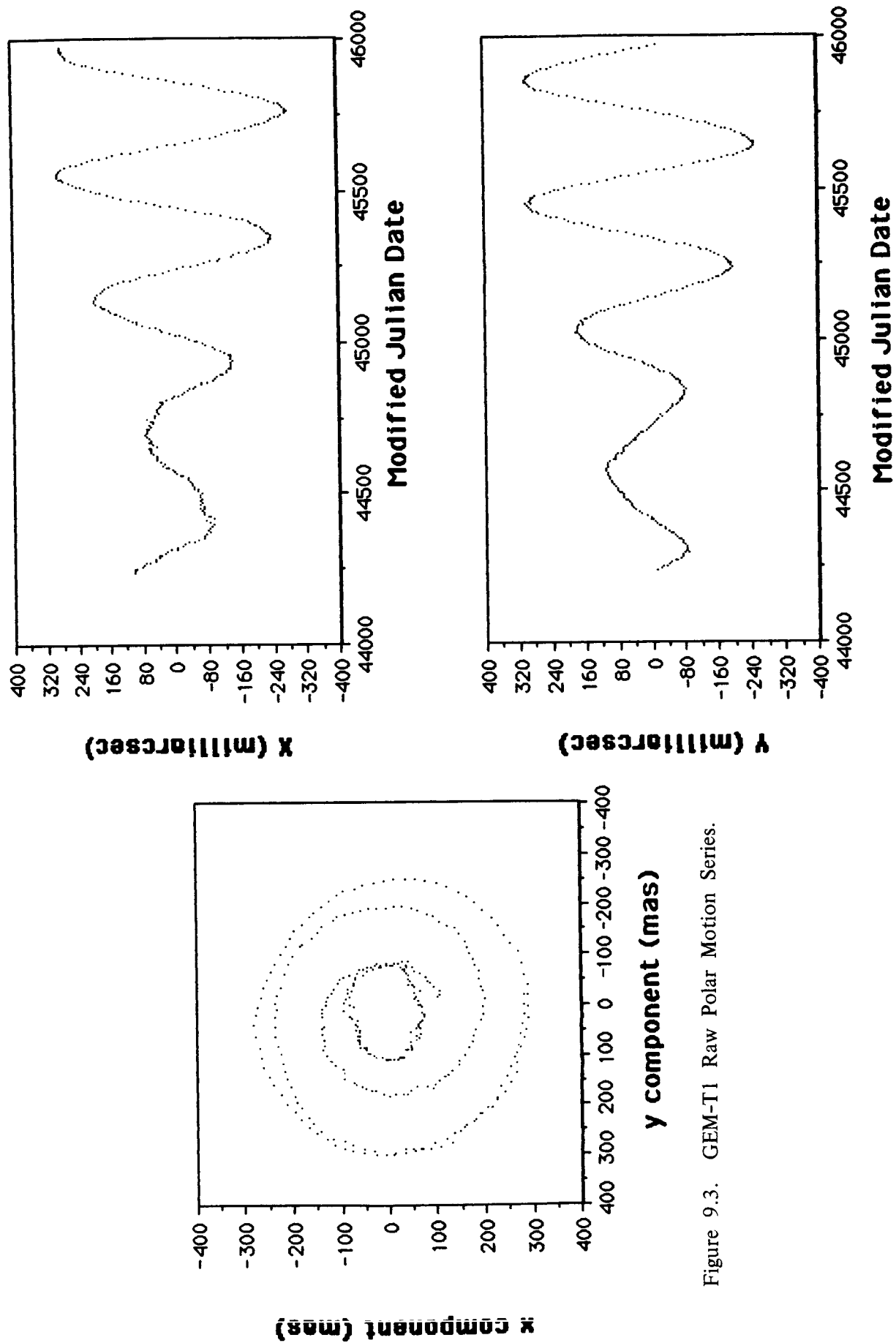
Figure 9.3. GEM-T1 Raw Polar Motion Series.

238
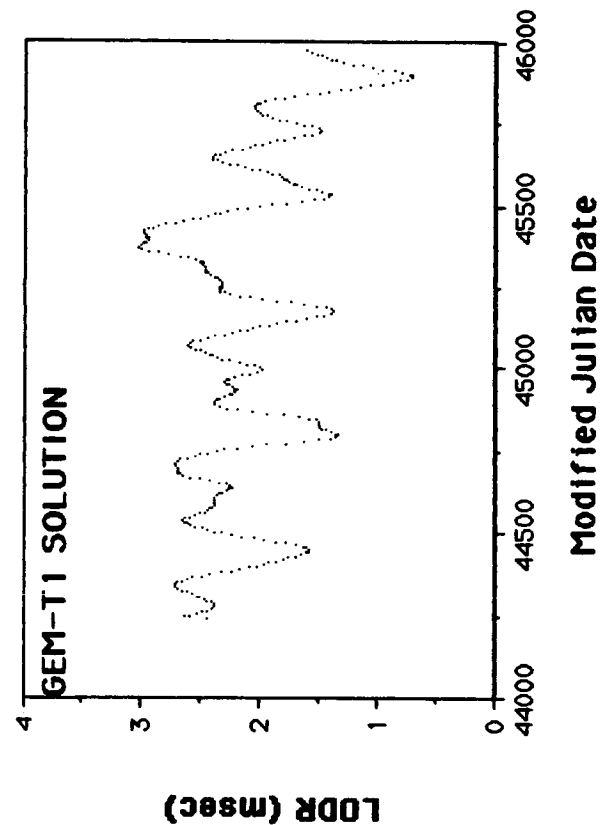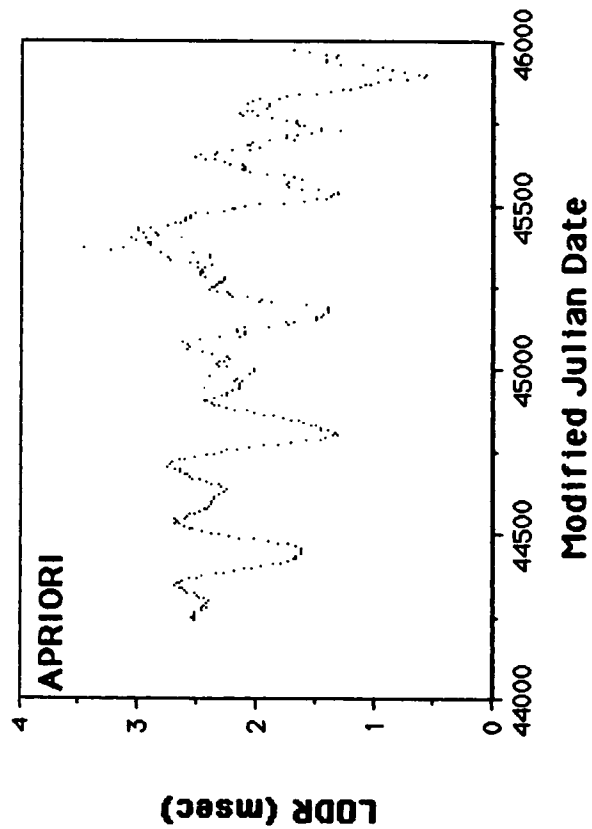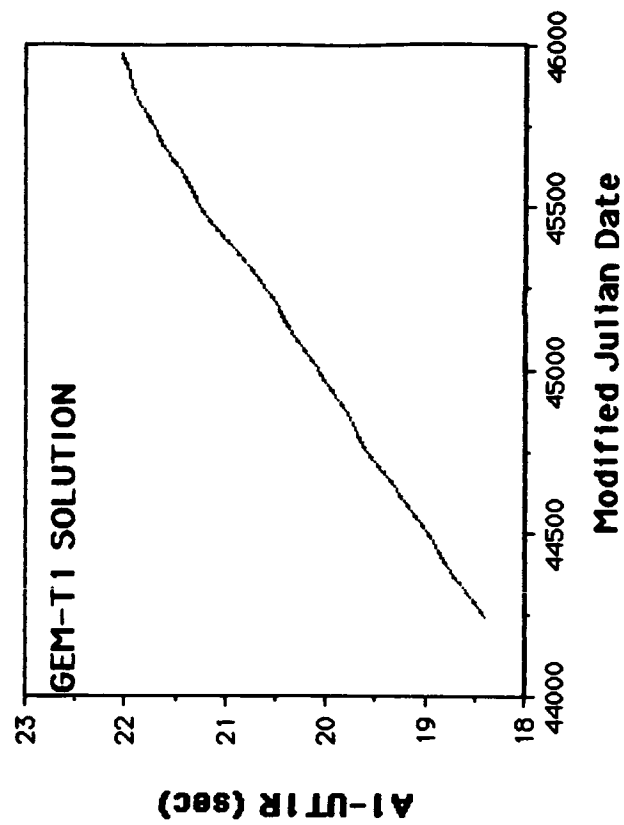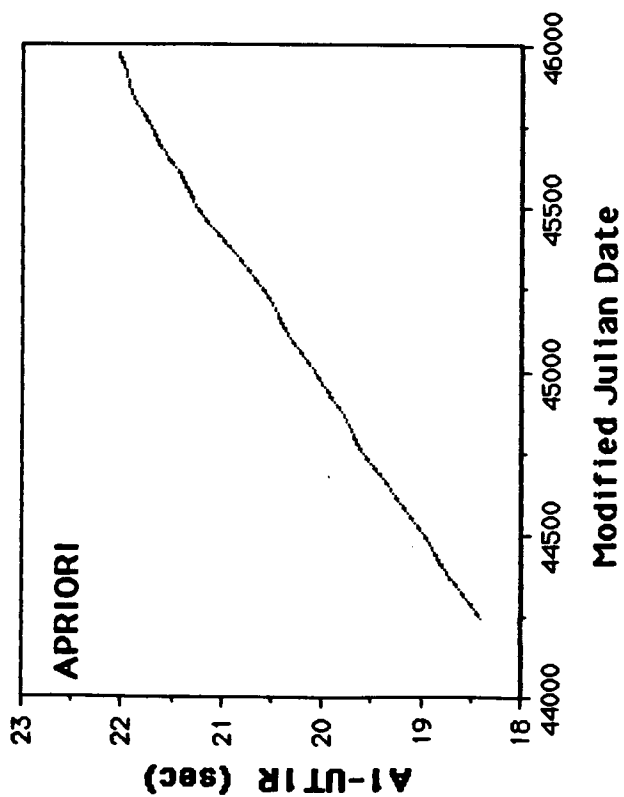
Figure 9.4. A Priori and GEM-T1 Vondrak Smoothed Earth Rotation Series.

9.4.3 The Annual and Chandler Cycles

To remove the coordinate system dependence of this evaluation we first transformed the GEM-T1 solution to the a priori series frame of reference. This was accomplished by the same least squares process that was used to determine the transformation parameters between the LAGEOS SL6 series and the BIH series in the creation of the a priori series (see Section 3.0). The results of this transformation are given in Table 9.10. The raw differences due to our adjustment are shown in Figures 9.5 and 9.6 for the polar motion and Earth rotation series respectively. The large b_1 rotation of 17.3 mas indicates a shift of the origin along the y_p-axis (that is in the negative Y-axis direction) as indicated in Figure 9.7. This has been resolved as an a priori bias of ~18 mas along the Goddard meridian (λ~283°) between the Z-axis of the a priori stations reference frame and the origin of the a priori polar motion. Since the station coordinates were held fixed during this solution, this rigid body rotation of the station network had to be accommodated by an opposite rotation of the estimated polar motion series.

An 18 mas rotation about an axis perpendicular to the Goddard meridian (λ~283°) can be decomposed in two components along the x_p and y_p axes; the magnitudes of these turn out to be 4.0 mas and 17.5 mas respectively. It thus becomes apparent that there is no real change in the reference frame of the TOPEX solution for polar motion, and the Z-axis of the CTRS is retained.

An argument similar to the above explains the large systematic rotation α_3=14.6 mas about the Z-axis. This was derived on the assumption that β_3=0. This however turns out to be incorrect since the transformation between the a priori TOPEX stations and the stations compatible with the a priori Earth orientation series indicates a systematic longitudinal rotation of -6.9 mas. On top of that, the

Table 9.10

GEM-T1 TO APRIORI TOPEX EARTH ORIENTATION SERIES TRANSFORMATION PARAMETERS

REFERENCE FRAME ROTATIONS

$$\beta_1 = 17.3 \pm 0.2 \text{ mas}$$

$$\beta_2 = 2.3 \pm 0.2 \text{ mas}$$

$$\beta_3 \equiv 0.0 \text{ mas}$$

$$\alpha_1 = -0.13 \pm 0.2 \text{ mas}$$

$$\alpha_2 = -0.03 \pm 0.2 \text{ mas}$$

$$\alpha_3 = 14.1 \pm 0.2 \text{ mas}$$

EOP SERIES RAW DIFFERENCES

RMS (Δx) : 4.0 mas

RMS (Δy) : 3.5 mas

RMS (ΔUT) : 1.2 ms

RMS (ΔLOD): 0.09 ms
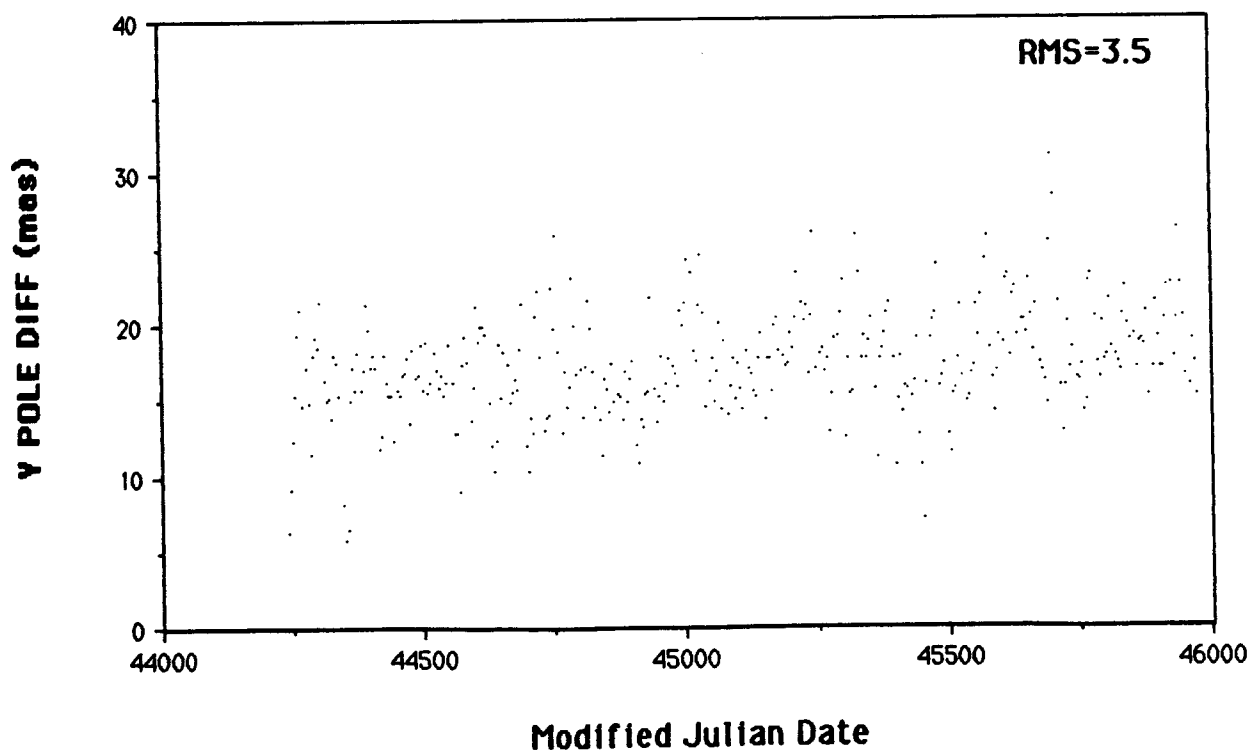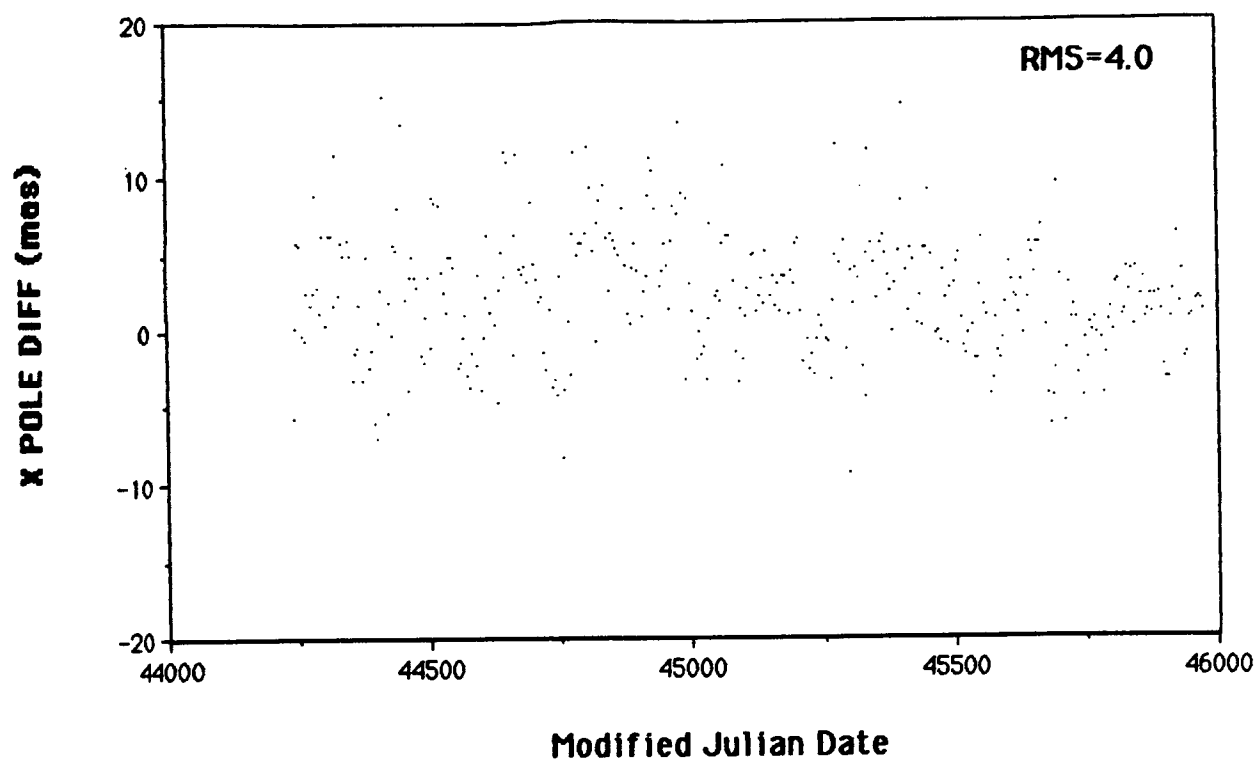
Figure 9.5. GEM-T1 Minus A Priori Polar Motion Series.

242
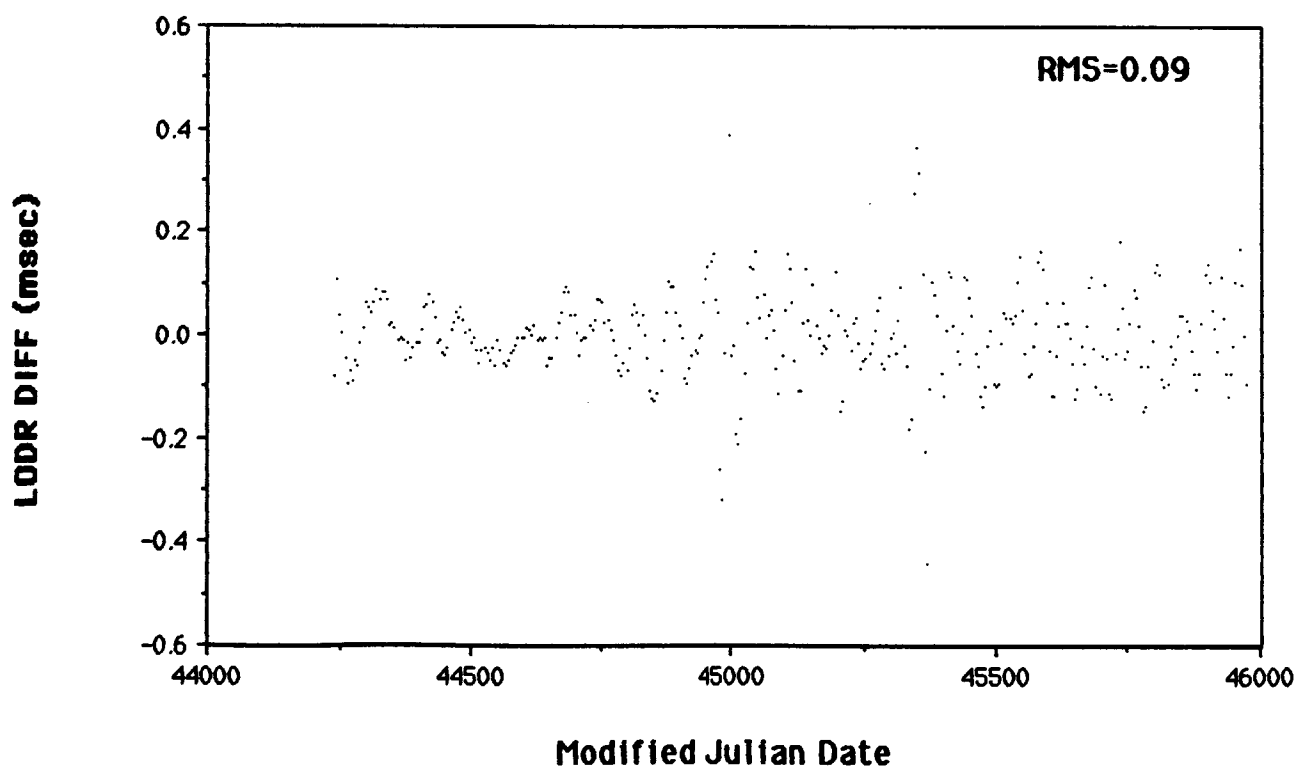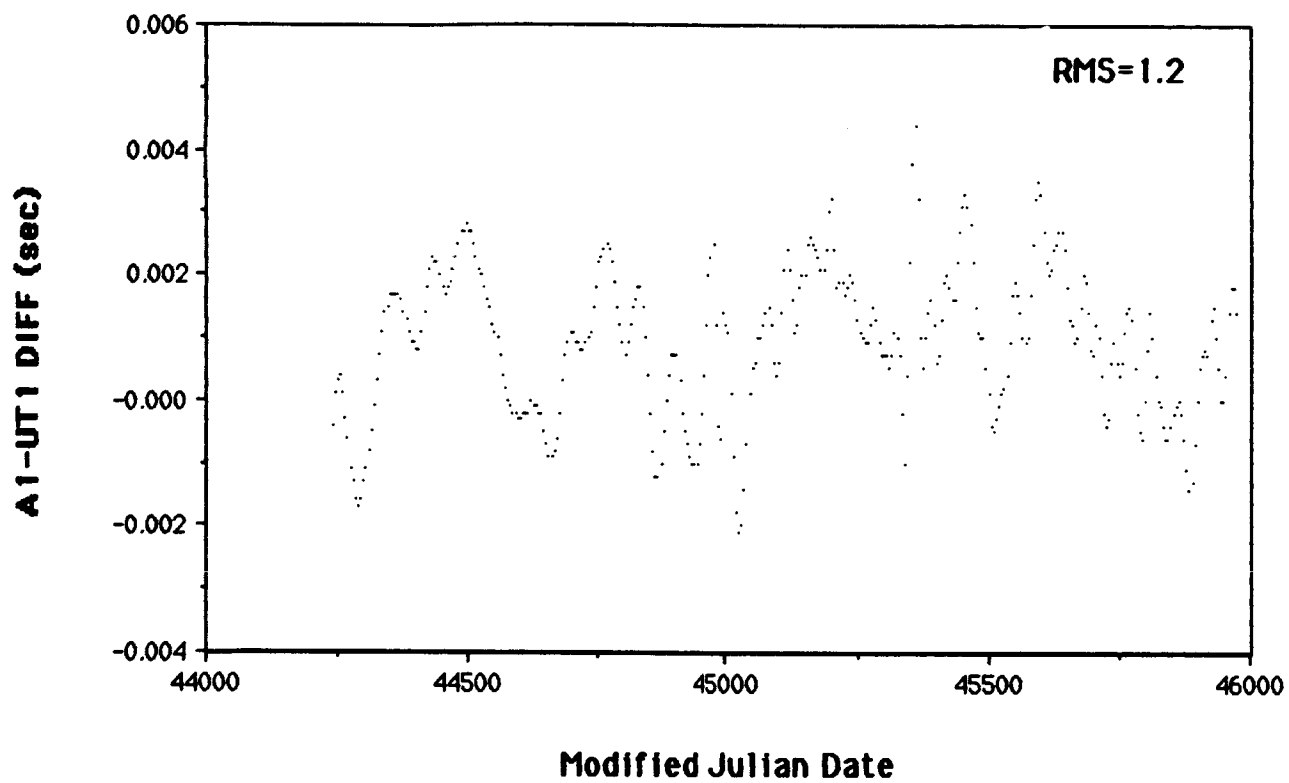
Figure 9.6. GEM-T1 (V-Smoothed) Minus A Priori Earth Rotation Series.

243
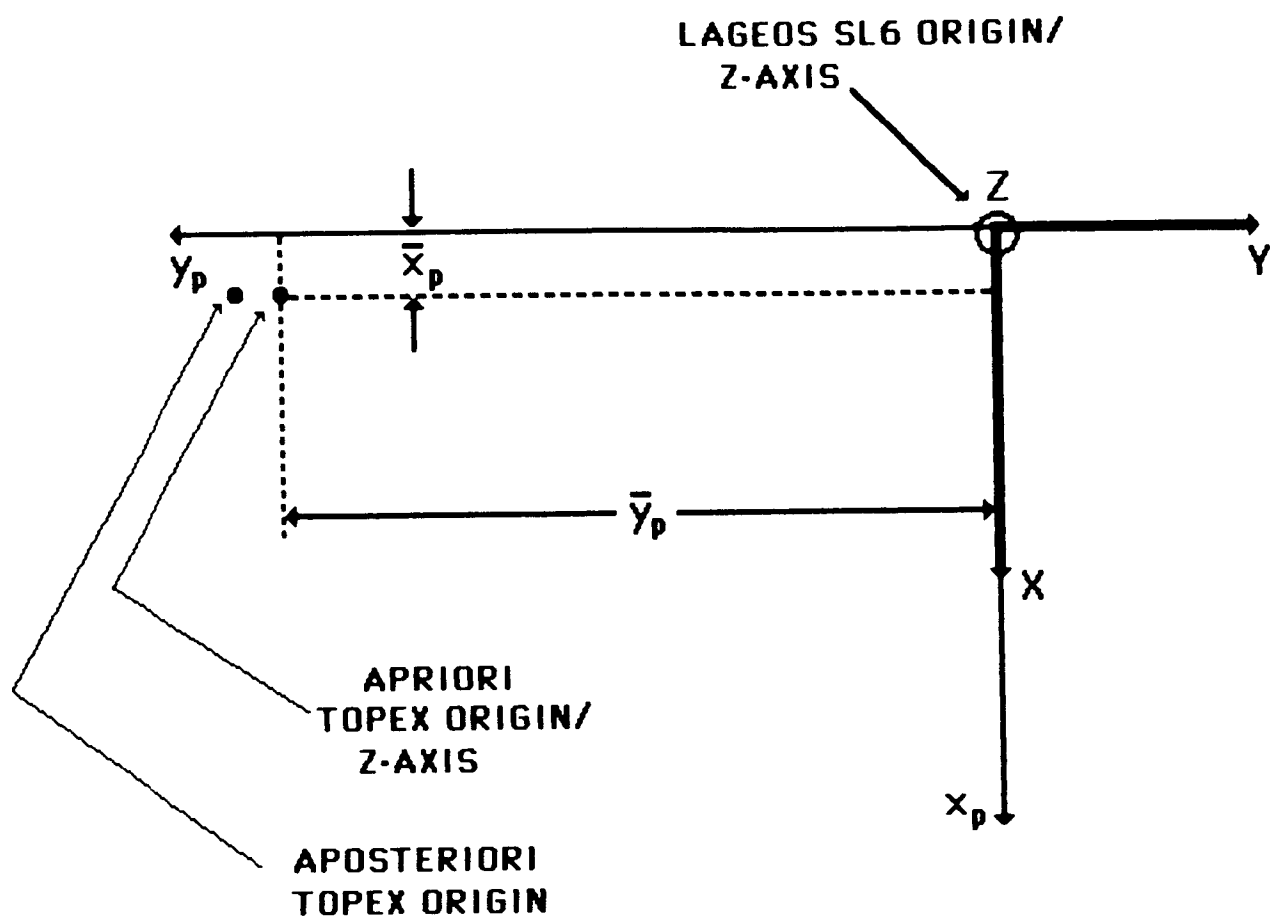
Figure 9.7.   GEM-T1 Polar Motion Origin.

Starlette arcs that contributed to the GEM-T1 solution are based on a set of stations developed during MERIT that have an additional longitude offset of -8.8 mas with respect to the set of stations used for all other earlier satellite data sets. This discrepancy was largely accommodated by shifting the right-hand sides when combining normal matrices to produce a single matrix with a common station set. However, all stations are not common, and those which did not shift have to be accommodated somehow in the least squares process. Therefore we modify our original estimate of $\beta_3 \equiv 0$ mas to $\beta_3 \equiv -15.7$ mas and conclude that $\alpha_3 \equiv -1.2$ mas which is an acceptable change considering the fact that this solution is based on the simultaneous adjustment of several arcs from various satellites through an intricate weighted least squares process. The a priori Earth rotation series is based largely on astrometry (75%) and only in the very recent years on the preliminary VLBI results (25%). The results of fitting the EOP series with the two frequency models are presented in Tables 9.11 and 9.12. Since aliasing is possible due to the incomplete coverage of the beat period (short by 1.25 years), the estimates listed here are only meant for relative comparisons. They should not be used to compare with those resulting from the analysis of series covering other time periods. It is rather clear that the GEM-T1 solution agrees to a great extent with the a priori series. This is what we expected and hoped for since the two series share the strongest data set over the intercomparison period, namely, the LAGEOS SLR data. Comparing the rms of fit with the observed oscillations in the two components we conclude that the two frequency model explains satisfactorily more than 95% of the original signal. We have further analyzed the residuals to this model by creating their power spectra and subsequently the coherence spectra between the a priori and GEM-T1 series. There is a better than 80% agreement between all of the series at periods longer than sixty days.

Table 9 11

COMPARISON OF
POLAR MOTION SERIES PARAMETERS
FOR THE
TWO FREQUENCY MODEL

$$\left.\begin{array}{c} x \\ y \end{array}\right\} = A + Bt + C_\alpha \cos\left(\frac{2\pi}{P_\alpha} t + \Phi_\alpha\right) + C_c \cos\left(\frac{2\pi}{P_c} t + \Phi_c\right)$$

	SERIES			
MODEL PARAMETER	APRIORI		GEM-T1	
	x	y	x	y
A (mas)	-2.5±1.3	12.3±1.3	-1.5±1.3	10.2±1.3
B (mas/yr)	0.7±0.5	-2.3±0.5	0.3±0.5	-1.4±0.5
C_α (mas)	103.5±1.2	103.3±1.5	103.8±1.2	102.8±1.4
P_α (days)	370.6±0.7	373.7±0.7	370.8±0.7	373.7±0.7
Φ_α (°)	138.1±1.7	237.4±1.8	138.1±1.7	237.5±1.7
C_c (mas)	180.1±1.2	179.0±1.5	180.1±1.2	178.4±1.5
P_c (days)	432.7±0.5	433.1±0.7	432.5±0.5	433.1±0.6
Φ_c (°)	1.5±0.9	95.9±1.1	1.3±0.9	95.8±1.1
RMS (mas)	11.9	11.8	12.0	11.2

t(days) = T T₀   T₀ = MJD 44239.0

Table 9.12

COMPARISON OF EARTH ROTATION SERIES PARAMETERS FOR THE TWO FREQUENCY MODEL

$$\left.\begin{array}{c} A1\text{-}UT1R \\ LODR \end{array}\right\} = A + Bt + C_\alpha \cos\left(\frac{2\pi}{P_\alpha}t + \Phi_\alpha\right) + C_s \cos\left(\frac{2\pi}{P_s}t + \Phi_s\right)$$

	SERIES			
MODEL PARAMETER	APRIORI		GEM-T1	
	A1-UT1	LODR[*]	A1-UT1	LODR[*]
A (ms)	18436.1±3.9	2.42±0.03	18436.8±3.9	2.42±0.03
B (mas/yr)	791.9±1.5	-0.13±0.01	792.0±1.5	-0.13±0.01
C_α (ms)	24.9±2.8	0.40±0.02	25.0±2.7	0.40±0.02
P_α (days)	340.8±4.3	365.0±2.3	338.7±4.2	363.6±2.2
Φ_α (°)	185.2±13.2	331.5±6.2	179.2±13.1	326.6±5.9
C_s (ms)	14.6±2.8	0.34±0.02	14.0±2.8	0.34±0.02
P_s (days)	183.5±2.0	182.4±0.6	180.4±2.2	182.3±0.6
Φ_s (°)	71.3±21.5	136.9±6.9	52.9±23.4	137.5±6.6
RMS (ms)	36.8	0.27	36.8	0.26

$t(days) = T - T_0$; T_0 = MJD 44239.0

[*] NOTE: LODR values refer to 2.5 days prior to T.

9.4.4 Summary

We have presented here an evaluation of the first Earth Orientation Parameters series obtained by the GEM-T1 solution. A continuous Earth rotation series was derived on the basis of the estimated Earth rotation variations (LODR). We have a viable technique to unify this inherently discontinuous series into a continuous one with satisfactory results and no apparent introduction of any distortions. The results indicate that all series agree very well with the a priori, a fact that was intuitively expected. A more comprehensive analysis of the EOPs will be possible (and more meaningful) when a complete solution (including station adjustments) becomes available.

SECTION 10.0

A CALIBRATION OF GEM-T1 MODEL ACCURACY

One of the difficulties faced in a numerical solution for a large number of physical parameters is the determination of meaningful accuracy estimates for the result beyond what is learned from formal solution uncertainties. As is well known, the process of fitting a model to observations provides an internal measure of precision on the assumption that the model is exact, i.e., formal statistics. But the value of this estimate is generally optimistic with respect to the real accuracy attained since the observations are inevitably represented by an approximate (incomplete) mathematical model. Yet, in our case without a better estimate of the accuracy of the geopotential, the results may have limited value, especially in non-orbital investigations.

In recent GEM solutions, a considerable effort has gone into the calibration of the field errors. The accuracy assessments, for example those found in Lerch et al, (1985), have relied almost exclusively on tests using independent data. These calibrations have been strengthened by having "satellite-only" models which exclude altimetry and surface gravimetry. One of the best ways of obtaining realistic errors for the models comes from comparing satellite derived information to independent and globally well distributed gravity anomaly and altimetry observations. Although independent data are employed, the calibration needs to be well designed, for there is a wide range of wavelengths spanned within a geopotential solution. Although these tests are never complete for every harmonic term in fields containing 1000 or more coefficients, they need to be diverse enough so that the long, intermediate and short wavelength portions of the field are calibrated in an overall fashion.

In previous GEM models, the accuracies of the fields have been successfully calibrated through the application of a single scaling factor applied to the formal variances of the solution. This approach is again undertaken here. However, it should be noted that, while the method is generally satisfactory, the lowest degree and order portion of the field is somewhat optimistically evaluated with this approach (by approximately 30%). This problem was found in the calibration of GEM-L2 (Lerch et al, 1985) and seems to apply equally to the calibration performed here on our new GEM-T1. Apparently, although it is not too surprising, systematic errors arising from the orbit determination procedures seem to more adversely alias the long rather than short wavelength portion of the gravity model. Still, as percentages of the full coefficient values, the errors found in the long wavelength terms in the model are much smaller than those found elsewhere in the field. Therefore, we have continued to produce error estimates based on a single scaling factor because the complexity introduced by using multiple scaling factors is presently unjustified and the single coefficient approach (our experience has shown) produces a good overall calibration. To more fully understand this calibration, the method of solution for GEM-T1 found in Section 8 should be consulted.

Based upon the data weights and scaling factors described in Section 8.2, the uncertainty in the GEM-T1 gravity solution is shown in Figure 10.1. When compared pictorially to other GEM models, as is done in Figure 10.2, one sees clearly the major reduction in errors that has been achieved, with our new gravity field modeling capabilities, in the GEM-T1 solution. The adequacy of these estimates of error is the subject of the remainder of this section. (The calibrated uncertainties for GEM-L2 and PGS-T2 have been previously shown in Figures 5.2.8a and 5.2.8b and may be consulted for comparison purposes.)

An interesting manifestation of our use of least squares collocation can be seen upon examination of Figure 10.1. The

ERRORS X 10⁹

Figure 10.1. Estimated Errors for GEM-T1 Coefficients.
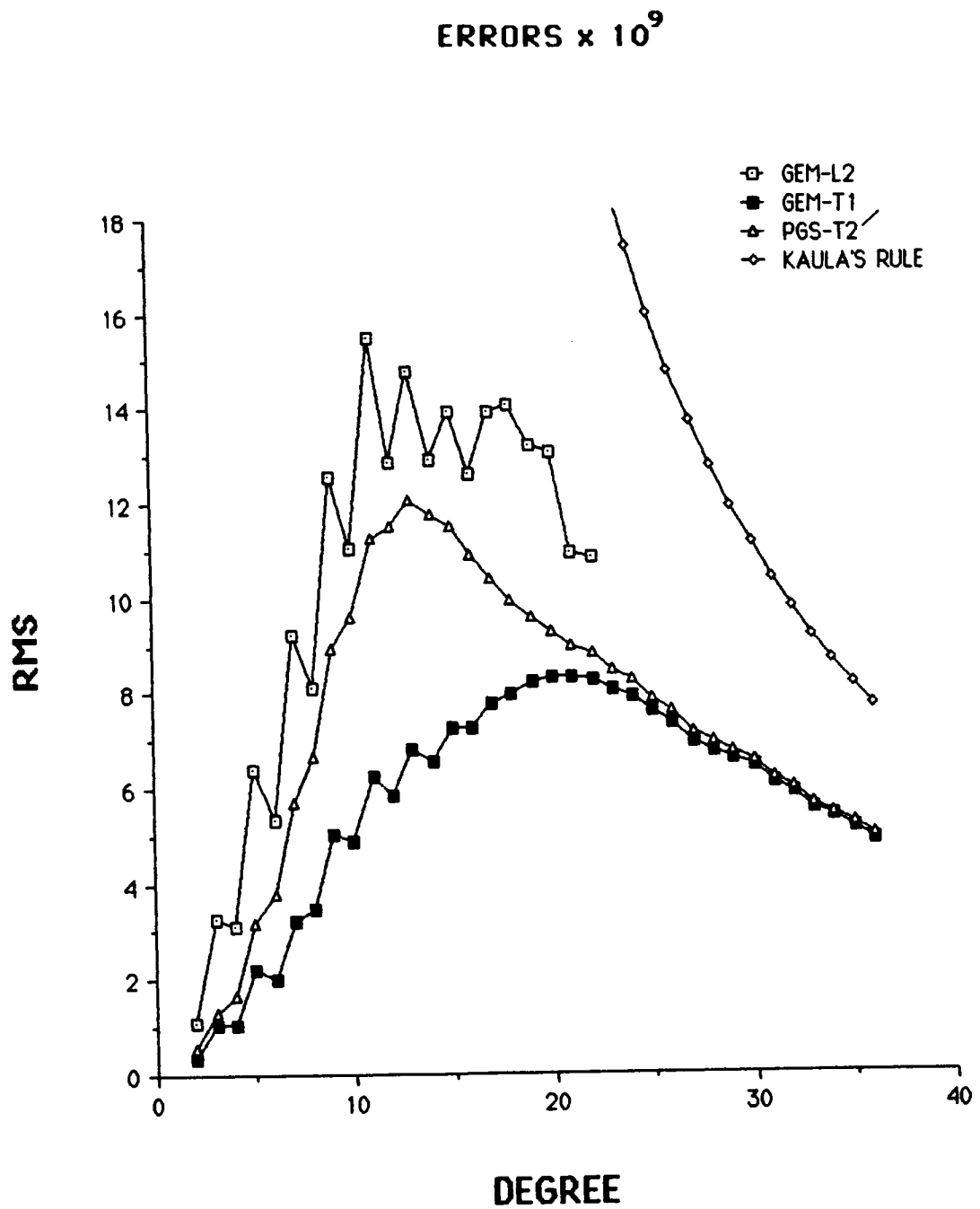
ERRORS × 10^9

Figure 10.2.   RMS of Coefficient Error Per Degree.

uncertainty for the highest degree terms in the model (except those of the zonal and resonant orders) are shown to be nearly 100% in error based upon their expected power. While collectively these terms contain valuable signal, individually, they are not well resolved. However, truncation of the field to a lower degree is unjustified, for as already shown in Figure 8.7, a significant amount of valuable information is lost by taking this approach. Nevertheless, based upon this preliminary scrutiny of the magnitude of the calibrated coefficient uncertainties, these high degree terms have been constrained to have no more than 100% of their expected power as their estimated error; and this is both a reasonable and desirable result for terms poorly resolved by dynamic orbital tracking data.

10.1 THE GEM-T1 CALIBRATION OF A SATELLITE MODEL'S ERRORS USING GRAVITY ANOMALY DATA

Mean free air gravity anomalies (on the geoid) can be calculated from the spherical harmonics of a gravity field as follows (Heiskanen and Moritz, 1967):

$$\Delta g_S = \sum_{\ell=2}^{\ell_{max}} \sum_{m=0}^{\ell} \gamma(\ell-1)B_\ell \left(\frac{a_e}{r}\right)^\ell \overline{P}_{\ell m}(\sin\phi) \left[\overline{C}_{\ell m}\cos m\lambda + \overline{S}_{\ell m}\sin m\lambda\right] \qquad (10.1)$$

where

γ is the mean value of equatorial gravity.

a_e is the earth's semi-major axis.

r is the radius to the surface of the best fitting earth ellipsoid.

$\overline{P}_{\ell m}(\sin\phi)$ is the fully normalized associated Legendre function for geocentric latitude ϕ.

λ is the geographic longitude,

B_ℓ is Pellinen's smoothing factor (described in Katsambalos, 1979) corresponding to the block size over which Δg_S is averaged over. (Note: $B_\ell=1$ for point anomaly values)

and

$\overline{C}_{\ell m}, \overline{S}_{\ell m}$ are the normalized spherical harmonics of the field with the reference ellipsoid zonal potential (even terms only) subtracted.

If

$\langle \; \rangle$ = global average value

E = statistically expected value and

ε_s = Error in Δg_s from coefficient commission errors

then

$$E \langle \varepsilon_s^2 \rangle = \sigma_{Model}^2 (\Delta g_s) = \sum_{\ell=2}^{\ell max} \sum_{m=0}^{\ell} \gamma^2 (\ell-1)^2 \; \sigma^2 (\overline{C}_{\ell m}, \overline{S}_{\ell m}) \; B_\ell^2 \qquad (10.2)$$

where

$E \langle \varepsilon_s^2 \rangle$ is the expected error in the gravity anomalies based upon the estimated errors in the satellite potential coefficients and $\sigma^2 (\overline{C}_{\ell m}, \overline{S}_{\ell m})$ is the variance of the pair of coefficients $\overline{C}_{\ell m}, \overline{S}_{\ell m}$.

Section 8.2 describes the data weights and scaling factors which have been determined to yield a well balanced solution for GEM-T1, and a solution which has realistic potential coefficient errors within its covariance. We wish to present the calibration this model has undergone based upon the best available and refined gravimetry and altimetry which we have employed as independent measures. Kaula (1966) showed how the errors (both of omission and commission) in a harmonic field can be estimated directly by comparison with independent global surface gravity data without forming harmonics for the surface information. The essential statistic is the difference between the global variance of the computed quantity and the covariance of computed and measured data. The expected value of this statistic is the expected global commission error of the model. If one also has reliable information on the errors in the surface data one can also estimate the omission (truncation) error in the harmonic field by computing the rms difference of the two data sets.

In terms of gravity anomalies as developed by Kaula (1966) the mean square commission errors are estimated for a given blocksize as:

$$E \langle \varepsilon_s^2 \rangle = \langle \Delta g_s^2 \rangle - \langle \Delta g \, \Delta g_s \rangle \qquad (10.3)$$

where the calculated value Δg_s is

$$\Delta g_s = \Delta g_{true} \text{ (for harmonics in the model) } + \varepsilon_s \text{ averaged over a}$$
$$\text{given blocksize}$$

and the measured Δg is

$$\Delta g = \Delta g_{true} + \Delta g_{omission} + \delta g_{data} \text{ averaged over the same block}$$
$$\text{size; } \delta g \text{ is measurement noise in } \Delta g.$$

The omission errors are estimated as:

$$E \langle \Delta g_{omission}^2 \rangle = \langle (\Delta g - \Delta g_s)^2 \rangle - [\langle \Delta g_s^2 \rangle - \langle \Delta g \, \Delta g_s \rangle] - \langle \delta g_{data}^2 \rangle \qquad (10.4)$$

To estimate a further scale factor in the coefficient uncertainties, we compare the estimated commission error from surface data, to model uncertainties and seek the scaling factor k in the equation:

$$\text{EST } \sigma_{true}(\Delta g_s) = E \langle \varepsilon_s^2 \rangle = k \, \sigma_{GEM-T1} \qquad (10.5)$$

where

k is to be determined from this analysis.

Unfortunately, for gravity anomalies the omission error for low degree fields is large and this simple estimate for commission error (Eq. 10.3) is unreliable for these terms. But the technique appears to give reliable results for complete high degree models especially in comparisons with global anomalies including marine values derived from altimetry. This calibration is most sensitive to the high degree and order field. Table 10.1 presents results of this calibration for GEM-T1.

The data sets used to calibrate our satellite geopotential models were obtained from two sources. Terrestrial surface gravimetric anomalies were obtained from Rapp, (1981). They were in 1°x1° observed (or geophysically predicted) areal means. Altimeter derived gravity anomalies from SEASAT were also used. These gravity anomalies were used in the form of 5° equal area mean anomalies computed from the original 1° values. The total estimated commission error for GEM-T1 based on the uncertainties in Figure 10.1 for 5° anomalies is given by:

$$
\sigma_{GEM\ T1}(\Delta g_s) = \gamma \left[\sum_{\ell=2}^{36} \sum_{m=0}^{\ell} B_\ell^2 (\ell-1)^2 \sigma^2(\bar{C}_{\ell m},\ \bar{S}_{\ell m}) \right]^{1/2} = 4.5\ \text{mgals}
$$

where:

B_ℓ is Pellinen's smoothing operator for 5° anomalies.

Table 10.1 presents the results of the calibrations in terms of the additional factor, k. This calibration, based on surface gravity alone, shows that our $\sigma_{\ell m}$ have been estimated to within 4%. However, when altimetry is also utilized, it seems that we have been conservative in the estimation of our field model uncertainties by nearly a factor of 2. We have chosen the more conservative estimate of field uncertainty. This discrepancy was not found to this extent in the calibration of GEM-L2 (Lerch et al., 1985b) and it appears to occur in GEM-T1 due to

its solution for higher degree terms. These terms have relatively more constraint within the collocation solution and have lowered power which is known to be unrealistic. The error estimator used here (Kaula's) will give a biased answer which favors a field with lower power. This can be seen in Equation (10.3) where the errors in a field with lower power is seen to have underestimated errors.

Figure 10.3 shows the agreement of SEASAT altimetry with recent GEM gravity models more directly. Again we use Rapp's 1°x1° estimates of oceanic gravity anomalies obtained from sea surface undulations. We have formed 5°x5° blocks from these values. In Figure 10.3.1 we show the computed residual gravity anomaly for the GEM models at different degrees of truncation. Note the GEM-T1 "satellite-only" model agrees much better with the Seasat altimetric information than does the GEM-L2 model which is its predecessor. GEM-T1 performs nearly as well as GEM-10B which utilized altimeter data. PGS 3163, shown here for comparison purposes, is a version of GEM-T1 which contains SEASAT altimeter data, and as expected, performs best in this comparison. Note also, the improvement over PGS-T2' found with the GEM-T1 model.

Richard Rapp has recently made available to us a new set of altimetrically based ocean gravity anomalies and these have been compared to GEM-T1 as was done in Figure 10.3.1. A comparison of GEM-T1 with both the original (1981) and most recent (1985) SEASAT and GEOS-3 gravity anomalies underscores the point that while the altimetry is quite good and a source for independent testing of our fields, it too, is subject to improvement. It is encouraging to see that progress in both global gravity modeling and altimeter analyses are converging to an unique and absolute answer. We are making the necessary changes to incorporate this new altimetric gravity data set into future calibration activities.

As alluded to earlier, these gravity anomaly data sets are somewhat insensitive to the longer wavelength gravity field. Figure 10.4

TABLE 10.1 CALIBRATION OF GEM-T1 SATELLITE MODEL ERRORS

$\sigma_{GEM\ T1}$ (Δg_s) = 4.5 mgals (using the preliminary estimate of commission error out to degree 36 derived from the $\sigma_{\ell m}$ found in Figure 10.1)

Calibration Distribution	Data Test Cases (Δg*)	Gravity Anomaly EST σ (Δg_s) (from Kaula Statistics)	Satellite Model Errors Factor: k
Global	5° equal area anomalies from surface gravimetry (Rapp, 1981 data set)	4.7 mgals	1.04
Global	5° equal area anomalies from SEASAT altimetry over the oceans and surface gravimetry over land (Rapp, 1981)	2.4	.53

*Data Sets Obtained From Rapp

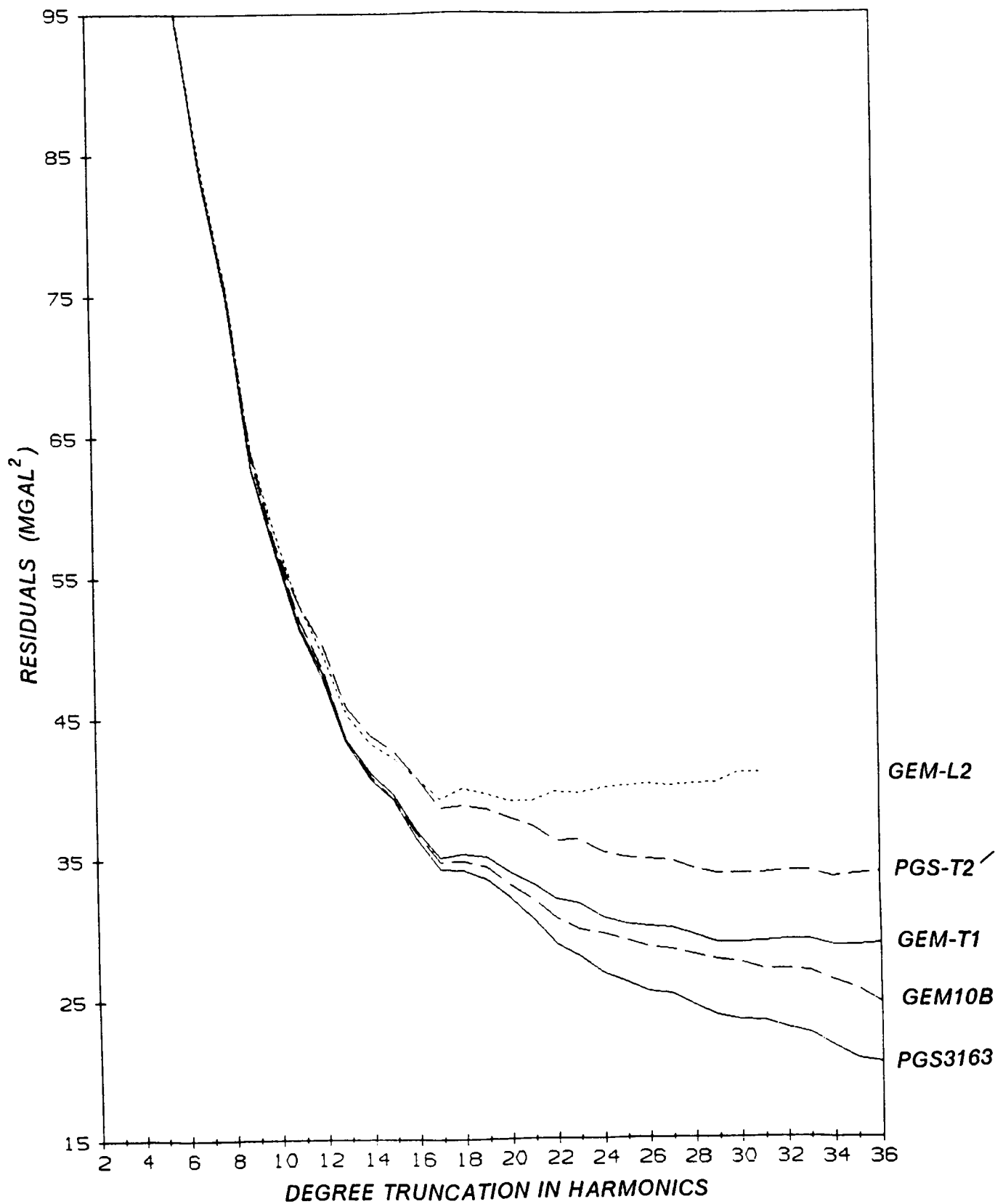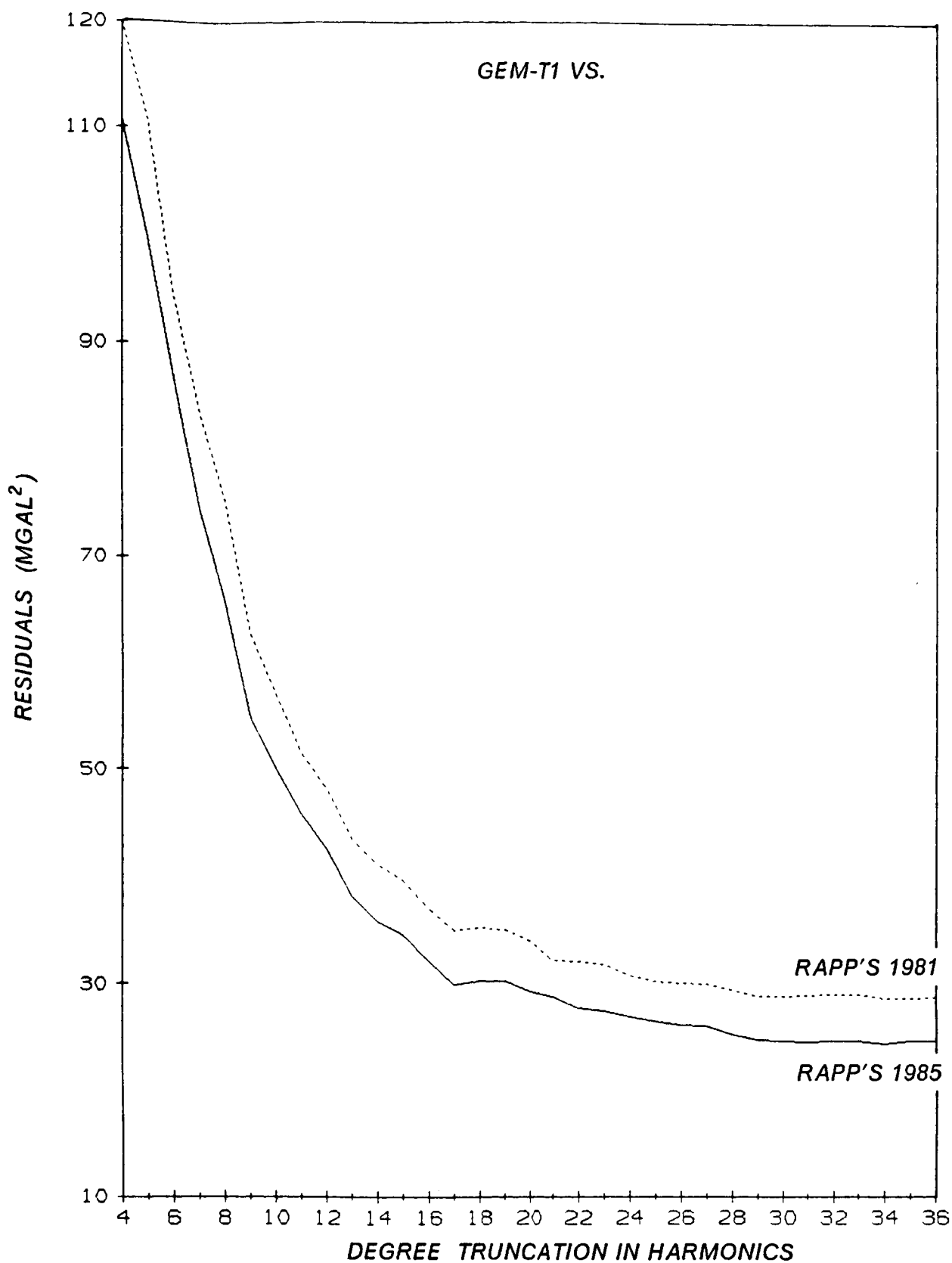Figure 10.3.1. Gravity Model Comparison with 1114 5° x 5° SEASAT Gravity Anomalies.

Figure 10.3.2. Gravity Model Comparison with 5° x 5° SEASAT Gravity Anomalies Using Two Recent Sets of Anomalies.
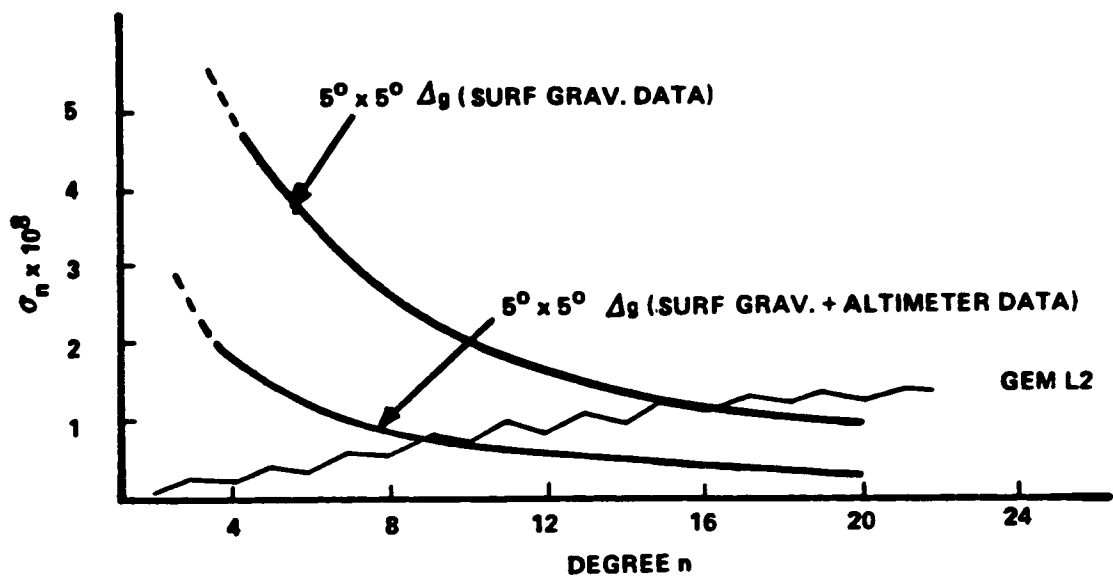
Figure 10.4. Coefficient Error Spectrum Per Degree n.

presents the error spectrum for GEM-L2 compared to that which is calcu-
lated from five-degree gravity anomalies. Based on Figure 10.4 the
calibration described in Table 10.1 does not reliably test those terms
below degree 8 in the GEM-T1 model. As indicated earlier the
calibration for high degree terms may not be completely reliable because
their low overall power in the GEM-T1 recovery may bias the Kaula error
estimator. Hence we substantiate this calibration with additional tests
as described throughout the remainder of this section.

10.2 CALIBRATION BASED UPON FIELD SUBSET SOLUTION TESTING

A new technique (Lerch, 1985a) has been developed for gravity
model calibrations of errors and applied to GEM-T1. First the new
method is reviewed along with test results which have verified the error
estimates for GEM-L2. GEM-L2 has been previously calibrated by a number
of different methods (Lerch et al., 1985b). If our new procedure yields
comparable results to those found earlier for GEM-L2, then we have some
verification of its performance.

A preliminary mathematical description of this new technique is
given. We will define quantities used in the calibration of the
geopotential coefficient errors between two fields, F and $\overline{F}$ where:

$$F : C_{\ell m}, S_{\ell m} , \sigma\text{'s (coeff. standard deviations)}$$

$$\overline{F} : \overline{C}_{\ell m}, \overline{S}_{\ell m}, \overline{\sigma}\text{'s} \qquad\qquad (10.6)$$

$$\Delta F: \Delta C_{\ell m} = (C_{\ell m} - \overline{C}_{\ell m}), \text{ likewise } \Delta S_{\ell m}, \Delta\sigma$$

263

(herein, the bar notation indicates the second model and is no longer used to denote field normalization.) The calibration quantities are further defined by

$$RMS_\ell(\Delta F) = \left[\sum_{m=0}^{\ell} \frac{\Delta C_{\ell m}^2 + \Delta S_{\ell m}^2}{2\ell + 1} \right]^{1/2} \qquad (\Delta: \quad \text{difference operator})$$

$$\sigma_\ell = \left[\sum_{m=0}^{\ell} \frac{\sigma_{(C_{\ell m})}^2 + \sigma_{(S_{\ell m})}^2}{2\ell + 1} \right]^{1/2} \qquad (\text{similarly for } \bar{\sigma}_\ell)$$

$$e_\ell^2 = E(RMS_\ell)^2 \qquad\qquad\qquad\qquad (10.7)$$

$$= \sigma_\ell^2 + \bar{\sigma}_\ell^2 \quad \text{when F is independent of } \bar{F} \qquad (10.7a)$$

$$= \sigma_\ell^2 - \bar{\sigma}_\ell^2 \quad \text{when data in F are fully contained in } \bar{F}. \qquad (10.7b)$$

Again, a calibration scale factor per degree, ℓ, is denoted as k_ℓ and is given by

$$k_\ell = \frac{RMS_\ell}{e_\ell}, \qquad\qquad\qquad\qquad (10.8)$$

From equations (10.7) and (10.8) we have two methods for calibrating errors: the first when the fields F and $\bar{F}$ are independent and contain no common data; the second when the data in F are wholly contained in $\bar{F}$. To satisfy the input criteria for this test the four models which were employed are described below:

o   GEM-9 is a satellite-only model which was published in Lerch et al, 1979. It is complete to degree and order 20. The gravity coefficients have no contributions from LAGEOS ranging, radar altimetry, or surface gravimetry. However, a limited amount of early STARLETTE laser data was utilized.

o   GEM-9A is a version of GEM-9 which was re-determined after removal of the STARLETTE data.

o   GEM-L2 is a satellite-only model which was published in Lerch et al., 1982. It was a solution which combined GEM-9 with LAGEOS laser ranging. Therefore, the data found within GEM-9 is entirely found within GEM-L2.

o   TEST FIELD was a special model developed from available sub-sets of normal equations. It contained recent LAGEOS and STARLETTE laser observations, surface gravimetry and SEASAT altimetry. It is therefore, by construction, a model whose data are completely independent of the data within GEM-9A described above.

Hence GEM-9A and TEST FIELD are evaluated with eq. (10.7a) for independent fields and GEM-9 and GEM-L2 are evaluated using eq. (10.7b) for dependent fields. Figure 10.5 presents the resulting calibration factors k_ℓ determined from each of the methods. Also shown are the averages of the calibration factors for the two methods. Clearly, the two methods show a good agreement for field calibrations. More important, the values of the estimated calibration factors, k_ℓ, are centered about $k_\ell=1$, which indicates that the overall uncertainties estimated by these methods agree well with the extensive calibration results previously obtained for the GEM-9 and GEM-L2 models. It is interesting to note that, as explained in the introduction to this section, the lower degree terms in the models may be optimistically

calibrated through our use of a scaled covariance for field uncertainty estimation. As seen in Figure 10.5, the low degree terms have a calibration scaling factor which exceeds 1.0, but only at most by 30% at its largest offset from unity. Therefore the results of this method for gravity model calibration overall agree quite well with what had earlier been determined for GEM-L2 using different techniques.

The method selected for assessing the reliability of the estimated GEM-T1 uncertainties corresponds to using eq. (10.7b) in which two models are used, where the first is obtained from data totally contained within the more complete data set found in the second. These calibrations required making several experimental gravity models based on subsets of the data used to obtain GEM-T1.

For the tests on GEM-T1 we examine several additional statistics. We calculate:

$$RMS_{\ell m} = (\Delta C^2_{\ell m} + \Delta S^2_{\ell m})^{1/2}$$

$$\epsilon_{\ell m} = (\sigma^2_{\ell m} - \overline{\sigma}^{-2}_{\ell m})^{1/2} \qquad\qquad (10.9)$$

$$k_{\ell m} = RMS_{\ell m}/\epsilon_{\ell m}$$

Coefficient statistics both by degree and by order are also evaluated through
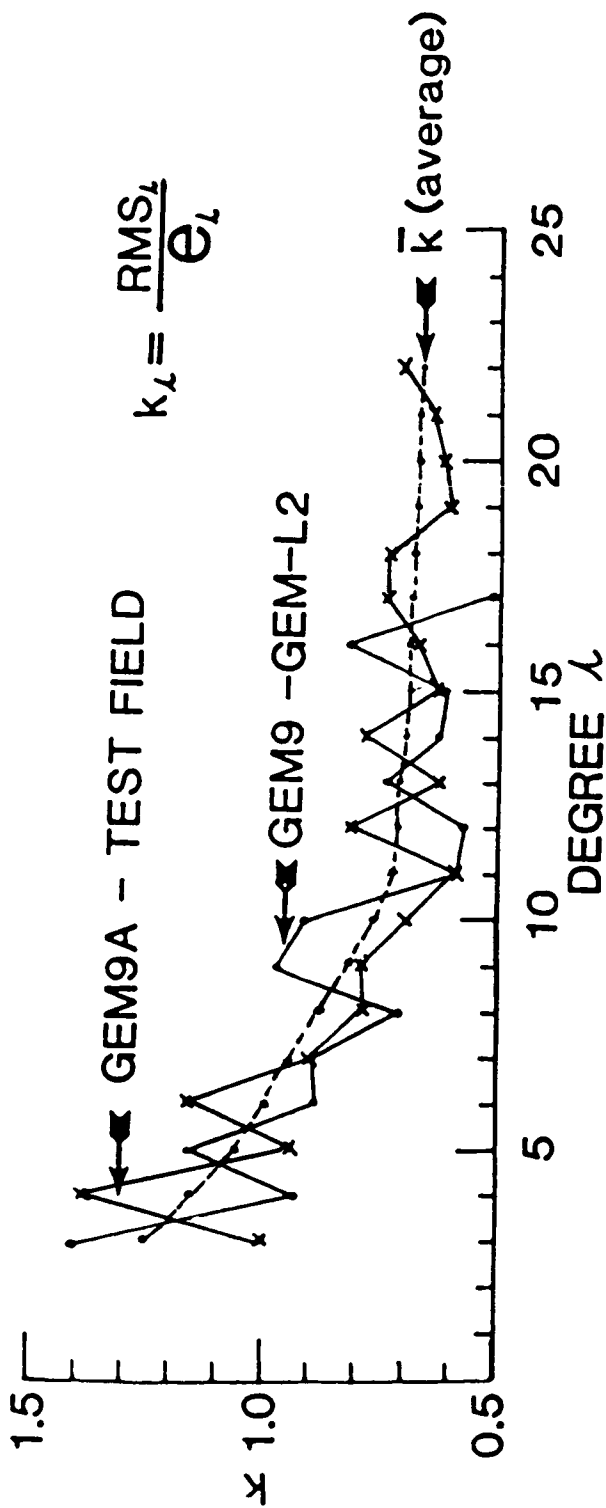
$$k_\ell = \left[\sum_{m=0}^{\ell} k^2_{\ell m}/(2\ell+1) \right]^{1/2}$$

$$(10.10)$$

$$k_m = \left[\sum_{\ell=m}^{36} k^2_{\ell m}/N_m \right]^{1/2}$$

266

Figure 10.5. Scale Variability for Errors.

where N_m equals the number of terms of order m (i.e., 36-m+1). As will be shown, similar results are obtained for either k_m or k_ℓ.

The scale factors k_ℓ are shown in Figure 10.6 for two cases:

(1) GEM-T1 has been compared to an experimental version of GEM-T1 which lacked the STARLETTE data, and

(2) GEM-T1 has been compared to a version of GEM-T1 which lacked the data from four laser satellites--BE-C, GEOS-1, GEOS-2 and GEOS-3.

The scale factors which were obtained by these calibrations (Figure 10.6) are close to unity for both cases with an overall average calibration factor of

$$\overline{k}_\ell = 1.1$$

(where the overbar indicates averaging)

The size of the subset of the potential coefficients used impacts the determination of these scaling parameters. For any individual coefficient, the factor would tend to be somewhat random. Therefore, the large subsets of coefficients (as indicated in (eq. 10.10)) provide a better determination of the overall calibration. Consequently, the slightly greater variability seen in Figure 10.6 for the low degree k_ℓ possibly is explained by the limited number of coefficients which are sampled ($2\ell + 1$) at these lower degrees. Figure 10.7 shows the σ_ℓ, e_ℓ, and RMS_ℓ for the second case. Figure 10.8 presents results for the k_m scaling parameters determined from both of these cases, but now sampling the coefficient subsets by order. When examined by order, the average scale factor is found to be

Figure 10.6. Calibration of Error Estimates Based Upon Subset Solutions.

269
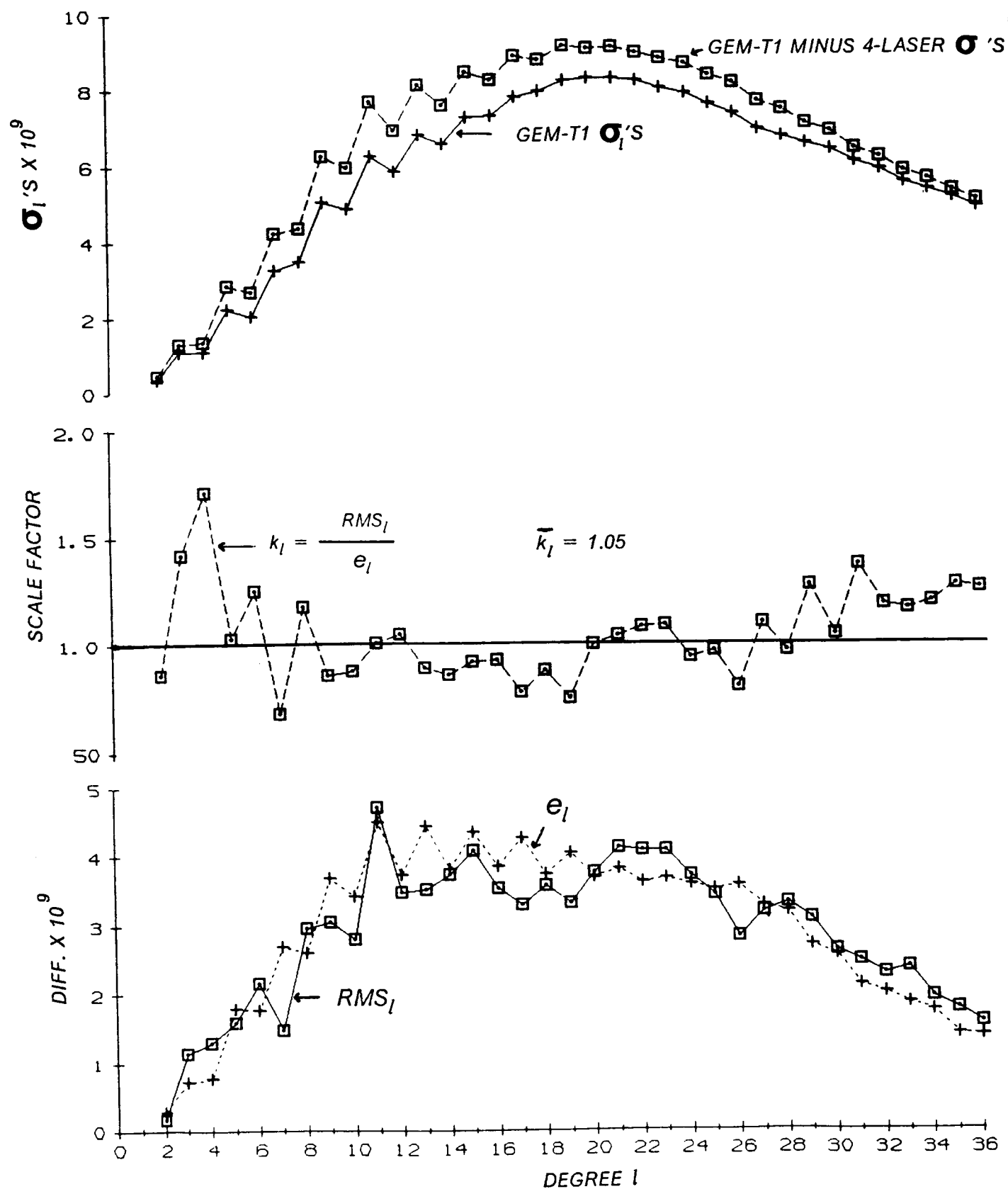
Figure 10.7.   Calibration Statistics GEM-T1 vs. GEM-T1 Without 4-Laser Satellites.
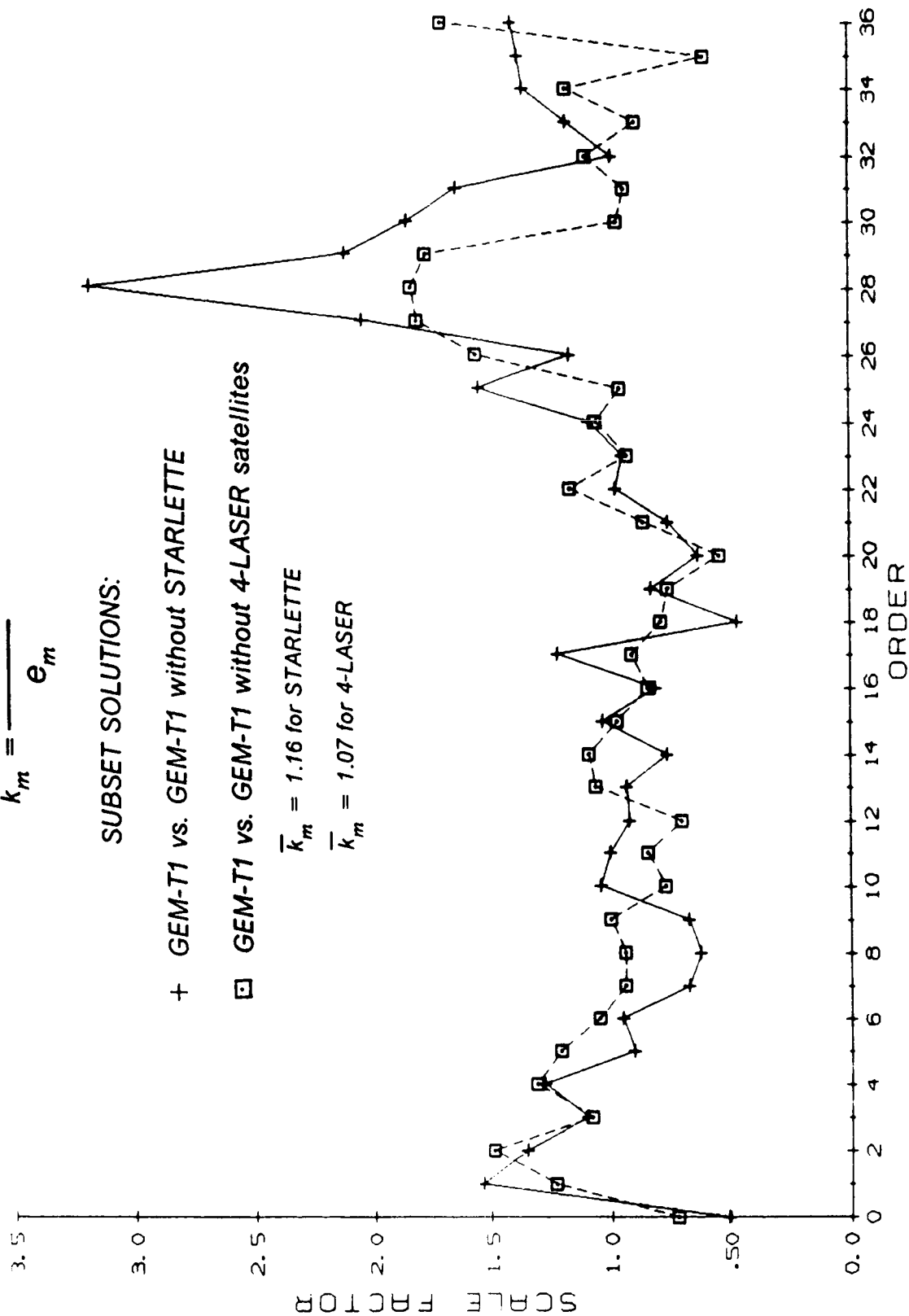
Figure 10.8. Calibration of Error Estimates Based Upon Subset Solutions.

$$\overline{k}_m = 0.99$$

Finally, the individual coefficient variability for these scaling parameters is shown in Figure 10.9. Overall, these fields seem to perform well when calibrated through these tests, and the overall scale factor obtained agrees well with that found using surface gravimetry and altimetry as described in Section 10.1.

Returning for a moment to Figure 10.8, one sees large scale factors for the orders where m=27 through 29 when STARLETTE data is eliminated from the solution. These orders have a strong secondary resonance with the STARLETTE orbit, and STARLETTE senses resonant terms beyond the 36th degree of truncation used when solving GEM-T1. Therefore, unconsidered aliasing error (due to STARLETTE's unique sensitivity to these orders) is perturbing the determination of the scale parameters for these orders. We have calculated and stored satellite measurement partial derivatives for the gravity model (nearly) complete to degree 50. When altimetry and surface gravity are introduced into the solution, STARLETTE's resonance will contribute to the determination of these m=27, 28, and 29 terms to ℓ=50 and this source of aliasing will be eliminated.

Two additional calibration tests were made. The first was one in which the inclusion of a preliminary set of altimetry in the GEM-T1 solution was assessed (and calibrated). The second directly evaluated the effect of significantly changing the value of the scaling factor, f, given in (eq. 8.8).

When speculating about the effect of using altimeter data within the GEM-T1 solution, we are attempting to project into the future and assess the accuracy of some yet-to-be-determined solution. A great deal of work remains to be done on improving our treatment of the altimeter data to eliminate non-geoidal signal (and it is scheduled for late

AVERAGE PER DEGREE = 1.0   AVERAGE PER ORDER = 1.1

$$k_{l,m} = \frac{RMS_{l,m}}{e_{l,m}}$$

ORDER

4-LASER SATELLITES : BE-C, GEOS-1 , GEOS-2 , GEOS-3

Figure 10.9.   Calibration Ratio ($k_{\ell, m}$) Based Upon GEM-T1 and GEM-T1 Without 4-Laser Satellites.

1987). However, the altimeter normal matrix we have obtained is similar to what will be available in the future, and for statistical purposes, it should be sufficient. Our first altimeter test model is PGS3163, whose gravity anomalies are compared to the SEASAT derived gravity anomalies in Figure 10.3. This model was computed giving very small weight to the altimeter data, since we did not wish to overwhelm the well calibrated GEM-T1 solution. However, for the present purposes, a second model was solved, called PGS3164, in which the altimetry was given five times the weight it had in PGS3163. The altimeter weight in PGS3164 more closely reflects the weight given to this data type in our previously published PGS-S4 solution. The calibration of this model is shown in Figure 10.10 where the overall scale factor of 1.02 which was obtained is in good agreement with those for either degree or order groupings of the coefficients. Shown in Figure 10.11 are the calibrated uncertainties for the PGS3164 model. The improvement over GEM-T1 is striking, and indicates that inclusion of the altimeter data in the future should have a substantial impact on further field improvements.

Finally, a calibration was performed on a field which was deliberately corrupted. In the discussion in Section 8.2, we show that a delicate balance of weights needs to be found to arrive at a good gravity model accompanied by realistic error covariances. We feel that this balance has been obtained in GEM-T1. However, looking at eq. (8.8) one can see that the value selected for f can alter both the overall scaling of the solution uncertainties and the balance between f and $\bar{f}$. A test solution, PGS3013, was made where f was multiplied upwards by a factor of 5 using a PGS-T2' base model (see Figure 8.4). The resulting standard deviations from this model, as expected, were about a factor of 2.5 better than those seen for GEM-T1. However, when this model was tested against surface gravity data, its performance was far worse (Table 8.2). PGS3013 was then calibrated using the same procedures which were utilized (as described in this section) for GEM-T1. For this model, the scaling parameter $\bar{k}_{\ell}$ was found to be approximately 2.5 When

GEM-T1 vs. GEM-T1 + SEASAT ALTIMETER

5 x ALTIMETER WEIGHT IN PGS3163

$$+ \; BY \; DEGREE \qquad k_l = \frac{RMS_l}{e_l} \qquad \overline{k_l} = 1.16$$

$$\boxdot \; BY \; ORDER \qquad k_m = \frac{RMS_m}{e_m} \qquad \overline{k_m} = 0.97$$
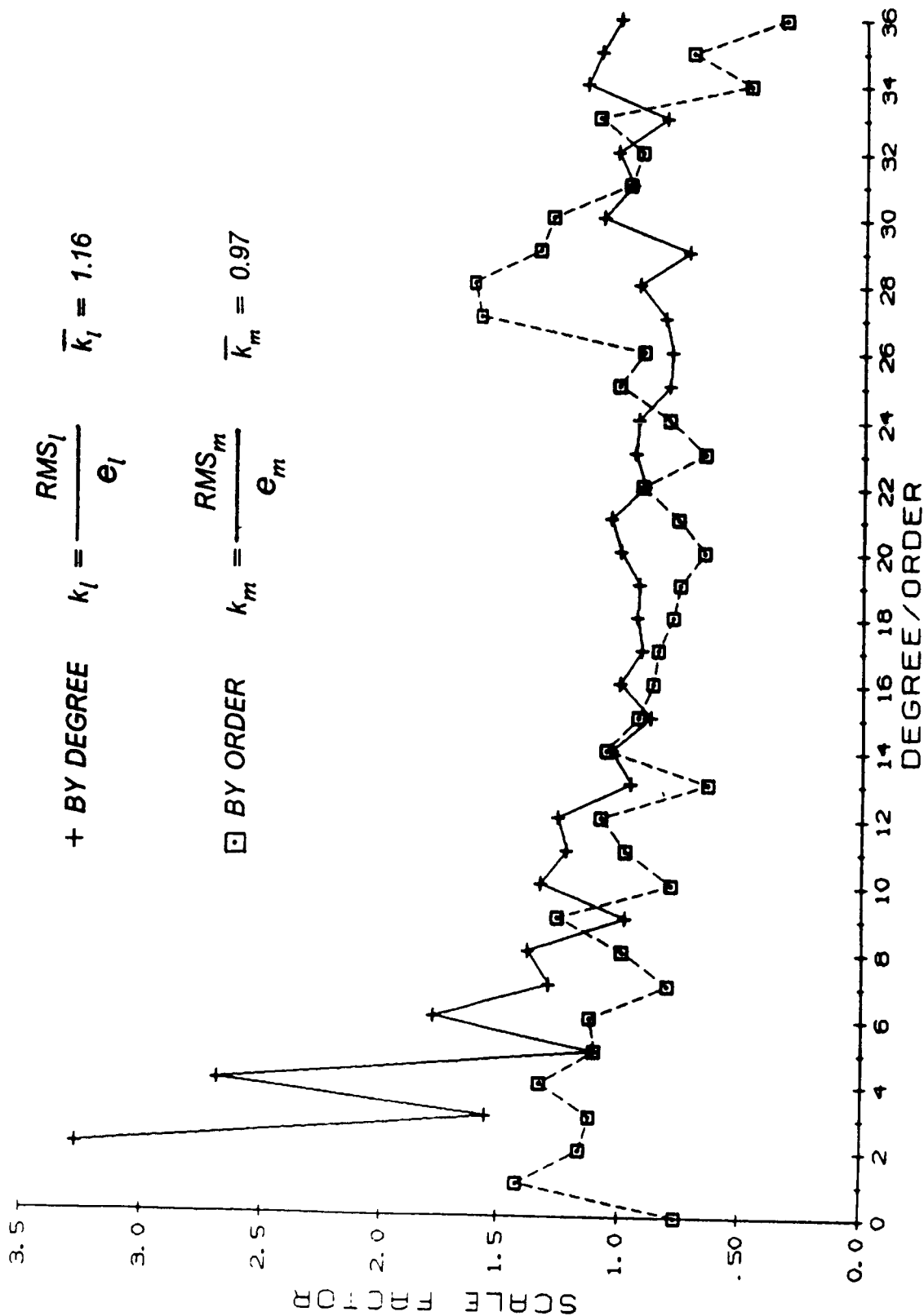
Figure 10.10. Calibration of Error Estimates Based Upon Subset Solutions.

275

(PGS3164 = GEM-T1 + SEASAT ALTIMETER)
ERRORS X 10^9

Figure 10.11. Estimated Errors for PGS3164 Coefficients.

the PGS3013 errors are scaled by this factor one obtains the results shown in Figure 10.12 which reveals a significant degradation of the PGS-T2' field. It is encouraging to note that the scaled errors for PGS3013 are worse than even GEM-L2, as is its performance on all of our tests using independent surface gravimetry and altimeter data.

In summary, we believe that valid methods for gravity model calibration have been developed and tested. The results confirm those which were obtained from comparisons with surface gravity and altimetry and indicate that a dramatic improvement has been achieved over previous satellite-only, Goddard Earth Models like GEM-L2. As shown by these calibrations, the uncertainties given for the GEM-T1 models in Figures 10.1 and 10.2 are realistic and can be applied to TOPEX simulated orbit testing.

10.3 COMPARISONS BETWEEN GEM-T1 AND GEM-L2

One of the important gains achieved with the complete re-calculation of a satellite-only gravity model lies in the ability to replace older data sets with more precise data which previously were unavailable. When assessing GEM-T1 in this light, we find that all of the laser data from BE-C, GEOS-1, GEOS-2, SEASAT and STARLETTE were not utilized in GEM-L2. Nor were the Doppler data from OSCAR and SEASAT previously used. There is an overlap with regards to the LAGEOS ranging, for GEM-L2 employed 2.5 years of the full-rate observations spanning January 1979 through June 1981. In GEM-T1, five years of LAGEOS two-minute normal-points have now been analyzed covering the years 1980 through 1984. Therefore, there is a considerable independent wealth of GEM-T1 information (approximately 75%) which has not been previously used in earlier GEM solutions. It is principally the older optical/early laser data sets, especially those used having low inclination orbits, which are a source of commonality between recent GEM models and GEM-T1. But even in these

277

ERRORS X 10^9
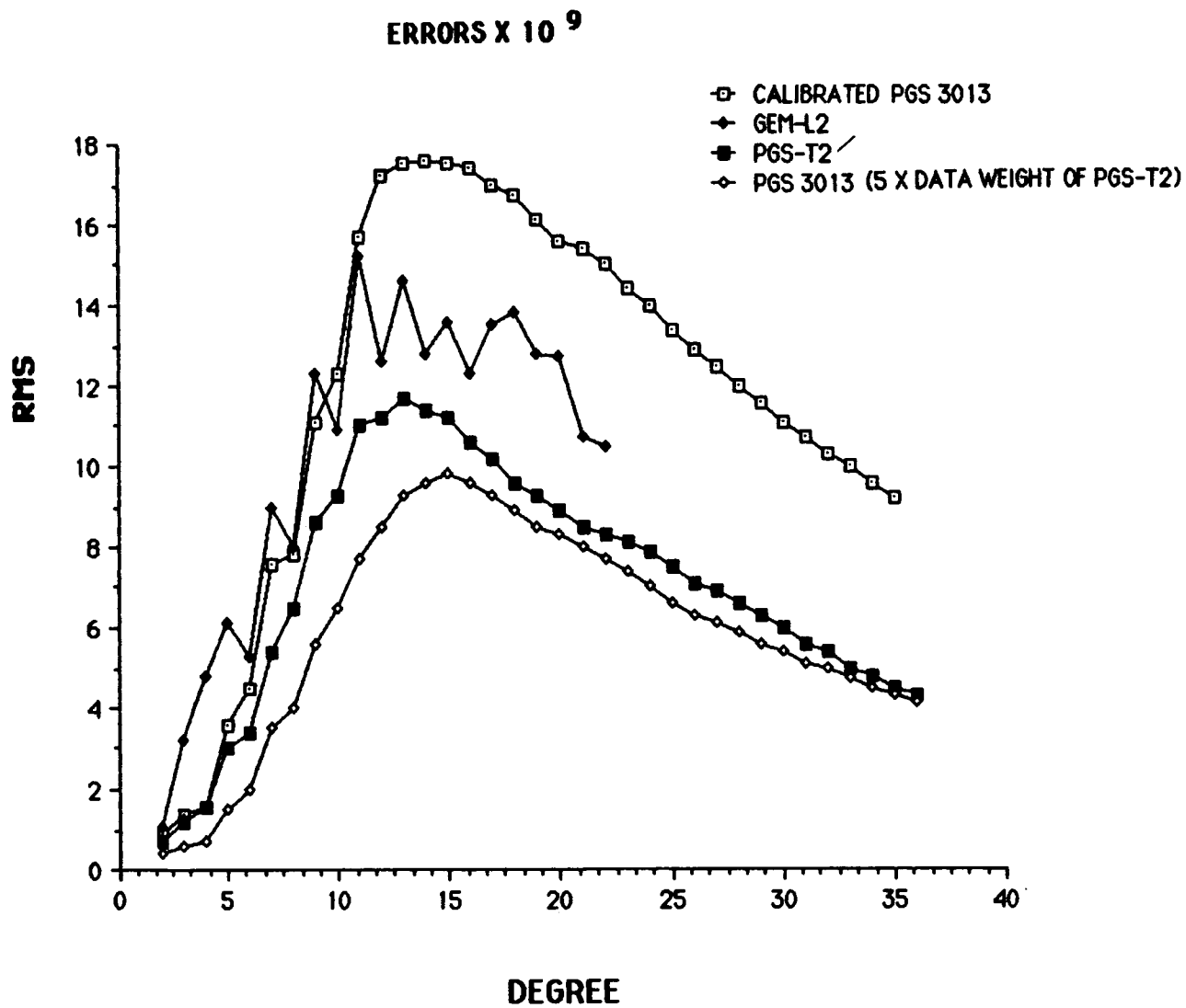
Figure 10.12.   RMS of Coefficient Error Per Degree.

278

cases, changes of approximately 25% in data selection have been made overall. Also of note, GEM-L2 used an additional 14 satellites which have not yet been included in GEM-T1. Another significant departure from GEM-L2 is the extension of the "satellite-only" model from 20x20 to degree 36 as was done in GEM-T1.

In a paper by Lambeck and Coleman (1983) the uncertainties published for GEM-L2 were directly questioned. It is of interest to revisit this issue here, and go beyond our direct response to that paper found in Lerch et al, (1986). There is a high degree of independence between GEM-T1 and GEM-L2. The models have been developed (a) using different computer programs, (b) in the presence of different constants, (c) with completely different treatment of earth/ocean tides, (d) with a new set of station positions in a new earth-fixed reference frame, (e) using a new model for nutations and a new third-body ephemerides (J2000), (f) with nearly a completely different set of tracking observations and finally (g) with the extension of the field from degree 20 (in GEM-L2) to degree 36 (in GEM-T1) which more than doubles the size of the field. We feel that a direct comparison of these recent models can shed meaningful light on the adequacy of our previous calibration methods. Figure 10.13 presents a histogram of the percent change in the individual coefficients (between GEM-T1 and GEM-L2) as:

$$P_C = \frac{\Delta \overline{C}_{\ell,m}}{\sigma_{C_{\ell,m}}} \times 100$$

(10.11)

$$P_S = \frac{\Delta \overline{S}_{\ell,m}}{\sigma_{S_{\ell,m}}} \times 100$$

279

where

$\Delta\overline{C}_{\ell,m}$ and $\Delta\overline{S}_{\ell,m}$ are the normalized potential coefficient differences between the two models,

$\sigma_{C_{\ell,m}}$, $\sigma_{S_{\ell,m}}$ are the published coefficient uncertainties found in Lerch et al, (1985) for the GEM-L2 model and

P_C, P_S are the percent changes in the coefficients.

It is clear from this figure, that nearly the entire GEM-T1 model is within one-sigma of GEM-L2.

Figure 10.14 shows the RMS coefficient differences by degree for both PGS-T2' and GEM-T1 with GEM-L2 again compared to the published estimate of GEM-L2's errors. (Again, PGS-T2' does not contain the low inclination satellite data.) Since the GEM-L2 errors are larger than those of GEM-T1 and PGS-T2', Figure 10.14 uses the GEM-L2 uncertainties as a basis for comparison. These last two figures show very good calibrated agreement between these nearly independent models and verify that our past calibration methods yielded reliable uncertainty estimates for GEM-L2.

10.4 THE NEED FOR LOW INCLINATION DATA-- REVISITED

Section 5.2.8 described some of the analyses which led us to introduce six more satellite data sets into our earlier PGS-T2 model. As described therein, the zonal harmonic coefficients in PGS-T2 were unsatisfactory due to the lack of adequate orbital inclination sampling in the field. The PGS-T2' model which will be referred to in this section was a version of the original PGS-T2 corrected for the GEOS-2
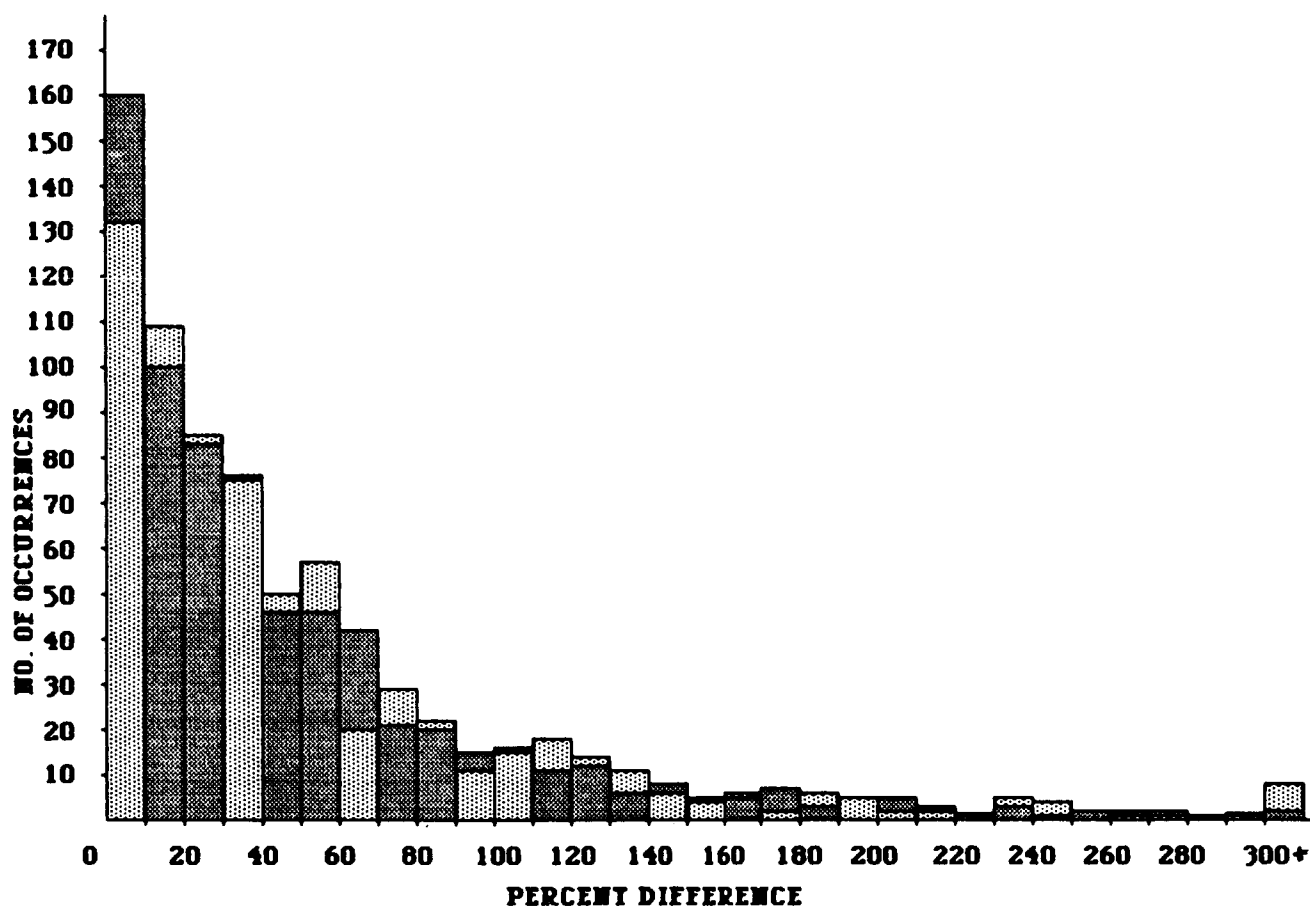
Figure 10.13. Comparison of GEM-T1 and GEM-L2 with Calibrated GEM-L2 Uncertainties.

GEM-L2 vs. OTHER FIELDS
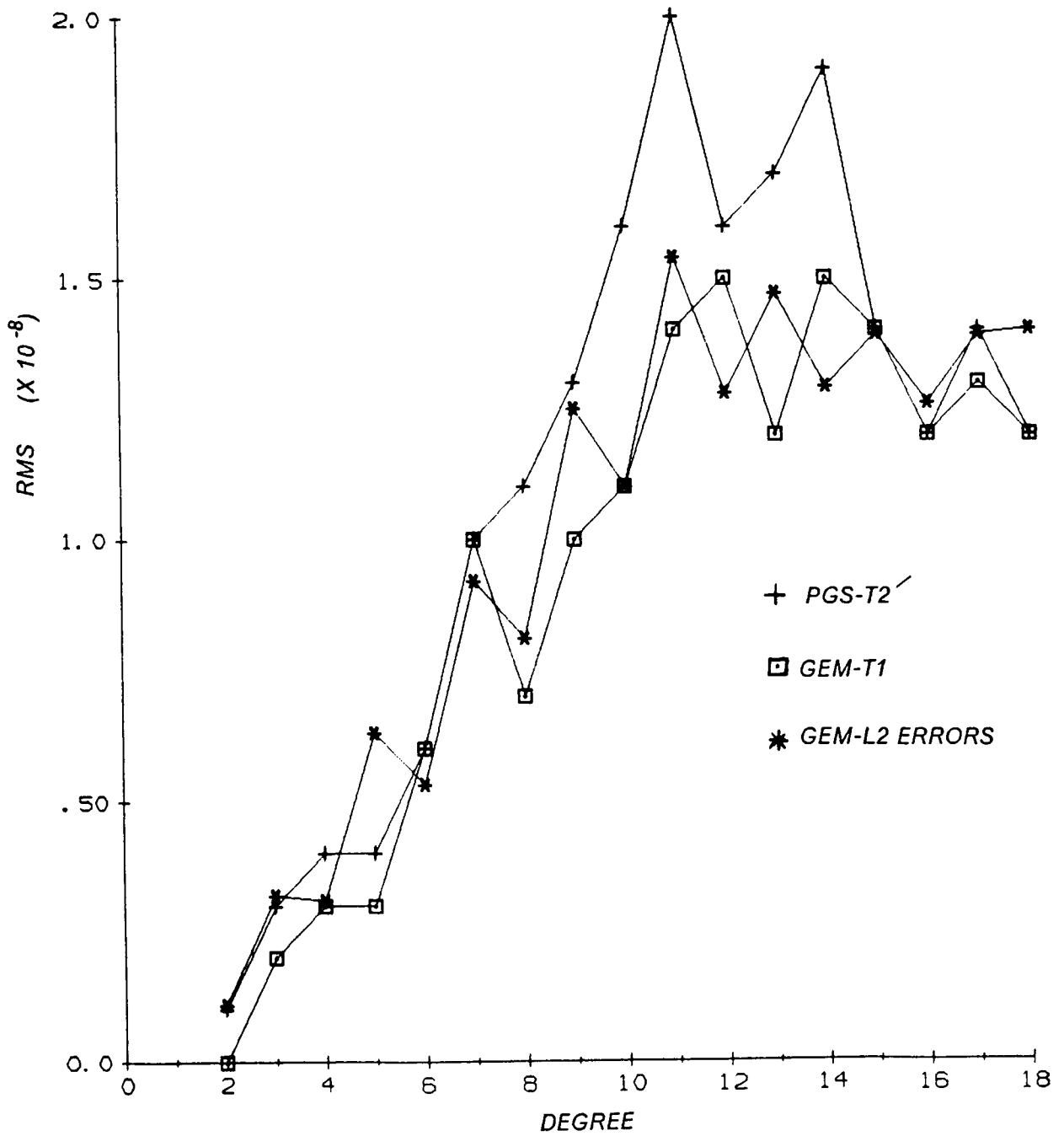
Figure 10.14.   RMS Coefficient Difference by Degree.

problem described in Section 8.2 (see Figure 8.3). The surprising large impact of the six low inclination data sets had on the solution (where GEM-T1 = PGS-T2' + (6 low i data sets)) has already been shown (in terms of field accuracy) in Figure 10.2. Figure 10.15 directly shows the improvement the addition of these data had on the zonal harmonic recovery. A further assessment of the importance of these low inclination satellite data sets is the subject of this subsection.

A good approach for measuring the influence of the low inclination data on the GEM-T1 solution is through an evaluation of the solution "condition numbers" for the harmonics when models with and without these observations are compared. Here, condition number C_i is defined as:

$$C_i = D_{ii} \, \sigma_{ii} \quad (10.12)$$

where

D_{ii} is the diagonal of the combined normal matrix (CN) given in equation (8.12), and

σ_{ii} is the diagonal of the inverse of the CN matrix given in (8.13)

It can be shown that these condition numbers demonstrate the loss of significant digits on the solution parameters in the reduction of the matrix. ($C_i = D_{ii} A_{ii}$/determinant where A_{ii} is the cofactor for the element D_{ii}.)
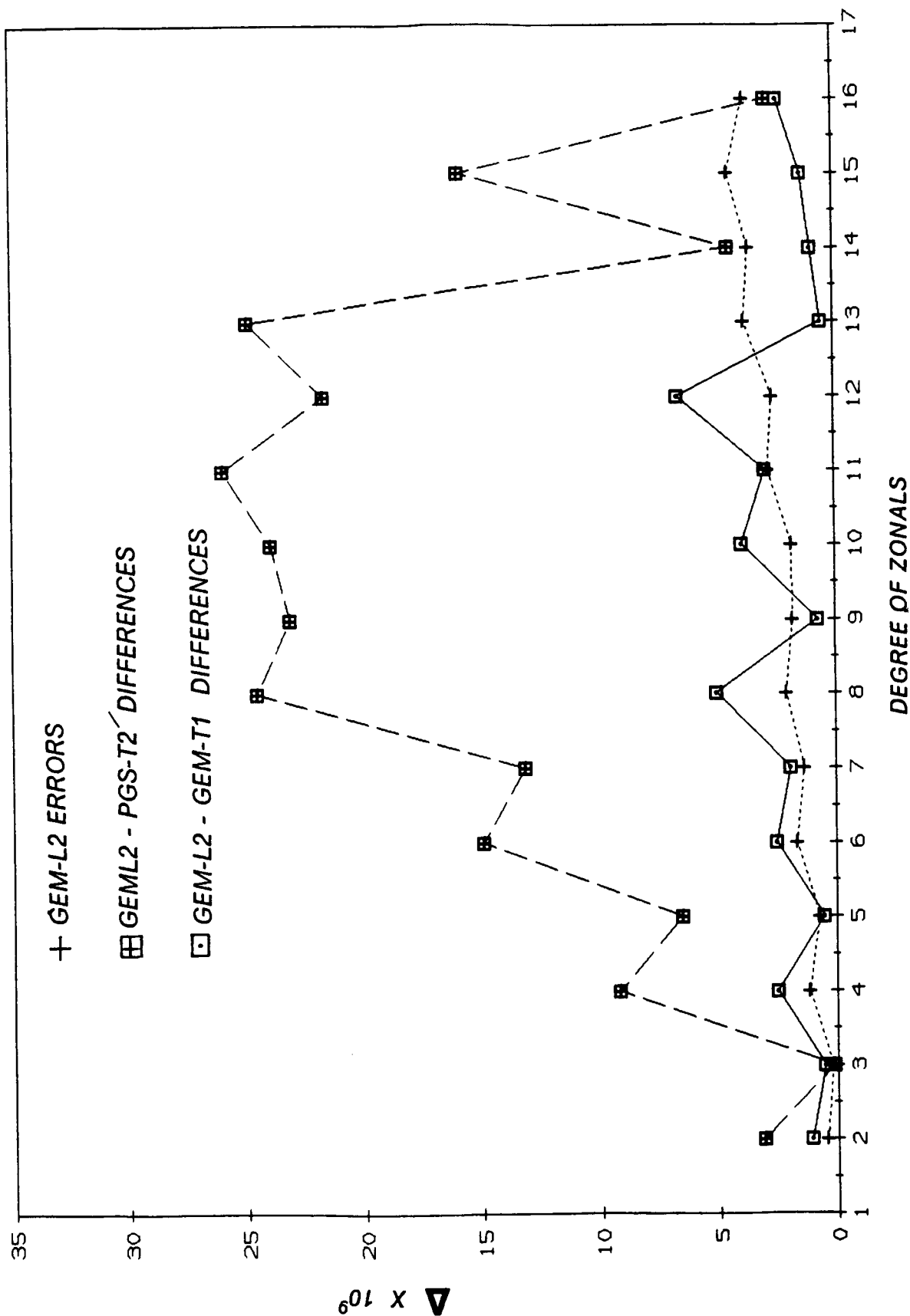
Figure 10.15. Zonal Coefficients.

284

Note that $C_i=1$, if there is no correlation present (i.e., $\sigma_{ij}=0$ for $i \neq j$) and

$$\sigma_{ii} = \frac{1}{D_{ii}} = \sigma_{ii}^{(o)} \qquad \begin{array}{l}\text{Idealized error variances for}\\ \text{the case where there is zero}\\ \text{correlation present.}\end{array} \qquad (10.13)$$

It can be shown that the condition number, C_i, will increase from unity depending on the extent of correlation in the inverse matrix (CN), and according to (10.12), σ_{ii} will increase as

$$\sigma_{ii} = C_i/D_{ii} = C_i \; \sigma_{ii}^{(o)} \qquad (10.14)$$

Equation (10.14) shows that the size of the condition number reflects the extent that correlation in the solution causes the variance to increase over the idealized variance. Hence, if the condition numbers are significantly reduced in a matrix, then the error variances are proportionately reduced.

The condition numbers in the comparison below reveal an interesting statistical property about the loss of resolution in the answers, due to cross-correlations among the parameters. If one takes the condition numbers obtained in a model (like PGS-T2') which lacked the low inclination data and divides them by the condition numbers obtained in GEM-T1 (as was done to produce Figure 10.16) the full impact of these data can be assessed. It is clear that the off-diagonal conditioning provided by the low inclination data penetrated into the central mid-degree sections of the model allowing a better resolution of the harmonics extending beyond improving the zonal determination. Obviously, these low inclination observations played a significant role in the determination of GEM-T1 which is somewhat surprising, given their level of observation imprecision and the low weight these data had in the combined solution.

GEM-T1 WITHOUT LOW INCLINATION SATELLITES OVER GEM-T1

RMS	DEGREE	\ORDER→ 0	1	2	3	4	5	6	7	8	9	10	11	12	13	14	15	16	17	18	19	20
3.0	2	4.8	2.9	1.5																		
3.6	3	7.8	2.1	2.1	1.1																	
3.4	4	8.3	2.9	2.9	2.0	1.2																
39.3	5	130.0	3.7	3.9	3.2	1.8	1.1															
7.0	6	22.8	5.9	5.1	3.8	1.7	1.2	1.0														
36.2	7	139.6	4.9	6.8	3.7	2.8	1.7	1.3	1.0													
8.1	8	29.6	8.4	6.4	4.4	2.3	1.6	1.5	1.2	1.0												
28.8	9	124.8	5.7	8.3	4.9	3.4	2.0	1.9	1.3	1.1	1.0											
10.9	10	45.7	7.2	9.0	4.2	2.5	1.6	1.7	1.5	1.2	1.1	1.1										
14.0	11	65.1	7.5	9.0	4.9	3.2	2.5	1.9	1.5	1.2	1.2	1.3	1.2									
7.6	12	31.0	10.8	8.4	4.2	2.9	1.8	1.7	1.4	1.3	1.2	1.6	1.3	1.0								
7.0	13	32.0	8.7	6.6	5.5	2.8	2.3	1.9	1.4	1.2	1.3	1.8	1.6	0.9	1.1							
5.8	14	20.0	8.6	5.1	3.6	2.7	2.0	1.6	1.2	1.1	1.2	1.4	1.5	0.8	1.2							
3.6	15	15.9	7.2	3.0	3.0	2.0	1.4	1.7	1.1	1.0	1.1	1.2	1.4	0.9	3.4	1.0						
3.0	16	11.9	5.8	5.1	1.7	1.4	1.3	1.5	1.1	0.9	1.0	1.0	1.1	0.5	4.4	1.1	1.0					
2.6	17	12.3	3.6	1.8	1.4	1.2	1.0	1.3	1.0	0.9	1.0	1.0	1.1	0.4	4.4	2.2	1.1	1.1				
2.3	18	8.7	3.6	1.3	1.3	1.1	0.9	1.2	0.8	0.9	0.9	0.9	1.0	0.5	3.2	1.1	1.3	1.0	1.0			
2.4	19	11.7	2.7	1.3	1.2	1.1	1.0	1.1	0.9	0.9	1.0	0.9	1.0	0.9	2.0	1.0	1.2	1.0	1.0	1.0	1.0	
2.2	20	4.0	2.1	1.0	1.0	1.0	0.9	1.0	0.8	0.9	0.9	0.9	1.0	0.7	1.2	1.0	1.1	1.0	1.0	1.0	1.0	1.0
2.3	21	12.2	1.3	1.0	1.0	1.0	1.0	1.0	0.9	0.9	1.0	1.0	1.0	0.8	1.1	1.1	1.0	1.0	1.0	1.0	1.0	1.0
1.9	22	3.2	1.5	1.0	0.8	0.7	0.9	0.9	1.0	0.9	1.0	0.9	1.0	0.9	1.0	1.0	1.0	1.0	1.0	1.0	1.0	1.0
2.2	23	10.7	1.2	0.9	1.0	1.0	1.0	1.0	1.0	0.9	0.9	0.9	1.0	0.7	1.0	1.0	1.0	1.0	1.0	1.0	1.0	1.0
2.1	24	2.5	1.4	1.0	0.9	0.9	0.9	1.0	0.9	0.9	1.0	0.9	1.0	0.8	0.9	1.0	1.0	1.0	1.0	1.0	1.0	1.0
1.1	25	3.9	1.2	0.8	0.8	0.9	0.8	0.9	0.8	0.9	0.9	1.0	1.0	0.8	1.0	1.0	1.0	1.0	1.0	1.0	1.0	1.0
1.0	26	2.2	1.0	1.0	1.0	1.0	0.9	0.9	0.9	1.0	1.0	0.9	1.0	0.9	1.0	1.0	1.0	1.0	1.0	1.0	1.0	1.0
1.0	27	2.2	1.2	0.9	0.9	1.0	1.0	0.9	1.0	1.0	0.9	1.0	1.0	0.9	1.0	1.0	1.0	1.0	1.0	1.0	1.0	1.0
1.0	28	1.5	0.9	1.0	0.9	1.0	0.9	0.9	0.9	0.9	1.0	0.9	1.0	0.9	1.0	1.0	1.0	1.0	1.0	1.0	1.0	1.0
1.0	29	1.6	1.1	1.0	0.9	1.0	1.0	1.0	0.9	1.0	1.0	0.9	1.0	0.9	1.0	1.0	1.0	1.0	1.0	1.0	1.0	1.0
1.0	30	1.4	1.0	0.9	0.9	1.0	1.0	1.0	0.9	0.9	1.0	1.0	0.9	0.9	1.0	1.0	1.0	1.0	1.0	1.0	1.0	1.0
1.0	31	1.3	1.0	1.0	0.9	1.0	1.0	1.0	1.0	1.0	1.0	0.9	1.0	0.7	1.0	1.0	1.0	1.0	1.0	1.0	1.0	1.0
1.0	32	1.2	0.9	0.9	0.9	0.9	0.9	0.9	0.9	0.9	1.0	0.9	1.0	0.8	1.1	1.0	1.0	1.0	1.0	1.0	1.0	1.0
1.0	33	1.3	1.0	0.9	1.0	0.9	1.0	1.0	1.0	0.9	0.9	1.0	1.0	0.7	1.0	1.0	1.0	1.0	1.0	1.0	1.0	1.0
1.0	34	1.3	0.9	0.9	0.9	0.9	0.9	0.9	0.9	0.9	1.0	0.9	1.0	0.8	1.1	1.0	1.0	1.0	1.0	1.0	1.0	1.0
1.0	35	1.1	1.0	0.9	0.9	1.0	1.0	1.0	1.0	0.9	1.0	1.0	1.0	0.9	1.0	1.0	1.0	1.0	1.0	1.0	1.0	1.0
1.0	36	1.2	1.0	0.9	0.9	0.9	1.0	1.0	0.9	0.9	1.0	1.0	1.0	0.8	1.1	1.0	1.0	1.0	1.0	1.0	1.0	1.0
RMS		42.5	4.7	3.5	2.5	1.8	1.4	1.2	1.1	1.1	1.1	1.1	1.3	1.2	1.0	1.2	1.1	1.0	1.0	1.0	1.0	1.0

ORDER

Figure 10.16. Ratio of Condition Numbers.

286

10.5 SUMMARY

This section has described a method for calibrating the errors found within our GEM-T1 gravity solution. The scaled covariance matrix obtained for the GEM-T1 solution, we believe, reflects an accurate estimate of both gravitational and tidal model errors. A good deal of this effort was made possible by the availability of our vectorized software which allowed us to make a large number of experimental fields at nominal cost, and the fact that we have made a "satellite-only" model which could then be evaluated through the use of altimetry and surface gravimetry.

SECTION 11.0
GRAVITY FIELD TESTING ON GEM-T1

11.1   ORBIT TESTING

One of the best ways, and in this project, one of the most relevant means for assessing the accuracy of the gravity model comes through tests using orbital tracking data. These tests typically fall into two categories: (a) orbital information extracted from previous analyses, such as "lumped harmonics" observed to explain the orbital evolution of deeply resonant objects, can be used to calibrate portions of the GEM-T1 field.   And (b), the tracking data on various artificial satellites can readily be used to assess improvements and weaknesses in the gravity models when RMS of fits to these observations are obtained and the resulting residuals are analyzed. This second category of testing also includes fits to precise laser observations, re-calculation of reference orbits to assess radial errors detected through altimeter cross-over misclosures, and the use of new and unrepresented satellite data sets for orbital reductions. All of these approaches are undertaken herein.

In the past, Goddard Space Flight Center has had to rely on so-called "tailored" gravity models to satisfy certain orbital accuracy requirements. This represented an admission on our part, that errors in the general models could not be effectively minimized to a satisfactory level for all considered satellites. Therefore, certain data sets were given inordinately high weights in special solutions to provide satellite-specific minimization of gravity errors. The consequences of this intentional mis-balancing of the weights within a field were predictable. Firstly, the objective of having good performance on a specific satellite orbit was achieved. For example the PGS-1331 model which was "tailored" for STARLETTE, does indeed perform better on this

satellite than any of the contemporary more general models. The same is true for the PGS-S4 model developed for SEASAT. However, this improvement was achieved at a cost, which is found in the aliasing of the coefficients within these "tailored" solutions--an aliasing which is considerably higher than that found in the general GEM models. It was hoped at the inception of this effort, that the good orbital performance seen with "tailored" models could be maintained with the development of an improved, general-purpose gravity solution. As shown in this section, GEM-T1 more than meets these earlier expectations.

Comparisons are made evaluating the performance of GEM-T1 with both general and "tailored" gravity models in the following subsections.

11.1.1 Orbital Tests on Laser Satellites

The deployment of a worldwide network of laser stations has dramatically improved the capabilities of satellite geodesy. Special spacecraft have been designed and launched into near-earth orbit to take advantage of the unique accuracies provided by these tracking systems. Third generation lasers have a precision on the order of <5 cm for 1 point per second ranges. These high data rates can be condensed through the formation of "normal" points at sampled time intervals which, for most purposes, are nearly noiseless. Systematic errors may exist within the laser ranges, but colocation testing and prepass and postpass ranging calibrations limit these errors so that they seldom exceed 5 cm. With mobile instruments occupying globally distributed sites, the accumulated data from many satellite missions can provide a highly accurate set of observations for gravity model testing.

Of primary interest are two special laser satellites. LAGEOS and STARLETTE are unique in several respects. They are passive, dense spheres covered with retroreflectors, whose sole purposes are to serve

as space-based laser ranging targets. Both of these satellites, by careful design, have a limited sensitivity to non-conservative force model effects, and are extremely good satellites for gauging gravity modeling improvements. The STARLETTE and LAGEOS orbits are, however, quite different. LAGEOS orbits the earth at nearly an earth's radius and thereby senses only the longest wavelength portion of the earth's geopotential due to attenuation. STARLETTE, on the other hand, is in a somewhat eccentric orbit (e=.02) with a perigee height of slightly more than 800km. In this orbit, STARLETTE experiences a much richer spectrum of gravity and tidal perturbations than does LAGEOS, especially those due to the shorter wavelength terms in the gravity model.

For LAGEOS orbits determined from a month's worth of tracking, gravity modeling is the dominant source of force model error. The orbit of LAGEOS is so clearly perturbed by the gravity field and little else, it is an ideal object for assessing long wavelength geopotential modeling accuracy. In order to isolate the gravity model error, LAGEOS monthly arcs require solution for the orbital state, a solar radiation pressure and along-track acceleration coefficient, as well as solution for earth orientation parameters. All of these were adjusted within each arc of LAGEOS used to test the fields.

Table 11.1 presents results from three typical monthly orbits found in the 1980-1984 time period. Intercompared are the RMS of fit to LAGEOS normal points (in cm) obtained within these orbital solutions when different general gravity models are used. GEM-T1 performs best with these data, with our GEM-L2 solution not far behind. The results from these two GSFC fields are considerably beyond the capabilities of other general fields shown for the determination of LAGEOS orbits. (In fact, GEM-L2 was adopted in 1984 for PROJECT MERIT's LAGEOS analyses). GEM-T1, however, included these observations. Table 11.2 intercompares GEM-T1 with GEM-L2 for an annual set of independent normal points, specifically those obtained during 1985. Again, GEM-T1 is shown to be

$C-4$

Table 11.1

<div style="border: 3px double black; text-align: center;">

GRAVITY MODEL TESTS:
LAGEOS (30^D ARCS)

RMS (cm)

</div>

MODEL	MAR. 81	AUG. 83	JUN. 84
GEM-10B	.162	.165	.184
GEM-L2	.084	.070	.131
GRIM 3B	.180	.251	.206
GRIM 3L1	.297	.398	.365
GEM-T1	.080	.061	.073

Table 11.2

COMPARISON OF GRAVITY MODELS
WITH LAGEOS LASER DATA:
ANNUAL 1985 SOLUTIONS ✪

MODEL	RMS (CM) FOR ANNUAL SOLUTION
GEM-L2	7.4
GEM-T1	6.0

✪ 1985 DATA HAS NOT BEEN UTILIZED IN EITHER
GEM-L2 OR PGS-T2. ANNUAL SOLUTION ADJUSTS
STATION COORDINATES AND POLAR MOTION.

Table 11.3

GRAVITY MODEL TESTS: STARLETTE

RMS (m)
840122 (5^D)

MODEL

GEM-10B	1.12
GEM-L2	1.26
GRIM 3B	3.65
GRIM 3L1	3.07
GEM-T1	0.16

an improved model. The 6 cm RMS of fit overall for the 1985 monthly arcs is quite good. At long wavelength, GEM-T1 seems to be a major advancement for LAGEOS orbit modeling.

STARLETTE is an excellent vehicle for field assessment. And by orbiting at a much lower orbit than LAGEOS, it complements LAGEOS for gravity field testing. Table 11.3 shows a sample STARLETTE five day orbit determined by various general gravity models. Surprisingly, GEM-T1 is nearly an order of magnitude improved over this complete set of recently published general fields. Test arcs spanning a variety of time periods are shown in Table 11.4 and Figure 11.1 where GEM-T1 is directly compared to the tailored model PGS-1331. The GEM-T1 model shows performance superior in every case by a factor of 2 to 3.

Other laser satellites, which are well represented in the general gravity models of the past five years, have also been used to test the performance of GEM-T1. Table 11.5 shows results for a sample five day arc using BE-C. Improvement comparable to that seen for both STARLETTE and LAGEOS is again seen for BE-C. BE-C was scheduled for high priority tracking to support crustal motion experiments in California. We have taken some of the short (two revolution) orbits which have been previously used in these investigations and re-computed them with GEM-T1. These results are shown in Table 11.6. GEM-T1 shows marked improvement in the ability to fit these BE-C observations, yielding results which are now at the noise levels of the laser instruments themselves in these two-revolution orbital arcs.

Tests using the GEOS-1,-2 and -3 satellites are shown in Table 11.7. In every case the RMS of fits are significantly better when GEM-T1 is used in the orbital modeling. The GEOS satellites are of special importance since their orbital inclinations are similiar to that planned for TOPEX/POSEIDON.
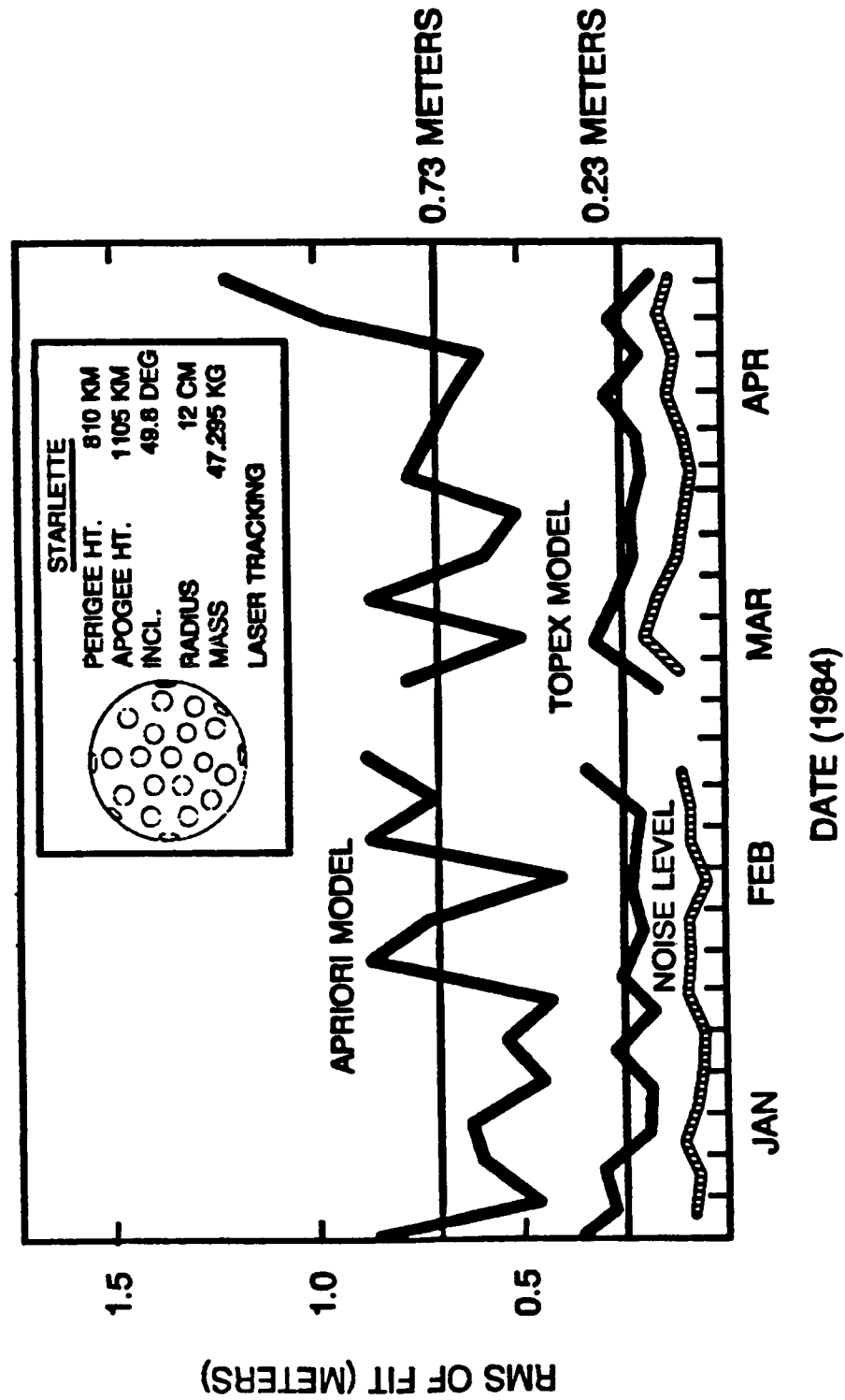
Figure 11.1. Precision Orbit Computations for the STARLETTE Satellite Using the May 1986 TOPEX Earth Gravity Model.

Table 11.4

ORBIT TESTS ON
STARLETTE

	RMS (cm)	
DATE	PGS-1331	GEM-T1
840112	64	20
840122	47	16
840206	56	18
840406	80	14
840511	93	20
840521	71	22
840526	76	19
840625	69	16
761027	43	23
761116	46	18
790320	49	25
790418	59	21

Table 11.5

**GRAVITY MODEL TESTS:
BE-C**
SAMPLE 5 DAY ARC

RMS (m)

MODEL

GEM-10B	0.75
GEM-L2	0.91
GRIM 3B	5.49
GRIM 3L1	3.03
GEM-T1	0.399

Table 11.6

BE-C SHORT ARCS
ORBITAL FITS ON INDEPENDENT
DATA SETS

(2 REVOLUTION ARCS)

DATE	RMS (cm) 7062		RMS (cm) 7051	
	GEM-9	GEM-T1	GEM-9	GEM-T1
740930	9.5	9.0	18.6	13.0
741001	14.6	9.9	14.5	13.0
741011	15.2	11.9	16.2	11.4
741017	12.5	11.1	18.8	10.4
AVERAGE	13.0	10.5	17.1	12.0
761028	12.7	8.5	22.1	12.4
761103	11.8	6.3	13.9	8.5
761104	13.8	10.5	11.5	11.3
AVERAGE	12.8	8.5	15.8	10.7
790414	16.9	6.8	23.5	6.6
790420	11.3	8.0	14.6	10.8
790421	14.7	7.9	18.7	11.3
790514	24.6	7.2	21.9	8.0
AVERAGE	14.1	7.5	19.7	9.2

Table 11.7

GRAVITY MODEL TESTS: GEOS Satellites
(5 DAY ARCS)
RMS (m)

MODEL	GEOS-1	GEOS-2	GEOS-3
GEM-10B	0.84	1.34	1.37
GEM-L2	0.95	1.06	1.57
GRIM 3B	1.82	3.32	3.71
GRIM 3L1	1.40	5.38	3.07
GEM-T1	0.71	0.69	0.74

Table 11.8

ORBIT TESTS USING AJISAI* LASER OBSERVATIONS

RMS (m)

| | GEM-T1 | | GEM-10B | |
EPOCH	OBS	RMS	OBS	RMS
860818	14087	0.18	14617	0.63
860823	6373	0.17	6282	0.56
860828	3213	0.04	3212	0.41

*
SEMI-MAJOR AXIS : 7870 KM
ECCENTRICITY : 0.0006
INCLINATION : 50.015

There are limited cases where laser data are available from a satellite which is not used in GEM-T1. The laser data overall, was considered essential in the development of this model. However, in the early summer of 1986, the Japanese launched a satellite called Ajisai which was equipped with laser retroreflectors. These data are not employed in any of the existent gravity models used for our analysis, and represent information on a unique orbit. Table 11.8 compares the RMS of fit we have obtained from two five-day arcs and one four-day arc using the Ajisai laser range data. When calibrating the orbits the estimated parameters included a daily drag coefficient (C_D), one radiation pressure coefficient (C_R) for each arc and one pole position at epoch, as well as the epoch state vector. The results of Table 11.8 show that the GEM-T1 field yields improvements ranging from a factor of 3 to a factor of 10 when compared to the GEM-10B field. Again, the results show more than a factor of three improvement obtained with the GEM-T1 field.

In summary, there is a very significant improvement in our ability to model the orbits of laser tracked satellites when using GEM-T1.

11.1.2 Orbit Tests On Doppler Satellites

Data acquired by globally distributed Doppler stations have been used in GEM-T1. There are contributions from two satellites tracked by these systems. OSCAR-14 is in a polar orbit and for the first time gives the GEM models a strong orbit at this inclination. The altimeter bearing SEASAT satellite is very important for assessing the radial error in the model and for providing a recent satellite which was tracked by both laser and Doppler systems. Therefore, SEASAT uniquely allowed us to inter-relate the Doppler and laser station coordinates into a unified global datum.

Table 11.9

> # GRAVITY MODEL TESTS: DOPPLER Satellites
>
> (6 DAY ARCS)
>
> RMS (cm/sec)

MODEL	SEASAT	OSCAR
GEM-10B	1.21	1.17
GEM-L2	1.49	1.46
GRIM 3B	2.56	2.34
GRIM 3L1	1.86	1.87
GEM-T1	0.62	1.16

There was only a limited amount of SEASAT and OSCAR Doppler data available, and all of it has been used in the development of the GEM-T1 field. Table 11.9 intercompares the performance of GEM-T1 against other global models with subsets of these Doppler data. However, in these comparisons, GEM-T1 has an advantage since these data were used in the solution. Therefore, while an improvement is noted, it is difficult to draw significant independent conclusions from these results. The PGS-S4 model is not a general field for it was "tailored" to the SEASAT orbit. To do so, this model used a significant amount of SEASAT altimetry. PGS-S4 is found to fit the SEASAT Doppler data at the same level as that shown for GEM-T1. Furthermore, it is difficult to achieve additional improvement beyond that seen with either of these fields given the apparent .6cm/sec noise seen for these Doppler observations.

There is a limited amount (6 days) of GEOSAT Doppler data which has been made available to us for test purposes. These observations have not been included in any of the gravity solutions. GEOSAT is in an orbit which is very similar to that of SEASAT, and fields which perform well on SEASAT would be expected to do well on GEOSAT. Table 11.10 confirms this speculation where the RMS of fit to the GEOSAT data is seen to be nearly equal for PGS-S4 and GEM-T1, with GEM-T1 doing slightly better. Both of these fields are a significant improvement over the results seen when using GEM-10B.

11.1.3 Tests Using Low Inclination Data

The level of aliasing present in the PGS-T2' model, which lacked the low inclination observations, was large. The low inclination satellite data were subsequently added to the solution to produce GEM-T1. Table 11.11 shows the RMS of fit obtained on three of these satellite data sets when using GEM-10B (which utilized these satellites), GEM-T1 (which also used them) and PGS-T2' (which lacked

Table 11.10

GRAVITY MODEL TESTS: GEOSAT (3^D ARC)

RMS (cm /sec)

MODEL

GEM-10B	1.47
PGS-S4	1.00
GEM-T1	0.98

Table 11.11

GRAVITY MODEL TESTS USING LASER TRACKING DATA FROM LOW INCLINATION SATELLITES

SATELLITE	EPOCH	RMS IN METERS		
		MODELS		
		GEM10B	PGS-T2 *	GEM-T1
DI-C	710615	2.58	2.42	1.65
	710622	2.23	1.99	1.50
DI-D	710507	1.93	1.76	1.22
	710710	1.87	.94	.94
PEOLE	710304	1.73	5.20	.89
	710527	2.82	12.62	.73

* THIS GRAVITY MODEL DOES NOT CONTAIN LOW INCLINATION TRACKING DATA

306

contributions from any satellite inclinations below 40 degrees). The degradation of the fit for the PEOLE laser data when using PGS-T2' is especially large. Again, GEM-T1 has an improved capability for modeling these orbits.

11.1.4 Radial Accuracy on SEASAT

Returning now to SEASAT, we have the ability to isolate the radial orbit modeling performance of different gravity fields through the use of altimeter data. The radial error can be assessed by evaluating the implied difference in the altimeter measured sea surface height at groundtrack crossover locations. Since the sea surface height is approximately equal to the geoid, (with small differences due to the general ocean circulation and errors due to mismodeled tides), its value at a specific geographical location would be expected to be nearly time-invariant. However, when the height of the sea surface above the reference ellipsoid at the same geographical point on the earth's surface is measured by crossing altimeter passes, the difference in the calculated sea surface heights is a reasonably strong measure of the non-geographically correlated radial orbit error. This assessment of radial error is incomplete, for there are correlated errors effecting both orbits equally. However, there remains a large time dependent radial error signal which can be detected and studied.

Table 11.12 gives a history of the altimeter crossover results which were obtained by GSFC during the efforts to "tailor" a field for SEASAT. Previously, the direct introduction of the SEASAT altimeter data into the solution was required to produce a model which gave better than 1m SEASAT radial orbit accuracy as measured by altimeter crossovers. As is shown by this table, GEM-T1, which lacks any altimeter data, performs significantly better than even the PGS-S4 field which used SEASAT altimeter data. Table 11.13 shows a comparison of the crossover performance on several test arcs using PGS-S4, the original PGS-T2,

Table 11.12

ALTIMETER CROSSOVER RESULTS FOR SEASAT

MODEL	DATA CONTENT	RADIAL ORBIT ERROR (M)
PGS-S1	GEM-9+ SEASAT LASER	2.1
PGS-S2	GEM-9+ SEASAT LASER AND S-BAND RADAR	1.8
PGS-S3	GEM-10B (GEOS-3 ALT) + SEASAT LASER/S-BAND	1.2
PGS-S4	PGS-S3 + SEASAT ALTIMETRY	0.7
GEM-T1	NEW SATELLITE ONLY MODEL WITH SEASAT DOPPLER DATA	0.5

Table 11.13

SEASAT ALTIMETER CROSSOVER RESULTS:

RMS (m) FOR 6 DAY ARCS

EPOCH	NO. OF CROSSOVERS	PGS-S4 1982	PGS-T2 AGU '86	GEM-T1	GEM-T1 + ALTIM
780727	1234	.623		0.933	
780802	1299	.868		0.688	
780808	1407	1.316	0.841	0.695	0.621
780917	1472	1.249	0.722	0.632	0.520
780923	1539	1.215	0.730	0.675	0.585
780929	1498	0.922	0.786	0.710	0.687
AVERAGE ÷ √2		0.72	0.54	0.51	0.42

309

GEM-T1 and a field which for test purposes combined GEM-T1 with SEASAT altimetry. The altimetry model represents only a preliminary attempt combining SEASAT altimeter data with the GEM-T1 satellite data base. A far more rigorous solution is in progress. Two conclusions can be drawn from this Table; first, GEM-T1 is a significant improvement over any field we have for modeling the radial trajectory of SEASAT. Second, when altimetry is added to the GEM-T1 model in the future, it will perform even better.

11.1.5 Tests Using the Longitudinal Acceleration on Ten 24-Hour Satellites

Carl Wagner (private communications) has used the longitude accelerations observed on ten 24-hour satellites to evaluate the accuracy of the low degree and order portion of several recent gravity fields. The 24-hour orbits (all circular) are resonant with all terms where the difference (parity) between degree and order is even. However, since these objects orbit at very high altitude, the size of the effects attenuate quickly, leaving the strongest gravitational perturbations arising from the specific harmonics of C,S(2,2), C,S(3,1) and C,S(3,3). These satellites, well-distributed in longitude, provide a special case where their deeply resonant orbit perturbations provide a strong independent test of the low degree and order fields.

Table 11.14 compares the weighted RMS residual obtained for the calculated longitudinal accelerations from different gravity fields with the longitude accelerations observed on these ten satellites. A weighted RMS = 1 would indicate that the satellite models predict these accelerations to the noise level of the observations.

When reviewing Table 11.14, there is a large difference in the low degree and order accuracy of the earlier models, like GEM-9 and GEM-10B, which lacked LAGEOS tracking as compared to those containing these laser

310

Table 11.14

```
+--------------------------------------+
|  TESTS OF GRAVITY MODELS             |
|            WITH                      |
|  24 - HOUR SATELLITE                 |
|  ACCELERATIONS                       |
+--------------------------------------+
```

MODEL	RMS WEIGHTED RESIDUAL
GEM 9	5.42
GEM 10B	3.84
GEM L2	1.21
PGS-T2	1.65
GEM-T1	1.34
PGS-3163	1.20

range measurements. All of the other models found in Table 11.14 contained LAGEOS data. The longitude accelerations calculated from the LAGEOS fields predict those observed on these satellites to a accuracy level near to that by which they have been observed directly. Although the performances are quite similiar on the latest LAGEOS fields, GEM-L2 still yields the best result for a "satellite-only" model. However, the performance of GEM-T1 is still quite satisfactory. Note the addition of altimetry into the GEM-T1 solution, even when preliminary as was done to form PGS-3163, improves the field performance on this test substantially.

11.2 GEOID MODELING

An improvement in gravity modeling requires a better determination of the individual harmonic coefficients (geoid representation) as well as improved "lumped harmonics" for orbital calculations. Given the fact that the earth has a unique gravity field, genuine improvements in gravity modeling require better representation (in spherical harmonics) of this physical reality. Therefore, part of our gravity modeling activity was directed towards achieving an improved global geoid modeling capability. This is of special interest within the TOPEX/POSEIDON framework because knowledge of the marine geoid is of critical importance.

Recalling Section 10, we find that GEM-T1 yields an improved geoid modeling capability which exceeds that which was found in any previous GSFC "satellite-only" solution. This is most clearly seen in Figure 10.3.1, where GEM-T1 is evaluated using altimeter derived gravity anomalies and is a clear and dramatic improvement over GEM-L2. Figure 9 in Lerch et al, (1985) shows that GEM-L2 was significantly better than any of the earlier GEM models when compared to altimeter anomalies. Also of note, is that the estimated commission error at degree 22 (which

is the size of the complete GEM-L2 model) using surface gravity data indicates approximately a factor of two improvement for GEM-T1 over GEM-L2. This level of improvement in reduced coefficient uncertainty is shown directly in Figure 10.2.

These results indicate that GEM-T1 is a "satellite-only" model which has less geoidal distortion than earlier such models. As such, it can serve as an improved "base" field for use in combination with local surface gravity and altimetry data.

11.3 ESTIMATED TOPEX/POSEIDON ORBITAL ACCURACY

Estimates of the orbital accuracy achievable for TOPEX/POSEIDON based upon our best estimate of gravity model uncertainty can be ascertained. To make these calculations we used the GSFC ERODYN Program [Englar et al., 1978] which is capable of propagating the full gravity model covariance error statistically into an RSS position error of the satellite's trajectory as a function of time. The scaled covariance matrix for GEM-L2, GEM-T1 and PGS-3163 (as described in Section 10) was used in these assessments. In Section 8.3 we raised some questions about the reliability of the full GEM-T1 covariance. At this point in our investigation we have been unable to develop a gravity model entirely free of constraint. Therefore, the following study must be accepted with some caution due to the difficulty we have had in assessing the full effect of least squares collocation on the correlations in our solution. However, in studies using AJISAI, the predicted range error for test arcs is 10 to 15cm RMS when using the independent GEM-T1 covariance matrix. This is in quite good agreement with the orbital fits (Table 11.8) we are obtaining when using GEM-T1 and fitting the actual full rate Ajisai laser data. We therefore have reason to believe that the forthcoming simulation for TOPEX yields reliable gravity modeling error estimates.

313

To obtain a realistic TOPEX orbital study, we simulated 3 days worth of Doppler data from a global network of 40 stations using the best available estimate of the TOPEX nominal orbit. These observations were made without any consideration for tracking system errors, including noise, since the only error we sought to assess was that arising from geopotential sources. These data were then orbitally reduced, and a set of normal equations (with their variational partials in time) were output for use in ERODYN.

Table 11.15 presents a summary of the results. Shown in this table is the RMS radial error caused by imperfections in the gravity model, for the TOPEX/POSEIDON orbit, as calculated for 1/2 day, 1 day and 3 day arc lengths. The results, as a function of time, are shown in Figure 11.2 for the 3 day arc length. These estimates indicate that a major improvement has been made towards reaching the orbit modeling goals set forth for the TOPEX/POSEIDON Mission. While preliminary, they are grounds for cautious optimism.

Figure 11.3 shows a preliminary breakdown of the gravity model contributions to the radial errors estimated for TOPEX when taking subsets of the coefficients by both degree and by order. The strongest signal is seen from an evaluation of the geopotential error contributions by order where there are two very significant problems. These spikes indicate that the uncertainies of the m=1 and m=13 harmonics are the most significant sources of error within the GEM-T1 field for TOPEX. The m=13 terms are at TOPEX's primary resonance. These terms should not present a problem for field improvement for even a little amount of TOPEX tracking data is capable of successfully resolving this orbital resonance. All of these m=13 terms produce a single, dominating, well defined resonance perturbation (with two nearby and much smaller sideband effects). This primary resonance is easily corrected in a multi-day orbital arc. Likewise, the most likely cause of the m=1 errors are those arising from the so-called "m-daily" perturbations

Table 11.15

TOPEX PROJECTED RADIAL ERRORS

ERRORS IN CENTIMETERS

SAMPLE INTERVAL = 10 MIN.

GRAVITY MODEL	1/2 DAY ARC	1 DAY ARC	3 DAY ARC
GEM-L2	51.6	61.9	65.7
GEM-T1	17.2	22.7	25.3
PGS3163	13.2	16.6	18.8

(PGS3163 = GEM-T1 + SEASAT ALTIMETER)
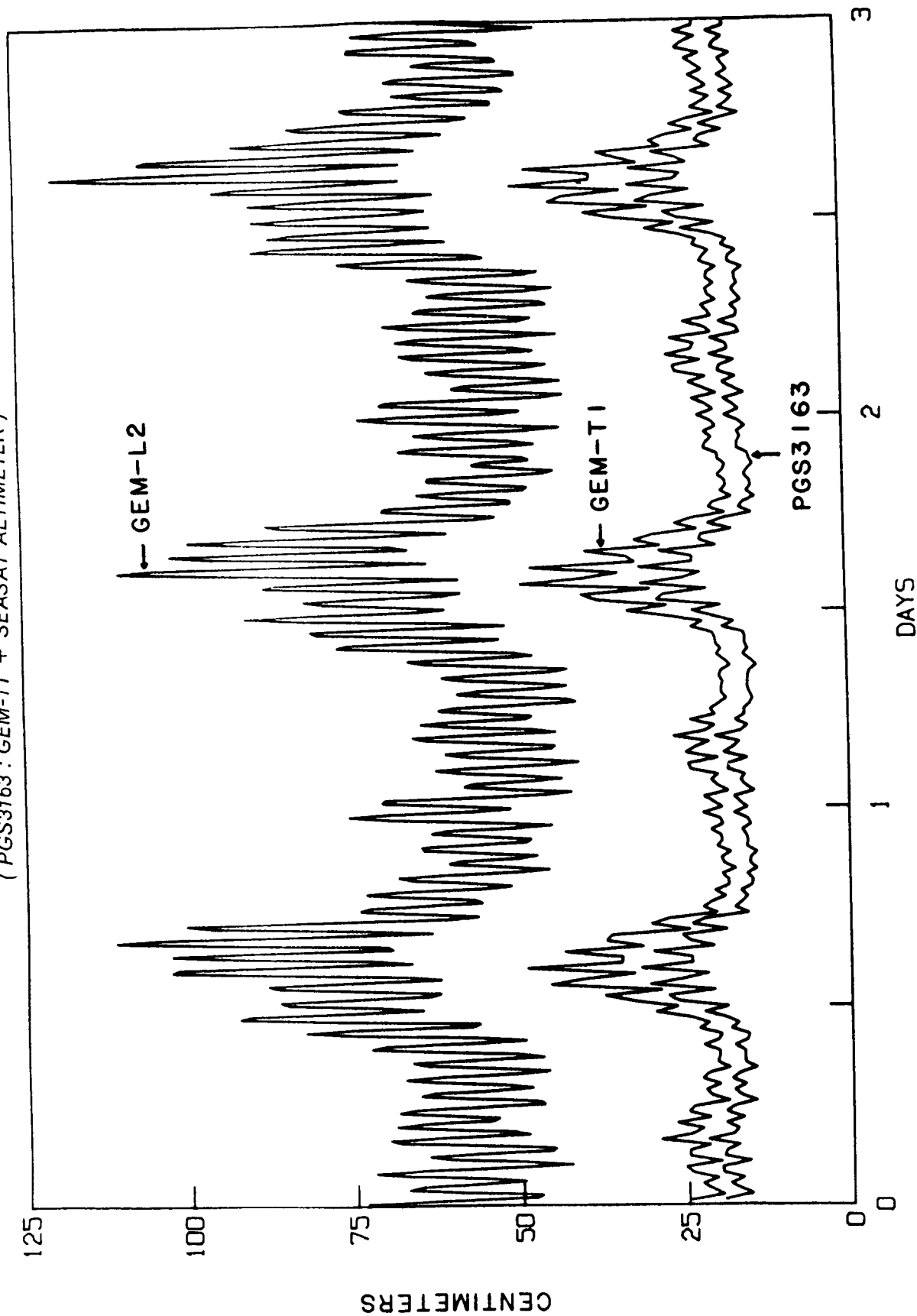
Figure 11.2. TOPEX Projected Radial Errors.

TOTAL RMS 25 CM.

RMS PER DEGREE

RMS PER ORDER
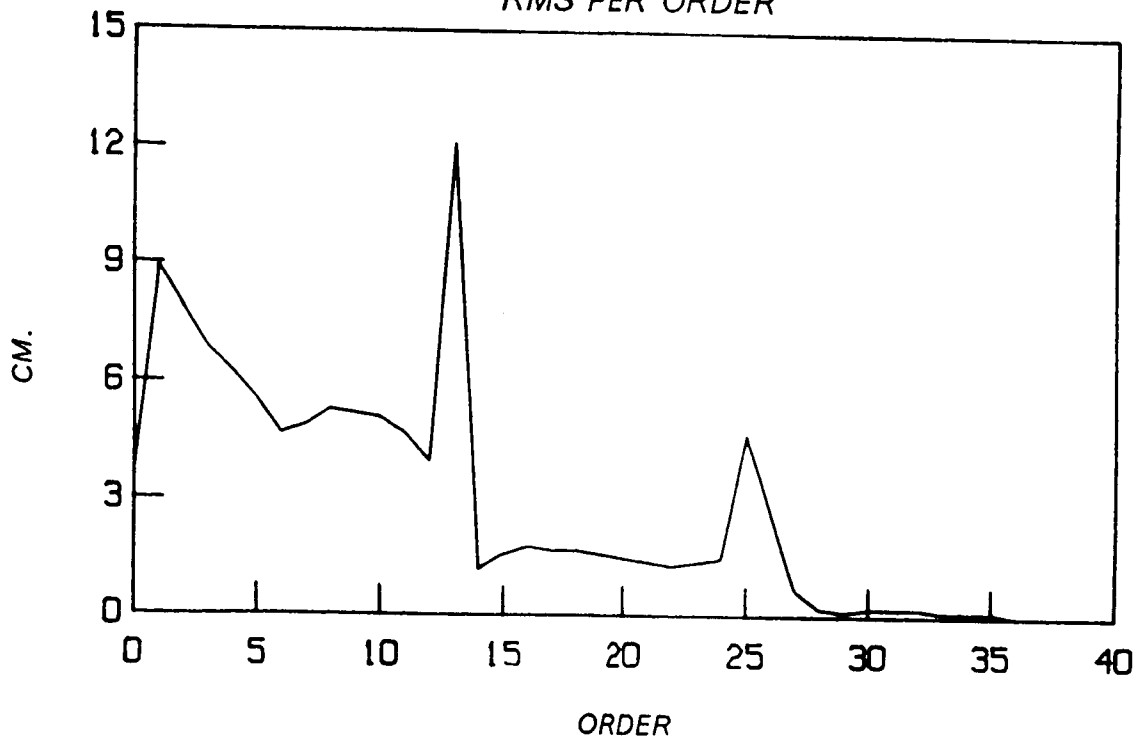
Figure 11.3. TOPEX Projected Radial Errors from GEM-T1.

317

which, for this order, have perturbations of one-cycle per day. These once per day cycles are clearly evident in Figure 11.2. Again, these m-daily terms should be modelled accurately if limited amounts of TOPEX/POSEIDON data are added to the gravity solution.

11.4 ORTHOMETRIC HEIGHTS COMPARISONS

One of the quantities related to the gravity model which can provide an external check on the field is the undulation at tracking station locations. If the orthometric heights are accurately known from surveys and the geometric height of the instrument is determined from its geodetic coordinates, then these data can be used to calibrate the undulations inferred by global geopotential models. If N denotes the undulation, h the geometric height above the reference ellipsoid, and H the orthometric height, then :

$$N = h - H \tag{11.1}$$

The ellipsoidal heights are derived from the estimated center-of-mass referred three-dimensional station positions. The orthometric heights are obtained at the tracking sites from spirit levelling. Consequently we can independently determine the undulation N at specific points on the earth's surface. These values can be compared to the values obtained from the gravity models (taken to infinite degree and order) that expresses N in terms of the potential coefficients. In practice we only have a finite set of potential coefficients and can get only approximate values of N; the error committed by omitting the coefficients above the truncation limit of the solution is termed omission error. The fact that the determined harmonics are in error, introduces an additional error, the so-called commission error. The mean sea level (orthometric) heights also have additional errors that vary, depending on the quality of the survey from which they were obtained. The surveying datum over the North American continent is expected to be of

good and of uniform accuracy. One of the comparisons we present here is for the Doppler-derived undulations at 750 North American stations compiled by NOAA's National Geodetic Survey. This data set has been used in other investigations such as [Tscherning and Goad, 1985], which has a detailed description of the data. The version which we used was obtained from Ohio State University (R.H. Rapp, private communication). Accompanying documentation from OSU indicates that the Doppler coordinates have been transformed into a geocentric system by applying the well known axial Z-shift of 4.0 meters, a scale change of -0.5 ppm and a Z-axis rotation of 0.5 mas. The undulations implied by various (recent) gravity field solutions were compared to those obtained from the Doppler sites. The mean differences and their RMS about the mean are listed in Table 11.16. The OSU fields are high degree expansions (to 180 x 180) and have much less omission error than the significantly smaller "satellite-only" fields. We have included them to provide some measure of the omission effects. It can be seen from this table that the new solutions compare favorably with others models. In most cases they are even better than satellite solutions which have included altimeter data and/or terrestrial gravity data (e.g. GEM10B, GRIM3).

A set of globally distributed undulations can also be used to infer the semi-major-axis of the best fitting ellipsoid. In theory the global undulation mean should be zero; one of the constraints in determining the size, shape and origin of the best fitting ellipsoid is having the undulations exactly mean to zero. In practice though we have only a limited number of point values where the geometric as well as the orthometric height are only approximately known. This determination therefore is only approximate and depends heavily on the distribution of the stations and the accuracy of the surveyed orthometric heights. The correction to the semi-major-axis is defined as the average misclosure in the equation relating N,h,H :

Table 11.16

GEOID HEIGHT COMPARISONS
BASED ON 750 DOPPLER-DERIVED UNDULATIONS IN NORTH AMERICA

FIELD DESIGNATION	MAXIMUM DEG.& ORD.	MEAN DIFFERENCE [cm]	RMS DIFFERENCE [m]
*GEM-10B	36, 36	-19	3.6
*GRIM 3	36, 36	-17	3.8
*GRIM 3L1	36, 36	12	3.3
*OSU '81	36, 36	-6	3.4
*OSU '78	180, 180	-41	2.9
GEM-L2	20, 20	13	4.1
PGS-T2	36, 36	6	3.4
GEM-T1	36, 36	15	3.5

*COMBINATION FIELDS

$$\Delta a_e = h_{SLR} - H - N$$

For this comparison, we have restricted our global station network to those stations with SLR tracking. The geometric relationship of the above defined quantities is depicted in Figure 11.4 . The results of this computation at thirty five stations are given in Table 11.17. A six meter editing criterion was applied. We have thus eliminated some isolated points where a 36 x 36 field cannot model sudden high frequency changes of the local gravity field or there is some error in the local survey/station position. The value of a_e from the remaining thirty stations agrees very well (to a few centimeters) with that derived from LAGEOS solutions. The large standard deviation of the sample indicates that this is not a particularly strong test of the models, which is a known fact when station locations are considered. Many stations are located on islands or in mountainous regions where local gravity features can be steep. However, although the quality of the GEM-T1 field is not directly assessed, its performance against other contemporary models is shown to be quite good.
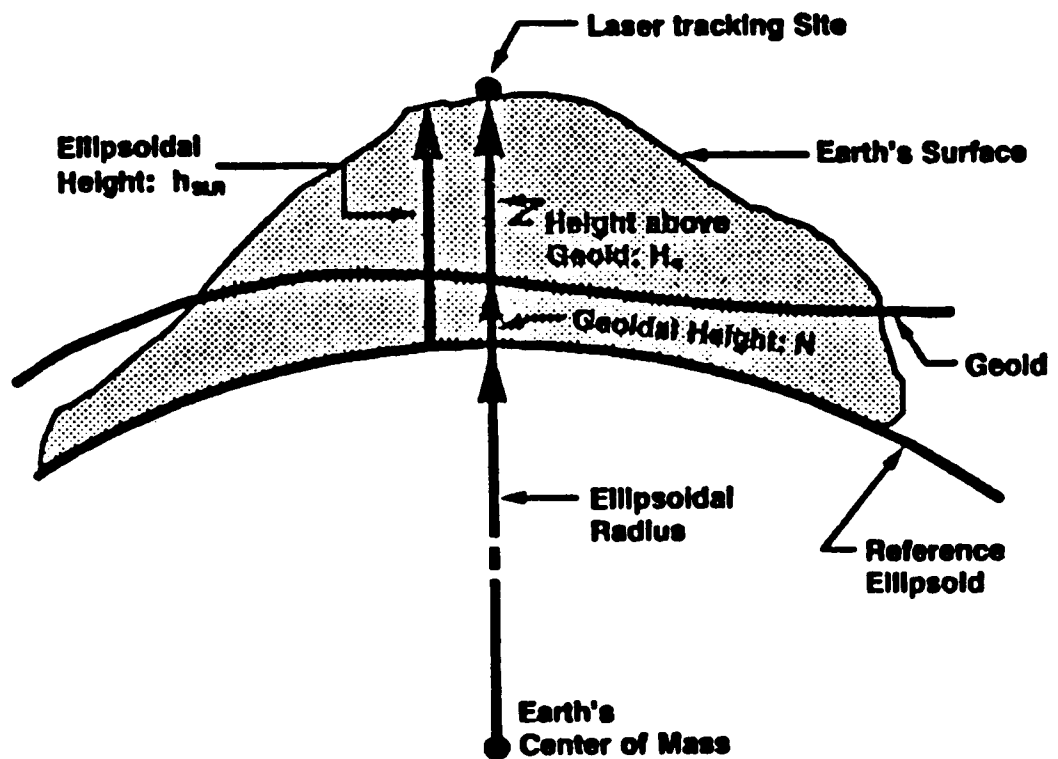
$$\Delta a_e = h_{SLR} - H_o - N$$

Figure 11.4. Determination of Earth's Semi-Major Axis.

TABLE 11.17

EARTH'S SEMI-MAJOR AXIS FROM GEM-T1

SITE LOCATION	NO.	ELLIPSOIDAL* HEIGHT m	MSL HEIGHT m	GEOIDAL** HEIGHT m	DELTA a_e m
EASTER I.	7061	115.82	119.14	-4.72	1.40
OTAY MT.	7062	988.59	1022.00	-35.12	1.71
BEAR LAKE	7082	1962.89	1976.51	-12.16	-1.46
FORT DAVIS	7086	1961.31	1983.21	-24.62	2.72
YARAGADEE	7090	241.30	266.56	-26.17	0.91
GREENBELT	7101	8.79	42.43	-34.63	0.99
GREENBELT	7102	17.95	51.81	-34.63	0.77
GREENBELT	7103	17.89	51.80	-34.63	0.72
GREENBELT	7105	19.13	53.40	-34.63	0.72
QUINCY	7109	1106.25	1129.85	-25.78	2.18
MON. PEAK	7110	1838.89	1870.79	-34.07	3.17
PLATTEVILLE	7112	1501.49	1519.91	-16.65	-1.77
OWENS VAL.	7114	1178.00	1203.80	-28.04	2.24
HAWAII (M1)	7120	3067.73	3048.25	4.30	15.18E
HUAHINE	7121	43.60	34.20	4.10	5.30E
MAZATLAN	7122	30.74	56.00	-22.28	-2.98
HAWAII	7210	3067.45	3047.95	4.30	15.20E
TLRS MON.PK.	7220	1838.74	1870.61	-34.07	2.20
BARSTOW	7265	895.92	926.72	-30.04	-0.76
SANTIAGO	7400	725.42	690.36	21.40	13.66E
CERRA TOLLO	7401	2158.59	2123.09	23.26	12.24E
FINLAND	7805	78.01	59.23	19.95	-1.17
KOOTWIJK	7833	93.42	49.80	45.27	-1.65
WETTZELL	7834	661.17	614.44	46.55	0.18
SIMOSATO	7838	99.48	60.43	36.52	2.54
GRAZ	7839	539.39	494.36	46.57	-1.54
GREENWICH	7840	75.33	30.68	49.11	-4.46
TLRS FT.DAVIS	7885	1961.33	1983.16	-24.62	2.79
TLRS QUINCY	7886	1109.51	1129.96	-25.78	5.33E
VANDENBURG	7887	601.34	636.45	-35.57	0.46
VERNAL	7892	1590.01	1607.70	-13.54	-4.15
AREQUIPA	7907	2492.25	2452.27	35.79	4.19
MT. HOPKINS	7921	2352.49	2383.38	-28.89	-2.00
MATERA	7939	535.86	490.52	39.90	5.44E
ORRORAL	7943	948.89	929.53	12.02	7.34E

The average a_e (edited E): 6378137.29 ± .43

SECTION 12.0
SUMMARY

The computation of GEM-T1 has been a major undertaking. To develop it, we have evaluated all of the overall solution design decisions made in the past for other GEM models and reconsidered them in light of the present state-of-the-art in Satellite Geodesy. As a result, we have achieved a level of internal consistency higher than for any earlier Goddard Earth Model. Moreover, this work was made possible by the redesign of our major software tools, GEODYN and SOLVE, for the Cyber 205 vector computer.

The GEM-T1 model provided a simultaneous solution for:

o a gravity model in spherical harmonics complete to degree and order 36;

o a subset of 66 ocean tidal coefficients for the long wavelength components of 12 major tides. This adjustment was made in the presence of 550 other ocean tidal coefficients representing 32 major and minor tides; and

o 5-day averaged earth rotation and polar motion parameters for the 1980 period onwards.

The model was derived exclusively from satellite tracking data acquired on 17 different satellites which ranged in inclination from 15 degrees to polar. In all, almost 800,000 observations were used, half of which were from third generation laser systems. A calibration of the model accuracies has been performed showing GEM-T1 to be a major improvement over all earlier GSFC "satellite- only" models for both orbital calculations and geoidal representations. And for terms of low

degree and order (to 8 x 8) GEM-T1 is a major advancement over all GEM models, even those containing altimetry and surface gravimetry.

When a simulation of the TOPEX/POSEIDON orbit was made using the covariances of the GEM-T1 model, preliminary estimated radial error was reduced to a level below 20cm RMS as compared to more than 50cm when using GEM-L2. This simulation evaluated only errors arising from geopotential sources. GEM-L2 was the best available model for TOPEX prior to the work described herein. A major step towards more accurate gravity modeling for TOPEX/POSEIDON has been achieved in this first of an expected new series of Goddard Earth Models.

ACKNOWLEDGEMENTS

REFERENCES

Balmino, G., Reigber, C. and Moynot, B., "The GRIM 2 Earth Gravity Field Model; Determination and Evaluation," EOS (2), 34, pp.55-78, 1978.

Barlier, F., Berger, C., Falin, K.L., Kockarts, G., Thuillier, G., "A Thermospheric Model Based Upon Satellite Drag Data," Ann. Geophys., +, 34, fasc1, 1978, pp. 9-24.

Bomford, G., Geodesy, Oxford University Press, 1980.

Christodoulidis, D.C., Smith, D.E., Klosko, S.M., & Dunn, P.J., "Solid Earth and Ocean Tide Paramters for LAGEOS", Proc. of the 10th International Symposium on Earth Tides (in press), 1986a.

Christodoulidis, D.C., Williamson, R.G., Chinn, D. & Estes, R., "On the Prediction of Ocean Tides for Minor Constituents", Proc. of the 10th International Symposium on Earth Tides (in press), 1986b.

Christodoulidis, D.C., Smith, D.E., Williamson, R.G. and Klosko, S.M., "Observed Tidal Braking in the Earth/Moon/Sun System," NASA Technical Memorandum 100677, June 1987.

Englar, T.S., Estes, R.H., Chin, D.C., and Maslyar, G.A., "ERODYN Program Mathematical Description Version 7809," BTS Contractor Report BTS-TR-78-69, September 1978.

Estes, R.H. and Majer, V., "SOLVE Program Mathematical Description," BTS Contractor Report prepared under NAS 5-27656, March 1986.

Gaposchkin, E.M., Smithsonian Standard Earth III S.A.O. Special Report, 353, 262-276, Smithsonian Astrophys. Observ., Cambridge, Mass., 1973.

Gaposchkin, E.M., "Gravity Field Determination From Laser Observations," Phil. Trans. R. Soc. A., 284, pp. 515-527, 1977.

Gaposchkin, E.M., "Pole Position Studied with Artificial Earth Satellites", in Rotation of the Earth, ed. by P. Melchoir & S. Yumi, pp.128-130, 1972.

Gilbert, F. & Dziewonski, A.M., "An Application of Normal Mode Theory to the Retrieval of Structural Parameters and Source Mechanisms from Seismic Spectra", Phil. Trans. R. Soc., Vol. A278, pp.187-269, 1975.

Heiskanen, W., and H. Moritz, 1967, Physical Geodesy, San Francisco, W.H. Freeman and Company.

Katsambalos, K.E., "The Effect of the Smoothing Operator on Potential Coefficient Determinations," Ohio State University, Dept. of Geodetic Science Report No. 287, 1979.

Kaula, W.M., Theory of Satellite Geodesy, Blaisdell Press, Waltham, Mass., 1966.

Kaula, W.M., "Tests of Satellite Determinations of the Gravity Field Against Gravimetry and Their Combination," Publication No. 509, Institute of Geophysics and Planetary Physics, University of California, 1966.

King-Hele, D.G. and D.M.C. Walker, "Evaluation of 15th Order Harmonics in the Geopotential From Analysis of Resonant Orbits," Proc. Roy. Soc., A379, 247-288, 1982.

Klosko, S.M. and Wagner, C.A., "Spherical Harmonic Representation of the Gravity Field From Dynamic Satellite Data," Planet Space Sci., Vol. 30, No. 1, pp. 5-28, 1982.

Lambeck, K., "Determination of the Earth's Pole of Rotation from Laser Range Observations to Satellites", Bull. Geod., Vol. 101, p.).263-281, 1971.

Lambeck, K. and Coleman, R. (1983), "The Earth's Shape and Gravity Field: A Report of Progress from 1958 to 1982," Geophys. J.R. Astr. Soc. (1983), 74, pp. 25-54.

Lambeck, K., "Polar Motion from the Tracking of Close Earth Satellites", in Rotation of the Earth, ed. by P. Melchoir & S. Yumi, pp.123-127, 1972.

Leick, A. & Van Gelder, B.H.W., "On Similarity Transformations and Geodetic Network Distortions based on Doppler Satellite Observations," Ohio State University, Dept. of Geodetic Science Report No. 235, 1975.

Lerch, F.J., Wagner, C.A., Richardson, J.A., Brownd, J.E., "Goddard Earth Models (5 and 6)," GSFC X-921-74-145, Greenbelt, Maryland, Dec. 1974.

Lerch, F.J., S.M. Klosko, R.E. Laubscher, and C.A. Wagner, "Gravity Model Improvement Using Geos 3," GSFC Document X-921-77-246, Goddard Space Flight Center, Greenbelt, Maryland, 1977.

Lerch, F.J., Klosko, S.M., Laubscher, R.E., Wagner, C.A., "Gravity Model Improvement Using GEOS-3 (GEM-9 and 10)," J. Geophys. Res., Vol. 84 (138), pp. 3897-3915, 1979.

Lerch, F.J., B.H. Putney, C.A. Wagner and S.M. Klosko, "Goddard Earth Models for Oceanographic Applications (GEM 10B and 10C)," Marine Geodesy, 5, 2, 145-187, 1981.

Lerch, F.J., Klosko, S.M., Patel, G.B., "Gravity Model Development From Lageos," Geophys. Res. Letters, Vol. 9, No. 11, pp. 1263-1266, 1982.

Lerch, F.J., Marsh, J.G., Klosko, S.M., Williamson, R.G., "Gravity Improvement for SEASAT," J. Geophys. Res., Vol. 87, No. C5, 3281-3296, April 30, 1982.

Lerch, F.J., "Error Spectrum of Goddard Satellite Models for the Gravity Field," Geodynamics Branch Annual Report-1984, NASA TM86223, August 1985a.

Lerch, F.J., Klosko, S.M., Wagner, C.A., & Patel, G.B., "On the Accuracy of Recent Goddard Gravity Models", J. Geophys. Res., Vol. 90, pp.9312-9334, 1985b.

Lerch, F.J., Klosko, S.M., & Wagner, C.A., "Comments on Lambeck and Coleman: 'The Earth's Shape and Gravity Field: A Report of Progress from 1958 to 1982'", Geophys. J. Roy. Astron. Soc., Vol. 86, pp.651-664, 1986.

Marsh, J.G., Lerch, F.J., & Williamson, R.G., "Precision Geodesy and Geodynamics Using Starlette Laser Ranging", J. Geophys. Res., V. 90, pp.9335-9345, 1985.

Marsh, J.G. et al, "An Improved Earth Gravity Model: A Status Report", EOS, V. 67, p.260 (abstract), 1986.

Marsh, J.G. & Born, G.H. TOPEX Gravity Model Development Team Activities During Fiscal Year 1984, NASA TM 86208, 1985.

Marsh, J.G. & Tapley, B.D. (editors), "TOPEX Gravity Model Improvement and Precision Orbit Determination Meeting Minutes," pp.A5-1 to A5-4, internal document, NASA/GSFC, 1985.

Marsh, J.G. et al., "A Global Station Coordinate Solution based upon Camera and Laser Data-GSFC 1973," NASA Report X-592-73-171, 1973, also published in Proceedings of the First International Symposium on the Use of Artificial Satellites for Geodesy and Geodynamics, Athens, Greece, May 1973.

Martin, T.V. & Eddy, W.F., "GEODYN System Documentation, Vol. 1," EG&G Washington Analytical Services Center, Inc., Prepared for B.H. Putney under contract NAS 5-22849, 1980.

Martin, T.V., Eddy, W.E., Rowlands, D.D., and Pavlis, D.E., "Volume 1 to 5, GEODYN II System Description," EG&G Contractor Report, April 1987.

McClure, P., "Diurnal Polar Motion," NASA document X-592-73-259, 1973.

Melbourne, W. Project MERIT Standards, Circular No. 167, U.S. Naval Observatory, Washington, D.C., 1983.

Moritz, H. "Least-Squares Collocation," Rev. of Geophysics & Space Physics, Vol. 16, 421-430, 1978.

Moritz, H., <u>Advanced Physical Geodesy</u>, Abacus Press, Tunbridge Wells Kent, Kent, England, 1980.

Munk, W.H. & Cartwright, D.E., "Tidal Spectroscopy and Prediction", <u>Phil. Trans. R. Soc.</u>, Vol. A259, pp.533-581, 1977.

National Geodetic Satellite Program, NASA SP-365, Washington, D.C., 1977.

Putney, B.H., "General Theory for Dynamic Satellite Geodesy", in <u>The National Geodetic Satellite Program</u>, pp.319-334, NASA SP-365, 1977.

Rapp, R.H., "The Earth's Gravity Field to Degree and Order 180 Using Seasat Altimeter Data, Terrestrial Gravity Data, and Other Data," <u>Dept. of Geodetic Science Report No. 322</u>, The Ohio State University, Columbus, Ohio, Dec. 1981.

Rapp, R.H., "The Determination of Geoid Undulations and Gravity Anomalies from Seasat Altimeter Data," <u>J. Geophys. Res.</u>, 88, C3, 1552-1562, 1983a.

Rapp, R.H., "The Development of the January 1983 1° x 1° Mean Free-Air Anomaly Data Tape," <u>Department of Geodetic Science and Surveying, Internal Report</u> Ohio State University, Columbus, Ohio, 1983b.

Rapp, R.H. <u>Geometric Geodesy</u>, Class notes, Dept. of Geodetic Science and Surveying, The Ohio State University, 1983.

Reigber, Ch., G. Balmino, B. Moynot and H. Mueller, "The GRIM3 Earth Gravity Field Model," <u>Manuscripta Geodaetica</u>, 8, 93-138, 1983.

Reigber, Ch., G. Balmino, B. Moynot, H. Mueller, Ch. Rizos and W. Bosch, "An Improved GRIM3 Earth Gravity Model (GRIM3B)," paper presented at <u>XVIII IUGG-IAG General Assembly</u>, Hamburg, 1983.

Safren, H.G., "Effect of a Drag Model Using a Variable Projected Area on the Orbit of the Beacon-Explorer C Satellite," NASA document X-921-75-210, 1975.

Schwarz, K.P., "Least-Squares Collocation for Large Systems," Bull. Geod. Sci., Aff., 35, 309-324, 1976.

Schwarz, K.P., "On the Application of Least-Squares Colloation Models to Physical Geodesy," in <u>Approximation Methods in Geodesy</u>, (H. Moritz and H. Šunkel, editors, H. Wichmann-Verlag, Karlsruhe, 1978.

Schwiderski, E.W. "Ocean Tides, Part I: Global Ocean Tide Equations", <u>Marine Geodesy</u>, Vol. 3, pp.161-217, 1980a.

Schwiderski, E.W. "Ocean Tides, Part II: Hydrodynamical Interpolation Model", <u>Marine Geodesy</u>, Vol. 3, pp.219-255, 1980b.

Smith, D.E., Kolenkiewicz, R., Dunn, P.J., & Torrence, M.H., "Determination of Station Coordinates from LAGEOS", in <u>The Use of Artificial Satellites for Geodesy and Geodynamics</u>, National Technical University, Athens, 1979.

Smith, D.E. et al, "Geodetic Applications of Laser Ranging", <u>Phil. Trans. R. Soc.</u>, A284, pp.529-536, 1977.

Smith, D.E. et al., "A Global Geodetic Reference Frame from LAGEOS Ranging (SL5-1AP)," <u>J. Geophys. Res.</u>, Vol. 90, pp. 9221-9235, 1985.

335

Wahr, J.M., "The Tidal Motions of a Rotating, Elliptical, Elastic, and Oceanless Earth," PhD Thesis, University of Colorado, 1979.

Wagner, C.A. and S.M. Klosko, "Gravitational Harmonics from Shallow Resonant Orbits," Celestial Mechanics, (16), 1977.

Wagner, C.A. and F.J. Lerch, "The Accuracy of Geopotential Models," Planet. Space Sci., Vol. 26, pp. 1081-1140, 1978.

Wagner, C.A. and Colombo, O., "Gravitational Spectra From Direct Measurements, J. Geophys. Res., 84, 4709, 1979.

Wagner, C.A., "The Accuracy of the Low-Degree Geopotential: Implications for Ocean Dynamics," J. Geophys. Res., 88, B6, 5083-5090, 1983.

Wagner, C.A., Lerch, F.J., Brownd, J.E. & Richardson, J.A., "Improvement In the Geopotential derived from Satellite and Surface Data (GEM 7 and 8)," NASA document X-921-76-20, 1976.

Williamson, R.G. & Marsh, J.G., "Starlette Geodynamics: The Earth's Tidal Response", J. Geophys. Res., Vol. 90, pp.9346-9352, 1985.

$$\boxed{\text{APPENDIX 1}}$$

APRIORI STATION POSITIONS
FOR GEM-T1

LASER, DOPPLER, S-BAND
TRACKING SITES

as of February 11, 1987

NAME	I.D.	X	Y	Z	LATITUDE	LONGITUDE	HEIGHT
SJEDOP	8	4083914.724000	-4209803.344000	-2499112.240000	-23 13 2.8860	314 7 49.3899	613.1566
MCMDOP	19	-1310713.158000	310460.103000	-6213366.502000	-77 50 51.7599	166 40 27.5094	-13.2180
MAHDOP	20	3602880.542000	5238222.012000	-515939.533000	-4 40 14.3724	55 28 46.4637	554.5197
UCLDOP	21	4027832.421000	307023.842000	4919538.285000	50 47 55.0127	4 21 32.3079	158.9292
SMGDOP	22	-3088047.508000	5333058.221000	1638811.523000	14 59 16.1057	120 4 21.0188	56.3766
GWMDOP	23	-5059777.437000	3591210.689000	1472782.183000	13 26 22.8863	144 38 4.2689	95.3281
TAFDOP	24	-6100051.840000	-997195.827000	-1568316.404000	-14 19 45.3734	189 17 3.1603	46.5015
MSADOP	27	-3857199.892000	3108659.442000	4004040.881000	39 8 6.5343	141 8 0.1677	118.7094
PRTDOP	105	5051978.523000	2725637.921000	-2774470.292000	-25 56 48.6108	28 20 51.7217	1607.4999
VIRDOP	107	1090140.067000	-4842520.407000	3991981.266000	38 59 43.7459	282 41 12.6096	85.5080
STFDOP	112	-3942240.273000	3468854.279000	-3608204.886000	-34 40 26.4569	138 39 17.3545	36.1642
NMXDOP	113	-1556216.306000	-5169444.382000	3387248.806000	32 16 43.9538	253 14 45.7264	1183.4823
ANCDOP	114	-2656164.201000	-1544366.537000	5570655.093000	61 17 0.4578	210 10 29.6066	76.9700
BSEDOP	116	4004964.422000	-96559.816000	4946541.129000	51 11 4.5706	358 37 7.9124	125.5878
TULDOP	118	539846.249000	-1388555.301000	6180980.376000	76 32 9.0692	291 14 42.7896	69.2382
ALTDOP	127	-3850349.834000	397640.976000	5052349.435000	52 43 41.9001	174 6 13.4618	74.2770
OTTDOP	128	1091450.380000	-4351283.878000	4518704.850000	45 23 59.9346	284 4 52.3700	47.6656
TEXDOP	192	-740293.270000	-5457073.446000	3207244.281000	30 23 1.1196	262 16 28.3958	218.8637
FLODOP	641	4522402.628000	898011.588000	4392486.373000	43 48 13.6779	11 13 51.9815	147.6731
POTDAM	1181	3800618.509000	882010.731000	5028856.705000	52 22 48.9239	13 3 55.3462	144.7284
MADSST	1425	4847873.416000	-353562.114000	4117035.733000	40 27 15.6631	355 49 43.4091	819.4767
ROSSST	1857	647216.476000	-5178143.313000	3656423.608000	35 11 56.3641	277 7 28.0414	858.3802
BDA3	6002	2308450.060000	-4874293.259000	3393401.139000	32 21 4.8493	295 20 31.5201	-13.8880
QUIS	6006	1263459.520000	-6255027.887000	-68797.595000	0 37 18.6378	281 25 10.4892	3592.2966
HAW3	6012	-5543841.363000	-2054556.810000	2387810.683000	22 7 34.6591	200 20 5.2415	1160.7495
GDS3	6016	-2354733.540000	-4646742.113000	3669444.112000	35 20 32.0640	243 7 35.1027	933.0909
ULA3	6018	-2282487.586000	-1453372.406000	5756710.824000	64 58 19.5128	212 29 12.9046	349.7586
MAD3	6022	4847758.757000	-353406.241000	4117201.143000	40 27 22.3866	355 49 49.6522	831.1639
MAD8	6023	4847822.178000	-353317.195000	4117139.507000	40 27 19.6721	355 49 53.6166	834.3747
GWM3	6024	-5069114.734000	3584103.540000	1458900.120000	13 18 38.2291	144 44 12.5497	140.8469
GDS8	6028	-2354766.548000	-4646777.247000	3669390.480000	35 20 29.7765	243 7 34.5657	939.8022
ROSS	6031	647202.274000	-5178317.177000	3656144.291000	35 11 45.7653	277 7 26.6321	836.9229
ORR3	6037	-4447485.440000	2676856.637000	-3695269.292000	-35 37 40.6738	148 57 25.4426	947.3843
MILA	6040	907138.484000	-5535192.616000	3026104.975000	28 30 29.6131	279 18 25.9814	-27.1839
MI23	6041	907078.144000	-5535232.599000	3026051.997000	28 30 27.6405	279 18 23.5539	-26.3718
AGO3	6054	1769867.176000	-5044471.100000	-3468390.273000	-33 9 3.6279	289 20 0.8442	727.6853
MIL3	6071	907006.114000	-5535206.236000	3026102.214000	28 30 29.4823	279 18 23.6370	-25.5543
ETCA	6091	1129867.308000	-4833147.503000	3992193.142000	38 59 54.2129	283 9 28.7975	23.5599
1UNDAK	7034	-521692.957000	-4242036.158000	4718733.844000	48 1 21.6883	262 59 19.9354	228.2115
1EDINB	7036	-828471.760000	-5657444.892000	2816825.976000	26 22 46.9803	261 40 7.9202	31.3196
1COLBA	7037	-191272.927000	-4967266.077000	3983269.628000	38 53 36.5000	267 47 41.3492	239.1561
1BERMD	7039	2308232.342000	-4873587.010000	3394578.597000	32 21 49.8477	295 20 35.5563	-1.6029
1PURIO	7040	2465070.227000	-5534913.914000	1985531.452000	18 15 28.9986	294 0 23.8776	9.1055
1GSFCP	7043	1130730.821000	-4831318.155000	3994143.543000	39 1 15.7027	283 10 21.0622	19.9526
1DENVR	7045	-1240462.201000	-4760221.025000	4048992.730000	39 38 48.2606	255 23 39.0016	1773.0005
GODLAS	7050	1130692.438000	-4831354.616000	3994112.117000	39 1 14.3647	283 10 19.1632	20.9531
QUINCO51	7051	-2516893.830000	-4198839.747000	4076416.458000	39 58 24.7867	239 3 37.5502	1059.9437
WALLAS	7052	1261570.901000	-4881573.970000	3893171.501000	37 51 36.0935	284 29 24.7514	-29.1658
MOBLAS	7053	1130704.646000	-4831318.517000	3994151.264000	39 1 16.0118	283 10 19.9993	20.4535
CRMLAS	7054	-2328184.126000	5299661.478000	-2669470.815000	-24 54 15.3778	113 42 58.5803	25.2383
GMISLS	7060	-5068966.309000	3584085.182000	1458762.160000	13 18 33.6245	144 44 14.0370	139.7523
EASTER	7061	-1884984.152000	-5357610.236000	-2892846.045000	-27 8 51.9069	250 36 59.2013	115.8812
OTAY MT	7062	-2428826.443000	-4799746.127000	3417278.409000	32 36 2.8875	243 9 32.8229	988.5455
STALAS	7063	1130714.033000	-4831362.670000	3994093.645000	39 1 13.6387	283 10 19.9610	19.2390
GORF064	7064	1130678.096000	-4831334.738000	3994134.113000	39 1 15.3807	283 10 18.7710	17.2255
GORF065	7065	1130694.399000	-4831348.899000	3994118.134000	39 1 14.6208	283 10 19.2967	20.7638
WFCLAS	7066	1261612.031000	-4881547.504000	3893201.667000	37 51 37.1712	284 29 26.6514	-22.7571
BDALAS	7067	2308538.082000	-4874075.622000	3393635.082000	32 21 14.0276	295 20 38.1253	-23.0299
GRNTURK	7068	1920482.803000	-5619475.234000	2318921.358000	21 27 38.0463	288 52 5.1988	-18.6689
RAMLAS	7069	917958.152000	-5548366.753000	2998783.678000	28 13 40.9313	279 23 39.4468	-23.5713
WFCMLAS	7070	1261570.285000	-4881564.364000	3893184.329000	37 51 36.6102	284 29 24.8254	-28.7573
1JUM24	7071	976288.131000	-5601387.375000	2880247.155000	27 1 14.3717	279 53 13.1683	-17.1686
1JUM40	7072	976291.901000	-5601381.235000	2880258.186000	27 1 14.7707	279 53 13.3413	-16.9689
1JUPC1	7073	976298.392000	-5601380.427000	2880256.241000	27 1 14.7097	279 53 13.5783	-17.5688
1JUBC4	7074	976299.001000	-5601377.656000	2880262.710000	27 1 14.9357	279 53 13.6173	-16.9686
1SUDBR	7075	692632.551000	-4347058.865000	4600492.858000	46 27 21.5533	279 3 10.9597	250.5663
1JAMAC	7076	1384174.482000	-5905661.874000	1966555.590000	18 4 34.8917	283 11 27.3567	435.2710
1GSFCN	7077	1130077.869000	-4833029.111000	3992265.813000	38 59 57.4187	283 9 38.4381	16.9530
WALMOT	7078	1261602.273000	-4881343.277000	3893447.085000	37 51 47.4404	284 29 28.3556	-30.1641
1CARVN	7079	-2328603.726000	5299341.378000	-2669685.615000	-24 54 23.4104	113 43 16.8575	2.9745
PATRICK	7081	917899.473000	-5548370.254000	2998789.456000	28 13 41.1908	279 23 37.3025	-26.2338
BEARLAKE	7082	-1735997.850000	-4425042.770000	4241435.989000	41 56 1.1377	248 34 45.5581	1962.9933
OWENS084	7084	-2410591.023000	-4477740.288000	3838653.927000	37 13 55.8799	241 42 15.1318	1178.0906
GLDST085	7085	-2353395.031000	-4641524.591000	3676904.548000	35 25 28.1911	243 6 48.9479	965.4002
MCDON086	7086	-1330125.959000	-5328522.319000	3236156.905000	30 40 37.5635	255 59 2.5634	1961.4090
YARAGADE	7090	-2389005.423000	5043325.366000	-3078532.454000	-29 2 47.6760	115 20 48.2987	241.3202

338

NAME	I.D.	X	Y	Z	LATITUDE	LONGITUDE	HEIGHT
HAYSTACK	7091	1492452.890000	-4457273.259000	4296821.737000	42 37 21.9617	288 30 44.5318	91.9873
KWADJLAS	7092	-6143447.454000	1364701.263000	1034160.176000	9 23 37.5885	167 28 32.5869	32.8943
SAMOALAS	7096	-6100045.486000	-996205.338000	-1568976.100000	-14 20 7.5069	189 16 30.5733	48.9818
GORF100	7100	1131355.271000	-4831163.669000	3994137.992000	39 1 15.7277	283 10 47.8010	10.1821
GORF101	7101	1131239.188000	-4831174.383000	3994154.926000	39 1 16.4817	283 10 43.0010	8.3861
GORF102	7102	1130685.810000	-4831347.958000	3994117.232000	39 1 14.6568	283 10 18.9580	17.9634
GORF103	7103	1130684.866000	-4831343.606000	3994122.634000	39 1 14.8838	283 10 18.9610	17.9052
GORF104	7104	1131095.124000	-4831191.890000	3994176.935000	39 1 17.3588	283 10 37.0040	9.9705
GORF105	7105	1130718.983000	-4831345.460000	3994112.813000	39 1 14.4407	283 10 20.3244	19.1645
QUINC109	7109	-2517235.448000	-4198550.859000	4076574.635000	39 58 30.2183	239 3 18.9461	1106.2919
MONPEAK	7110	-2386278.541000	-4802349.879000	3444887.127000	32 53 30.4746	243 34 38.3005	1838.9476
VANDENB	7111	-2668830.842000	-4530782.286000	3598709.230000	34 33 58.7920	239 30 0.1313	626.7517
PLATVL	7112	-1240679.001000	-4720458.044000	4094486.505000	40 10 58.2580	255 16 26.3902	1501.5515
OWENS114	7114	-2410423.050000	-4477797.657000	3838692.069000	37 13 57.4359	241 42 22.2338	1177.9945
GLDST115	7115	-2350862.271000	-4655541.514000	3661003.506000	35 14 54.1284	243 12 28.9809	1038.5943
MAUILAS	7120	-5465998.744000	-2404405.737000	2242230.454000	20 42 27.4667	203 44 38.1444	3067.7242
HUAHINE	7121	-5345864.877000	-2958248.945000	-1824620.993000	-16 44 0.5754	208 57 32.0009	43.5516
MAZATLAN	7122	-1660089.961000	-5619097.054000	2511644.801000	23 20 34.5020	253 32 27.2487	30.8389
GORF1251	7125	1130743.438000	-4831365.212000	3994084.486000	39 1 13.2206	283 10 21.1271	20.6016
HOLLAS	7210	-5466006.852000	-2404425.027000	2242189.498000	20 42 26.0470	203 44 38.6415	3067.4500
MONPEAKT	7220	-2386292.850000	-4802343.054000	3444886.538000	32 53 30.4541	243 34 37.6908	1838.8421
BARSTOW	7265	-2356476.427000	-4646613.334000	3668430.278000	35 19 52.5993	243 6 31.2485	895.8857
MTLAGUNA	7274	-2386291.134000	-4802340.426000	3444886.484000	32 53 30.5076	243 34 37.7049	1836.1954
SNTIAGOL	7400	1769700.612000	-5044619.215000	-3468256.468000	-33 8 58.4901	289 19 52.8881	725.3650
CERROTL	7401	1815518.227000	-5213470.794000	-3187995.444000	-30 10 20.6561	289 11 59.8451	2158.5624
ASKITES	7510	4353445.920000	2082674.201000	4156503.948000	40 55 40.7134	25 33 58.6765	184.1009
DIONYSOS	7515	4595217.892000	2039442.831000	3912626.422000	38 4 42.7711	23 55 57.1260	512.1019
ROUMELLI	7517	4728694.568000	2174383.801000	3674569.898000	35 24 15.1174	24 41 39.3802	104.1018
KARITZ	7520	4596043.243000	1733486.324000	4055718.246000	39 44 3.1556	20 39 53.7644	599.9742
JRUSLM	7530	4436653.779000	3131126.067000	3335786.090000	31 44 2.6143	35 12 43.7988	757.9412
MATERA40	7540	4641968.380000	1393063.494000	4133231.399000	40 38 55.0053	16 42 16.5601	516.7544
MATERA41	7541	4641993.122000	1393048.174000	4133230.248000	40 38 54.5695	16 42 15.6330	530.6437
PUNSAMEN	7545	4893400.699000	772679.294000	4004140.157000	39 8 7.6904	8 58 22.9807	232.1879
TRIESTE	7550	4336739.199000	1071281.849000	4537909.914000	45 38 34.5399	13 52 32.4804	448.4463
MTGENERO	7590	4390311.858000	696761.146000	4560853.602000	45 55 39.5797	9 1 4.3478	1663.4743
WETZL596	7596	4075584.698000	931843.821000	4801558.909000	49 8 38.8751	12 52 43.5497	660.2469
WETZL597	7597	4075604.248000	931833.091000	4801546.599000	49 8 38.2065	12 52 42.8187	661.8388
WETZL599	7599	4075516.968000	931760.151000	4801629.999000	49 8 42.4533	12 52 40.2703	658.6266
SAFLAS	7804	5105611.229000	-555233.140000	3769639.160000	36 27 45.4103	353 47 36.5916	67.9012
METSAHVI	7805	2892595.047000	1311815.105000	5512609.368000	60 13 2.2114	24 23 40.8263	78.2898
HAULAS	7809	4578354.440000	457992.130000	4403170.357000	43 55 56.3997	5 42 45.1244	706.5983
ZIMRWALD	7810	4331285.030000	567559.507000	4633143.586000	46 52 38.0360	7 27 55.2402	955.5510
CANISL	7819	5440495.604000	-1501675.583000	2961259.663000	27 50 37.4029	344 34 10.3013	121.2828
DAKLAS	7820	5886274.041000	-1845649.974000	1615245.180000	14 46 2.8382	342 35 27.9817	48.1843
HELWAN	7831	4728281.385000	2879673.940000	3156890.992000	29 51 32.3280	31 20 33.8847	130.1489
KOOTWIJK	7833	3899223.487000	396749.080000	5015074.070000	52 10 42.2477	5 48 35.6243	93.4801
WETTZELL	7834	4075529.405000	931787.187000	4801617.581000	49 8 41.7460	12 52 41.4339	661.1067
GRASSE	7835	4581691.193000	556164.708000	4389359.447000	43 45 16.8840	6 55 16.2747	1322.9373
SHANGHAI	7837	-2831099.391000	4676208.174000	3275167.461000	31 5 50.9148	121 11 30.2116	29.2218
SIMOSATO	7838	-3822387.162000	3699366.723000	3507566.454000	33 34 39.4932	135 56 13.2192	99.0526
GRAZ	7839	4194426.092000	1162699.512000	4647245.773000	47 4 1.6445	15 29 36.3548	539.4764
RGOLAS	7840	4033463.109000	23668.353000	4924305.460000	50 52 2.5912	0 20 10.3476	75.2802
GRASSE	7842	4582050.519000	554736.161000	4389150.208000	43 45 7.8481	6 54 10.9638	1311.7171
NATMAP	7843	-4446475.905000	2678122.786000	-3696256.267000	-35 38 10.6996	148 56 21.6480	1350.2505
CABSL882	7882	-1997242.190000	-5528036.285000	2468364.902000	22 55 3.5269	250 8 7.9954	111.0910
MCDON885	7885	-1330126.074000	-5328522.270000	3236156.903000	30 40 37.5638	255 59 2.5588	1961.3910
QUINC886	7886	-2517243.158000	-4198548.760000	4076577.109000	39 58 30.2346	239 3 18.6220	1109.5399
VANDN887	7887	-2668868.722000	-4530738.717000	3598690.293000	34 33 58.6232	239 29 57.9836	600.9262
MTHOPKIN	7888	-1936744.915000	-5077634.665000	3332000.152000	31 41 6.6096	249 7 18.5466	2331.2920
GORF889	7889	1131364.030000	-4831163.716000	3994135.281000	39 1 15.6177	283 10 48.1551	10.0624
AUSTIN	7890	-754162.717000	-5459056.967000	3200750.958000	30 18 56.0496	262 8 3.9743	257.2461
FLAGSTAF	7891	-1923977.301000	-4850866.722000	3658580.761000	35 12 52.5769	248 21 55.6633	2144.2609
VERNAL	7892	-1631485.491000	-4589128.521000	4106755.294000	40 19 36.8912	250 25 44.9131	1590.3207
YUMA	7894	-2196778.378000	-4887334.614000	3448434.259000	32 56 21.1695	245 47 48.6551	241.6952
JPLLAS	7896	-2493212.494000	-4655224.980000	3565580.077000	34 12 20.2046	241 49 39.7315	441.6185
MCDON897	7897	-1330802.109000	-5328719.688000	3235713.110000	30 40 19.2891	255 58 39.7219	2040.5716
GORF899	7899	1131364.030000	-4831163.717000	3994135.282000	39 1 15.6177	283 10 48.1551	10.0638
ORGLAS	7901	-1535788.518000	-5166982.633000	3401042.783000	32 25 24.8068	253 26 47.0671	1626.6594
OLILAS	7902	5056122.298000	2716520.205000	-2775767.582000	-25 57 36.0836	28 14 52.6461	1569.4682
AREQUIPA	7907	1942791.903000	-5804080.070000	-1796911.637000	-16 27 56.4184	288 30 24.7320	2492.2662
GORF18	7918	1130708.448000	-4831340.981000	3994124.391000	39 1 14.8705	283 10 19.9404	21.2007
GORF19	7919	1130693.793000	-4831336.327000	3994133.143000	39 1 15.2517	283 10 19.3913	20.5958
GORF20	7920	1130744.819000	-4831365.034000	3994086.238000	39 1 13.2619	283 10 21.1847	21.8145
HOPLAS	7921	-1936760.950000	-5077702.716000	3331929.098000	31 41 3.4660	249 7 18.8984	2352.9399
NATAL	7929	5186467.775000	-3653857.284000	-654316.651000	-5 55 39.9399	324 50 7.3422	39.5952
GRELAS	7930	4595222.026000	2039459.557000	3912615.037000	38 4 42.2692	23 55 57.6844	513.3957
DODAIR	7935	-3910418.452000	3376364.722000	3729239.156000	36 0 20.7222	139 11 30.3195	902.9204
MATERA	7939	4641964.690000	1393074.846000	4133261.132000	40 38 55.7423	16 42 17.0680	535.9172
DIONYSOS	7940	4599578.363000	2040864.682000	3906778.504000	38 0 42.2298	23 55 37.8905	501.1291
ORRORAL	7943	-4447547.753000	2677129.639000	-3695000.954000	-35 37 29.9285	148 57 17.4255	948.9088

339

NAME	I.D.	X	Y	Z	LATITUDE	LONGITUDE	HEIGHT
KOOT883	8833	3899237.136000	396775.269000	5015055.290000	52 10 41.4604	5 48 36.9228	88.5977
OLISAO	9902	5056122.298000	2716520.205000	-2775767.582000	-25 57 36.0836	28 14 52.6461	1569.4682
ARESAO	9907	1942791.903000	-5804080.070000	-1796911.637000	-16 27 56.4184	288 30 24.7320	2492.2662
HOPSAO	9921	-1936760.950000	-5077702.716000	3331929.098000	31 41 3.4660	249 7 18.8984	2352.9399
NATSAO	9929	5186467.775000	-3653857.284000	-654316.649000	-5 55 39.9399	324 50 7.3422	39.5950
GRESAO	9940	4595214.996000	2039466.003000	3912612.430000	38 4 42.2788	23 55 58.0431	508.7882
ACSDOP	10068	6119386.038000	-1571424.522000	-871688.464000	-7 54 28.1129	345 35 52.6247	46.2993
KWJDOP	10214	-6160997.731000	1339618.542000	960416.572000	8 43 6.9791	167 43 58.1446	35.7283
QUIDOP	30121	1280855.752000	-6250961.609000	-10805.525000	0 5 51.6484	281 34 47.7272	2711.6928
SHIDOP	30123	6104423.692000	-611086.597000	-1740830.697000	-15 56 34.8342	354 17 0.3124	603.3940
HONDOP	30188	-5511608.533000	-2226970.519000	2303886.656000	21 18 52.5588	202 0 4.3794	20.4519
STODOP	30280	1743940.474000	-5022701.110000	-3512033.120000	-33 37 26.0082	289 8 51.3537	448.5113
CALDOP	30414	-1659604.189000	-3676719.050000	4925498.638000	50 52 17.1118	245 42 23.2134	1248.3641
NAPDOP	30448	-4923683.543000	270895.598000	-4031782.997000	-39 27 31.6054	176 51 2.9697	18.7144
EASDOP	30730	-1888662.883000	-5355677.851000	-2893870.151000	-27 9 30.4145	250 34 29.8655	48.9958
TVEDOP	30793	-5037686.750000	3301866.496000	-2090790.183000	-19 15 43.8524	146 45 28.2275	66.0787
BGKDOP	30800	-1139091.837000	6089774.901000	1510692.599000	13 47 32.9828	100 35 41.0666	-13.3294
DGCDOP	30939	1915631.725000	6030276.750000	-801056.456000	-7 15 49.0645	72 22 35.6272	-57.4495
LAJDOP	30966	4432069.966000	-2258084.956000	3973470.407000	38 46 51.3245	332 53 57.0433	132.7341
BDADOP	30967	2293704.122000	-4883222.062000	3390598.216000	32 19 16.9668	295 9 35.8925	-4.7505
PERDOP	30968	-2353567.078000	4877202.497000	-3358333.914000	-31 58 39.4446	115 45 37.1833	13.1668
CNIDOP	30970	5384988.857000	-1576474.618000	3023843.496000	28 28 54.5056	343 40 56.7134	626.5256
UKIDOP	51960	-2713391.456000	-4144609.641000	4004304.887000	39 8 16.2157	236 47 16.9749	170.0838
POTSDAM	18113901	3800618.509000	882010.731000	5028856.705000	52 22 48.9239	13 3 55.3462	144.7284
QUINO511	70510101	-2516895.280000	-4198842.164000	4076418.824000	39 58 24.7868	239 3 37.5502	1063.6237
QUINO512	70510202	-2516895.254000	-4198842.117000	4076418.769000	39 58 24.7865	239 3 37.5501	1063.5472
QUINO513	70510203	-2516895.254000	-4198842.131000	4076418.778000	39 58 24.7865	239 3 37.5504	1063.5622
QUINO514	70510804	-2516895.110000	-4198841.926000	4076418.548000	39 58 24.7860	239 3 37.5512	1063.2229
EASTER1	70611201	-1884984.664000	-5357611.696000	-2892846.837000	-27 8 51.9068	250 36 59.2014	117.6193
EASTER2	70611202	-1884984.664000	-5357611.696000	-2892846.837000	-27 8 51.9068	250 36 59.2014	117.6193
OTAYMT1	70620201	-2428827.802000	-4799748.813000	3417280.328000	32 36 2.8873	243 9 32.8229	992.1153
OTAYMT2	70620302	-2428827.818000	-4799748.845000	3417280.357000	32 36 2.8875	243 9 32.8230	992.1611
OTAYMT3	70620303	-2428827.812000	-4799748.810000	3417280.322000	32 36 2.8871	243 9 32.8226	992.1136
OTAYMT4	70621104	-2428829.163000	-4799747.956000	3417280.275000	32 36 2.8885	243 9 32.7615	991.9603
OTAYMT5	70621205	-2428827.125000	-4799747.476000	3417279.376000	32 36 2.8875	243 9 32.8230	990.3399
STALAS1	70632101	1130714.571000	-4831364.967000	3994095.557000	39 1 13.6387	283 10 19.9610	22.2757
GORF0641	70640101	1130678.623000	-4831336.991000	3994135.988000	39 1 15.3807	283 10 18.7710	20.2036
GORF0642	70640102	1130678.623000	-4831336.980000	3994135.982000	39 1 15.3808	283 10 18.7711	20.1915
GORF0651	70650201	1130695.004000	-4831351.484000	3994120.285000	39 1 14.6208	283 10 19.2967	24.1806
GORF0652	70650203	1130695.017000	-4831351.530000	3994120.307000	39 1 14.6204	283 10 19.2968	24.2316
GORF0653	70650302	1130694.853000	-4831351.610000	3994120.252000	39 1 14.6182	283 10 19.2894	24.2285
WFCL0661	70662701	1261613.824000	-4881554.445000	3893207.239000	37 51 37.1712	284 29 26.6514	-13.6775
BDALAS1	70670101	2308539.420000	-4874078.448000	3393637.063000	32 21 14.0276	295 20 38.1253	-19.3284
BDALAS2	70670102	2308539.410000	-4874078.444000	3393637.052000	32 21 14.0274	295 20 38.1250	-19.3410
GTILAS1	70680201	1920483.885000	-5619478.384000	2318922.667000	21 27 38.0463	288 52 5.1990	-15.0903
GTILAS2	70680202	1920483.882000	-5619478.480000	2318922.712000	21 27 38.0466	288 52 5.1978	-14.9902
RAMLAS1	70692201	917958.646000	-5548166.239000	2998785.303000	28 13 40.9313	279 23 39.4468	-20.1361
WFCL0701	70700201	1261570.949000	-4881566.932000	3893186.391000	37 51 36.6102	284 29 24.8254	-25.3976
PATLAS1	70810201	917899.965000	-5548373.228000	2998791.074000	28 13 41.1908	279 23 37.3025	-22.8126
BARLAS1	70820101	-1735998.872000	-4425045.384000	4241438.513000	41 56 1.1377	248 34 45.5583	1966.7679
BARLAS2	70820102	-1735998.883000	-4425045.418000	4241438.537000	41 56 1.1376	248 34 45.5584	1966.8105
BARLAS3	70821103	-1735998.035000	-4425046.288000	4241437.531000	41 56 1.1025	248 34 45.6064	1966.5103
BARLAS4	70821104	-1735997.926000	-4425046.270000	4241437.600000	41 56 1.1054	248 34 45.6105	1966.5144
OWNS0841	70840201	-2410592.341000	-4477742.737000	3838656.041000	37 13 55.8799	241 42 15.1318	1181.5839
GLDS0851	70850101	-2353396.463000	-4641527.398000	3676906.786000	35 25 28.1911	243 6 48.9476	969.2653
MCDN0861	70860101	-1330126.754000	-5328525.475000	3236158.844000	30 40 37.5638	255 59 2.5631	1965.1974
MCDN0862	70861102	-1330127.026000	-5328526.018000	3236157.350000	30 40 37.5122	255 59 2.5582	1964.9449
MCDN0863	70862403	-1330121.606000	-5328527.968000	3236153.351000	30 40 37.3910	255 59 2.7734	1963.4028
YARAG1	70900501	-2389006.624000	5043327.876000	-3078534.003000	-29 2 47.6761	115 20 48.2991	244.5048
HAYSTK1	70910301	1492453.768000	-4457275.873000	4296824.275000	42 37 21.9617	288 30 44.5319	95.7350
HAYSTK2	70910702	1492453.680000	-4457275.629000	4296824.015000	42 37 21.9612	288 30 44.5316	95.3681
KWAJL1	70920801	-6143450.492000	1364701.891000	1034160.674000	9 23 37.5881	167 28 32.5884	36.0359
SAMOAL1	70960601	-6100048.544000	-996205.837000	-1568976.891000	-14 20 7.5069	189 16 30.5733	52.1796
GORF1001	71000301	1131355.891000	-4831166.327000	3994140.204000	39 1 15.7277	283 10 47.8009	13.6953
GORF1002	71000402	1131355.856000	-4831166.075000	3994140.005000	39 1 15.7279	283 10 47.8019	13.3732
GORF1011	71010602	1131239.098000	-4831176.841000	3994157.002000	39 1 16.4856	283 10 42.9741	11.5366
GORF1012	71010801	1131239.046000	-4831176.808000	3994157.029000	39 1 16.4872	283 10 42.9723	11.5194
GORF1021	71020305	1130686.437000	-4831350.557000	3994119.473000	39 1 14.6586	283 10 18.9587	21.4515
GORF1022	71020402	1130686.374000	-4831350.385000	3994119.248000	39 1 14.6567	283 10 18.9578	21.1685
GORF1023	71020403	1130686.414000	-4831350.328000	3994119.224000	39 1 14.6570	283 10 18.9600	21.1174
GORF1024	71020404	1130686.420000	-4831350.378000	3994119.229000	39 1 14.6565	283 10 18.9598	21.1594
GORF1025	71020501	1130686.381000	-4831350.390000	3994119.245000	39 1 14.6565	283 10 18.9581	21.1717
GORF1031	71030601	1130685.399000	-4831346.029000	3994124.644000	39 1 14.8837	283 10 18.9596	21.0980
GORF1032	71030602	1130685.427000	-4831346.031000	3994124.591000	39 1 14.8822	283 10 18.9607	21.0711
GORF1041	71040701	1131095.729000	-4831194.201000	3994178.959000	39 1 17.3610	283 10 37.0066	13.1002
GORF1051	71050701	1130719.513000	-4831347.838000	3994114.808000	39 1 14.4413	283 10 20.3233	22.3133
GORF1052	71050702	1130719.513000	-4831347.838000	3994114.808000	39 1 14.4413	283 10 20.3233	22.3133
GORF1053	71050703	1130718.983000	-4831345.460000	3994112.813000	39 1 14.4407	283 10 20.3244	19.1645
GORF1054	71050704	1130718.983000	-4831345.460000	3994112.813000	39 1 14.4407	283 10 20.3244	19.1645
QUINIO91	71090801	-2517236.706000	-4198552.978000	4076576.716000	39 58 30.2186	239 3 38.9466	1109.5173

NAME	I.D.	X	Y	Z	LATITUDE	LONGITUDE	HEIGHT
QUIN1092	71090802	-2517236.680000	-4198552.934000	4076576.619000	39 58 30.2173	239 3 18.9465	1109.4158
QUIN1093	71091503	-2517235.448000	-4198550.859000	4076574.635000	39 58 30.2183	239 3 18.9461	1106.2919
LAGU1101	71100301	-2386279.860000	-4802352.528000	3444889.032000	32 53 30.4744	243 34 38.3004	1842.4669
LAGU1102	71100402	-2386279.761000	-4802352.301000	3444888.842000	32 53 30.4736	243 34 38.2999	1842.1560
VAND1111	71111101	-2668830.288000	-4530786.549000	3598710.144000	34 33 58.7540	239 30 0.2349	630.0635
PLATVL1	71120201	-1240679.684000	-4720460.634000	4094488.774000	40 10 58.2581	255 16 26.3901	1505.0619
OWNS1141	71140201	-2410424.425000	-4477800.195000	3838694.258000	37 13 57.4358	241 42 22.2335	1181.6171
OWNS1142	71141102	-2410424.314000	-4477799.072000	3838695.370000	37 13 57.4850	241 42 22.2159	1181.4608
OWNS1143	71141103	-2410424.264000	-4477799.144000	3838695.409000	37 13 57.4852	241 42 22.2191	1181.5160
GLDS1151	71150301	-2350863.626000	-4655544.133000	3661005.598000	35 14 54.1287	243 12 28.9797	1042.2096
MAUI1201	71200101	-5466001.828000	-2404407.104000	2242231.716000	20 42 27.4663	203 44 38.1447	3071.3259
HUAHNE1	71210101	-5345867.943000	-2958250.648000	-1824622.047000	-16 44 0.5754	208 57 32.0011	47.2137
MAZATL1	71220601	-1660090.795000	-5619099.854000	2511646.062000	23 20 34.5020	253 32 27.2484	34.0210
GORF1251	71251501	1130743.438000	-4831365.212000	3994084.486000	39 1 13.2206	283 10 21.1271	20.6016
HOLLAS1	72102301	-5466007.345000	-2404425.239000	2242190.501000	20 42 26.0714	203 44 38.6414	3068.3066
MNPK2201	72201101	-2386293.129000	-4802345.089000	3444889.510000	32 53 30.5008	243 34 37.7160	1842.0906
MNPK2202	72201102	-2386292.850000	-4802343.054000	3444886.538000	32 53 30.4541	243 34 37.6908	1838.8421
BARSTOW1	72651101	-2356478.931000	-4646614.953000	3668432.680000	35 19 52.6145	243 6 31.1890	899.3767
MTLAGUNA	72741101	-2386291.134000	-4802340.426000	3444886.484000	32 53 30.5076	243 34 37.7049	1836.1954
SNTI4001	74001101	1769700.612000	-5044619.215000	-3468256.468000	-33 8 58.4901	289 19 52.8881	725.3650
CERR4011	74011101	1815518.227000	-5213470.794000	-3187995.444000	-30 10 20.6561	289 11 59.8451	2158.5624
ASKITES	75101501	4353445.920000	2082674.201000	4156503.948000	40 55 40.7134	25 33 58.6765	184.1009
DIONYS	75151501	4595217.892000	2039442.831000	3912626.421000	38 4 42.7711	23 55 57.1260	512.1012
ROUM1716	75171601	4728694.568000	2174383.801000	3674569.898000	35 24 15.1174	24 41 39.3802	104.1018
KARITZ	75215010	4596043.243000	1733486.324000	4055718.246000	39 44 3.1556	20 39 53.7644	599.9742
JRUSLM	75300000	4436653.778000	3131126.067000	3335786.090000	31 44 2.6143	35 12 43.7988	757.9405
MATERA40	75401501	4641986.380000	1393063.494000	4133231.399000	40 38 54.6412	16 42 16.3399	529.8350
MATERA41	75411601	4641993.122000	1393048.174000	4133230.248000	40 38 54.5695	16 42 15.6330	530.6437
PUNSAMEN	75450000	4893400.699000	772679.294000	4004140.157000	39 8 7.6904	8 58 22.9807	232.1879
TRIESTE	75501601	4336739.199000	1071281.849000	4537909.914000	45 38 34.5399	13 52 32.4804	448.4463
MTGENERO	75900000	4390311.858000	696761.146000	4560385.602000	45 55 39.1743	9 1 4.3478	1650.5420
WETZ0105	75961502	4075584.698000	931843.821000	4801558.909000	49 8 38.8751	12 52 43.5497	660.2469
WETZ5961	75961601	4075584.698000	931843.821000	4801558.909000	49 8 38.8751	12 52 43.5497	660.2469
WETZ5971	75971501	4075604.248000	931833.091000	4801546.599000	49 8 38.2065	12 52 42.8187	661.8388
WETZ5991	75991501	4075516.968000	931760.151000	4801629.999000	49 8 42.4533	12 52 40.2703	658.6266
METZAHVI	78053301	2892595.047000	1311815.105000	5512609.368000	60 13 2.2114	24 23 40.8263	78.2898
ZIMRWLD1	78104801	4331285.030000	567559.507000	4633143.586000	46 52 38.0360	7 27 55.2402	955.5510
HELWAN1	78314601	4728281.385000	2879673.940000	3156890.992000	29 51 32.3280	31 20 33.8847	130.1489
KOOTWIK1	78333201	3899223.487000	396749.080000	5015074.070000	52 10 42.2477	5 48 35.6243	93.4801
WETZELL	78343001	4075529.405000	931787.187000	4801617.581000	49 8 41.7460	12 52 41.4339	661.1067
GRASSE1	78353101	4581691.193000	556164.708000	4389359.447000	43 45 16.8840	6 55 16.2747	1322.9373
SHNGHAI1	78373701	-2831089.391000	4676208.174000	3275167.461000	31 5 50.9148	121 11 30.2116	29.2218
SIMOSATA	78383601	-3822388.419000	3699367.939000	3507567.615000	33 34 39.4932	135 56 13.2192	101.1518
GRAZ1	78393401	4194426.092000	1162699.512000	4647245.773000	47 4 1.6445	15 29 36.3548	539.4764
RGOLAS1	78403501	4033463.109000	23668.353000	4924305.460000	50 52 2.5912	0 20 10.3476	75.2802
NATMAP1	78432501	-4446475.905000	2678122.786000	-3696256.267000	-35 38 10.6996	148 56 21.6480	1350.2505
CABO8821	78821201	-1997242.723000	-5528037.760000	2468365.566000	22 55 3.5270	250 8 7.9954	112.7941
MCDN8851	78851101	-1330126.247000	-5328524.621000	3236159.986000	30 40 37.6114	255 59 2.5738	1964.9618
QUIN8861	78861101	-2517243.158000	-4198548.760000	4076577.109000	39 58 30.2346	239 3 18.6220	1109.5399
QUIN8862	78861102	-2517243.158000	-4198548.760000	4076577.109000	39 58 30.2346	239 3 18.6220	1109.5399
VNDN8871	78871101	-2668870.125000	-4530742.008000	3598691.031000	34 33 58.5776	239 29 58.0017	604.2663
MTHOPKN1	78881101	-1936745.913000	-5077638.237000	3332000.678000	31 41 6.5612	249 7 18.5595	2334.7109
GORF8891	78891201	1131364.574000	-4831165.237000	3994138.563000	39 1 15.6676	283 10 48.1627	13.3757
GORF8892	78891302	1131364.590000	-4831165.242000	3994138.549000	39 1 15.6671	283 10 48.1633	13.3735
AUSTIN1	78901101	-754162.240000	-5459060.531000	3200751.323000	30 18 56.0015	262 8 3.9849	260.5025
AUSTIN2	78901102	-754164.193000	-5459059.415000	3200753.004000	30 18 56.0639	262 8 3.9321	260.5466
FLGSTAF1	78911101	-1923979.299000	-4850868.905000	3658582.712000	35 12 52.5769	248 21 55.6216	2147.6448
VERNAL1	78921101	-1631485.501000	-4589131.270000	4106757.427000	40 19 36.8896	250 25 44.9517	1593.6783
VERNAL2	78921102	-1631485.474000	-4589131.400000	4106757.467000	40 19 36.8920	250 25 44.9519	1593.6528
YUMA1	78941101	-2196778.378000	-4887334.614000	3448434.259000	32 56 21.1695	245 47 48.6551	241.6952
JPL1	78961101	-2493213.111000	-4655226.798000	3565583.186000	34 12 20.2535	241 49 39.7438	444.9326
MCDN8971	78971101	-1330802.872000	-5328723.160000	3235713.379000	30 40 19.2377	255 58 39.7257	2043.7685
MCDN8972	78971102	-1330802.873000	-5328723.262000	3235713.478000	30 40 19.2388	255 58 39.7266	2043.9043
GORF8991	78991101	1131364.574000	-4831165.238000	3994138.563000	39 1 15.6676	283 10 48.1627	13.3765
GORF8992	78991102	1131364.590000	-4831165.242000	3994138.550000	39 1 15.6671	283 10 48.1633	13.3742
AREQUI71	79074001	1942791.873000	-5804080.083000	-1796911.642000	-16 27 56.4185	288 30 24.7309	2492.2703
GORF1813	79181301	1130708.884000	-4831342.845000	3994125.943000	39 1 14.8705	283 10 19.9404	23.6651
GORF1914	79191401	1130694.251000	-4831338.287000	3994134.775000	39 1 15.2517	283 10 19.3913	23.1871
GORF2011	79201101	1130745.039000	-4831366.608000	3994089.505000	39 1 13.3119	283 10 21.1787	25.1010
GOR22011	79201102	1130744.819000	-4831365.034000	3994086.238000	39 1 13.2619	283 10 21.1847	21.8145
HOPLAS71	79214301	-1936760.949000	-5077702.714000	3331929.105000	31 41 3.4662	249 7 18.8984	2352.9417
NATAL71	79294101	5186467.770000	-3653857.284000	-654316.651000	-5 55 39.9399	324 50 7.3422	39.5952
DODAIR	79350000	-3910418.452000	3376364.722000	3729239.156000	36 0 20.7222	139 11 30.3195	902.9204
MATERA1	79394101	4641964.690000	1393074.846000	4133261.132000	40 38 55.7423	16 42 17.0680	535.9172
DIONYS71	79404701	4599578.363000	2040864.682000	3906778.504000	38 0 42.2298	23 55 37.8905	501.1291
ORRORL71	79434201	-4447547.753000	2677129.639000	-3695000.954000	-35 37 29.9285	148 57 17.4255	948.9088
KOOT8331	88331501	3899237.136000	396775.269000	5015055.290000	52 10 41.4604	5 48 36.9228	88.5977
KOOT8332	88331602	3899237.136000	396775.269000	5015055.290000	52 10 41.4604	5 48 36.9228	88.5977
KOOT8333	88331603	3899237.136000	396775.269000	5015055.290000	52 10 41.4604	5 48 36.9228	88.5977
OLIS9902	99024001	5056122.298000	2716520.205000	-2775767.582000	-25 57 36.0836	28 14 52.6461	1569.4682
AREQUI91	99074001	1942791.873000	-5804080.083000	-1796911.642000	-16 27 56.4185	288 30 24.7309	2492.2703
HOPLAS91	99214301	-1936760.949000	-5077702.714000	3331929.105000	31 41 3.4662	249 7 18.8984	2352.9417
NATAL91	99294101	5186467.770000	-3653857.284000	-654316.651000	-5 55 39.9399	324 50 7.3422	39.5952
DIONYS91	99404701	4595214.996000	2039466.003000	3912612.430000	38 4 42.2788	23 55 58.0431	508.7882
ORRORL91	99434201	-4447547.753000	2677129.639000	-3695000.954000	-35 37 29.9285	148 57 17.4255	948.9088

341

APPENDIX 2

APRIORI STATION POSITIONS FOR GEM-T1

OPTICAL & DOPPLER TRACKING SITES

as of February 11, 1987

343

TOPEX GEODETIC FILE CREATED 02/11/87
SEMI-MAJOR AXIS: 6378137.00   FLATTENING: 1/298.257

NAME	I.D.	X	Y	Z	LATITUDE	LONGITUDE	HEIGHT
1BPOIN	1021	1118042.673000	-4876303.718000	3942974.315000	38 25 50.1059	282 54 49.0319	-35.1079
1FTMYR	1022	807877.886000	-5651970.293000	2833513.886000	26 32 53.5470	278 8 4.5896	-22.3786
1OOMER	1024	-3977275.856000	3725643.767000	-3302983.031000	-31 23 25.1614	136 52 15.6789	135.9607
1SATAG	1028	1769719.956000	-5044619.692000	-3468246.138000	-33 8 58.0878	289 19 53.5863	725.4544
1MOJAV	1030	-2357228.652000	-4646321.402000	3668322.198000	35 19 48.2390	243 5 59.4610	898.5917
1JOBUR	1031	5084791.750000	2670402.009000	-2768144.919000	-25 53 1.0486	27 42 26.2858	1550.2946
1NEWFL	1032	2602767.335000	-3419137.999000	4697657.623000	47 44 29.6192	307 16 46.7707	77.0941
1COLEG	1033	-2299248.779000	-1445691.272000	5751818.453000	64 52 18.4528	212 9 37.1439	181.2022
1GFORK	1034	-521692.908000	-4242035.759000	4718733.398000	48 1 21.6883	262 59 19.9354	227.6111
1WNKFL	1035	3983119.138000	-48488.686000	4964717.894000	51 26 45.9081	359 18 9.1498	117.3075
1ULASK	1036	-2282348.390000	-1452629.676000	5756906.658000	64 58 37.2922	212 28 30.8390	308.8093
1ROSMN	1037	647535.550000	-5177922.122000	3656717.613000	35 12 7.5231	277 7 41.6406	880.8541
1ORORL	1038	-4447486.306000	2677158.222000	-3695055.561000	-35 37 32.0848	148 57 15.1933	949.9060
1ROSMA	1042	647529.510000	-5177922.522000	3656716.313000	35 12 7.4952	277 7 41.4017	879.8166
1TANAN	1043	4091868.993000	4434290.059000	-2064734.326000	-19 0 32.2311	47 17 59.3996	1374.9833
MADGAR	1122	4091329.793000	4434216.058000	-2065984.225000	-19 1 15.1045	47 18 11.2313	1385.0988
MADGAS	1123	4091343.393000	4434216.058000	-2065970.925000	-19 1 14.6291	47 18 10.7968	1386.7038
ROSRAN	1126	647205.415000	-5178319.808000	3656150.566000	35 11 45.8756	277 7 26.7424	842.9914
ULASKR	1128	-2282490.491000	-1453373.076000	5756716.860000	64 58 19.5130	212 29 12.8287	356.4167
CARVON	1152	-2328231.626000	5299695.978000	-2669340.215000	-24 54 10.8344	113 42 59.6354	16.2215
MOROC	1804	5105598.670000	-555231.211000	3769632.040000	36 27 45.4693	353 47 36.6141	53.4608
CANARI	1819	5440484.420000	-1501663.783000	2961260.039000	27 50 37.6249	344 34 10.6083	109.1496
HOWARD	2001	1122551.680000	-4823067.408000	4006490.821000	39 9 48.7587	283 6 7.6568	126.8940
NEWMEX	2003	-1555975.516000	-5169337.536000	3387501.796000	32 16 53.8729	253 14 53.3592	1173.4164
SANHES	2008	4083900.485000	-4209792.868000	-2499123.925000	-23 13 3.4584	314 7 49.2870	601.7412
MISAWA	2013	-3779644.939000	3024716.790000	4138986.003000	40 43 13.9770	141 19 51.3907	51.4191
ANCHOR	2014	-2656171.683000	-1544363.513000	5570648.254000	61 17 0.2115	210 10 29.1787	73.3496
TAFUNA	2017	-6100011.515000	-997195.143000	-1568454.805000	-14 19 50.0579	189 17 3.3549	42.0909
THOLEG	2018	539395.656000	-1388369.682000	6181056.264000	76 32 20.1842	291 13 53.9457	64.7609
MCMURD	2019	-1310714.228000	310461.061000	-6213364.320000	-77 50 51.7053	166 40 27.4044	-15.0854
AUSTIN	2092	-741620.291000	-5462204.839000	3198143.740000	30 17 19.7384	262 16 5.0021	165.0000
WAHIWA	2100	-5504142.805000	-2224142.821000	2325303.722000	21 31 15.5563	202 0 10.4627	411.0386
LACRES	2103	-1556205.009000	-5169441.832000	3387263.869000	32 16 44.4660	253 14 46.1116	1186.7089
LASHAM	2106	4005440.205000	-71745.392000	4946709.632000	51 11 9.1373	358 58 25.7826	228.3128
APLMND	2111	1122659.254000	-4823035.989000	4006472.801000	39 9 48.4329	283 6 12.3176	110.6957
SMITHL	2112	-3942235.661000	3468855.745000	-3608201.826000	-34 40 26.4213	138 39 17.1916	32.3723
PRETOR	2115	5051977.208000	2725634.308000	-2774460.696000	-25 56 48.3713	28 20 51.6299	1600.7180
ASAMOA	2117	-6100015.715000	-997194.583000	-1568457.905000	-14 19 50.1229	189 17 3.3138	46.7867
SANMIG	2121	-3088055.247000	5333061.128000	1638815.384000	14 59 16.1733	120 4 21.1942	63.5512
WALDOP	2203	1261687.864000	-4881237.408000	3893561.151000	37 51 51.9753	284 29 32.8297	-24.1640
CANTON	2706	-6303360.092000	-923454.804000	-308728.340000	-2 47 35.2090	188 20 4.7574	34.5854
MAHE	2717	3602875.617000	5238223.545000	-515928.740000	-4 40 14.0263	55 28 46.6236	552.1180
ASCENS	2722	6118431.429000	-1571559.409000	-878444.905000	-7 58 9.9380	345 35 40.6060	96.9358
COCOS	2723	-741966.658000	6190797.586000	-1338588.853000	-12 11 45.2618	96 50 3.4690	-19.2995
MOSLAK	2738	-2127818.698000	-3785834.127000	4656062.131000	47 11 7.6401	240 39 42.9984	355.2917
SHEMAL	2739	-3851514.689000	397264.310000	5051466.845000	52 42 55.7756	174 6 39.7958	50.3803
BELTSV	2742	1130796.551000	-4830813.278000	3994724.458000	39 1 40.0688	283 10 28.5062	15.4582
STNVIL	2745	-84982.690000	-5327948.044000	3493465.591000	33 25 32.4685	269 5 10.2810	13.5933
CARGIL	2809	-4313785.893000	893041.467000	-4596956.426000	-46 24 43.7262	168 18 13.7845	5.3052
PARIBO	2815	3623309.482000	-5214208.712000	601537.041000	5 26 53.3756	304 47 42.3949	-0.1532
MESHED	2817	2604359.352000	4444166.828000	3750327.345000	36 14 25.9684	59 37 44.2297	972.4892
FRTLMY	2822	6023417.038000	1617938.536000	1331706.781000	12 7 53.8046	15 2 6.7821	316.7621
NATLDP	2837	5186372.100000	-3654218.808000	-653027.495000	-5 54 57.7605	324 49 55.9422	35.9026
APLTWO	2911	1122714.880000	-4823027.109000	4006402.121000	39 9 48.5861	283 6 14.6582	119.6539
1UNDAK	7034	-521692.957000	-4242036.158000	4718733.844000	48 1 21.6883	262 59 19.9354	228.2115
1EDINB	7036	-828471.760000	-5657444.892000	2816825.976000	26 22 46.9803	261 40 7.9202	31.3196
1COLBA	7037	-191272.927000	-4967266.077000	3983269.628000	38 53 36.5000	267 47 41.3492	239.1561
1BERMD	7039	2308232.342000	-4873587.010000	3394578.597000	32 21 49.8477	295 20 35.5563	-1.6029
1PURIO	7040	2465070.227000	-5534913.914000	1985531.452000	18 15 28.9986	294 0 23.8776	9.1055
1GSFCP	7043	1130730.821000	-4831318.155000	3994143.543000	39 1 15.7027	283 10 21.0622	19.9526
1DENVR	7045	-1240462.201000	-4760221.025000	4048992.730000	39 38 48.2606	255 23 39.0016	1773.0005
GODLAS	7050	1130692.438000	-4831354.616000	3994112.117000	39 1 14.3647	283 10 19.1632	20.9531
QUINC051	7051	-2516893.830000	-4198839.749000	4076416.458000	39 58 24.7867	239 3 37.5502	1059.9437
WALLAS	7052	1261570.901000	-4881573.970000	3893171.501000	37 51 36.0935	284 29 24.7514	-29.1658
MOBLAS	7053	1130704.646000	-4831318.517000	3994151.264000	39 1 16.0118	283 10 19.9993	20.4535
CRMLAS	7054	-2328184.126000	5299661.478000	-2669470.815000	-24 54 15.3778	113 42 58.5803	25.2383
GMISLS	7060	-5068966.309000	3584085.182000	1458762.160000	13 18 33.6245	144 44 14.0370	139.7523
EASTER	7061	-1884984.612000	-5357611.709000	-2892846.844000	-27 8 51.9071	250 36 59.2033	117.6181
OTAY MT	7062	-2428826.443000	-4799746.127000	3417278.409000	32 36 2.8875	243 9 32.8229	988.5455
STALAS	7063	1130714.033000	-4831362.670000	3994093.645000	39 1 13.6387	283 10 19.9610	19.2390
GORF064	7064	1130678.096000	-4831334.738000	3994134.113000	39 1 15.3807	283 10 18.7710	17.2255
GORF065	7065	1130694.399000	-4831348.899000	3994118.134000	39 1 14.6208	283 10 19.2967	20.7638
WFCLAS	7066	1261612.031000	-4881547.504000	3893201.667000	37 51 37.1712	284 29 26.6514	-22.7571
BDALAS	7067	2308538.082000	-4874075.622000	3393635.082000	32 21 14.0276	295 20 38.1253	-23.0299
GRNTURK	7068	1920482.803000	-5619475.234000	2318921.358000	21 27 38.0463	288 52 5.1988	-18.6689
RAMLAS	7069	917958.152000	-5548366.753000	2998783.678000	28 13 40.9313	279 23 39.4468	-23.5713

NAME	I.D.	X	Y	Z	LATITUDE	LONGITUDE	HEIGHT
WFCMLAS	7070	1261570.285000	-4881564.364000	3893184.329000	37 51 36.6102	284 29 24.8254	-28.7573
1JUM24	7071	976288.131000	-5601387.374000	2880247.155000	27 1 14.3717	279 53 13.1683	-17.1695
1JUM40	7072	976291.901000	-5601381.235000	2880258.186000	27 1 14.7707	279 53 13.3413	-16.9689
1JUPC1	7073	976298.392000	-5601380.427000	2880256.240000	27 1 14.7097	279 53 13.5783	-17.5693
1JUBC4	7074	976299.006000	-5601377.656000	2880262.710000	27 1 14.9357	279 53 13.6175	-16.9678
1SUDBR	7075	692632.551000	-4347058.865000	4600492.858000	46 27 21.5533	279 3 10.9597	250.5663
1JAMAC	7076	1384174.482000	-5905661.874000	1966555.590000	18 4 34.8917	283 11 27.3567	435.2710
1GSFCN	7077	1130077.869000	-4833029.111000	3992265.813000	38 59 57.4187	283 9 38.4381	16.9530
WALMOT	7078	1261602.272000	-4881343.277000	3893447.085000	37 51 47.4404	284 29 28.3556	-30.1643
1CARVN	7079	-2328603.726000	5299341.378000	-2669685.615000	-24 54 23.4104	113 43 16.8575	2.9745
DELFTH	8009	3923405.024000	299909.552000	5002981.668000	52 0 6.3424	4 22 16.5137	73.1644
ZIMWLD	8010	4331310.700000	567543.231000	4633125.666000	46 52 37.0879	7 27 54.3207	958.4242
MALVRN	8011	3920168.247000	-134706.054000	5012732.350000	52 8 35.9096	358 1 55.0516	161.5850
HAUTEP	8015	4578328.737000	457997.648000	4403198.266000	43 55 57.6133	5 42 45.4853	707.9391
NICEFR	8019	4579479.626000	586622.290000	4386423.525000	43 43 32.8750	7 17 58.9994	431.3883
MUDONI	8030	4205642.568000	163747.065000	4776554.051000	48 48 22.0630	2 13 46.8840	222.5547
1ORGAN	9001	-1535736.898000	-5166990.635000	3401055.124000	32 25 25.2673	253 26 49.0477	1627.3368
1OLFAN	9002	5056124.398000	2716514.805000	-2775771.682000	-25 57 36.2134	28 14 52.4394	1570.6283
WOOMER	9003	-3983793.232000	3743086.410000	-3275536.467000	-31 6 2.2261	136 47 3.4590	166.1201
1SPAIN	9004	5105596.429000	-555212.070000	3769671.060000	36 27 46.5702	353 47 37.3686	73.1944
1TOKYO	9005	-3946701.784000	3366284.120000	3698830.457000	35 40 22.6368	139 32 16.5965	97.4377
1NATAL	9006	1018193.658000	5471111.932000	3109615.511000	29 21 34.2701	79 27 27.5562	1881.9966
1QUIPA	9007	1942791.749000	-5804079.617000	-1796911.493000	-16 27 56.4183	288 30 24.7320	2491.7665
1SHRAZ	9008	3376878.004000	4404003.001000	3136259.449000	29 38 13.5471	52 31 11.7222	1592.2059
1CURAC	9009	2251841.307000	-5816910.568000	1327176.578000	12 5 25.3067	291 9 44.6674	-9.8095
1JUPTR	9010	976306.929000	-5601383.489000	2880250.753000	27 1 14.4847	279 53 13.8643	-16.0690
1VILDO	9011	2280591.315000	-4914582.504000	-3355397.399000	-31 56 34.4100	294 53 36.4518	638.7421
1MAUIO	9012	-5466046.730000	-2404297.754000	2242186.928000	20 42 26.1383	203 44 34.0628	3052.7508
HOPKIN	9021	-1936761.465000	-5077706.425000	3331923.185000	31 41 3.2404	249 7 18.9303	2352.9393
AUSBAK	9023	-3977783.956000	3725095.767000	-3303009.930000	-31 23 25.9706	136 52 43.9634	146.7573
DODAIR	9025	-3910447.481000	3376358.232000	3729214.022000	36 0 19.7245	139 11 31.2730	902.4885
DEZEIT	9028	4903753.689000	3965224.700000	963855.471000	8 44 50.8070	38 57 33.6719	1916.5855
NATALB	9029	5186466.971000	-3653856.721000	-654316.421000	-5 55 39.9358	324 50 7.3421	38.5952
COMRIV	9031	1693805.245000	-4112343.673000	-4556637.708000	-45 53 12.1867	292 23 9.3821	203.0141
JUPGEO	9049	976296.864000	-5601385.468000	2880245.476000	27 1 14.3287	279 53 13.4923	-18.2692
AGASSI	9050	1489749.695000	-4467460.382000	4287314.575000	42 30 22.0210	288 26 30.5904	146.3939
ATHENG	9051	4606872.302000	2029756.782000	3903548.846000	37 58 36.1806	23 46 40.6745	230.2932
MALVRN	9080	3920171.696000	-134721.226000	5012742.827000	52 8 36.0163	358 1 54.2604	172.2922
GREECE	9091	4595164.574000	2039477.178000	3912661.522000	38 4 44.3632	23 55 59.3014	506.3560
EDWAFB13	9113	-2449990.048000	-4624418.526000	3635038.437000	34 57 50.8759	242 5 8.2223	753.5172
COLDLK14	9114	-1264845.049000	-3466885.553000	5185467.766000	54 44 33.9608	249 57 22.3359	687.6346
OSLONR15	9115	3121281.524000	592659.860000	5512725.385000	60 12 39.0078	10 45 4.2127	623.0307
JOHNST17	9117	-6007406.974000	-1111883.065000	1825753.157000	16 44 39.1301	190 29 9.4086	33.7610
COLDLK24	9424	-1264827.430000	-3466879.952000	5185469.308000	54 44 34.2880	249 57 23.1537	682.3706
EDWAFB25	9425	-2449990.048000	-4624418.526000	3635038.437000	34 57 50.8759	242 5 8.2223	753.5172
OSLONR26	9426	3121281.524000	592659.860000	5512725.385000	60 12 39.0078	10 45 4.2127	623.0307
JOHNST27	9427	-6007406.974000	-1111883.065000	1825753.157000	16 44 39.1301	190 29 9.4086	33.7610
RIGLAT	9428	3183913.279000	1421526.773000	5322765.729000	56 56 53.3549	24 3 33.8538	14.7034
RIGALA	9431	3183883.925000	1421491.579000	5322808.034000	56 56 55.2158	24 3 32.6607	27.7186
UZHGOR	9432	3907416.268000	1602450.327000	4763917.190000	48 38 1.6238	22 17 55.5773	232.9081
HELSIK	9435	2884535.666000	1342151.531000	5509526.419000	60 9 42.9720	24 57 7.8651	58.1214

APPENDIX 3

APRIORI OCEAN TIDE MODEL

Doodson Number	Tide Name	Degree & Order No.		Interpolated Model C's	Interpolated Model ε's	Schwiderski Model C's	Schwiderski Model ε's
056.5545	SA	2	0 *	0.092	229.97		
		3	0	0.006	23.14		
		4	0	0.021	81.87		
		5	0	0.041	270.26		
		6	0	0.054	143.61		
057.5555	SSA	2	0	0.566	230.75	0.622	221.72
		3	0	0.038	25.47	0.031	2.42
		4	0	0.129	82.47	0.162	92.88
		5	0	0.248	269.77	0.262	251.40
		6	0	0.320	143.33	0.437	145.84
058.5545		2	0	0.032	231.63		
		3	0	0.002	28.34		
		4	0	0.007	83.11		
		5	0	0.014	269.20		
		6	0	0.018	143.00		
065.4555	MM	2	0	0.538	241.96	0.532	258.97
		3	0	0.024	88.82	0.031	94.48
		4	0	0.141	89.76	0.099	68.70
		5	0	0.205	261.62	0.229	292.14
		6	0	0.178	136.37	0.065	39.69
075.5555	MF	2	0	0.860	261.07	0.853	251.96
		3	0	0.104	145.41	0.095	148.22
		4	0	0.259	99.12	0.298	102.87
		5	0	0.241	239.65	0.297	223.21
		6	0	0.125	8.99	0.088	107.99
075.5655		2	0	0.354	261.15		
		3	0	0.043	145.49		
		4	0	0.107	99.16		
		5	0	0.099	239.51		
		6	0	0.052	8.51		

* Due to symmetries in the harmonic
expansion of the m=o tides (the
prograde and retrograde components
sum), the amplitude values shown
reguire doubling when included in
the tidal potential model.

Doodson Number	Tide Name	Degree & Order No.		Interpolated Model C's	ε's	Schwiderski Model C's	ε's
135.6555	Q1	2	1	0.530	313.70	0.537	313.77
		3	1	0.316	104.18	0.314	107.47
		4	1	0.293	288.12	0.293	288.93
		5	1	0.215	112.27	0.221	112.47
		6	1	0.041	286.69	0.040	288.25
		-2	1	0.238	165.27	0.244	167.48
		-3	1	0.210	351.92	0.208	352.78
		-4	1	0.106	338.07	0.105	339.05
		-5	1	0.081	153.31	0.086	155.75
		-6	1	0.019	195.21	0.020	187.46
145.5455	O1F	2	1	0.466	313.85		
		3	1	0.226	93.70		
		4	1	0.267	278.37		
		5	1	0.193	110.02		
		6	1	0.034	284.24		
		-2	1	0.206	156.40		
		-3	1	0.192	338.56		
		-4	1	0.104	330.63		
		-5	1	0.081	153.44		
		-6	1	0.025	202.63		
145.5555	O1	2	1	2.482	313.85	2.420	313.74
		3	1	1.202	93.64	1.314	83.69
		4	1	1.422	278.32	1.431	276.30
		5	1	1.029	110.01	0.950	109.18
		6	1	0.181	284.23	0.187	282.93
		-2	1	1.099	156.35	1.063	150.11
		-3	1	1.025	338.50	1.074	335.01
		-4	1	0.554	330.59	0.581	326.62
		-5	1	0.433	153.44	0.382	147.25
		-6	1	0.132	202.65	0.126	223.92
155.4555	M1	2	1	0.060	314.03		
		3	1	0.023	72.46		
		4	1	0.037	267.31		
		5	1	0.026	107.30		
		6	1	0.004	280.78		
		-2	1	0.027	145.08		
		-3	1	0.028	324.01		
		-4	1	0.015	323.22		
		-5	1	0.012	153.57		
		-6	1	0.005	206.96		
155.6555	M1F	2	1	0.172	314.04		
		3	1	0.065	71.92		
		4	1	0.107	267.11		
		5	1	0.074	107.25		
		6	1	0.012	280.71		
		-2	1	0.077	144.86		
		-3	1	0.080	323.75		
		-4	1	0.044	323.09		
		-5	1	0.035	153.57		
		-6	1	0.013	207.02		

Doodson Number	Tide Name	Degree & Order No.		Interpolated Model C's	e's	Schwiderski Model C's	e's
162.5565	PI1	2	1	0.054	314.22		
		3	1	0.019	43.09		
		4	1	0.037	258.16		
		5	1	0.024	104.77		
		6	1	0.003	276.89		
		-2	1	0.025	134.56		
		-3	1	0.029	312.91		
		-4	1	0.016	317.60		
		-5	1	0.012	153.66		
		-6	1	0.005	209.25		
163.5555	P1	2	1	0.906	314.24	0.902	313.91
		3	1	0.326	39.89	0.296	40.18
		4	1	0.630	257.28	0.636	258.26
		5	1	0.401	104.50	0.413	104.58
		6	1	0.058	276.45	0.058	276.79
		-2	1	0.432	133.50	0.430	135.45
		-3	1	0.494	311.91	0.488	312.71
		-4	1	0.269	317.08	0.262	317.94
		-5	1	0.210	153.67	0.217	154.60
		-6	1	0.093	209.43	0.096	204.99
164.5565	S1	2	1	0.021	314.26		
		3	1	0.008	36.68		
		4	1	0.015	256.41		
		5	1	0.010	104.24		
		6	1	0.001	275.99		
		-2	1	0.010	132.43		
		-3	1	0.012	310.91		
		-4	1	0.006	316.56		
		-5	1	0.005	153.68		
		-6	1	0.002	209.61		
165.5455	K1F	2	1	0.053	314.28		
		3	1	0.019	33.66		
		4	1	0.038	255.58		
		5	1	0.024	103.98		
		6	1	0.003	275.53		
		-2	1	0.026	131.41		
		-3	1	0.030	309.98		
		-4	1	0.016	316.07		
		-5	1	0.013	153.69		
		-6	1	0.006	209.77		
165.5555	K1	2	1	2.677	314.28	2.816	315.16
		3	1	0.990	33.50	0.889	34.14
		4	1	1.908	255.54	1.912	254.20
		5	1	1.195	103.97	1.211	104.74
		6	1	0.170	275.51	0.164	282.14
		-2	1	1.296	131.36	1.349	132.60
		-3	1	1.511	309.93	1.524	310.96
		-4	1	0.817	316.04	0.852	317.31
		-5	1	0.635	153.69	0.656	156.16
		-6	1	0.288	209.78	0.318	203.59

Doodson Number	Tide Name	Degree & Order No.		Interpolated Model C's	ε's	Schwiderski Model C's	ε's
165.5655	K1S	2	1	0.360	314.28		
		3	1	0.133	33.32		
		4	1	0.257	255.49		
		5	1	0.161	103.95		
		6	1	0.023	275.48		
		-2	1	0.174	131.30		
		-3	1	0.203	309.87		
		-4	1	0.110	316.01		
		-5	1	0.085	153.69		
		-6	1	0.039	209.79		
166.5545	PSI1	2	1	0.021	314.30		
		3	1	0.008	30.34		
		4	1	0.015	254.67		
		5	1	0.009	103.69		
		6	1	0.001	275.01		
		-2	1	0.010	130.27		
		-3	1	0.012	308.95		
		-4	1	0.006	315.53		
		-5	1	0.005	153.70		
		-6	1	0.002	209.95		
167.5555	PHI1	2	1	0.037	314.32		
		3	1	0.014	27.23		
		4	1	0.027	253.80		
		5	1	0.017	103.41		
		6	1	0.002	274.50		
		-2	1	0.018	129.18		
		-3	1	0.022	307.99		
		-4	1	0.012	315.02		
		-5	1	0.009	153.70		
		-6	1	0.004	210.12		
175.4555	J1	2	1	0.127	314.60		
		3	1	0.072	359.10		
		4	1	0.110	244.32		
		5	1	0.060	99.94		
		6	1	0.007	267.07		
		-2	1	0.072	116.76		
		-3	1	0.093	298.08		
		-4	1	0.048	309.50		
		-5	1	0.036	153.80		
		-6	1	0.019	211.71		
185.5555	OO1	2	1	0.057	315.08		
		3	1	0.057	341.27		
		4	1	0.064	234.05		
		5	1	0.029	94.84		
		6	1	0.003	251.77		
		-2	1	0.041	102.60		
		-3	1	0.057	288.45		
		-4	1	0.027	303.46		
		-5	1	0.020	153.91		
		-6	1	0.012	213.14		

Doodson Number	Tide Name	Degree & Order No.		Interpolated Model C's	ε's	Schwiderski Model C's	ε's
245.6555	N2	2	2	0.651	317.51	0.653	321.73
		3	2	0.089	164.54	0.109	172.01
		4	2	0.215	138.70	0.214	141.96
		5	2	0.073	2.73	0.084	5.17
		6	2	0.077	345.44	0.067	346.51
		-2	2	0.155	92.42	0.166	96.47
		-3	2	0.057	356.03	0.040	14.76
		-4	2	0.132	18.84	0.146	29.03
		-5	2	0.160	267.60	0.165	274.19
		-6	2	0.030	146.63	0.038	157.04
255.5455	M2S	2	2	0.109	316.82		
		3	2	0.019	178.09		
		4	2	0.037	129.22		
		5	2	0.013	2.22		
		6	2	0.013	326.48		
		-2	2	0.023	77.60		
		-3	2	0.006	344.65		
		-4	2	0.018	20.36		
		-5	2	0.026	261.47		
		-6	2	0.005	144.38		
255.5555	M2	2	2	2.939	316.81	2.957	310.56
		3	2	0.516	178.13	0.361	168.73
		4	2	0.984	129.18	1.006	124.88
		5	2	0.353	2.22	0.274	357.00
		6	2	0.340	326.40	0.411	329.01
		-2	2	0.606	77.52	0.522	59.66
		-3	2	0.158	344.56	0.303	335.85
		-4	2	0.493	20.37	0.457	353.69
		-5	2	0.703	261.44	0.701	249.14
		-6	2	0.125	144.37	0.095	108.07
265.4555	L2	2	2	0.070	315.86		
		3	2	0.017	188.77		
		4	2	0.025	116.99		
		5	2	0.009	1.60		
		6	2	0.009	303.03		
		-2	2	0.014	51.80		
		-3	2	0.002	277.01		
		-4	2	0.008	23.92		
		-5	2	0.017	252.64		
		-6	2	0.003	140.43		
271.5575		2	2	0.002	314.93		
		3	2	0.001	194.75		
		4	2	0.001	106.75		
		5	2	0.000	1.08		
		6	2	0.000	287.22		
		-2	2	0.001	28.18		
		-3	2	0.000	219.53		
		-4	2	0.000	31.80		
		-5	2	0.001	243.99		
		-6	2	0.000	135.25		

Doodson Number	Tide Name	Degree & Order No.		Interpolated Model C's	ε's	Schwiderski Model C's	ε's
272.5565	T2	2	2	0.057	314.81		
		3	2	0.018	195.31		
		4	2	0.023	105.61		
		5	2	0.008	1.03		
		6	2	0.010	285.71		
		-2	2	0.013	25.73		
		-3	2	0.004	217.09		
		-4	2	0.004	33.49		
		-5	2	0.014	242.92		
		-6	2	0.002	134.48		
273.5555	S2	2	2	0.969	314.69	0.931	314.07
		3	2	0.312	195.86	0.265	201.82
		4	2	0.386	104.47	0.372	103.13
		5	2	0.138	0.97	0.137	3.96
		6	2	0.169	284.24	0.172	280.45
		-2	2	0.223	23.33	0.155	2.19
		-3	2	0.067	214.98	0.096	223.69
		-4	2	0.061	35.54	0.064	55.63
		-5	2	0.232	241.84	0.213	240.04
		-6	2	0.029	133.66	0.031	137.73
274.5545		2	2	0.008	314.57		
		3	2	0.003	196.40		
		4	2	0.003	103.32		
		5	2	0.001	0.91		
		6	2	0.001	282.81		
		-2	2	0.002	20.98		
		-3	2	0.001	213.14		
		-4	2	0.000	38.09		
		-5	2	0.002	240.73		
		-6	2	0.000	132.78		
275.5555	K2	2	2	0.255	314.44	0.260	315.16
		3	2	0.087	196.92	0.095	194.91
		4	2	0.104	102.16	0.106	103.64
		5	2	0.037	0.84	0.038	0.77
		6	2	0.047	281.40	0.047	281.34
		-2	2	0.062	18.68	0.071	28.61
		-3	2	0.021	211.53	0.019	199.15
		-4	2	0.013	41.29	0.015	39.03
		-5	2	0.061	239.59	0.064	242.56
		-6	2	0.007	131.82	0.008	135.32
285.4555		2	2	0.011	312.22		
		3	2	0.006	202.96		
		4	2	0.006	86.66		
		5	2	0.002	359.93		
		6	2	0.003	266.16		
		-2	2	0.004	354.66		
		-3	2	0.002	200.63		
		-4	2	0.001	171.06		
		-5	2	0.003	221.65		
		-6	2	0.000	104.96		

Doodson Number	Tide Name	Degree & Order No.		Interpolated Model C's	Interpolated Model ε's	Schwiderski Model C's	Schwiderski Model ε's
295.5555		2	2	0.002	309.07		
		3	2	0.002	207.64		
		4	2	0.002	72.13		
		5	2	0.000	358.75		
		6	2	0.001	255.90		
		-2	2	0.002	340.76		
		-3	2	0.001	196.63		
		-4	2	0.001	186.39		
		-5	2	0.001	199.95		
		-6	2	0.000	30.24		

Report Documentation Page

1. Report No.	2. Government Accession No.	3. Recipient's Catalog No.
NASA TM 4019		

4. Title and Subtitle	5. Report Date
An Improved Model of the Earth's Gravitational Field: GEM-T1	July 1987
	6. Performing Organization Code 621.0

7. Author(s) J.G.Marsh, F.J.Lerch, D.C.Christodoulidis, B.H.Putney, T.L.Felsentreger, B.V.Sanchez, D.E.Smith, S.M.Klosko, T.V.Martin, E.C.Pavlis, J.W.Robbins, R.G.Williamson, O.L.Colombo, N.L.Chandler, K.E.Rachlin, G.B.Patel, S.Bhati, D.S.Chinn	8. Performing Organization Report No. 87B0451
	10. Work Unit No.

9. Performing Organization Name and Address	11. Contract or Grant No.
Goddard Space Flight Center Greenbelt, Maryland 20771	
	13. Type of Report and Period Covered Technical Memorandum

12. Sponsoring Agency Name and Address	
National Aeronautics and Space Administration Washington, DC 20546-0001	**14. Sponsoring Agency Code**

15. Supplementary Notes

Authors Marsh through Smith are in the Geodynamics Branch of GSFC; authors Klosko through Rachlin are affiliated with EG&G Washington Analytical Services Center Inc. and authors Patel through Chinn are with Science Applications and Research Corporation

16. Abstract

A new generation of Goddard Earth Models is under development at the NASA/Goddard Space Flight Center to satisfy the requirements of future geodetic and oceanographic missions. GEM-T1, a model which has been developed from an analysis of direct satellite tracking observations, is the first in this series of models to be produced. GEM-T1 is complete to degree and order 36. It was developed using consistent reference parameters, extensive earth and ocean tidal models, and simultaneously solved for gravitational and tidal terms, earth orientation parameters and the orbital parameters of 580 individual satellite arcs. The solution used exclusively satellite tracking data acquired on 17 different satellites and is predominantly based upon the precise laser data taken by third generation systems. In total, 800,000 observations were used. A major improvement in field accuracy has been obtained with GEM-T1. For marine geodetic applications, nearly a factor of two improvement in long wavelength geoidal modeling has been achieved over that available from earlier "satellite-only" GEM models. Orbit determination accuracy has also been substantially advanced over a wide range of satellites which have been tested.

17. Key Words (Suggested by Author(s))	18. Distribution Statement
gravitational models geopotential satellite geodesy satellite data analysis satellite laser ranging	Unclassified-Unlimited Subject Category - 46

19. Security Classif. (of this report)	20. Security Classif. (of this page)	21. No. of pages	22. Price
Unclassified	Unclassified		